MECHANISTIC, SYNTHETIC AND THEORETICAL STUDIES OF HIGH VALENT METALLACYCLES AND METAL ALKYLIDENES

Thesis by

Eric Van Anslyn

In Partial Fulfillment of the Requirements

for the Degree of

Doctor of Philosophy

California Institute of Technology

Pasadena, California

1988

(Submitted November 2, 1987)

To my loving wife,

Roxanna,

and supportive parents,

Sam and Dorothea.

ACKNOWLEDGMENTS

Caltech has been a special and unique experience for me. My friends and colleagues have created an atmosphere for open discussion and scientific curiosity. Most notably, the leadership style of Bob Grubbs encourages self-motivation and creates a relaxed atmosphere in which research can be pursued not only enthusiastically but also carefully and accurately. I thank Bob for the chance to work in his group and for his guidance. I also thank Bob for the trust and opportunity to be an NMR GLA. It has been an invaluable educational experience.

In addition to Bob Grubbs, I would like to thank Bill Goddard. Part of this thesis discusses ab initio electronic structure theory calculations that were performed under the guidence and trust of Bill.

The Grubbs research group (members past and present) has helped me to grow as a scientist and has given me many friendships. Special mention should be made about Doug Meinhart (NMR education), Bill Tumas (helpful discussions), Scotty Virgil (Cp*) and several close friends and supporters: Bill Finch, John Stille, Tim Swager, Bruce Novak, Dave Wheeler and Mike Petti. A special thanks to Mark Brusich for his time and patience with VAX computer problems.

The X-ray crystallographic work in this thesis was done in collaboration with Bernard Santarsiero; my thanks for his expertise. I would also like to thank Union Carbide for a fellowship.

My parents have always supported and helped my every goal and ambition, and I am deeply grateful.

Finally, Roxanna has shared my goals and hopes and understood my fears and obsessions from the very beginning. I could not ask for a more supportive and loving wife.

PREFACE

The primary focus of this thesis is on the mechanism of olefin metathesis and ring opening metathesis polymerizations. In addition, several reactions of metal alkylidenes and metallacycles which are not traditionally viewed as part of the olefin metathesis reaction are presented. Olefin metathesis involves the 2+2 cycloaddition of metal alkylidenes with olefins and the 2+2 cycloreversion of metallacyclobutanes. These reactions are becoming common place in organometallic reaction mechanisms and join the traditional oxidative additions, reductive eliminations, ligand substitutions, intramolecular insertions, nucleophilic attacks on coordinated ligands and ligand fluxtionalities as the commonly sited organometallic reactions. A current goal of organometallic chemistry is to understand the influence of oxidation state, electron count, ligand sterics, ligand electronics and substituent effects upon each of these reactions.

The knowledge of mechanisms is essential to be able to understand and rationally manipulate chemical processes. The knowledge also allows for the capability to catagorize mechanistic theories as an organizing device for understanding organometallic chemistry as a whole. Organometallic chemistry, however, is not easily catagorized due to the large complexity of bonding types and structures that inorganic chemistry produces. The work in this thesis has utilized some techniques of physical organic chemistry to study mechanisms and reactive intermediates. These techniques include kinetics, substituent effects, isotope effects, stereochemical studies and theoretical calculations.

Organic chemistry has greatly benefited from the advent and subsequent development of the pericyclic theory for the understanding of covalent bonding, frontier orbitals and symmetry. These same notions have met with various levels of success

in organometallic chemistry. The success of theoretical studies in organometallic systems very often depends upon the level of electron correlation and the extent to which the exchange integrals are calculated. The theory presented in this thesis utilizes a fully ab initio method with electron correlation. The structure of organometallic complexes is examined as a function of the nodal planes of the individual metal ligand bonds and their influence on the bonding of other ligands within the same complex. In addition, reactivity of the complexes are probed as a function of the symmetry and energy of the bonding and empty orbitals.

In chapter one, data and speculations relating to the mechanism of cleavage of titanocene metallacyclobutanes is presented. The reactive intermediate is postulated to be a titanocene methylidene-olefin adduct. Chapter two further expands upon these mechanistic studies by presenting the kinetics and polydispersities of the ring opening metathesis polymerizations of slightly strained olefins. Chapter three presents work which utilizes ab initio electronic structure theory calculations to determine the energetics of the 2+2 cycloaddition of molybdenum alkylidene and imido complexes with olefins. In chapters 4, 5 and 6, reactivity different than the normal cycloadditions of metal alkylidenes and cycloreversions of metallacycles is examined. In chapter 4, an electron transfer mechanism for the reaction of titanocene methylidene with activated halides is presented. Chapter 5 discusses the reactivity of titanocene methylidene with inorganic carbonyls. The titanocene methylidene does not perform methylene transfer as is seen with organic carbonyls, but instead, the resultant oxametallacycle rearranges to yield a titanocene ketene complex. Finally, in chapter six, ab initio electronic structure theory calculations are again presented. They are used to explore the interconversion of a metallacyclobutadiene to a metallatetrahedrane. The two complexes are found to be energetically

similar due to a balance between the strength of σ and π bonds and the role of strain and resonance effects. Each chapter was written as an individual study and thus includes an Abstract, Introduction, Results and Discussion section and a Summary or Conclusion. Thus, this thesis presents work that attempts to add a little more knowledge to the mechanistic and theoretical understanding of organometallic reaction mechanisms.

TABLE OF CONTENTS

LIST OF TABLES

LIST OF FIGURES, SCHEMES AND GRAPHS

Chapter 6.

CHAPTER 1

THE MECHANISM OF TITANOCENE

METALLACYCLOBUTANE CLEAVAGE AND THE

NATURE OF THE REACTIVE INTERMEDIATE

ABSTRACT

Titanocene metallacyclobutanes react with olefins and acetylenes and display either first or second order kinetics. Second order kinetics is due to a competition between the trap and the latent olefin for the titanocene methylidene reactive intermediate. The metallacycles display saturation kinetics at high concentrations of trapping reagents. Kinetic studies on titanocene methylidene phosphine adducts implicate a rate limiting loss of phosphine followed by rapid trapping of titanocene methylidene. Competition trapping studies on titanocene methylidene phosphine adducts and titanocene metallacyclobutanes demonstrate that the reactions proceed through different intermediates. The reactive intermediates formed from the metallacycles are postulated to be titanocene methylidene olefin adducts. Electron withdrawing and electron donating substituents on the cyclopentadienyl ligands slow the rate of metallocyclobutane cleavage. Electron withdrawing substituents preferentially stabilize the ground state, and electron donating substitutents preferentially destabilize the transition state. Secondary deuterium isotope effect studies demonstrate that the CH_2 modes of the methylidene ligand are lower in energy than the typical CH_2 modes of olefins.

INTRODUCTION

Titanocene metallacyclobutanes[1] show a wide variety of reactivities with organic and inorganic reagents. Their reactions include methylene transfer to organic carbonyls,[2] formation of enolates,[2a,2e,3] electron transfer from activated alkyl chlorides,[4] olefin metathesis,[5] ring opening polymerization[6] and complexation with metal halides.[7] All these reactions presumably occur through a reactive intermediate which exhibits behavior consistent with that of a transition metal carbene. The intermediate has been postulated to be free titanocene methylidene[5d] **A** or a titanocene methylene olefin complex[5d] **B**. The cleavage of the metallacycle to give the reactive intermediate is the rate determining step in all the above reactions. Controlling the rate of cleavage and understanding the nature of the reactive intermediate could lead to better catalyst design, better selectivity in organic reactions and higher stereocontrol in polymerization.[8]

$$Cp_2Ti = CH_2 \qquad\qquad Cp_2Ti = CH_2$$
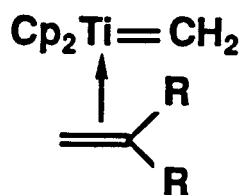
A **B**

The metallacycle can be envisioned to lose olefin in a one step process or by a slipping mechanism in which a methylidene-olefin complex forms first and then the olefin dissociates. This question has been approached theoretically

by several groups. Rappé has found, by the Generalized Valence Bond method[9] and the Orbital Phase Continuity Principle,[10] that an olefin can react with the methylidene in a concerted 2+2 reaction which is allowed due to the second angular node present in d orbitals.[11] He found no energy well for an olefin-methylidene complex. However, Hoffmann and coworkers[12] have studied this system using the Extended Hückel method and found the metallacycle substantially less stable than the olefin-methylidene complex (by approximately 20 kcal./mol). Furthermore, they found the global potential energy minimum to be the geometry Rappé found to be a saddle point, namely the olefin methylidene complex. Thus, two radically opposing views exist on the stability of a titanocene methylidene olefin complex.

The nature of the titanocene methylidene has also been studied theoretically by several groups, all of which agree on its basic features.[13] The titanocene methylidene has its π bond electron density in a plane between the two cyclopentadienyl rings and has an empty orbital of A_1 symmetry in the same plane. Figure 1 represents the frontier orbitals of the titanium and CH_2.[14] The hypothetical free uncoordinated titanocene methylidene is a 16 electron species which has an empty orbital to which Lewis bases could possibly coordinate. Addition of a two electron donor Lewis base would achieve a full 18e- count for the titanium. Herein, it is reported that the reactivity of the titanocene methylidene is intimately tied to the nature of empty and bonding orbitals and whether or not a Lewis base adduct is stable.

For later transition metal olefin metathesis systems,[15] the metallacycle is the unstable reactive intermediate which can cleave nonproductively to give starting materials or in a productive manner, to yield metathesized olefin.

Figure 1: Frontier orbitals of Cp$_2$Ti and CH$_2$.
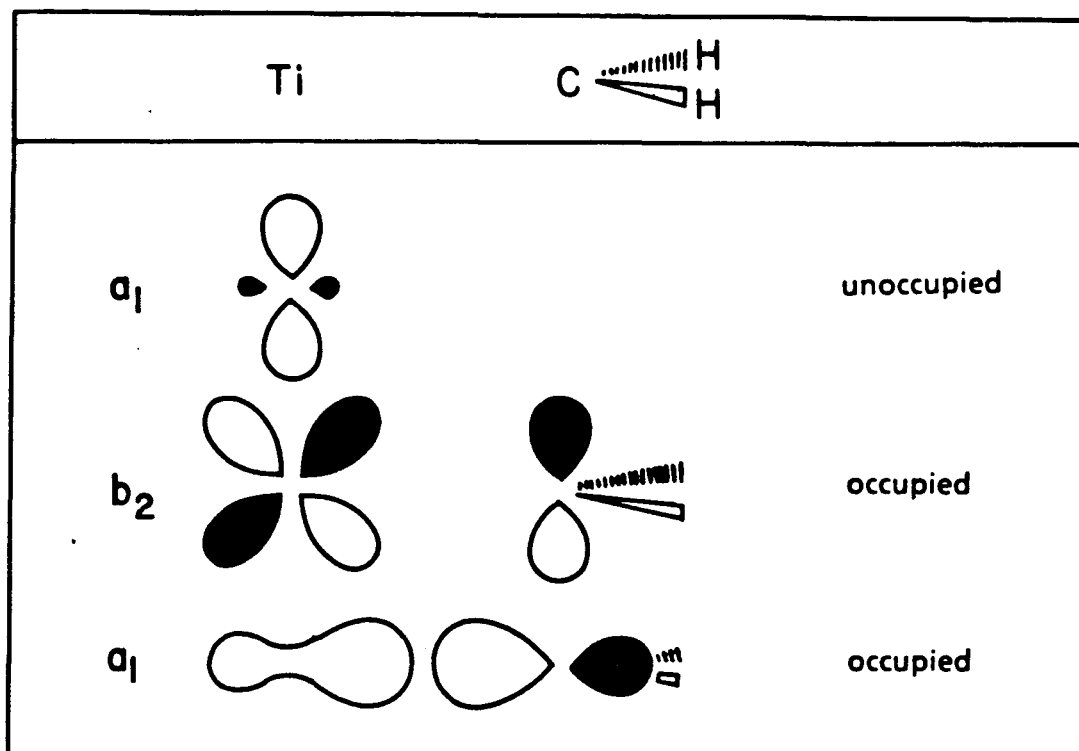
Because of the reversibility of this process, the product distribution is thermodynamically controlled. Only in the case where metathesized olefin cannot react with the carbene is relative reactivity information gained.

The reactivity of the titanocene metathesis system directly contrasts the later metal systems. The stable chain propagating catalyst is the metallacycle, not the methylidene. The methylidene can be trapped with olefins and internal acetylenes to yield metallacyclobutanes and metallacyclobutenes, respectively. These olefin and acetylene traps can be chosen so that the reaction is not reversible. In these systems relative reactivity information can be obtained.

RESULTS AND DISCUSSION

A. Rate Expressions and Reaction Orders

In order to probe the reaction mechanism, it was first decided to study the reaction order of several metallacycles. The reaction order gives information on the number of molecules that are involved in the rate determining step, or in multi-step reactions, it can reflect contributions from several different steps. This information, therefore, gives some initial insight into relative sizes of rate constants in multi-step reactions and plausible mechanisms. This was done because preliminary results suggested that the reaction order changed with metallacycle and substrate.

The proposed mechanisms of metallacycle cleavage to a reactive titanocene methylidene intermediate are presented in Figure 2. In mechanisms 1 and 3, the reactive intermediate is free titanocene methylidene **A**. In mechanism 2 and 4, the reactive intermediate is a titanocene methylidene olefin complex **B**. Mechanism 3 also involves the titanocene methylidene olefin intermediate, but it then forms the free titanocene methylidene which reacts with the trapping reagent. The rate expressions for each mechanism are also presented and were derived using the steady state approximation for all intermediates. The basic form of the kinetic expressions for mechanism 1, 2 and 3 are the same. They all have a product of rate constants preceding the [R][T] term in the numerator and additive [O] and [T] terms in the denominator with a constant for mechanism 2. In contrast, mechanism 4 has no trap term in the denominator. The mathematical form was tested for by

Table 1.

Compound	Number	Cleavage Temperature
Cp$_2$Ti	1	55
Cp$_2$Ti	2	0
Cp$_2$Ti	3	5
Cp$_2$Ti	4	-5
Cp$_2$Ti	5	65
Cp$_2$Ti	6	45
Cp$_2$Ti—Al, Cl	7	-78 with added pyridine
Cp$_2$Ti=CH$_2$ ← PMe$_3$	8	20
Cp$_2$Ti=CH$_2$ ← PMe$_2$Ph	9	0
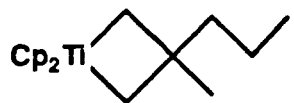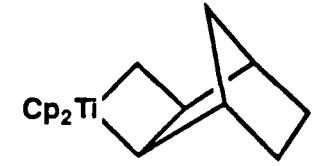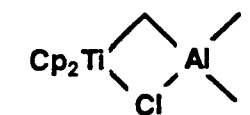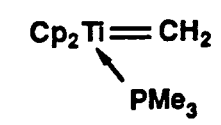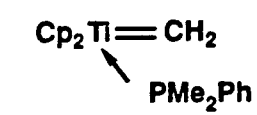
Figure 2: Metallacycle Proposed Mechanisms.
Legend
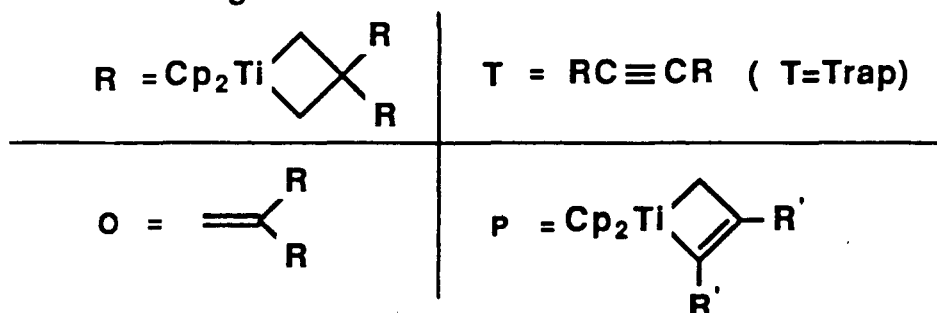
$$R = Cp_2Ti\diamond\!\!\!<^R_R \qquad\qquad T = RC\equiv CR \quad (\ T=Trap)$$

$$O = \;=\!\!<^R_R \qquad\qquad P = Cp_2Ti\diamond\!\!\!-^{R'}_{R'}$$

Mechanism 1

$$Cp_2Ti\diamond\!\!\!<^R_R \xrightleftharpoons[k_{-1}]{k_1} Cp_2Ti=CH_2 \;+\; =\!\!<^R_R$$

$$\big\downarrow k_2RC\equiv CR$$

$$Cp_2Ti\diamond\!\!\!-^{R'}_{R'}$$

Kinetic Expression

$$\frac{d[P]}{dt} = \frac{k_1k_2[R][T]}{k_{-1}[O]+k_2[T]}$$

Mechanism 2

$$Cp_2Ti\diamond\!\!\!<^R_R \xrightleftharpoons[k_{-1}]{k_1} Cp_2Ti=CH_2 \xrightleftharpoons[k_{-2}]{k_2R'C\equiv CR'} Cp_2Ti=CH_2 \;+\; =\!\!<^R_R$$

$$Cp_2Ti\diamond\!\!\!-^{R'}_{R'}$$
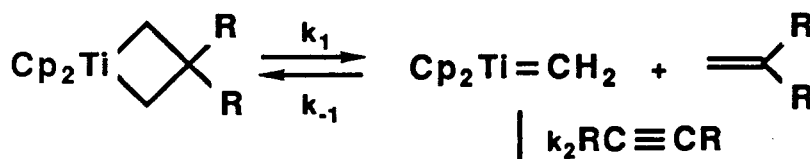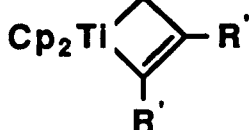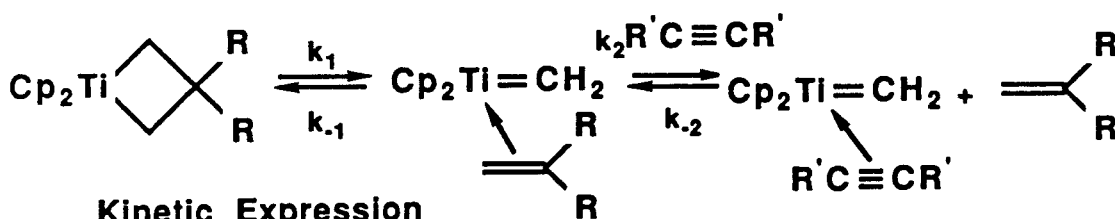
Kinetic Expression

$$\frac{d[P]}{dt} = \frac{k_1k_2k_3[R][T]}{k_3k_{-1}+k_{-2}k_{-1}[O]+k_2k_3[T]}$$

Mechanism 3

Kinetic Expression

$$\frac{d[P]}{dt} = \frac{k_1 k_2 k_3 k_4 [R][T]}{(k_4 + k_{-3})k_{-2}k_{-1}[O] + (k_{-1} + k_2)k_3 k_4 [T]}$$

Mechanism 4

Kinetic Expression

$$\frac{d[P]}{dt} = \frac{k_1 k_2 k_3 [R][T]}{k_{-1} k_{-2}[O] + (k_{-1} + k_2)k_3}$$
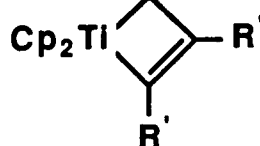
manipulation of reaction orders and observation of saturation behavior. Table 1 presents the compounds discussed and the temperatures which give roughly equal rates of cleavage.

Mechanisms 1, 2 and 3 will exhibit first order behavior under the appropriate conditions. For mechanisms 1 and 3, the rate expression reduces to first order when [T] > >[O] or when the rate constants preceding [T] in the denominator are much greater than the rate constants preceding [O]. Conditions for attaining first order behavior for mechanism 2 are more stringent. When [T] > >[O], k_{-1} must also be small compared to $k_2[T]$ before first order behavior is observed. Finally, in mechanism 4, first order behavior only occurs for high concentrations of trapping reagent.

When the olefin and trap terms of the denominator are comparable in mechanisms 1, 2 or 3, then reduction to first order is not possible. This occurs when the rate constants preceding [O] and [T] are roughly equal. The reaction is now second order because [O] is going up exactly proportional to the drop in [T] and because the initial [R] and [T] are roughly equal. The denominator is now approximately a constant. Therefore, the observation of both first and second order behavior can be due to the ability of the trap and the olefin to compete for the reactive intermediate. When the free olefin produced by the metallacycle is competitive with the added trapping reagent, the reaction displays second order behavior. When the added trap is much better at trapping the reactive intermediate than the olefin produced, the reaction displays first order behavior for mechanisms 1, 2 and 3.[18]

In Graph 1a, a first order plot of the reaction of metallacycle 1 with one equivalent of diphenylacetylene is displayed. In Graph 1b, a second order plot

of the same reaction is displayed. Clearly, the reaction more closely follows first order behavior. Graph 2a shows the first order plot of **3** when trapped with one equivalent of diphenylacetylene. In Graph 2b, the second order plot of the same data is displayed. The reaction now more closely follows second order behavior. Mechanism 4 can be ruled out solely based on this data since it should display only second order behavior under these conditions. This behavior can, however, be explained by mechanisms 1, 2 and 3. It is due to a greater difference between the trapping rate constants of the trap versus the olefin released for metallacycle **1**, compared to metallacycle **3**. In other words, isobutylene is a more comparable trap to diphenylacetylene at a temperature of 10°C than is neohexene at a temperature of 55°C. For metallacycle **3**, the denominator of the rate expressions cannot be simplified by neglecting the olefin term as it can be in the reaction of **1**.

Along with each graph is presented the rho value for the line and the standard deviation of the y value. Very often scatter can contribute to a low rho or high standard deviation and yet the line will be linear. In constrast, a high rho or small standard deviation can be associated with low scatter and yet the line will be visually curved. Since the scatter in all our graphs are low, visual inspection of the graphs was done rather than relying solely on mathematical error analysis. The graphs shown are typical examples of the experimental data, and the rate constants derived were always repeatable with an error margin of ten percent.

The reaction orders can also be reversed by using different traps or by changing concentrations. Graph 1c shows the kinetics of the reaction of **1** with diphenylacetylene when 3.9 equivalents of neohexene is added. Now the
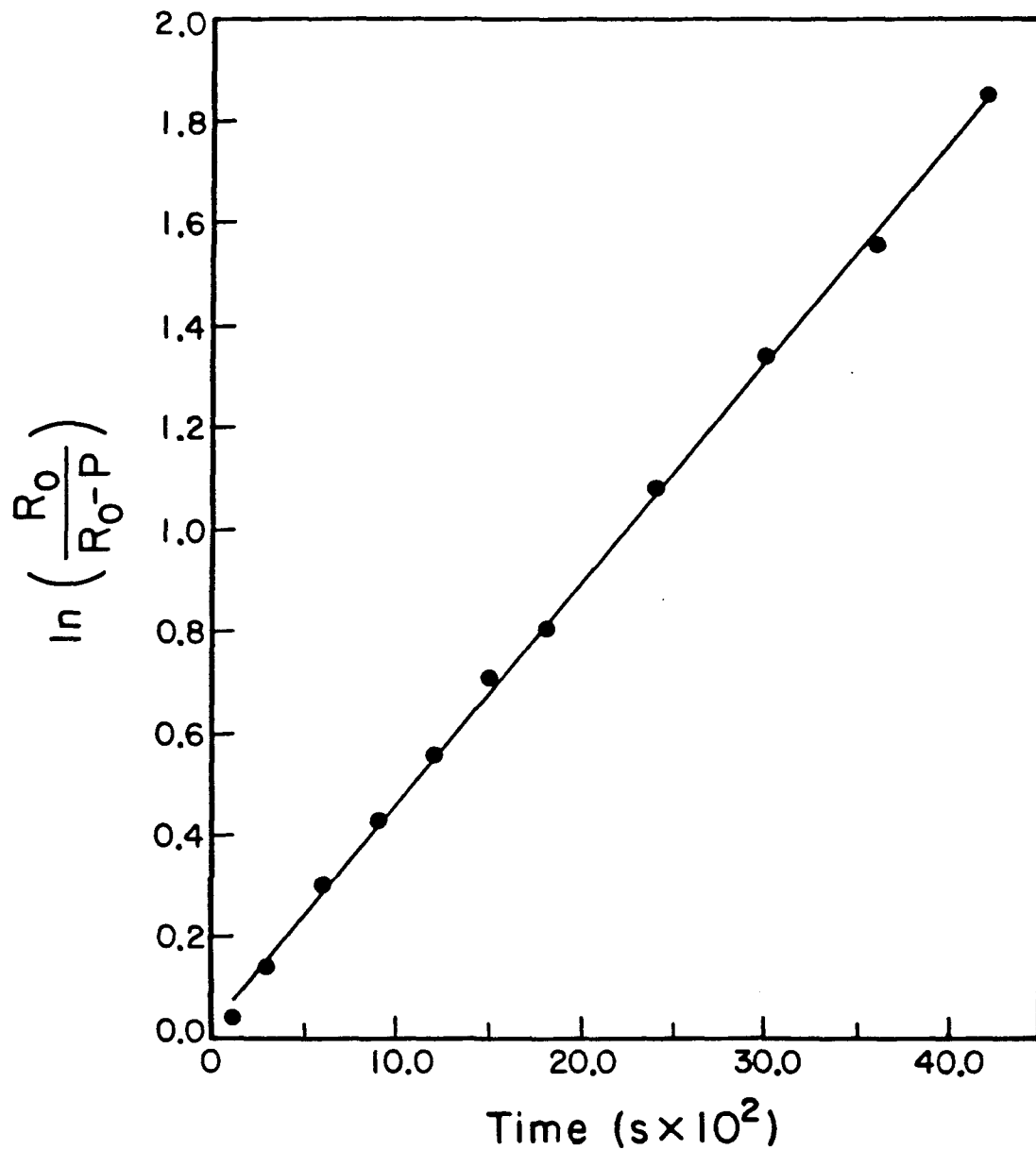
Graph 1a: First Order plot for the reaction of 1 with 1.1 eq of diphenylacetylene. The graph is linear. Rho=0.999, Standard Deviation $y = 0.0224$.
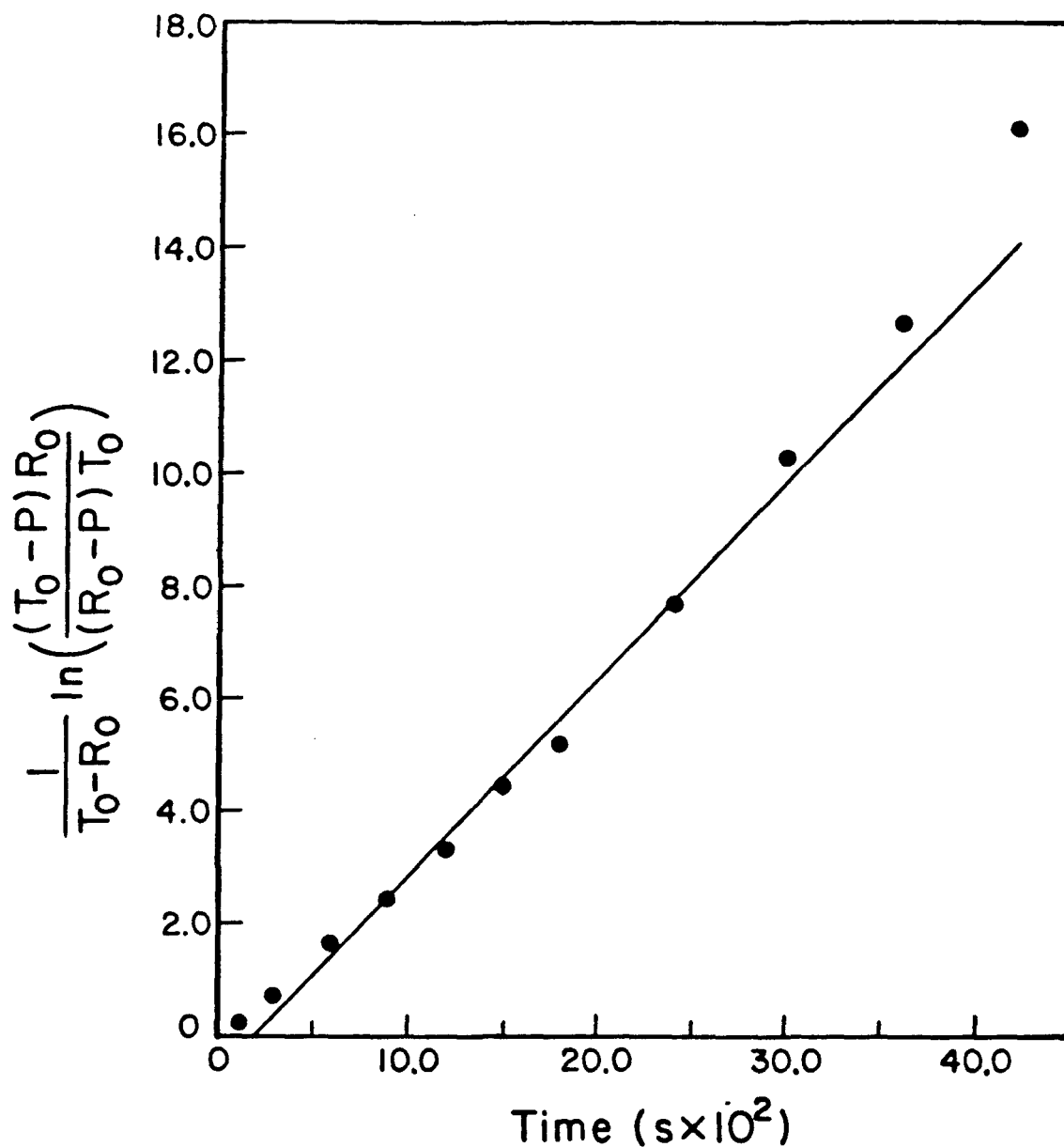
Graph 1b: Second Order plot for the reaction of 1 with 1.1 eq of diphenylacetylene. The graph curves up. Rho = 0.993, Standard Deviation y = 0.578.
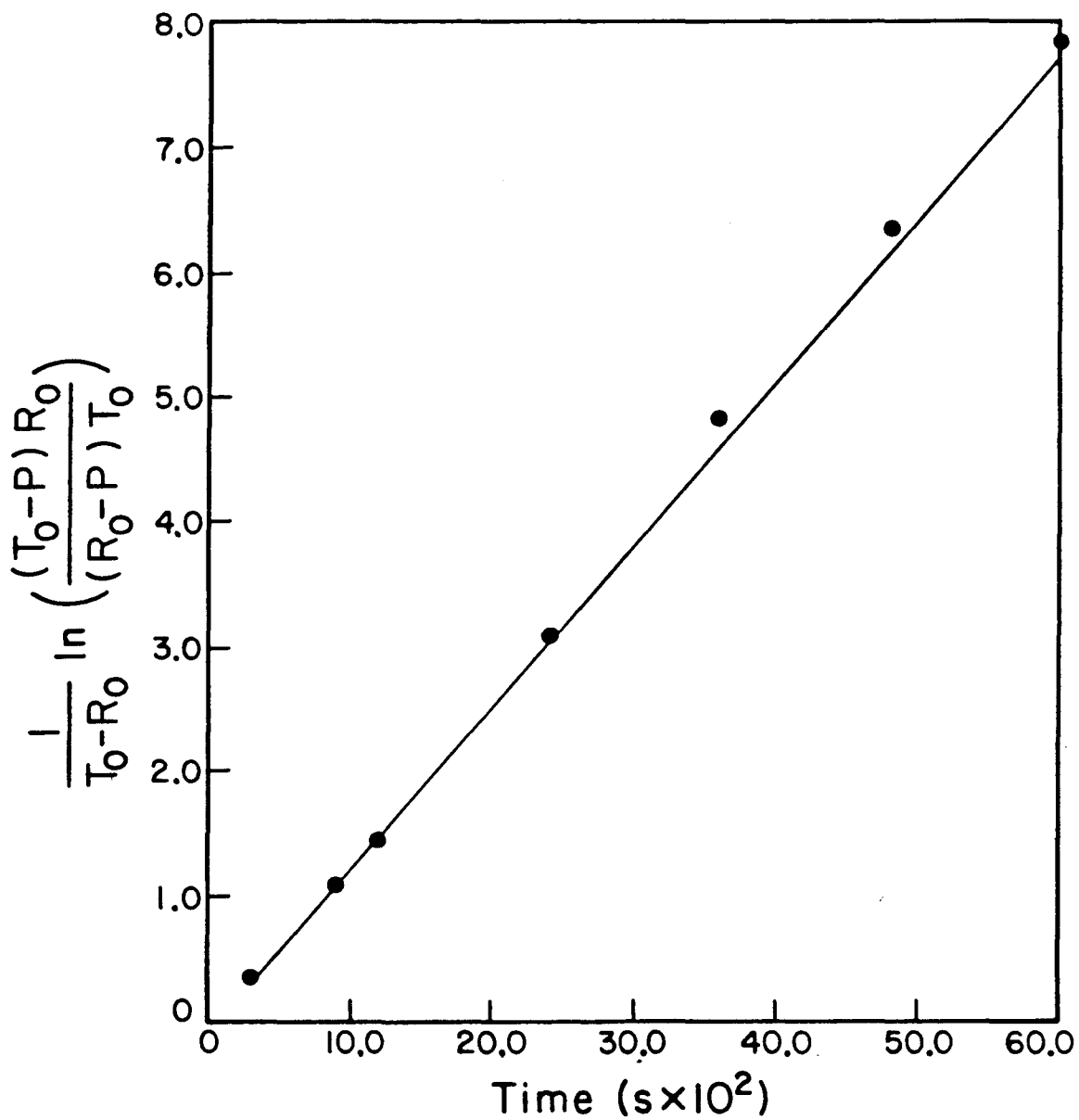
Graph 1c: Second Order plot for the reaction of 1 with 1.1 eq of diphenylacetylene and 2.5 eq of neohexene. The graph is linear. Rho = 0.998.
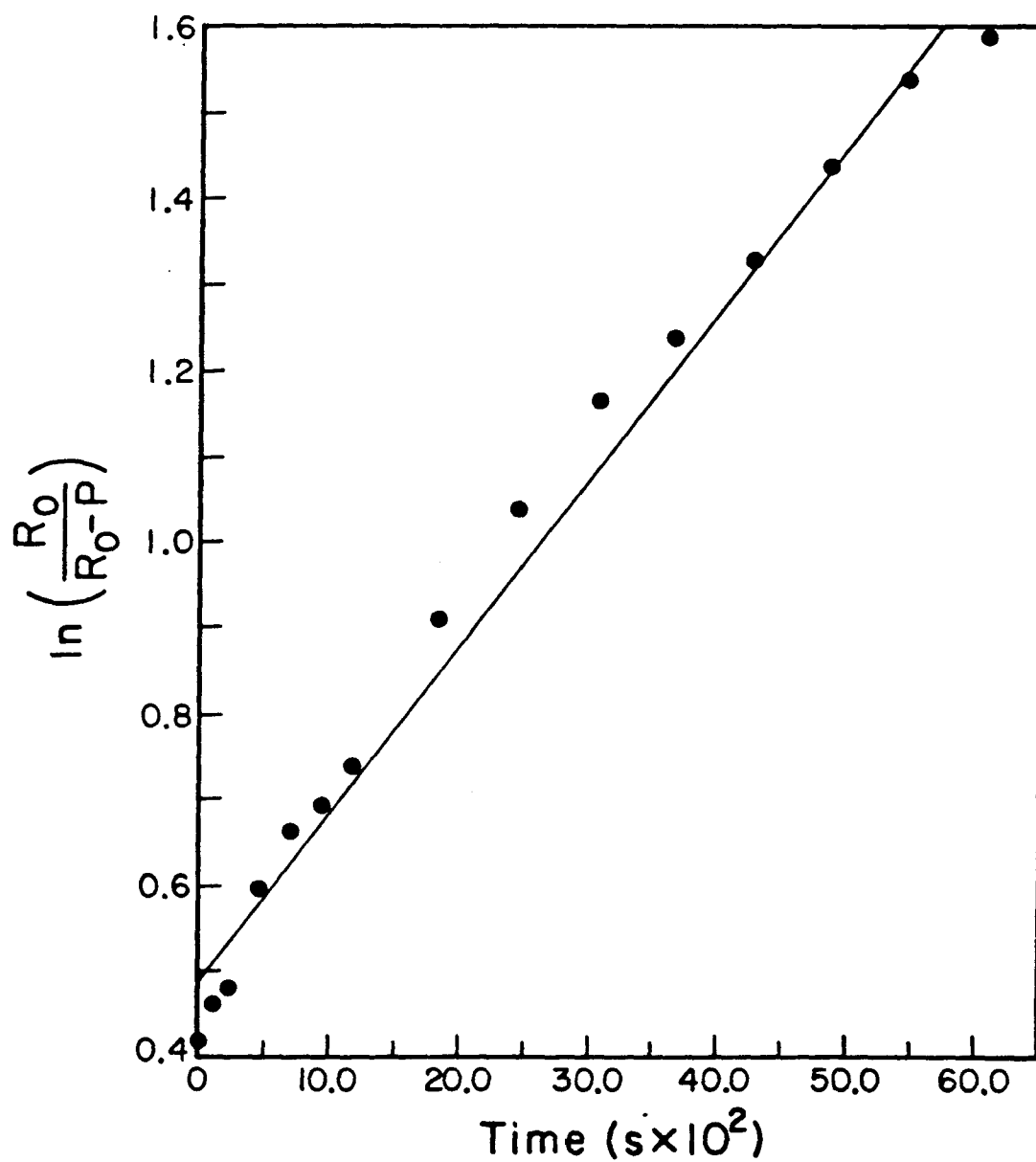
Graph 2a: First Order plot for the reaction of **3** with 1.1 eq of diphenylacetylene. The graph curves down. Rho = 0.993, Standard Deviation $y = 0.047$.
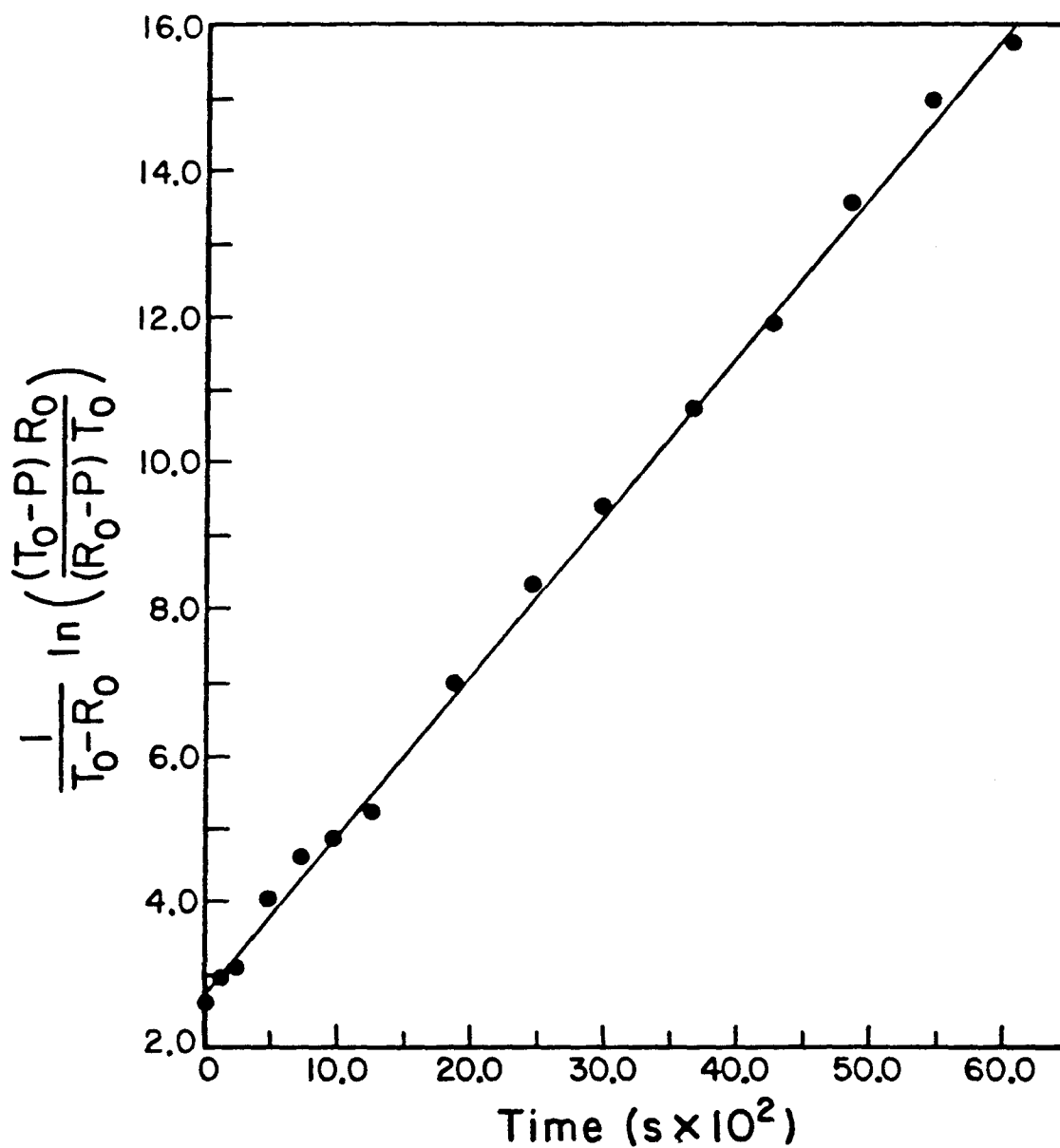
Graph 2b: Second Order plot for the reaction of 3 with 1.1 eq of diphenylacetylene. The graph is linear. Rho=0.998, Standard Deviation $y = 0.257$.
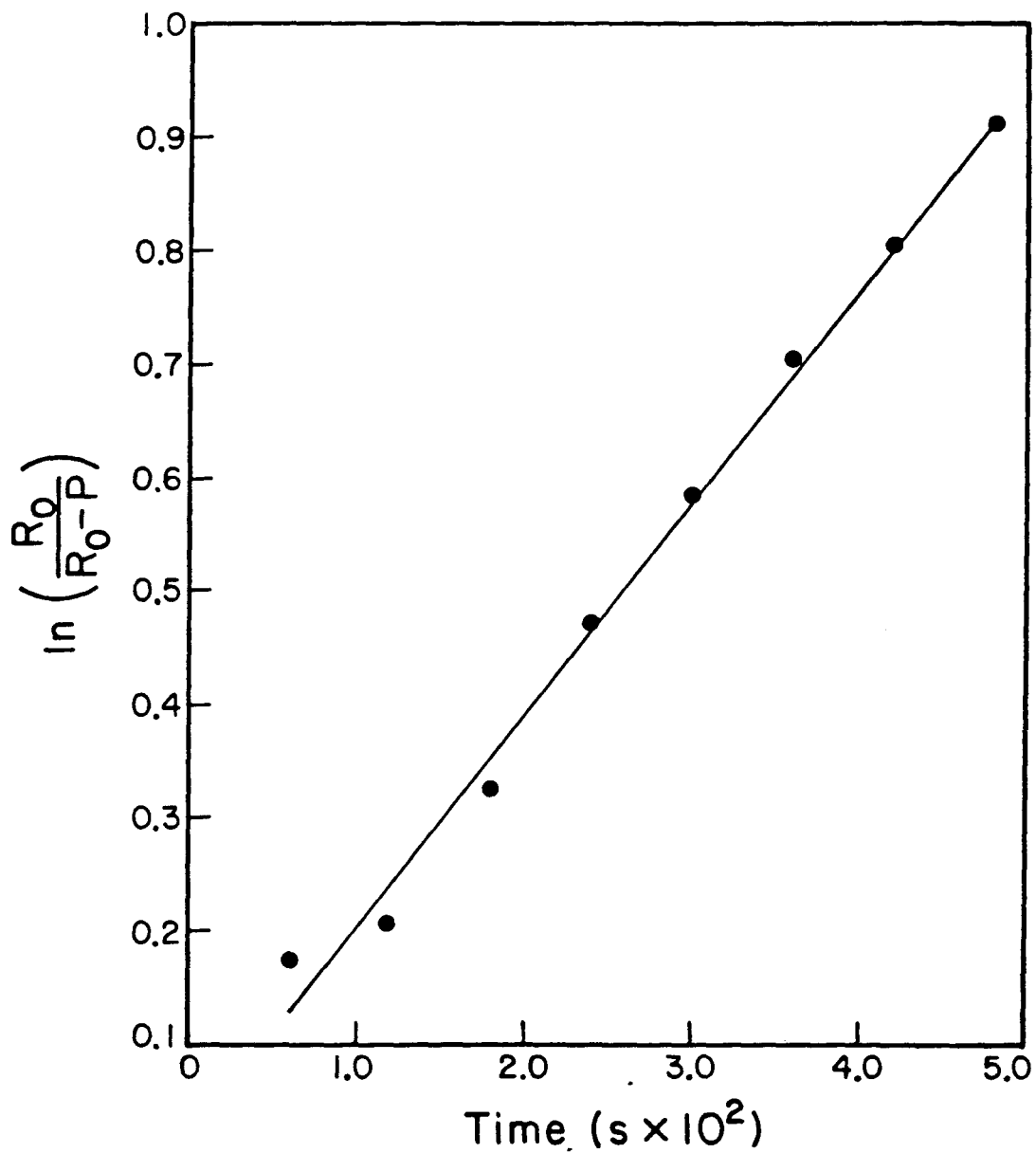
Graph 2c: First Order plot for the reaction of **3** with **8** eq of diphenylacetylene. The graph is linear. Rho = 0.995, Standard Deviation $y = 0.0169$.
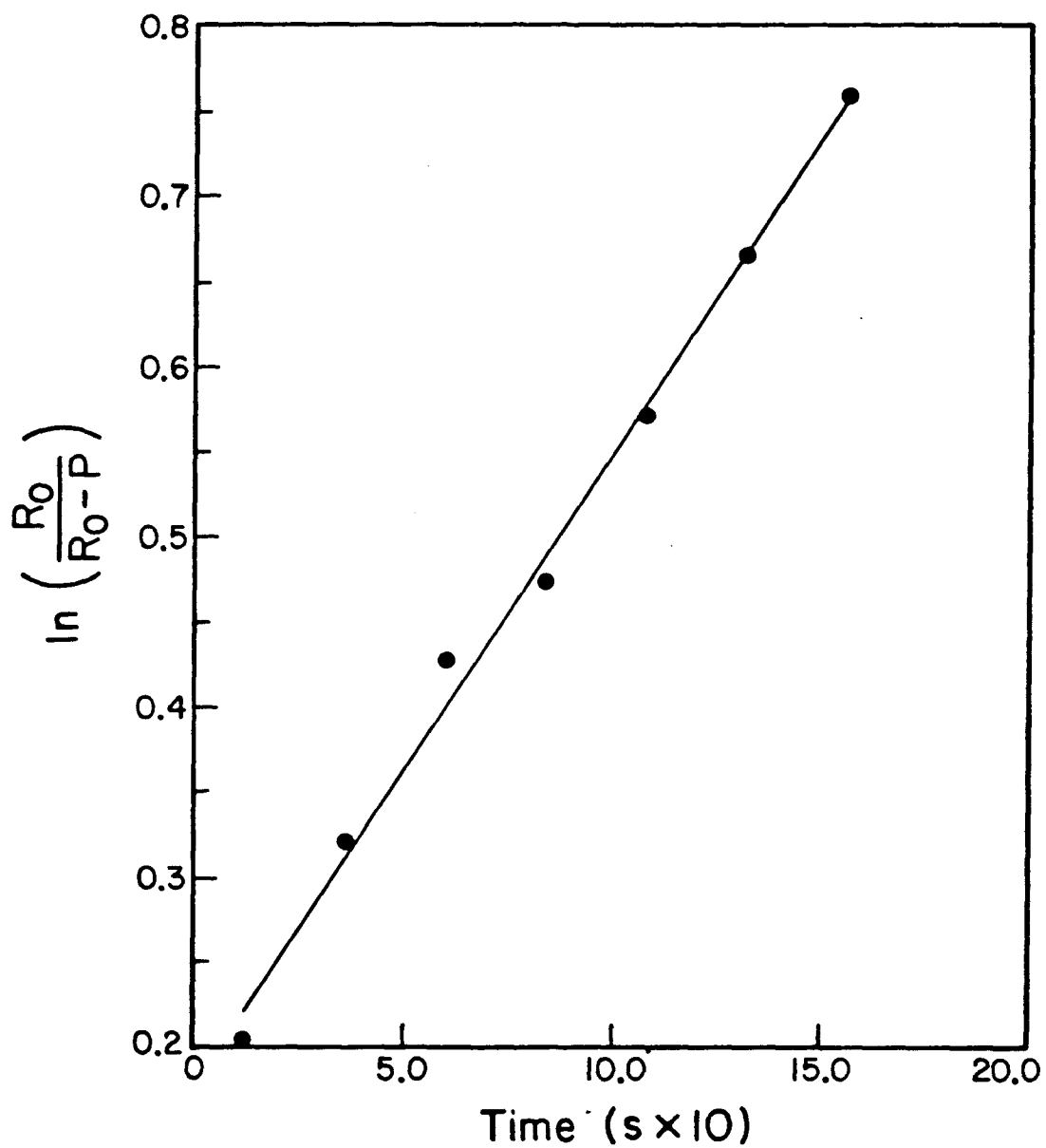
Graph 2d: First Order plot for the reaction of **3** with 1.1 eq of dimethylacetylene. The graph is linear. Rho = 0.997, Standard Deviation $y = 0.0172$.

reaction displays second order behavior and is slower (the rate dropped by 30 percent). This is due to the terms in the denominator of the rate expressions becoming closer in value since the olefin concentration has been increased. Conversely, the reaction of 3 with diphenyacetylene is first order and faster if a large excess of diphenylacetylene is used (Graph 2c). Now the trap term in the denominator of the kinetic expressions for mechanisms 1, 2 and 3 is much larger than the olefin term. The same effect can be achieved by using a better acetylene trap for 3. If 2-butyne is used as the acetylene trap (Graph 2d), then the reaction is first order in 3. Now the rate constants of the trap term are so large that the olefin cannot compete for the reactive intermediate.

These studies have shown the delicate balance between reaction orders in the titanocene metallacycle systems. The reaction order is determined by a competition between the free olefin released and the trapping reagent for the reactive intermediate. This competition can be manipulated easily by changing traps or trap concentrations and therefore changing reaction orders. The rate of reaction of olefins versus acetylenes for the reactive intermediate are, therefore, comparable.

It must be emphasized that the conclusion of first or second order behavior is based on whether the graphs *better fit* a first or second order logarithm. The reactions really are between first and second order behavior since it would be unlikely that the olefin reaction terms were exactly equal to zero (pure first order behavior) or the olefin and trap terms were exactly equal to one another (pure second order behavior).

B. Saturation Behavior

Mechanisms 1, 2 and 3 predict a pseudo first order rate constant that approaches k_1 as the concentration of the trap increases, whereas mechanism 4 does not. Mechanism 4 would not saturate because there is no trap term in the denominator of the kinetic expression and, therefore, the reaction cannot reduce to first order. In order to test for this behavior and also to determine the k_1 values for different metallacycles, the reactions were monitored under saturation conditions.

In all metallacycles studied, the rate determining step in the reaction of the metallacycle with a trap at high concentration is the formation of a reactive titanocene methylidene intermediate. All of the metallacycles studied show saturation behavior at high trapping concentrations. This behavior is predicted by mechanisms 1, 2 and 3. In these three mechanisms, as the trapping term becomes large compared to the olefin term in the denominators, all of the expressions reduce to first order in metallacycle and give a rate which is independent of trap concentration.

Graphs 3 and 4 show saturation behavior on metallacycles 2 and 3 with three different traps: neohexene, 2-butyne and diphenylacetylene. The more efficient trapping agent shows more rapid approach to saturation as predicted by all three mechanistic schemes. The better trapping agent competes more effectively than the olefin at a lower trapping agent concentration. All the traps saturate to the same level as predicted above. The trapping ability of the acetylene increases with the electron richness of the triple bond and decreases with increasing size of the R groups. Error bars are excluded on
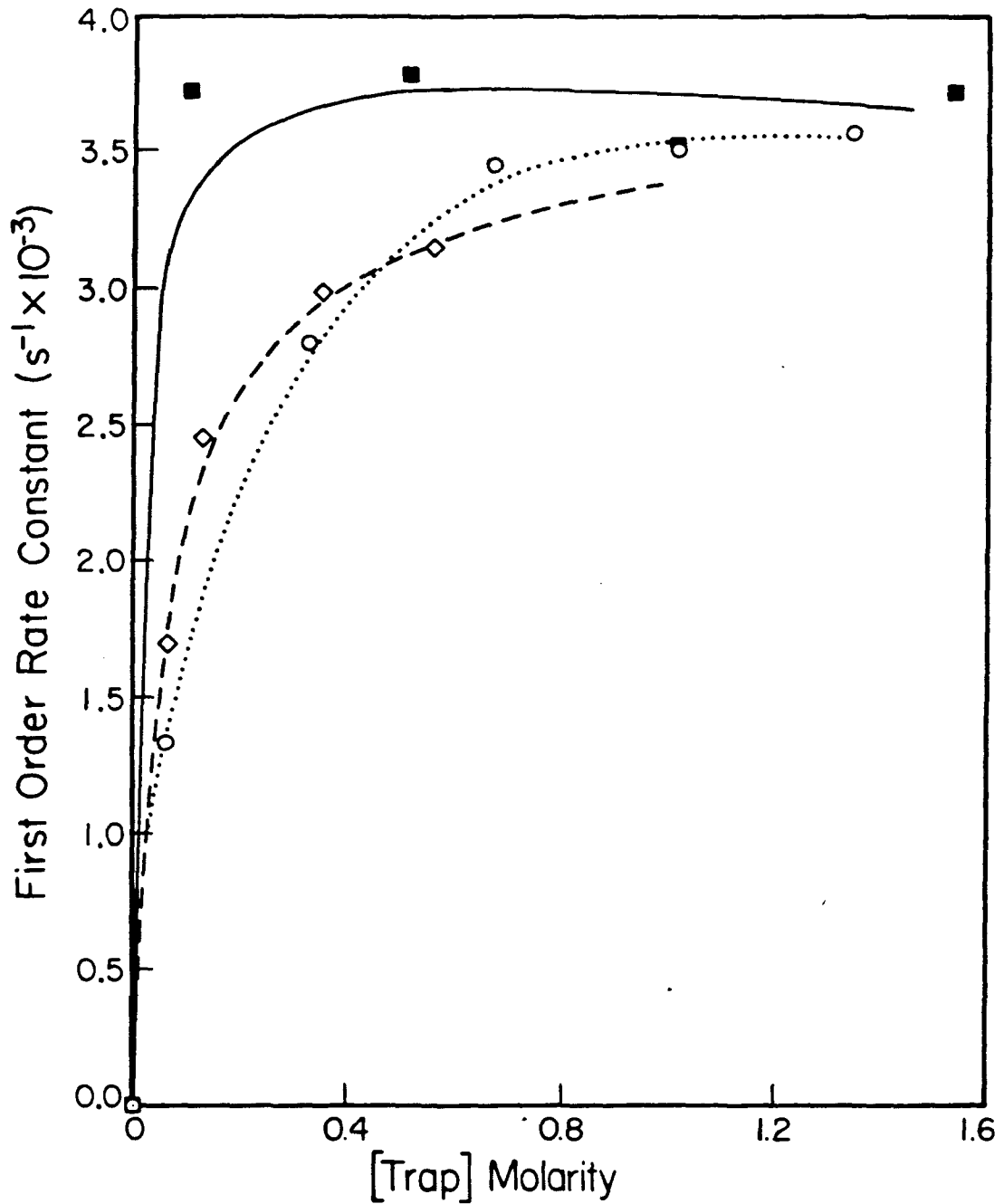
Graph 3: Saturation kinetics on 0.1 M 2 with ■ = diphenylacetylene, ◇ = dimethylacetylene, and ○ = neohexene.
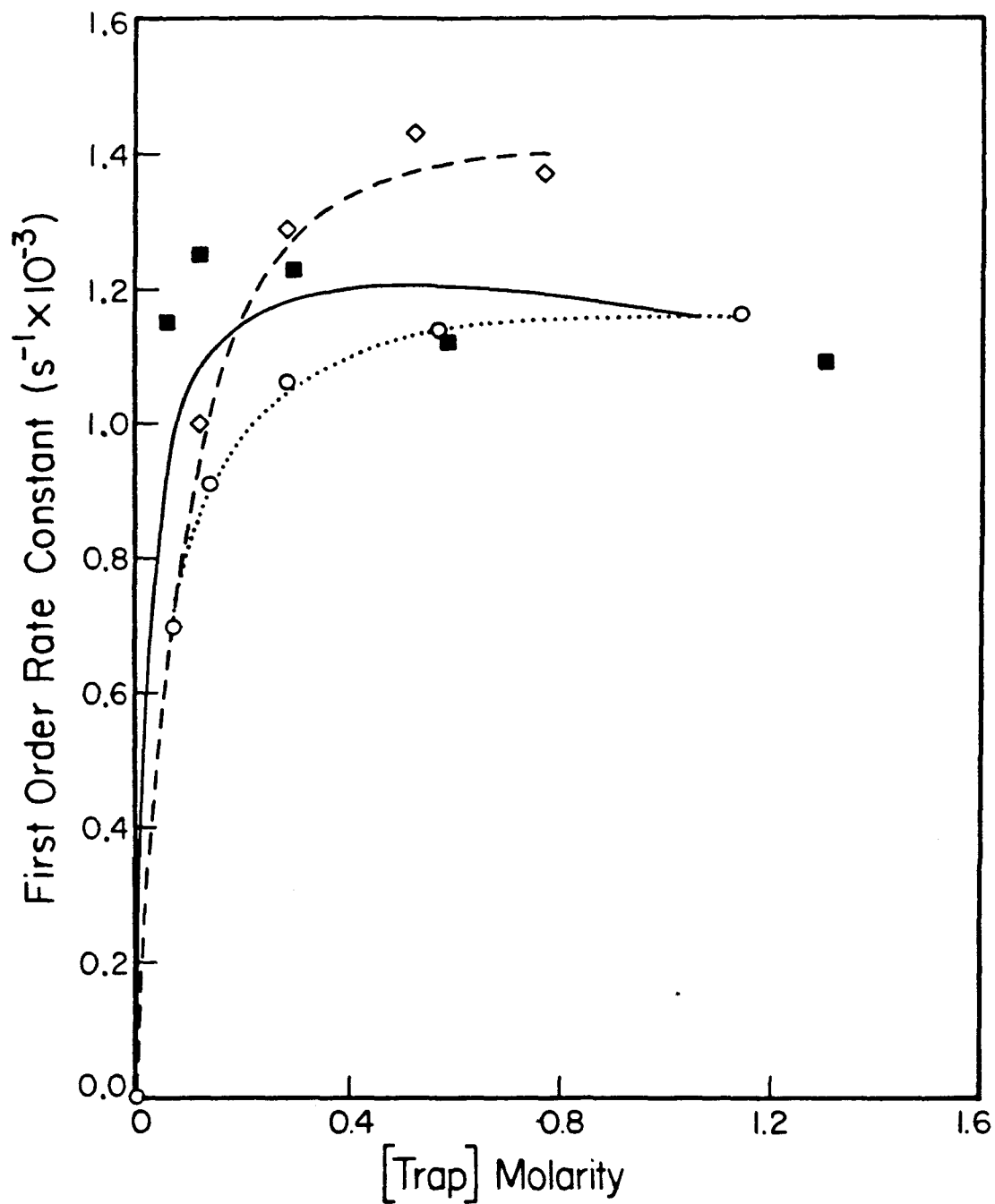
Graph 4: Saturation kinetics on 0.1 M 3 with ■ = dimethylacetylene, ◇ = diphenylacetylene and ○ = neohexene.

these graphs for clarity but would be plus or minus 10 percent. Metallacycles 1, 2, 3, 5 and 6 have all been studied under saturation conditions. Graph 3 represents a typical case. Graph 4 shows the worst case.

Mechanism 4[19] could saturate at high trap concentrations analogous to Michaelis-Menton Enzyme kinetics.[20] In order for this to be true, however, the rate determining step would have to be dissociation of the metallacycle-olefin complex. This would mean that at the point of saturation, the concentration of this complex would be substantial and detectable. No intermediates are ever seen when following these reactions by ^{1}H NMR.

There is another argument against this alternative. If the incoming trap induces cleavage of the metallacycle by prior coordination, each trap should do this at a different rate. Each trapping reagent would show saturation behavior with the metallacycles to a different rate determining k_1. Graphs 3 and 4 show this not to be the case. Therefore, prior coordination of the olefin is rejected.

In summary, these studies show that the olefin term in the denominator can be ignored at high trap concentrations, reducing the reaction order to first order. This also shows that the rate determining step is metallacycle cleavage and that the trapping rates are orders of magnitude faster. Finally, only mechanisms 1, 2 and 3 are consistent with the data of the last two sections.

C. Phosphine Adduct Kinetics Analogy

Titanocene methylidene phosphine adducts can be synthesized from metallacycles.[16] These adducts also yield metallacycles when reacted with olefins or acetylenes. A study was commenced on these adducts in order to enter the same reaction pathway as the metallacycles via a different route and also because titanocene methylidene phosphine adducts could show similar associative or dissociative reaction pathways as an olefin complex and hence serve as a model for the post rate limiting step in the olefin reaction.

Mechanisms 5, 6, 7 and 8 represent the alternatives for phosphine adduct reactions with trapping reagents (Figure 3). Using ideas presented in sections A and B, mechanisms 6 and 7 would show saturation kinetics and first order kinetics (in phosphine adduct) with high concentration of trap or with very good traps. Mechanisms 5 and 8 would give second order behavior (first order in phosphine adduct and first order in trap) or pseudo first order behavior for high trap concentrations. Mechanism 8, however, would also show inhibition by added phosphine. Graph 5 shows pseudo first order behavior for 8 with several trapping reagents. The lines appear linear when trapping with neohexene and diphenylacetylene. When 3-hexyne and 4-octyne are used as the trapping reagents, the lines appear linear when a trap molarity of 0.5 to 3.2 is used. The reaction order in 3-hexyne and 4-octyne, however, are 0.45 and 0.40, respectively. When a 3-hexyne or 4-octyne concentration of 6.5 and 5.1, respectively, are employed, the graphs appear to be bending down. There are large error bars on these points in Graph 5 since the solution is three quarters acetylene, and the ^{1}H NMR integration of the product and reactant

Figure 3:   Proposed phosphine adduct mechanisms.

Legend

$R = Cp_2Ti{=}CH_2$ ← PMe_3 $T = R'C{\equiv}CR'$

$O = PMe_3$ $P = Cp_2Ti$⟨◇⟩$-R$, R

Mechanism 5

$Cp_2Ti{=}CH_2$ ← PMe_3 $\xrightarrow[k_1]{R'C{\equiv}CR'}$ Cp_2Ti⟨◇⟩$-R$, R + PMe_3
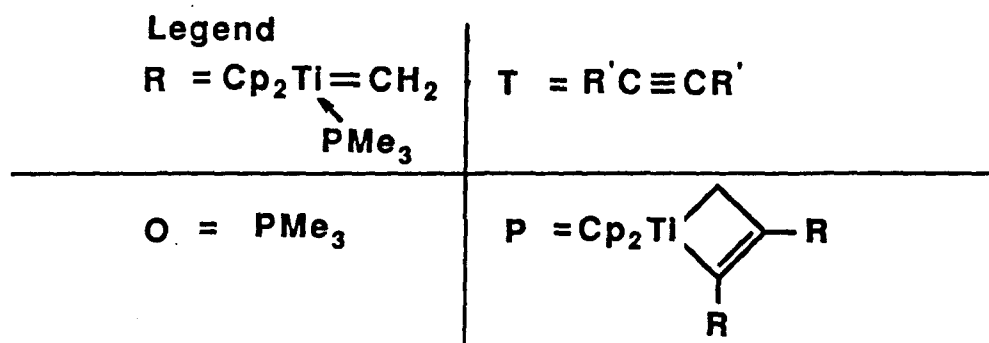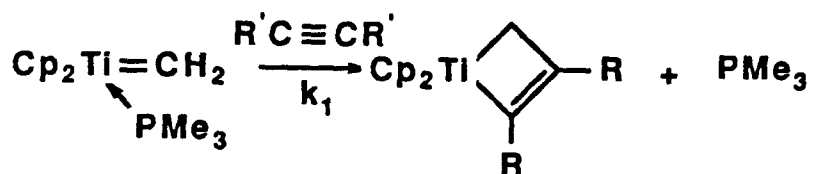
Kinetic Expression

$$\frac{d[P]}{dt} = k_1[R][T]$$

Mechanism 6

$Cp_2Ti{=}CH_2$ ← PMe_3 $\underset{k_{-1}}{\overset{k_1}{\rightleftharpoons}}$ $Cp_2Ti{=}CH_2$ + $PMe3$ $\xrightarrow[k_2]{R'C{\equiv}CR'}$ Cp_2Ti⟨◇⟩$-R$, R

Kinetic Expression

$$\frac{d[P]}{dt} = \frac{k_1 k_2[R][T]}{k_{-1}[O] + k_2[T]}$$

Mechanism 7

$$Cp_2Ti = CH_2 \underset{k_{-1}}{\overset{k_1}{\rightleftharpoons}} Cp_2Ti = CH_2 + PMe_3$$

with PMe₃ coordinated to the left Cp₂Ti=CH₂.

$$k_{-2} \uparrow\downarrow \quad k_2 R'C \equiv CR'$$

$$Cp_2Ti = CH_2$$

Kinetic Expression

$$R'C \equiv CR' \xrightarrow{k_3} Cp_2Ti$$

forming the titanacyclobutene ring with substituents R, R.
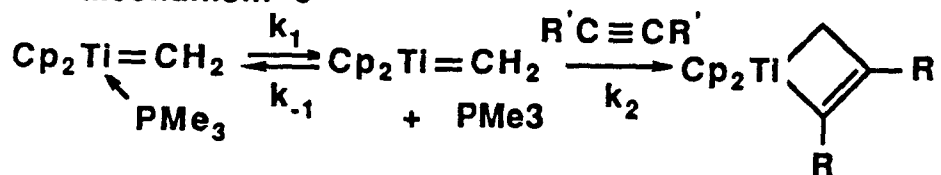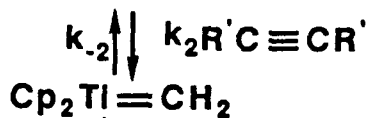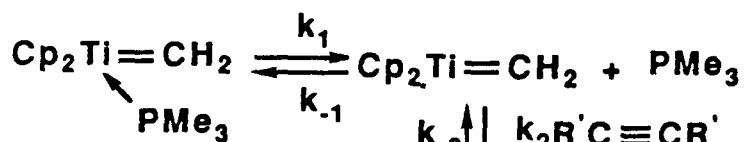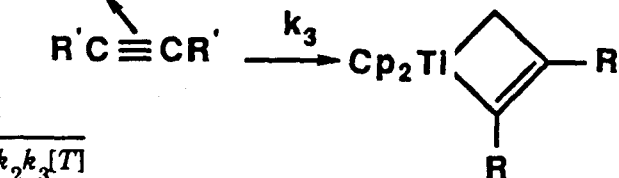
$$\frac{d[P]}{dt} = \frac{k_1 k_2 k_3 [R][T]}{(k_{-2} + k_3)k_{-1}[O] + k_2 k_3 [T]}$$

Mechanism 8

$$k_1 R'C \equiv CR'$$

$$Cp_2Ti = CH_2 \underset{k_{-1}}{\overset{}{\rightleftharpoons}} Cp_2Ti = CH_2 + PMe_3$$

with PMe₃ coordinated to the left Cp₂Ti=CH₂ and R'C≡CR' on the right.

$$\downarrow k_2$$

Kinetic Expression

$$\frac{d[P]}{dt} = \frac{k_1 k_2 [R][T]}{k_{-1}[O] + k_2}$$

$$Cp_2Ti \text{ forming titanacyclobutene with substituents } R, R$$
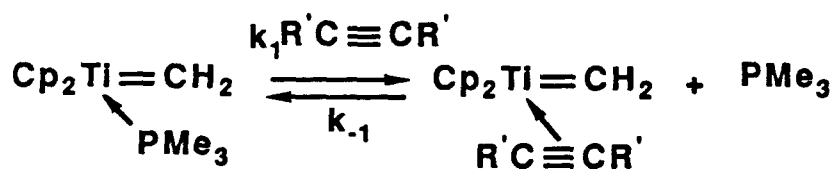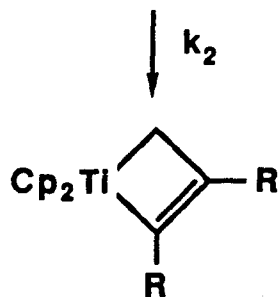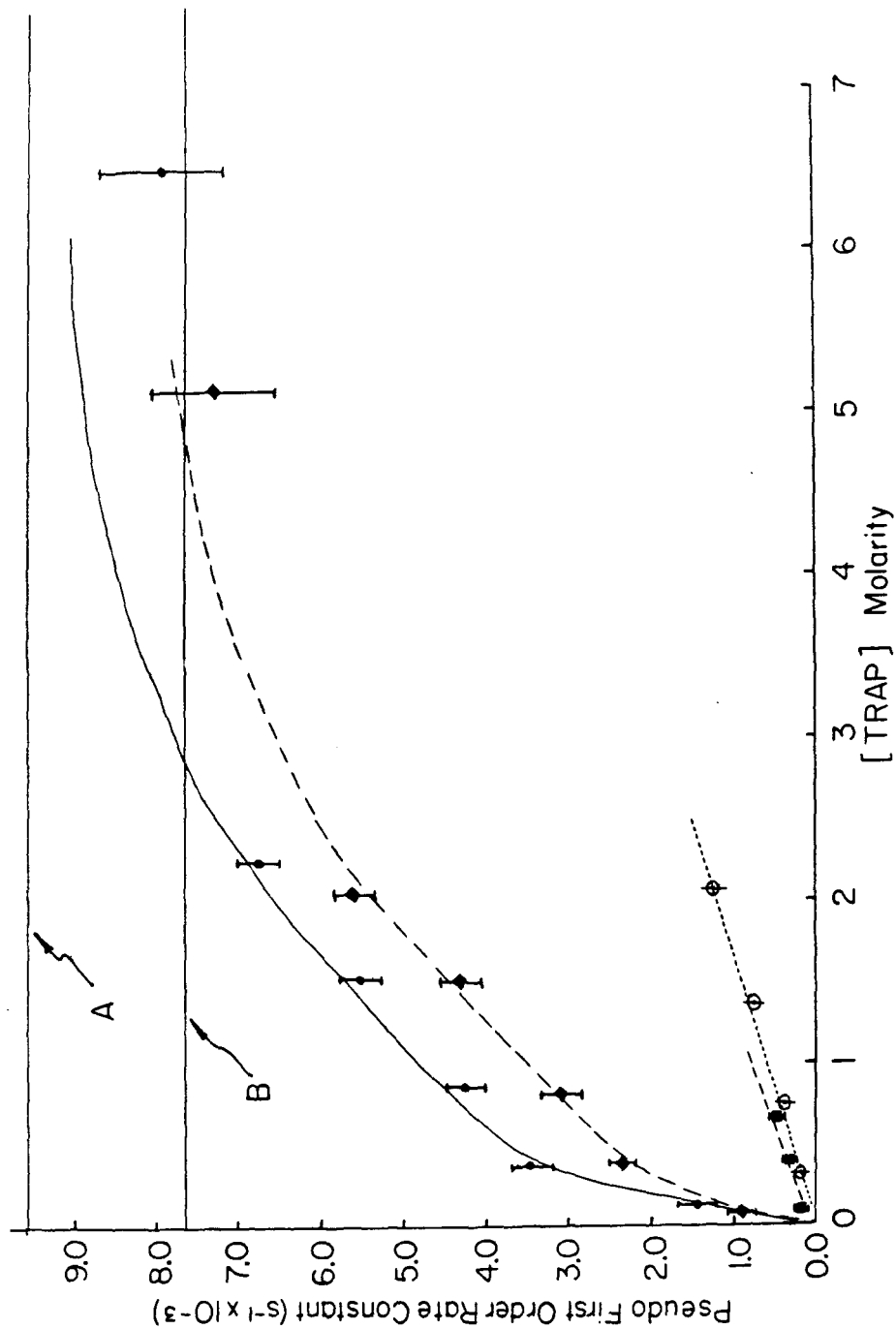
Graph 5: Pseudo first order kinetics on 0.1 M 8 with ◆=4-octyne, ⬟ =3-hexyne, ■=diphenylacetylene and O=neohexene.

cyclopentadienyl resonances have large errors. All attempts at performing the reactions in neat acetylene failed due to the low signal to noise of the ^{1}H NMR resonances of the cyclopentadienyl resonances of the product and reactant. It appears that saturation behavior is observed, but the rate of reaction of 8 with acetylenes has not yet reached a rate limiting k_1 value even at a 72 fold excess of 3-hexyne. To test for saturation behavior, two experiments were performed.

In order to not have reached a saturation level, the back reaction of phosphine with free methylidene in mechanisms 6 and 7 must be so great that the [O] term in the kinetic expressions outweighs the other term in the denominator, even at very high trap concentrations. Thus, the kinetic expressions would never reduce to first order behavior. The first test of this possibility was to measure the relative trapping abilities of trimethylphosphine versus 3-hexyne. This was done by adding trimethylphosphine and 3-hexyne to a solution of Tebbe's reagent. There was immediate formation of the phosphine adduct and metallacyclobutene. The reaction of the phosphine adduct to metallacyclobutene was then followed by NMR. The kinetics were then extrapolated back to time zero to determine the initial ratio of phosphine adduct and metallacyclobutene. It was found to be 10.9. This yields the relative trapping abilities. A calculation was then performed to determine the extent of saturation that should be present when the trap is in a 25 fold excess (as with 3-hexyne, Graph 6), and the trapping rate constant by phosphine is 10.9 times that of the acetylene. The result is approximately 70%. (See Experimental section for details.) Since at a 25 fold excess of 3-hexyne, the rate is predicted to be 70% of the saturated rate, one

can calculate the rate limiting k_1 value. It was found to be $9.64 \cdot 10^{-3} s^{-1}$. This rate limiting k_1 value is displayed in Graph 5 as line A.

A second experiment to determine the predicted rate limiting k_1 value was performed. The reciprocal of the kinetic expression for mechanism 6 is given in equation A.

$$\frac{1}{k_{obs}} = \left(\frac{k_{-1}[O]}{k_1 k_2 [T]} + \frac{1}{k_1} \right) \frac{1}{[R]} \qquad \text{eq. A}$$

When one monitors the kinetics of several reactions of 8 with varying ratios of a large concentration of both 3-hexyne and trimethylphosphine, a plot of $1/k_{obs}$ versus [O]/[T] yields an intercept of $1/k_1$ and a slope of $k_{-1}/k_1 k_2$. The results are displayed in Graph 6. The k_1 value was found to be $7.58 \cdot 10^{-3} s^{-1}$. This rate limiting k_1 value is displayed in Graph 5 as line B. the k_{-1}/k_2 ratio was found to be 6.7. Thus, we conclude that Graph 5 displays saturation behavior for the reaction of 8 with 3-hexyne and 4-octyne. This narrows the mechanistic possibilities to mechanisms 6 and 7 in Figure 3. The titanocene methylidene phosphine adducts react by a rate limiting dissociation of phosphine to yield uncoordinated titanocene methylidene. The titanocene methylidene then reacts with acetylenes or olefins by either forming an adduct which closes to product (mechanism 6) or by a concerted closure (mechanism 7). In support of a rate limiting loss of phosphine, an Eyring plot for the reaction of 8 with diphenylacetylene yields an $\Delta H^{\ddagger}$ of 26.5 kcal/mol and an $\Delta S^{\ddagger}$ of 15.3 e.u.

In order to further probe the mechanism of ligand exchange in titanocene methylidene adducts, the kinetics of equilibration of two different phosphine adducts was studied. Two possible mechanisms are presented in Figure 4.
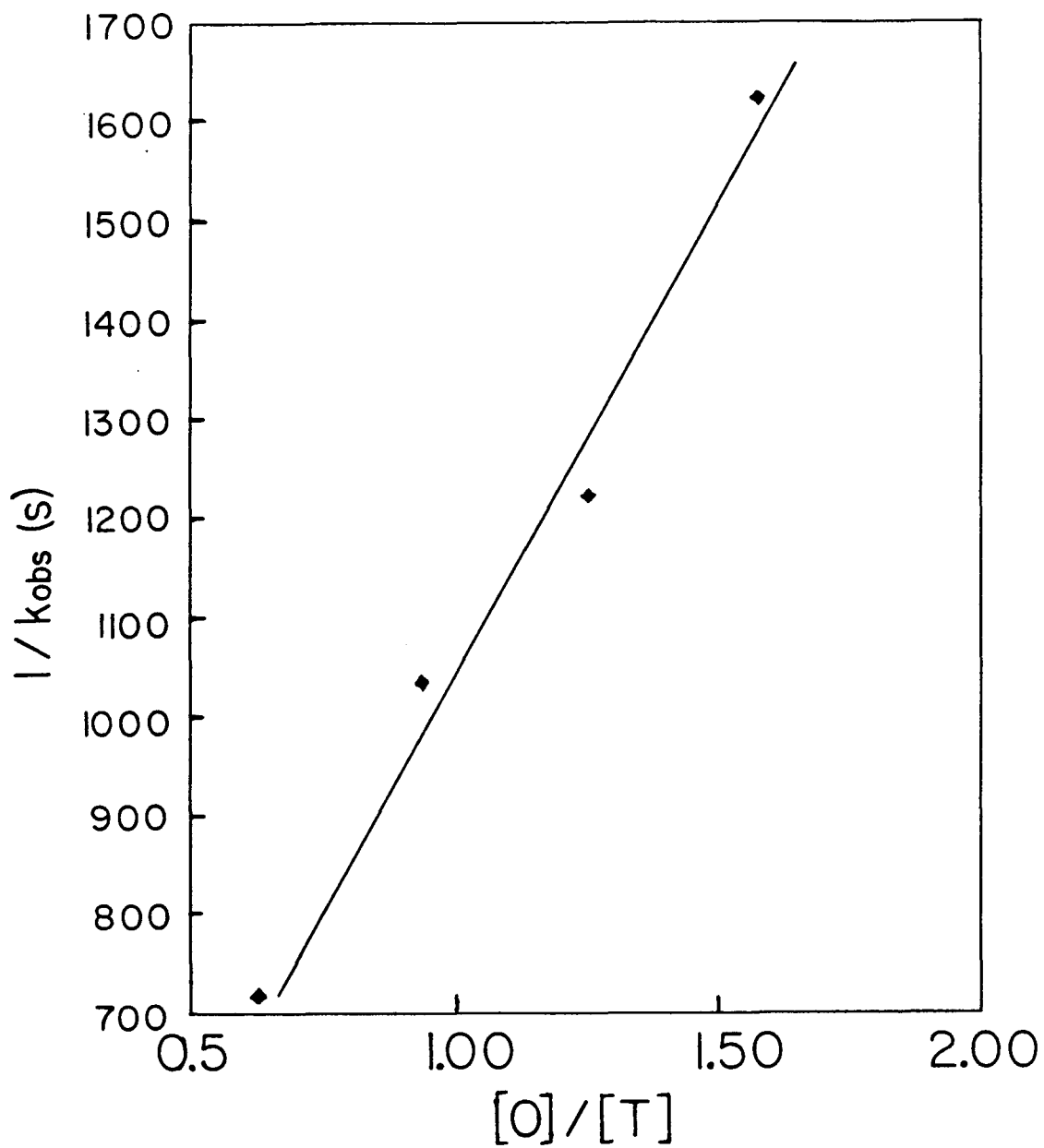
Graph 6: $1/k_{obs}$ versus [O]/[T] for the reaction of **8** and 3-hexyne. Rho = 0.992.

Figure 5: Mechanisms for phosphine equilibration.
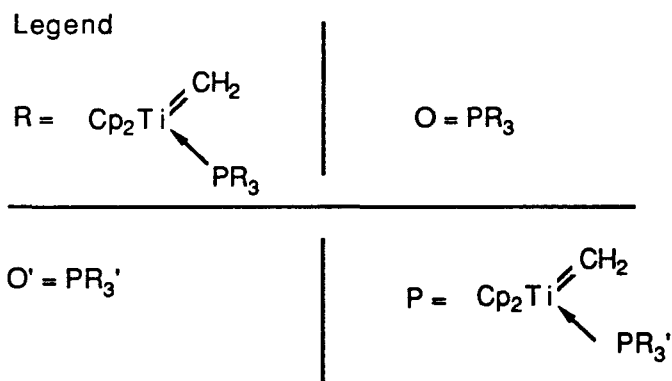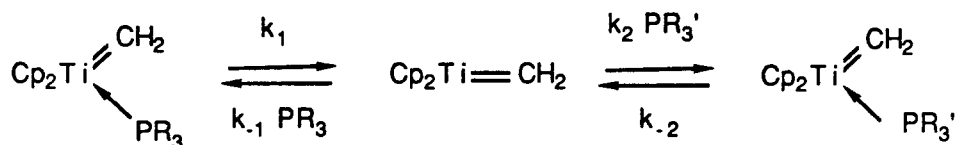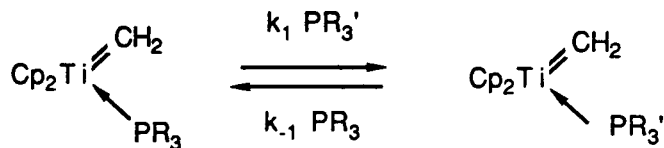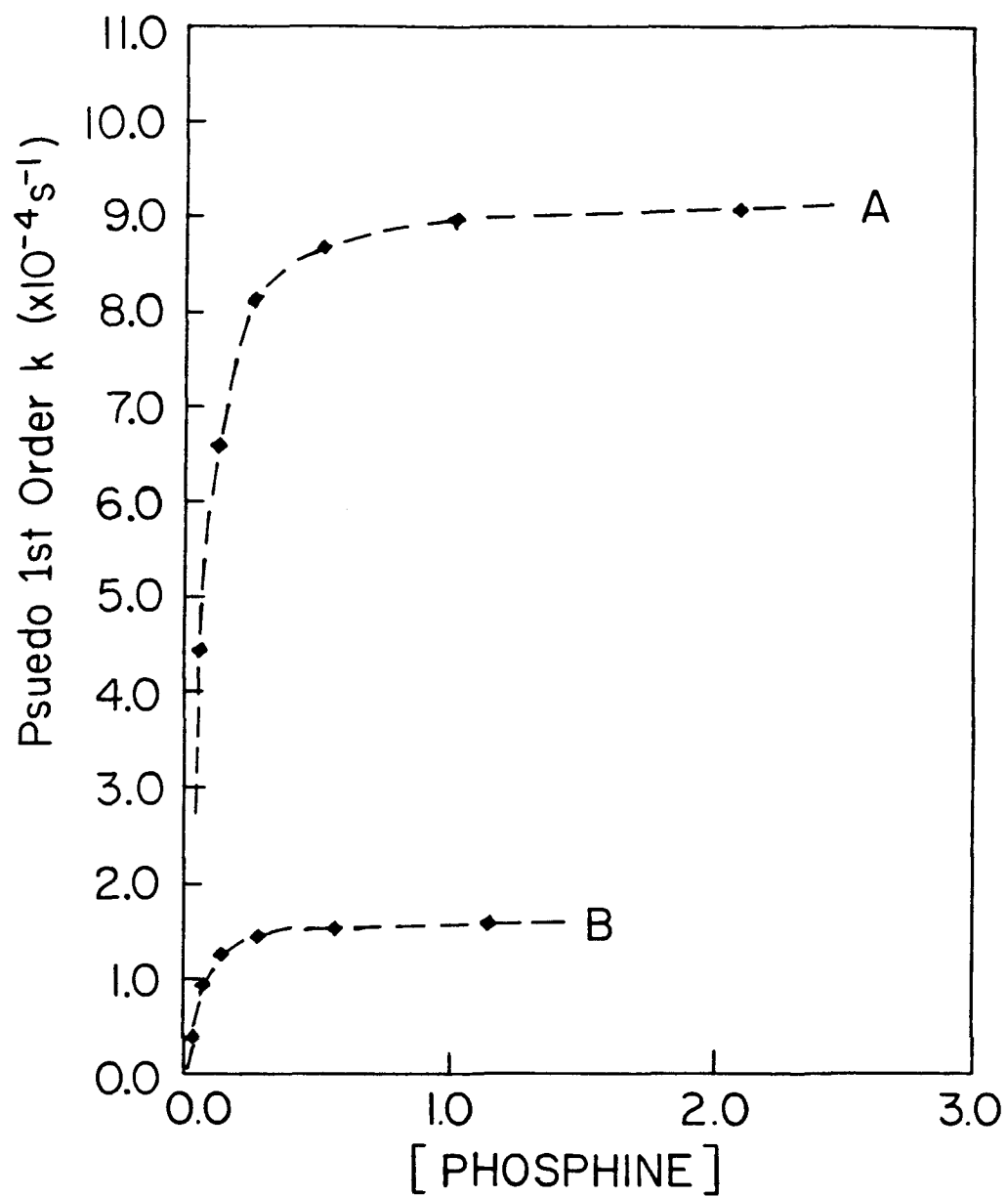
Graph 7: A) Saturation kinetics on **9** with PMe₃, B) Saturation kinetics on **8** with PMe₂Ph.

Mechanism 9 is expected based on the results from the reaction of **8** with acetylenes and olefins. Mechanism 10 would yield first order kinetics in both the titanocene methylidene phosphine adduct and the uncoordinated phosphine. Mechanism 9 would yield very different kinetic behavior. This mechanism would exhibit saturation behavior with a rate limiting k_1 value at high concentrations of added phosphine. In order to distinguish these two mechanistic possibilities, the kinetics of the reaction of **8** with PMe$_2$Ph was determined. Only initial rates of equilibration (first twenty percent of reaction) were measured since the rate to equilibrium slows as equilibrium is approached. In addition, the reaction of Cp$_2$Ti(CH$_2$)PMe$_2$Ph **9** with PMe$_3$ was also studied. The results are shown in Graph 7. The kinetics clearly exhibit saturation behavior at large phosphine concentrations. Thus, the kinetic results are best explained by mechanism 10. The reaction proceeds by a rate determining dissociation of phosphine from the titanocene methylidene phosphine adduct, followed by rapid trapping of titanocene methylidene by phosphine. These results further support mechanisms 6 and 7 in Figure 3. The results also support that the kinetics presented in Graph 5 have not yet reached a saturated level.

Two analogies can be drawn from the phosphine adduct mechanism. First, an acetylene-methylidene complex is possibly involved in the phosphine adduct reaction, and it is conceivable that it is also possibly a viable intermediate in the metallacycle reaction. Secondly, the phosphine adduct is a good model for an acetylene methylidene complex. Although the phosphine complex is a more stable adduct, it could show similar displacement or dissociative reaction pathways. Taking what has been learned from the

phosphine adduct mechanism, still leaves mechanisms 1, 2 and 3 as the viable possibilities for metallacycle cleavage. The key difference between the phosphine-methylidene adduct and the olefin-methylidene adduct is their stability. An olefin-methylidene complex could be so much more unstable that it rapidly dissociates to free olefin and free methylidene before a trap can displace the olefin. This is the key difference between mechanisms 1, 2 and 3. There is also the possibility that an acetylene or an olefin is a poor nucleophile and cannot displace a phosphine. In order for reaction to occur between 8 and an acetylene or an olefin, the phosphine must first dissociate. This does not, however, demonstrate that an olefin cannot displace another olefin in a hypothetical titanocene methylidene olefin adduct (mechanism 2). Mechanisms 1, 2 and 3, however, can be easily differentiated if several methylidene sources are competitively trapped with two different trapping reagents.

D. Competition Trapping

The titanocene methylidene in mechanisms 1 and 3 is independent of the olefin produced by cleavage of the metallacycle. Mechanism 2, however, involves a titanocene methylidene olefin complex. Therefore, if several different methylidene sources are competitively trapped with two different trapping reagents, the ratio of products derived from the two competing traps should be the same in mechanisms 1 and 3 but not necessarily the same for mechanism 2. Mechanism 2 could show a memory of its origin because of the coordinated olefin. To test this possibility, a number of titanocene

methylidene sources that would yield a range of $Cp_2Ti=CH_2 \cdot L$ species were studied by the use of competitive traps.

Table 2 shows several different titanocene methylidene sources, all of which give different trapping ratios with several different traps. Successive experiments showed that the ratios were reproduced within 15 percent of each other. This lends credence to mechanism 2. In addition, the metallacycles give very different trapping ratios than the phosphine adducts, confirming the different reactive intermediates generated from the two species. As shown in the last section, the titanocene methylidene phosphine adducts react via uncoordinated titanocene methylidene. Thus, the competitive trapping ratios for 8 and 9 in Table 2 reflect the relative abilities of the competing traps to react with titanocene methylidene. These competitive trapping ratios are always about twice the values found for the metallacycles. Therefore, the metallacycle reactive intermediate is not uncoordinated titanocene methylidene.

Further analysis of Table 2 uncovers several trends. When competing diphenylacetylene against neohexene, the difference in product ratios derived from several metallacycles are small (case 1). When competing diphenylacetylene against cyclopentene, the differences in product ratios (case 2) become larger. Finally, when competing 4-octyne and diphenylacetylene, the differences are on the order of a factor of 2 (case 3). The different product ratios (for an individual titanocene methylidene source) reflect the different ability of the traps to displace the coordinated olefin or trap the uncoordinated titanocene methylidene source. As the inequivalence between the traps increases, so does the difference in products ratios between

Table 2

Methylidene Source	Case 1	Case 2	Case 3
	PhC≡CPh **vs** (CH₂=CH–C(CH₃)₃ type alkene)	PhC≡CPh **vs** (cyclopentene)	(internal alkyne) **vs** PhC≡CPh
	Cp₂Ti–(cyclobutene)–Ph, Ph	Cp₂Ti–(cyclobutene)–Ph, Ph	Cp₂Ti–(cyclobutene with ethyl groups)
	Cp₂Ti–(cyclobutane with C(CH₃)₃)	Cp₂Ti–(bicyclic)	Cp₂Ti–(cyclobutene)–Ph, Ph
Cp₂Ti–(cyclobutane, gem-dimethyl)	2.2	5.9	9.9
Cp₂Ti–(cyclobutane, methyl/propyl)	2.1	4.8	10.8
Cp₂Ti–(cyclobutane, isopropyl)	1.9	3.8	5.2
Cp₂Ti=CH₂ · PMe₃	2.7	10.2	22.2
Cp₂Ti=CH₂ · PMe₂Ph	2.6	8.6	18.9
Cp₂Ti–(CH₂)–Al(CH₃)₂–Cl	2.8	9.5	22.7

the different titanocene methylidene sources. In case 1, diphenylacetylene and neohexene are equally efficient trapping reagents and, therefore, displace the leaving groups equally well. In cases 2 and 3, one trap is significantly better than the other and, therefore, the difference in product ratios depending on titanocene methylidene source can be observed. In case 3, 4-octyne is a much better trap than diphenylacetylene and, therefore, displaces the most selective (harder to displace) leaving group more efficiently. This is analogous to traditional Sn2 chemistry. A good leaving group reacts less selectively (more statistically) with nucleophiles than a poor leaving group.[21]

The magnitude of the differences between the ratios of products in cases 1, 2 and 3 are small compared to organic Sn2 reactions. Pseudo Sn2 reactions at metal centers have not been extensively studied. There are three possible reasons for this small difference. If the transition state for Sn2 displacement is late along the reaction coordinate, it will not have much character of the leaving group. A second possible explanation is that the mechanism of metallacycle reaction is a combination of mechanisms 2 and 3. In other words, there are two reactive intermediates, both the titanocene methylidene complex and a free titanocene methylidene. To whatever extent the free methylidene exists in solution to react, it would suppress the difference in trapping ratios between different starting reactants. Other studies in our group support this theory. Thirdly, the initial differences in displacement of the metallacycle olefin from the olefin-titanocene methylidene complex by two different traps could be washed out by scrambling of the traps. In other words, the trap-titanocene methylidene complex can react with other traps and, therefore, the initial influence of the metallacycle olefin would be lost. The

product ratio would then more reflect the relative rate of closure of the trap-titanocene methylidene complexes and not the initial rate of displacement of olefin. This dependence on the rate of closure of the trap-titanocene methylidene complex is an outcome of the Curtin Hammett principle.[22]

Besides giving evidence for a different intermediate from several different titanocene methylidene sources, competition kinetics can reveal differences in selectivities of the reactive intermediates. It is intriguing that the metallacycle reaction orders were different from one metallacycle to another. As already explained, this behavior is due to the differential reactivity of the intermediate toward olefin or trapping agent. This competition between olefin and trap should have a temperature dependence. A temperature dependence could reveal differences in $\Delta S^{\ddagger}$ for trapping the reactive intermediate with olefins or acetylenes.

In section A, the behaviors of 1 and 3 were contrasted. In addition, metallacycles 2 and 4 more closely exhibit second order behavior than first order behavior when reacted with diphenylacetylene. In contrast metallacycle 5 more closely exhibits first order behavior than second order.[6] The available data suggest that metallacycles which decompose at higher temperatures show first order behavior, whereas, those which cleave at lower temperatures show second order behavior. In fact, as the temperature is lowered in the reaction of metallacycle 1 with diphenylacetylene, the first order kinetic plots start to curve and begin to suggest second order behavior. Conversely, as the temperature is raised in the reaction of 3 with diphenylacetylene, the curves bend more to resemble first order. In section A, the reaction orders were related to a competition between the olefin (liberated

by the metallacycle) and the trap for the reactive intermediate. Thus, it appears that as the temperature is raised, the olefin becomes a poorer trap relative to an acetylene.

To test this behavior, competition trapping studies of several metallacycles with an olefin and an acetylene trap at different temperatures were commenced. As seen in Graph 8, at high temperature, the acetylene preferentially traps the intermediate. This trend is also observed in competitive trapping studies with phosphine adducts and Tebbe's reagent.[7] The experiments were restricted to diphenylacetylene and neohexene traps since these substrates are roughly equal in trapping ability, and hence, the trends can be uncovered. The data in Graph 8 confirms that at higher temperatures the diphenylacetylene is a better trap than the olefin released.

The neohexene used to compete against diphenylacetylene is not the olefin released from 2, 3 or 4. Therefore, this temperature dependent trend is only applicable to the explanation of observed first or second order kinetics for 2, 3 and 4 if the critical difference between the traps is that one is an alkene and one is an alkyne. It is proposed that the critical difference is in the steric interaction on approach of the trap to the titanocene methylidene. The terminal R groups of an olefin are forced to interact with the cyclopentadienyl ligands as the metallacycle is formed. The alkyne R groups will begin to bend back out of the way of the cyclopentadienyl ligands as the metallacycle is formed. This steric argument is also confirmed by the Rappé calculation.[11] He found that as ethylene approaches the titanium of $Cl_2Ti = CH_2$, the chlorines bent back to avoid the incoming olefin. This steric hindrance should be accentuated in the real system since cyclopentadienyl ligands are
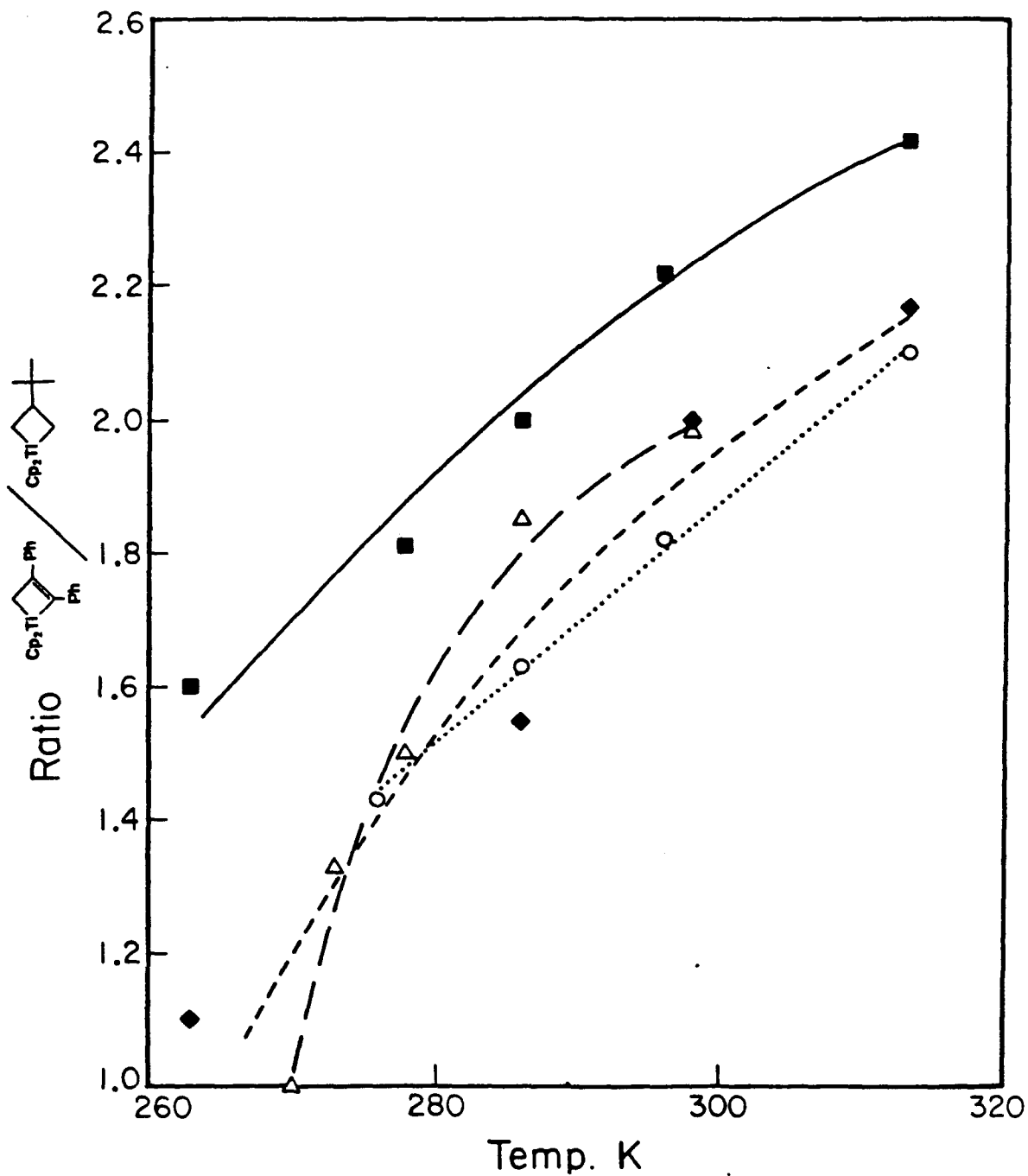
Graph 8: Competition kinetics versus temperature using diphenylacetylene and neohexene as traps. ■ = 7, ◆ = 3, △ = 2, O = 8.

undeniably larger than chlorines, and the olefins all have alkyl or aryl substituents and not just hydrogens. If steric hindrance is taken as contributing to $\Delta S^{\ddagger}$, then $\Delta S^{\ddagger}$ should be more positive for acetylenes than for olefins since their approach to the titanocene moiety is less sterically crowded. Therefore, the temperature dependence can be explained if $\Delta S^{\ddagger}$ is greater for alkynes, and hence, they will be favored over alkenes as the temperature is raised.

In summary, these experiments reveal an image of the transition-state for reaction of titanocene methylidene, with an acetylene being less crowded than reaction with an olefin. This combined with the fact that an acetylene is more electron rich than an alkene and, thus, is a better trapping agent for the electrophilic titanocene methylidene, makes an acetylene an overall better trap electronically and a more entropically favored trap. These experiments also lent further credence to the existence of an olefin titanocene methylidene complex since each titanocene methylidene source gave different product ratios when competitively trapped.

E. Crossover Experiments

In order to test for the existence of a free titanocene methylidene, crossover experiments were performed. If $6\text{-}d_2$ and perprotio 1 are stirred together without any trap for more than one half life of 1, the crossover products perprotio 6 and $1\text{-}d_2$ are observed to an extent of approximately 10%.

If mechanism 2 were rigorously true, no crossover products should be observed. If, however, there is a reactive pathway to free methylidene, crossover products would appear as is observed. Therefore, in the absence of

trapping reagents, there appears to be a pathway to free methylidene. The question then arises if this pathway is significant in the presence of trapping reagents. This question has not been fully answered. A comparison of the scrambling rate to that of the reaction with trap revealed that the scrambling is about 80% slower. Therefore, the free methylidene is being formed at a slower rate than the main reactive intermediate is formed. This evidence shows that there is another reactive intermediate in solution beside free titanocene methylidene. The actual amount of crossover is questionable since any Lewis Base impurity or decompositon of the metallacycles to yield olefin could scramble all the olefins of the proposed olefin titanocene methylidene adducts.
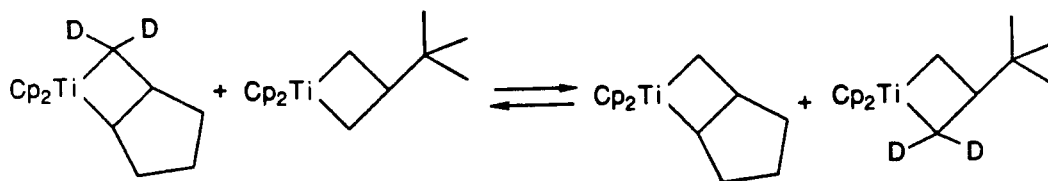
F. Deuterium Isotope Effects.

The past five sections have concentrated on identifying the mechanism of reaction of metallacyclobutanes and phosphine titanocene methylidene adducts. Strong evidence was presented for the role of an olefin-titanocene methylidene adduct in these reactions. To further develop an understanding of the rate determining step of metallacyclobutanes and the bonding in the olefin-titanocene methylidene adduct, the examination of several secondary deuterium isotope effects was done.

There are two possible isotope effects in these systems to study. The first isotope effect studied was on the rate of cleavage of the metallacycles. The second was an intramolecular competitive isotope effect on the direction of cleavage of the metallacycles.

Table 3 summarizes the kinetic deuterium isotope effects on the rate of cleavage of metallacycles 1 and 6 with diphenylacetylene. In both cases, the effect of deuterium substitution on the methylene carbons of the metallacycle decreases the rate of cleavage. When a metallacycle cleaves, the hybridization of the α carbons change from sp^3 to sp^2. A secondary isotope effect of $k_H/k_D \approx 1.2$ was observed and is in the correct range for rehybridization changes of this type.[21] Each isotope effect was repeated two to three times, and the measured values were always within seven percent of each other.

Table 3:   X=H or D

Reactant	Eq. of Trap	k_H/k_D
(Cp$_2$Ti structure, X, X; bicyclic cyclopentane)	1.1	1.30
(Cp$_2$Ti structure, X, X; bicyclic cyclopentane)	8	1.45
(Cp$_2$Ti structure, X, X; cyclobutane with tert-butyl)	1.1	1.23
(Cp$_2$Ti structure, X, X; cyclobutane with tert-butyl)	8	1.17
(Cp$_2$Ti structure, X, X; cyclobutane with tert-butyl, D, D)	1.1	1.26
(Cp$_2$Ti structure, X, X; cyclobutane with tert-butyl, D, D)	8	1.29
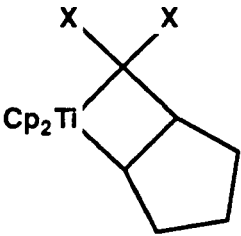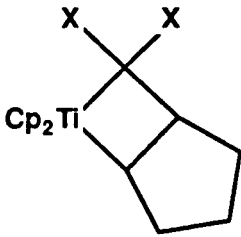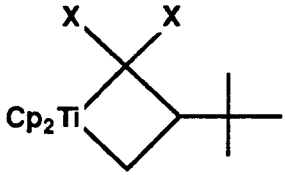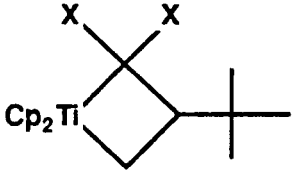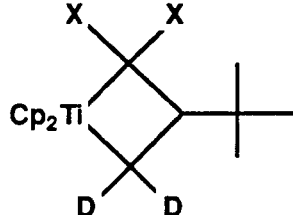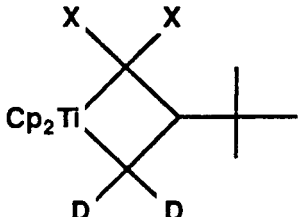
In the case of metallacycle **6**, the isotope effect is due to the deuterated metallacycle going directly to deuterated methylidene. The case of 1-d_2 is a combination of effects. The deuterium can either end up on the olefin or on the methylidene. Finally, in the case of 1-d_4, the effect is due to both carbons changing from a deuterated sp^3 carbon to a deuterated sp^2 carbon. As each α carbon of the metallacycle is deuterated, an isotope effect of approximately 1.2 was observed. Therefore, the zero point energy differences between 1-d_0 and 1-d_2 that lead to the isotope effects are approximately the same difference between 1-d_2 and 1-d_4. In addition, since these isotope effects are independent of trap concentration, the effect is solely in the rate determining cleavage of the metallacycle to the titanocene methylidene and is not reflecting any rate differences in subsequent steps.

When large trapping agent concentrations are used, one can obtain a competitive isotope effect by trapping metallacycle 1-d_2 (Figure 5). This metallacycle can cleave in two directions to give two intermediates, which are immediately trapped due to the high trap concentration. By measuring the deuterium incorporated in the metallacyclobutene product in comparison to the deuterium incorporated in the olefin liberated, the competitive isotope effect is found to be 1.47 favoring deuterium incorporation in the olefin.

An intramolecular secondary effect of 1.47 favoring deuterium incorporation in the olefin is quite large. This effect must be due to a significant zero point energy difference between deuterated methylidene and deuterated olefin in the olefin titanocene methylidene complex. The transition state should resemble the olefin-titanocene methylidene adduct since the reaction is endothermic by approximately 25 kcal/mol, and the
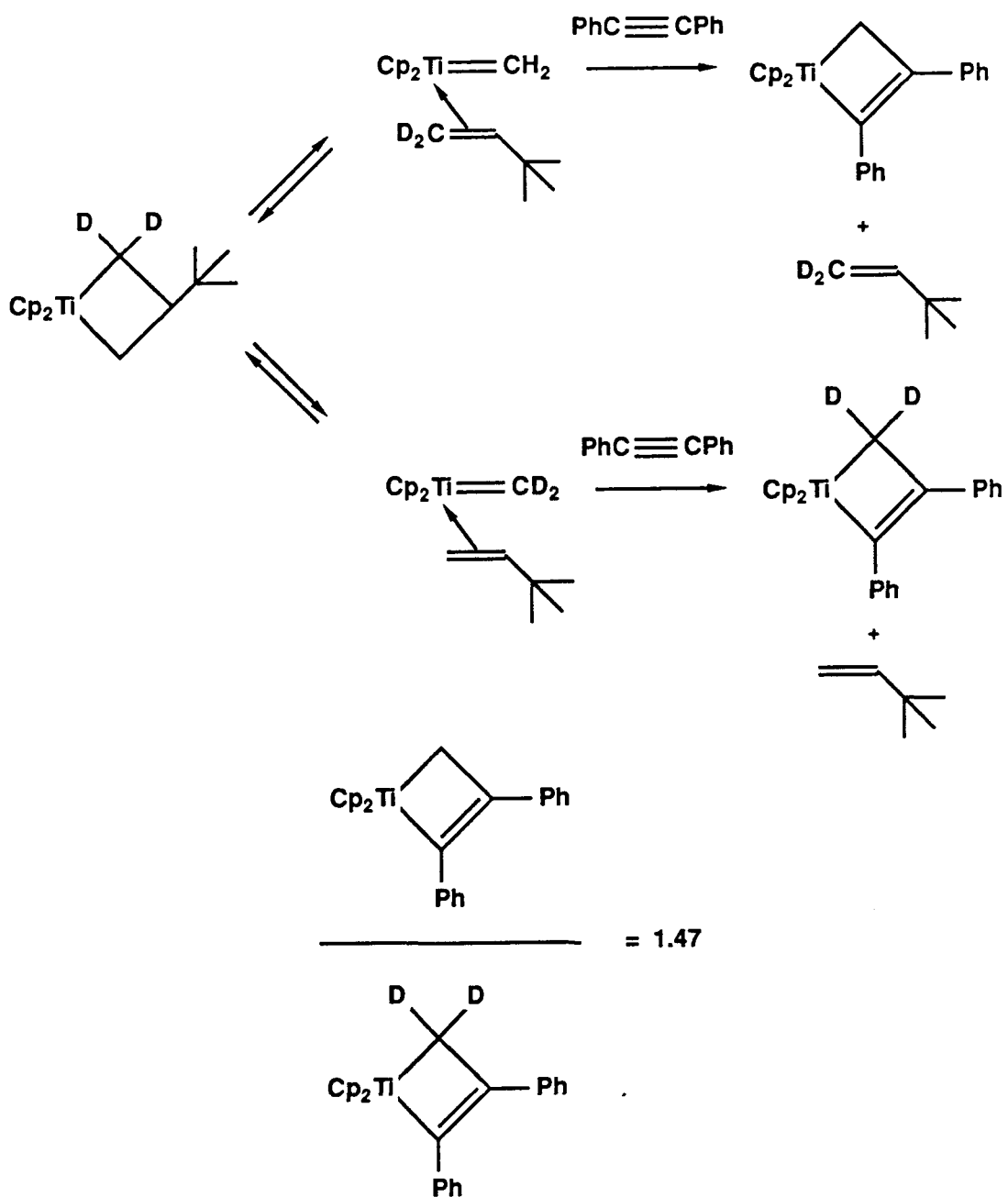
Figure 5: Competitive deuterium isotope effect.

transition state is, therefore, late along the reaction coordinate. This assumption is also predicted by the Rappé calculation, which places the transition state for metallacycle cleavage at almost the same geometry as an olefin-titanocene methylidene complex. Therefore, the competitive isotope effect can be used to gain insight into the bonding of the olefin titanocene methylidene adduct.

The large intramolecular competitive isotope effect of 1.47 is due to the carbon hydrogen bonds of the methylidene carbon being significantly weaker than the carbon hydrogen bonds of the olefin carbon. This effect is the same (within experimental error) as the k_{H_4}/k_{D_4} isotope effect on metallacycle 1 and the k_{H_2}/k_{D_2} effect of metallacycle 6. These results all taken together demonstrate that the majority of the isotope effect stems from the metallacycle α carbons undergoing the most hybridization change when transforming to the methylidene carbon rather than to the olefin carbon. A qualitative energy diagram (Figure 6) shows the relative activation energy differences for the reactions studied.

Separation a gives the activation energy difference between perprotio metallacycle cleavage and dideuterio metallacycle cleavage to yield dideuterio olefin. This should be roughly the same activation energy difference between tetradeuterio metallacycle cleavage and dideuterio metallacycle cleavage to yield dideuterio methylidene (separation c). Finally, the largest separation b is the difference between dideuterio metallacycle placing deuterium on the olefin versus methylidene during cleavage. Activation energy difference b accounts for the intramolecular competitive isotope effect, whereas $a + b$ accounts for the isotope effect on metallacycle 6
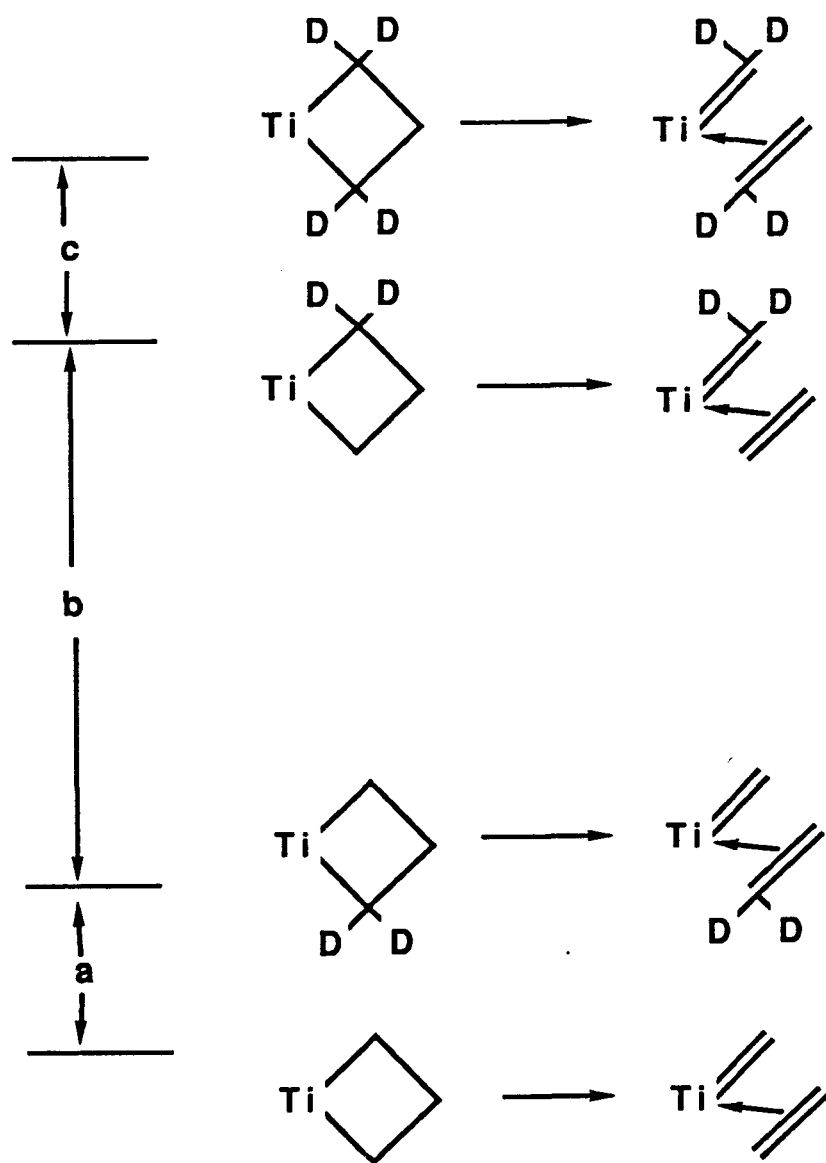
Figure 6: Relative activation energy differences for deuterated metallacycle cleavage: a and c = 6 cm^{-1}, b= 77 cm^{-1}.

and $a+b+c$ accounts for the k_{H_4}/k_{D_4} isotope effect on metallacycle 1. This energy diagram explains the seeming coincidence of three different isotope effects, since a and c are small compared to b.

A potential energy curve which includes the vibrational levels of the protio and deuterio metallacycle is shown in Figure 7. The zero point vibrational energy gaps x, y, and z can be related to the isotope effects in Table 3 and Figure 4 by equations 1, 2 and 3.

$$\frac{D_0}{D_2} = \frac{2e^{-(E_0-2z+x+y)/RT}}{e^{-(E_0-z+y)/RT} + e^{-(E_0-z-x)/RT}} = 1.23 \tag{Eq 1}$$

$$\frac{D_2}{D_4} = \frac{e^{-(E_0+z+y)/RT} + e^{-(E_0-z+x)/RT}}{2e^{-E_0/RT}} = 1.25 \tag{Eq 2}$$

$$\frac{D_0}{D_4} = \frac{e^{-(E_0-2z+x+y)/RT}}{e^{-E_0/RT}} = 1.54 \tag{Eq 3}$$

Simplification yields three equations with three unknowns (Eqs. 1', 2' and 3'). In addition, the competitive isotope effect yields equation 4. The equations are internally consistent but not independent.

$$\frac{e^{(z-y)/RT} + e^{(z-x)/RT}}{e^{(z-y)/RT} e^{(z-x)/RT}} = 1.626 \tag{Eq 1'}$$

$$e^{(z-y)/RT} + e^{(z-x)/RT} = 2.50 \tag{Eq 2'}$$
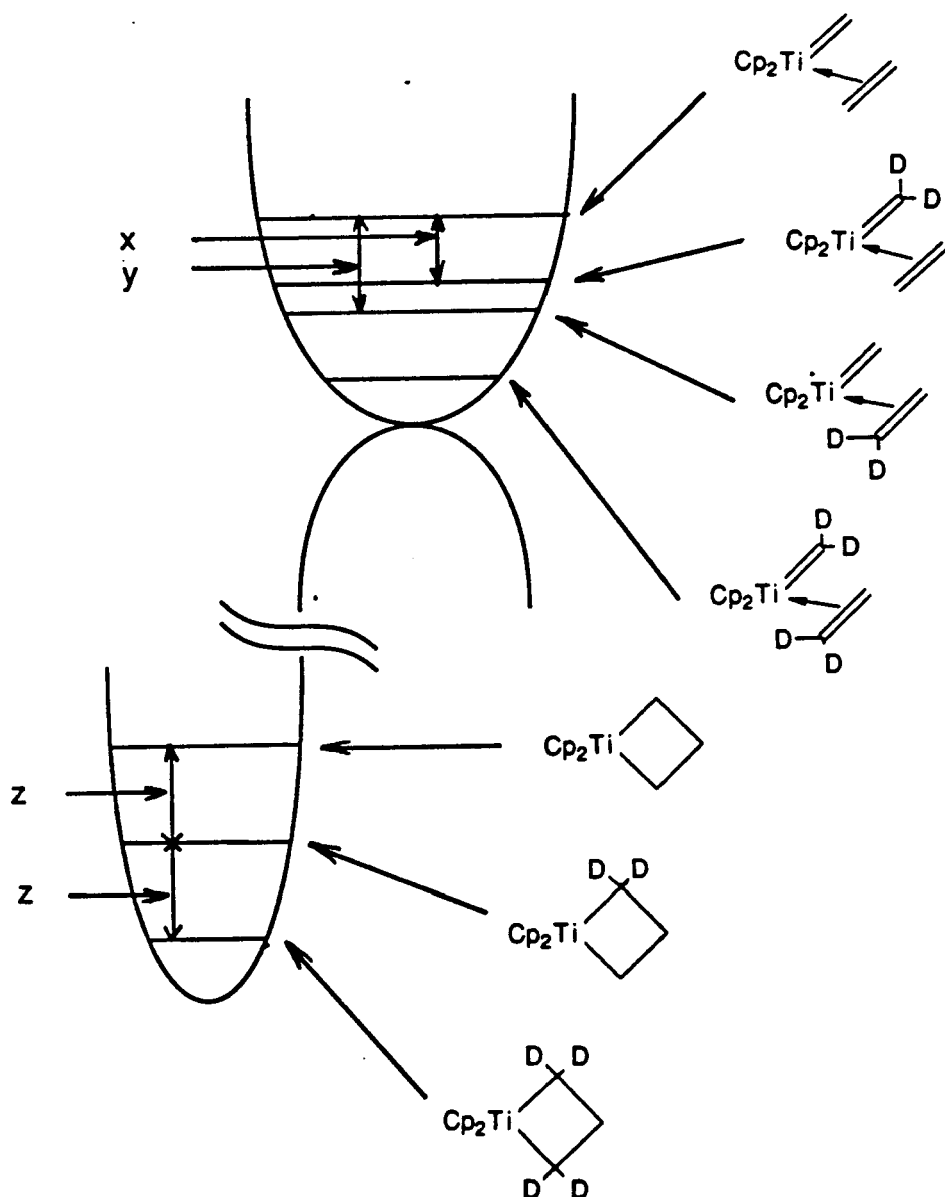
Figure 7: Potential energy curve for deuterated metallacycle cleavage showing the relative zero point energy gap sizes: $z = 2800$ cm^{-1}, x and y $= 2570$ cm^{-1}, y-x $= 77$ cm^{-1}.

$$e^{(z-y)/RT} \, e^{(z-x)/RT} = 1.54 \qquad \text{(Eq 3')}$$

$$\frac{e^{(z-x)/RT}}{e^{(z-y)/RT}} = 1.47 \qquad \text{(Eq 4)}$$

Using these equations, one solves for the energy gap b between olefin d_2-methylidene adduct and d_2-olefin methylidene adduct. This is found to be 77 cm^{-1}. In addition, one can solve for $a + b + c$ (Figure 6). This is found to be 89 cm^{-1}. Finally, this allows for the calculation of energy gaps a and c to be roughly 6 cm^{-1}.

With these experimentally measured zero point energy differences, one can now model the energy gaps z, x and y by identifying infrared stretching frequencies. Table 4 shows the frequency shifts used. Those modes for 1 that were not found in the I.R. spectrum are modeled by CH_2Cl_2 [32], and those modes for 8 that were not found are modeled by ethylene.[32] The zero point energy gap is estimated to be 2800 cm^{-1} for the d_0 versus d_2 metallacycle (z in Figure 7). The zero point energy gap is estimated to be 2569 cm^{-1} for the d_0 versus d_2 phosphine methylidene adduct (x or y in Figure 7).

The origin of a secondary isotope effect lies in the analysis of all the vibrational modes between reactant and product. Deuterium prefers the strongest bond. In a homolytic cleavage, an sp^2 C−H bond is stronger than an sp^3 C−H bond, yet deuterium prefers an sp^3 C−H bond, as in the Cope reaction.

To achieve the correct reasoning, all the modes must be considered including the rock, wag, twist and scissor. When these modes are included, then the zero point energy gap between d_0 and d_2 for an sp^3 center is larger
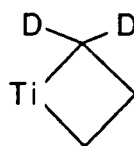
Mode	Frequency cm^{-1}	Frequency cm^{-1}	Difference
s-stretch	3001	2245	756
a-stretch	2985	2180	805
scissor *	1467	1052	415
twist *	1153	826	327
rock *	898	712	186
wag *	1268	957	311
		Total	2800
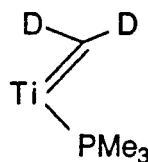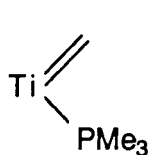
Mode	Frequency cm^{-1}	Frequency cm^{-1}	Difference
s-stretch	2940	2165	775
a-stretch	2885	2095	790
scissor #	1444	1077	367
twist #	825	580	245
rock #	949	720	229
wag #	943	780	163
		Total	2569

*=modeled by CH_2Cl_2

#=modeled by C_2H_4

Table 4: Infrared frequencies for metallacycles and phosphine adducts. The total difference for the sp^3 and sp^2 centers is 231cm^{-1}.

than for an sp[2] center. This is due to the extremely weak wag and twist modes for an sp[2] CH_2 group.

The calculated difference between sp[3] and sp[2] centers in the titanocene systems studied is 231 cm^{-1}, which gives a calculated secondary isotope effect of 3.0. This value is obviously too large, but does show that z, x and y are much larger than the value of $y - x$.

In Figure 7, $y - x$ represents the energy difference that gives rise to the competitive isotope effect. This difference has been shown to be 77 cm^{-1} (b in Figure 6). This secondary effect is much larger than traditionally observed (1.45 versus 1.2) for an equilibrium between a sp[2] and a sp[3] center. Furthermore, the observed isotope effect is really due to an equilibrium between deuterium on the coordinated olefin or on the methylidene. Therefore, it is partitioning between two psuedo sp[2] centers. There are two possible explanations for this very large competitive isotope effect. The first is that the CH vibrational modes of the methylidene are much weaker than the CH modes of a normal sp[2] center. The second possibility is that the olefin methylidene adduct resembles a titanacyclopropane donor singlet carbene adduct (B).

In structure B, the competitive isotope would be expected to be quite large due to a differentiation between a pseudo sp[3] center and a donor carbene center. The twist and wag vibrational frequencies of a singlet carbene are expected to be much weaker than a triplet carbene and further accentuate the competitive isotope effect.
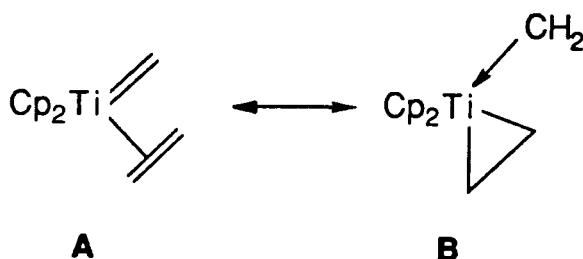
The structure **B** corresponds to the calculated intermediate from the Hoffmann group[12], and **A** corresponds to the calculated intermediate from the Rappé group.[11]

The isotope effects of Table 3 and Figure 5 can also be used as further support for the concerted nature of the reaction. If the reaction was stepwise, starting with either heterolytic or homolytic $Ti-C$ bond cleavage, the intramolecular competitive isotope effect would have been the reverse of that observed due to the propensity of deuterium prefering a sp^3 center.

G. Substituent Effects

This section begins with the synthesis of the chlorocyclopentadienyl ligand. Then the influence of electron withdrawing and donating groups (attached to the cyclopentadienyl ligands) on the electron density at titanium in several titanocene complexes is explored by physical techniques. Finally, the effect of these substituents on the rate of cleavage of metallacyclobutanes is discussed.

Only a few cyclopentadienyl ligands with electron withdrawing substituents have been synthesized. These include chlorocyclopentadienyl thallium[41] and trifluoromethylcyclopentadienyl thallium.[42] The literature preparation for $Cp^{Cl}_2TiCl_2$ ($Cp^{Cl} = C_5H_4Cl$) uses chlorocyclopentadienyl thallium[41] and yields only 180 mg of bis-chlorocyclopentadienyl titanium dichloride. Scaling up the literature preparation by several fold proved laborious and often resulted in very poor yields. Due to the toxicity of thallium,[43] its high price on multigram scale and the initial unsuccessful results, another synthetic pathway was sought. This route yields 8-10 grams of bis-chlorocyclopentadienyl titanium dichloride in an overall 40% yield from α-1-hydroxydicyclopentadiene.[44] This quantity of product would require approximately 420 g CpTl and 192 g TlOEt if synthesized by the current literature procedure.[41]

Our synthesis starts with α-1-hydroxydicyclopentadiene which was originally made by R.B. Woodward[44] as presented in Figure 8. The alcohol is converted to the chloride with CCl_4 and $P\varnothing_3$. The dimer is then cracked by vacuum transfer pyrolysis and the chlorocyclopentadiene selectivity deprotonated with nBuLi. The ring substituted titanocene metallacyclobutanes used in this study are listed in Table 5 with their compound numbers.

Table 5

Compound	Number
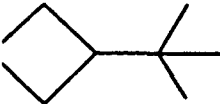
Cp$^{Cl}_2$Ti ⌑⟩—⟨   10

Cp$^{'}_2$Ti ⌑⟩—⟨   11
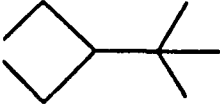
CpCp'Ti ⌑⟩—⟨   12
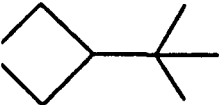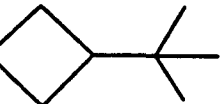
Cp<Cp>Ti ⌑⟩—⟨   13

The uv/vis spectra of several ring-substituted titanocene dichlorides are recorded in Table 6. They all exhibit a weak absorbance (ε ca. 200 M^{-1} cm^{-1}) between 500 and 560 nm, which in titanocene dichloride has been assigned to a symmetry forbidden $A_1 \to A_2$ transition.[34] This band moves to lower energy as electron donating substitutents are added to the rings and moves to higher energy as electron withdrawing substituents are added to the rings. The absorption spectra of the compounds having single substituents on the rings are qualitatively similar to the spectrum of titanocene dichloride. In addition to the band between 500 nm and 560 nm, they exhibit a broad region of
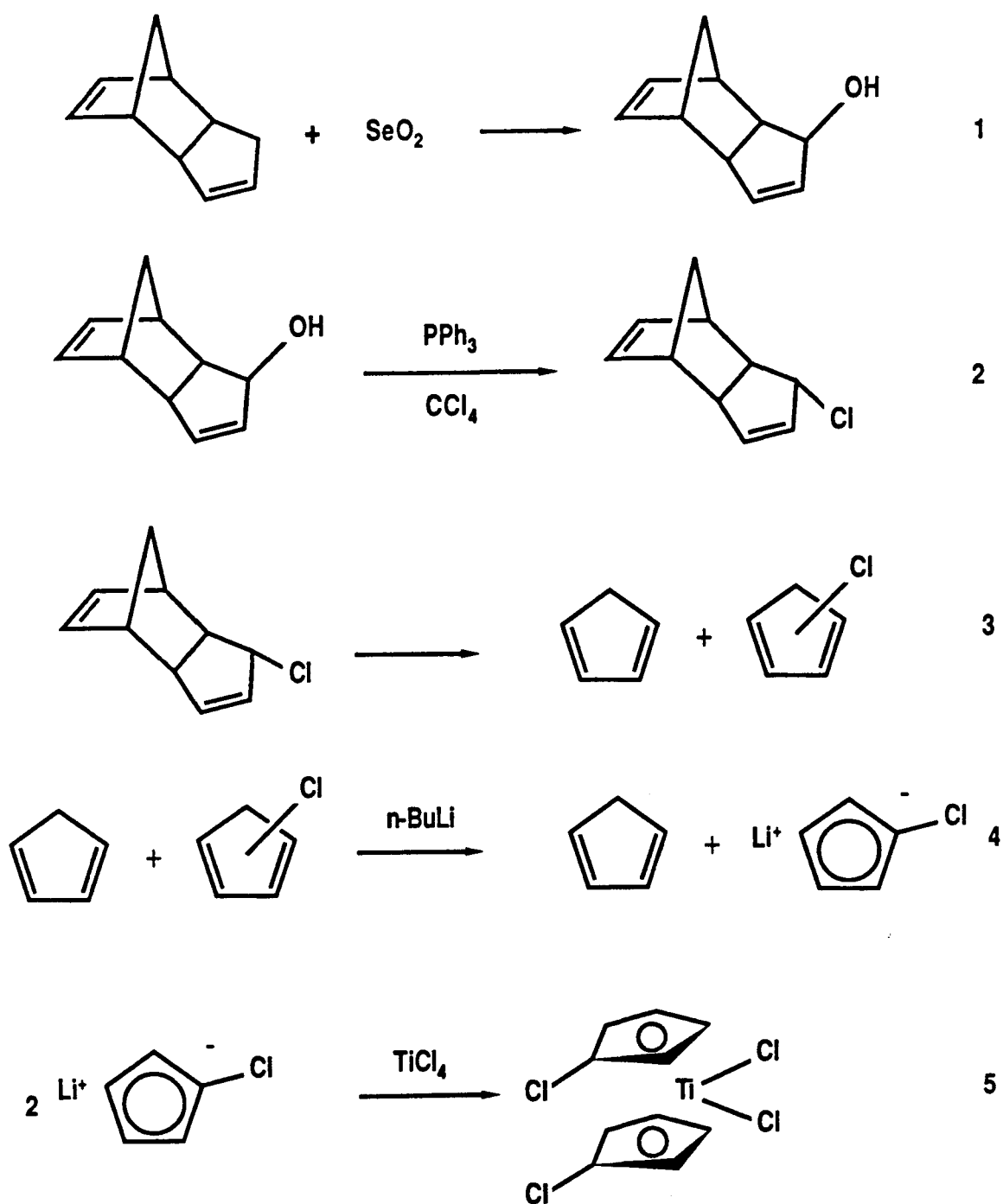
Figure 8: Synthesis of bis-chlorocyclopentadienyl titanium dichloride.

absorption between 260 and 410 nm. The compounds with more highly substituted rings, *i.e.* those with $<Cp>$ and Cp^* ligands, not only exhibit this broad region of absorption but also a band between 470 and 490 nm.

Table 6. Absorption Maxima of Lowest Energy Transitions in the uv/vis Spectra of Ring-Substituted Titanocene Dichlorides

Compound[a]	λ_{max}[b]	Ref.
$Cp_2^*TiCl_2$	560	33
$<Cp>_2TiCl_2$	536	
$Cp^{TMS}CpTiCl_2$	532	33
Cp'_2TiCl_2	528	33
$Cp'CpTiCl_2$	525	33
Cp_2TiCl_2	523	33
$CpCp^{Cl}TiCl_2$	517	
$Cp_2^{Cl}TiCl_2$	514	
$CpCp^{CF3}TiCl_2$	513	
$<Cp>CpTiCl_2$	510	33

(*a*) 3.3×10^{-3} M solutions in $CHCl_3$ (*b*) λ in nm

Thus, it is observed from the absorption spectra of various titanocene dichlorides that ring substitution affects the energy difference between the ground and first excited states of these complexes. It seems that electron donating groups on the rings tend to make this energy difference smaller; there are exceptions to this generalization, cf. the absorption spectrum of

<Cp>CpTiCl₂. The UV spectra of the titanocene dichlorides can give at least an indication of relative electron density at the metal center.

The $^{(49,47)}$Ti NMR spectra of these ring-substituted titanocene dichlorides were also recorded (Table 7). Both the ^{49}Ti and ^{47}Ti resonances

Table 7. $^{(49,47)}$Ti NMR^a of a Number of Titanium Compounds

Compound	$\delta(47,49)$Ti (ppm)^b	$\nu_{\frac{1}{2}}^{49}$Ti (Hz)	$\nu_{\frac{1}{2}}^{47}$Ti (Hz)	Ref.
Cp₂TiCl₂	-771.8	44	84	33
Cp'CpTiCl₂	-744.8	66	184	
Cp'₂TiCl₂	-719.3	125	235	
Cp^{TMS}CpTiCl₂	-747.3	85	257	33
<Cp>CpTiCl₂	-666.4	107	195	
<Cp>₂TiCl₂	-568.5	115	---	
Cp*₂TiCl₂	-442.3	70	213	33
Cp^{Cl}CpTiCl₂	-740.1	110	---	
Cp^{Cl2}TiCl₂	-708.8	136	---	
CpCp^{CF3}TiCl₂	-776.7	82	---	

(a) ^{49}Ti (5.51%; I=7/2, Q=0.24 x 10^{-28} M²; ^{47}Ti (7.28%; I=5/2, Q=0.29 x 10^{-28} M²).
See Ref. 32 and 42

appear in the same spectrum with the ^{49}Ti resonance 268.1 ppm downfield of the ^{47}Ti resonance. Due to its higher quadrapole moment, the ^{47}Ti resonance is always broader than the ^{49}Ti resonance. Increasing methyl substitution of the rings causes an increasingly downfield shift of the $^{(49,47)}$Ti resonances.

Substitution of the electron-donating TMS (trimethylsilyl) group and the electron-withdrawing Cl and CF_3 groups onto the rings also causes a downfield shift of the $^{(49,47)}Ti$ resonances.

NMR chemical shift values are not always an indication of electron density at the atom being observed. A striking example of this is found in the $^{49,47}Ti$ NMR data for a number of ring-substituted titanocene dichlorides (Table 7). Replacing two chlorides in $TiCl_4$ with more electron donating cyclopentadienyl rings does shift the Ti resonances upfield as expected, but the titanocene dichloride complex that should be the most electron-rich at titanium, $Cp^*_2 TiCl_2$, exhibits the lowest field $^{49,47}Ti$ resonance. Gassman[37] has found an inverse relationship between core electron binding energy and $^{49,47}Ti$ chemical shift for Cp_2TiX_2, Cp^*CpTiX_2, and $Cp^*_2TiX_2$ (X = F, Cl, Br) compounds.

A plot of the observed δ $^{49,47}Ti$ values $vs.$ the wave length of the observed lowest energy transition in the spectrum of a number of ring-substituted titanocene dichlorides is presented in Graph 9. Linear correlations are not expected since both σ_p and σ_d will change with substitutions on the rings. In general, it does seem that the lower the energy of the first optical transition, the farther downfield the observed $^{49,47}Ti$ resonance. In addition, a fairly linear correlation is found among sets of titanocene dichlorides which are substituted with the same substituents.

From the ring substituted titanocene dichlorides, the corresponding titanocene methyl chlorides can be prepared in good yield (eq. 5).
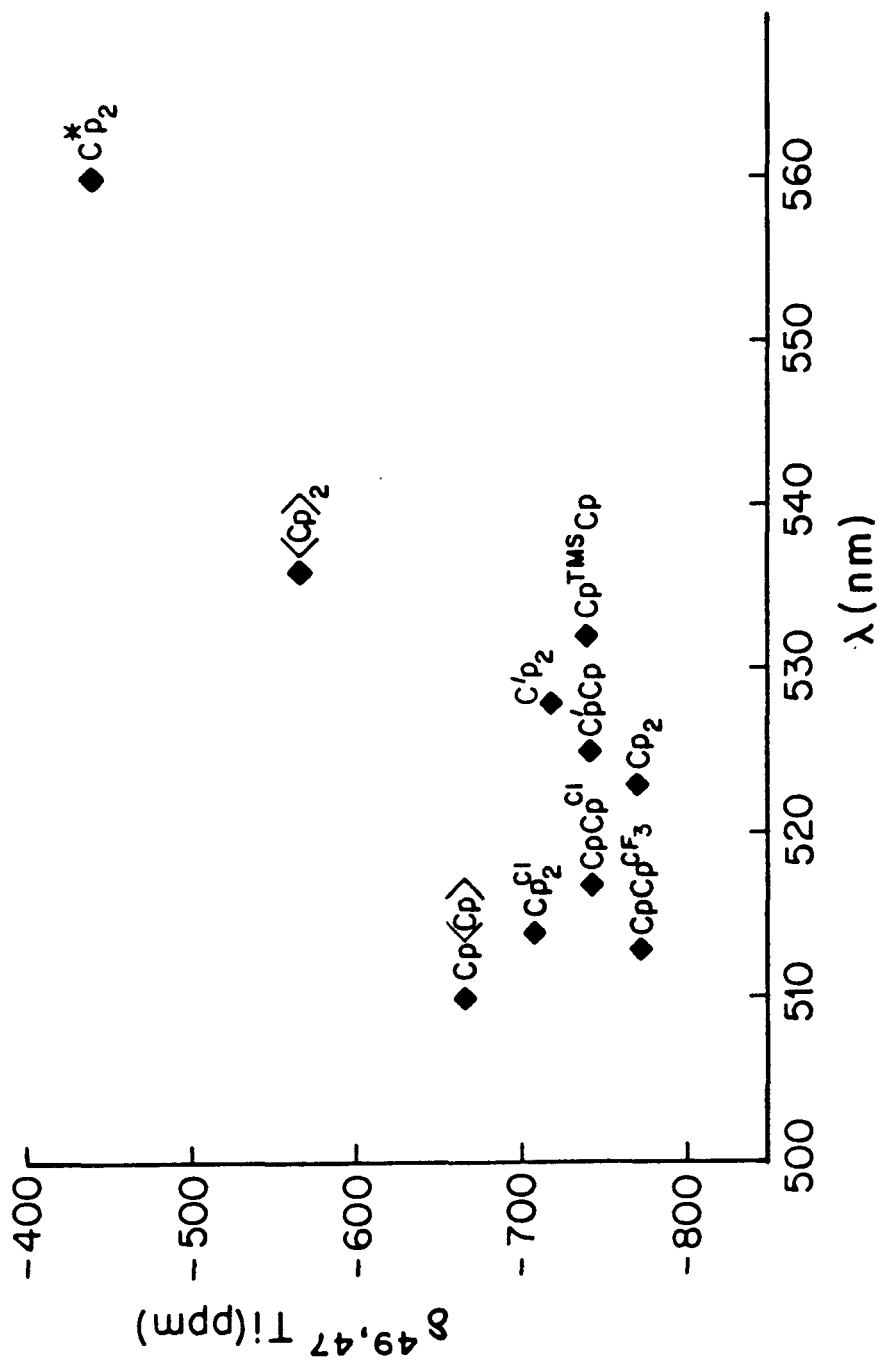
Graph 9: Plot of $\delta_{49,47}Ti$ vs λ_{max} (lowest energy transition of a number of ring substituted titanocene dichlorides.

$$\overline{C}p\,\overline{C}p\,TiCl_2 + AlMe_3 \rightarrow \overline{C}p\,\overline{C}p\,TiMeCl + AlMe_2Cl \tag{5}$$

$$\overline{C}p = \text{substituted or unsubstituted ring}$$

The C-H coupling constants of the methyl group bonded to titanium are included in Table 8. The C-H coupling constant decreases with increasing methyl substitution of the cyclopentadienyl rings and increases with electron withdrawing substituents.

Table 8. C-H Coupling Constants of Methyl Groups
Attached to a Metal Center

Compound	J_{CH} (Hz)	Ref.
CpCp^{CF_3}TiMeCl	129.9	
Cp^{Cl_2}TiMeCl	129.9	
Cp^{Cl}CpTiMeCl	129.1	
Cp$_2$TiMeCl	128.9	33
Cp'CpTiMeCl	128.4	33
Cp'$_2$TiMeCl	128.2	33
<Cp>CpTiMeCl	127.7	33
Cp*CpTiMeCl	127.2	33
<Cp>$_2$TiMeCl	126.7	
Cp*$_2$TiMeCl	126.5	33

The C−H coupling constants of methyl groups depend on the amount of *s*-character at carbon in the C−H bonds.[38] To a first approximation, the amount of *s*-character depends on the effective electronegativity of the group to which the methyl group is bonded: the larger the electronegativity of this group the lower the *s*-character of its bond with the methyl carbon. This leaves more s-character in the C−H bonds, and hence, increasing the electronegativity of the group attached to the carbons should increase the C−H coupling constant observed for a methyl group. Conversely, decreasing the electronegativity of the group attached to carbon should lower the C−H coupling constant. Increasing the electron density at the atom to which the methyl group is bonded effectively lowers the electronegativity and should lower the C−H coupling constant.

Increasing the electron-density at Ti by adding methyl groups to the cyclopentadienyl rings causes a lowering of the J_{CH} of the methyl group bonded directly to the metal center. Conversely, substitution of electron-withdrawing chlorides or a triflurormethyl group on the rings causes an increase in J_{CH}.

Since J_{CH} is a direct relative measure of the hybridization of the Ti-CH_3 bond, of the methods presented here, it best reflects the relative electron density at the metal center. In addition, no exceptions were found to the predicted trends and, therefore, the J_{CH} is the most reliable measure of the electron donating or withdrawing nature of the cyclopentadienyl and possibly other ligands.

The methyl ring-substituted titanocene methyl chlorides are the best starting materials for the preparation of methyl ring-substituted analogs of

the Tebbe reagent (eq. 6).

$$\overline{C}p\,\overline{C}pTiMeCl + AlMe_3 \rightarrow \overline{C}p\,\overline{C}p\,\overline{TiCH_2Al(Me)_2C}\,l + CH_4 \qquad (6)$$

The materials are identical to materials produced by the direct reaction of the titanocene dichlorides with two equivalents of $AlMe_3$.[35] The electron withdrawing ring-substituted titanocenes dichlorides must be used to make the Tebbe reagent.

The kinetics of the reaction of the t-butylmetallacycles

$Cp_2Ti\overline{CH_2CH(tBu)C}\,H_2$, 1, $Cp_2^{Cl}Ti\overline{CH_2CH(tBu)C}\,H_2$, 10, $Cp_2'Ti\overline{CH_2CH(tBu)C}\,H_2'$, 11,
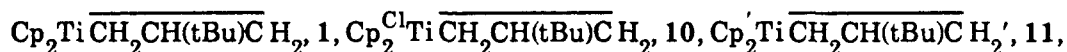
trans-12, cis-12, trans-13 and cis-13 with diphenylacetylene were studied. The results are shown in Table 9. Activation parameters for the reaction of 1,

Table 9. Relative rates of reaction of $CpCpTiCH_2CH(tBu)CH_2$ at 55°C. $CpCpTiCH_2CH(tBu)CH_2$ + $PhC\equiv CPh \rightarrow$ $CpCpTiCH_2C(Ph)C(Ph)$ + $CH_2=CH(tBu)$

Cp	Metallacycle	k_{obs} $(\times 10^{-5}\,s^{-1})$	Relative Rate	Ref.
Cp_2	1	68	16	33
Cp'Cp	trans 12	40	9.3	33
Cp'Cp	cis 12	40	9.3	33
Cp'_2	11	10	2.3	33
<Cp>Cp	trans 13	4.5	1.1	33
<Cp>Cp	cis 13	4.3	1.0	33
Cp^{Cl_2}	10	32	7.4	

11, 10, *cis* and *trans*-13 with diphenyl acetylene were derived from kinetics data obtained in a temperature range between 45°C and 75°C and are listed in Table 10.

Table 10. Activation Parameters for the reaction of $CpCpTiCH_2CH(tBu)CH_2$ at 55°C. $CpCpTiCH_2CH(tBu)CH_2$ + $PhC \equiv CPh \rightarrow CpCpTiCH_2C(Ph)C(Ph) + CH_2 = CH(tBu)$

Cp	Metallacycle	$\Delta H^\ddagger$ (kcal/mol)	$\Delta S^\ddagger$ (e.u.)	Ref.
Cp_2'	11	30.1(6)	15(2)	33
<Cp>Cp	*trans* 13	30.1(4)	13(1)	33
<Cp>Cp	*cis* 13	28.3(9)	8(3)	33
Cp_2	1	25.0(5)	10(2)	
Cp^{Cl}_2	10	27.2(4)	8(2)	

Ring-substitution can affect these complexes electronically. Gassman[36] has shown from ESCA data that substitution of two Cp* ligands for the two Cp ligands in titanocene dichloride produces an effect on the titanium core orbitals equivalent to a one-electron reduction at titanium. Thus, electron donating substituents on the rings increase the electron density at the metal center.

Since these kinetics were done under saturation conditions, they essentially give us only information about the relative energies of the titanacyclobutanes and the first transition state. The results reveal how the relative energy difference varies as a function of ring-substitution. The data does not allow for determination of the relative stabilities of metallacycles

having different substituents on the cyclopentadienyl rings. Thus, one cannot separate ground state from transition state effects.

It is seen from all our kinetic results that increasing methyl substitution of the rings decreases k_{obs}. Steric effects seem to be playing a very small part in determining the observed rate.

Electronic effects then seem to play the major role in determining the relative reactivities of the metallacycles studied. The cleavage of a metallacyclobutane to a carbene-olefin complex is formally a reductive process. In a carbene-olefin complex, the CH_2 group can be considered either a dianionic donor or a neutral donor. Thus, in these titanium systems the oxidation state of titanium metallacycles is Ti[IV], while in the carbene-olefin complex, the titanium can have some Ti[II] character (eq. 7). Hoffmann[12] has

$$Cp_2Ti \diagup \diagdown \qquad Cp_2Ti \diagup CH_2 \diagdown \qquad (7)$$
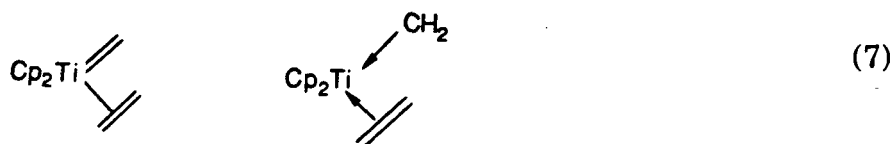
studied these systems using the extended Hückel method. While quantitatively incorrect, his calculations lead to a qualitative understanding of this system. He calls the titanacyclobutanes d[0] complexes and carbene-olefin complexes d[2]. A more convincing argument for a reductive process is electron counting. The metallacycles are $16e^-$ species and possess an empty $1a_1$ orbital of largely metal character. In the $18e^-$ carbene-olefin complex this orbital is filled.

In fact, this is the exact reactivity that would be predicted from the Rappé, Upton Generalized Valence Bond calculations.[11] Their calculations

predict a metallacycle cleavage to yield a titanocene methylidene olefin adduct which has some donor olefin character. Their calculations, however, found no energy minimum for this carbene-olefin complex.

By the Hammond[39] postulate the transition state for the endothermic formation of carbene-olefin from metallacycle should most closely resemble the carbene-olefin species. Thus, effects that change the stability of carbene-olefin relative to metallacycle should cause similar changes to the stability of the transition state relative to metallacycle. Since the formation of carbene-olefin from metallacycle involves formal reduction at titanium, increasing the electron density at titanium by increasing the electron-donating ability of the ancillary ligands should destabilize the carbene olefin relative to the metallacycle. Thus, it is predicted that increasing methyl substitution of the cyclopentadienyl rings, making them better donors, should slow cleavage of metallacycle to carbene-olefin. This prediction is observed. All the Cp_2TiCl_2 UV/VIS and $Cp_2TiMeCl$ $C-H$ coupling constant data lead to the conclusion that the methyl substitution on the cyclopentadienyl ligands does increase the electron density on the Ti. Similar effects of ring substitution were observed in the formation of the Tebbe reagent from mixed-ring titanocene dichlorides.[35] In that system, increasing methyl substitution of the cyclopentadienyl rings lowered the kinetic acidity of the α-hydrogens of a L_nTi-Me intermediate.

The chloro substitution on the cyclopentadienyl rings should decrease their electron-donating ability, which seems confirmed by the fact that the J_{CH} coupling constant of the methyl bonded to titanium in $Cp^{Cl_2}TiMeCl$ is larger than the corresponding constant in $Cp_2TiMeCl$. From the above argument, it

would be predicted that **10** should react faster with diphenylacetylene than would the plain-ring analog, **1**. It was found, however, the k_{obs} for the reaction of **10** with diphenylacetylene is smaller than k_{obs} for the same reaction of **1**. One possible explanation for this result is that while the transition state is stabilized by the chloro substitution (relative to the plain-ring transition state), the metallacycle ground state is stabilized to a greater extent. Evidence for this argument is found in the preparation of the Cp^{Cl}_2 analog of the Tebbe reagent. It is made difficult because of the formation of a large amount of $Cp^{Cl}_2TiMe_2$ in the reaction of $Cp^{Cl}_2TiCl_2$ with $AlMe_3$. In fact,, in order to successfully synthesize the Cp^{Cl}_2 analog of the Tebbe reagent, an extra equivalent of $AlMe_2Cl$ was necessary to shift the equilibrium toward $Cp^{Cl}_2TiMeCl$. This was accomplished by starting with $Cp^{Cl}_2TiCl_2$ and two equivalents of $AlMe_3$ instead of $Cp^{Cl}_2TiMeCl$ and one equivalent of $AlMe_3$.

To further elucidate this effect, the equilibrium constants of several CpCpTiMeCl complexes with CpCpTiMe$_2$ complexes were measured (eq. 8). The titanocene methylchlorides are in equilibrium with dimethyl titanocenes when treated with one equivalent of trimethyl aluminum (eq. 8).

$$\overline{C}p\,\overline{C}pTiClMe + AlMe_3 \rightleftharpoons \overline{C}p\,\overline{C}pTiMe_2 + AlMe_2Cl \tag{8}$$

The equilibrium constants lie further to CpCpTiMe$_2$ as electron withdrawing substituents are substituted on the cyclopentadienyl ligands and lie further to CpCpTiMeCl with increasing methyl substitution on the cyclopentadienyl ligands. The equilibrium constants are tabulated in Table 11. The K_{eq} increased with decreasing methyl substitution and increased with electron withdrawing substitutents. Since the aluminum reagents are the same in all

the equilibriums studied, the K_{eq}'s reflect relative thermodynamics of the titanocene methyl chlorides and dimethyl titanocenes. Electron withdrawing cyclopentadienyl ligands make the titanium center less electro-positive and, therefore, the complex prefers the more electron donating methyl than electron withdrawing chlorine. A second possible explanation is that the chloro substituted cyclopentadienyl rings are removing s-character from the titanium leaving more d-character to form stronger metal carbon bonds in the metallacycle.[40] The other substituted titanocene dichlorides studied do not readily form Cp_2TiMe_2. Thus, dialkyls including metallacyclobutanes, in the Cp^{Cl}_2Ti system may enjoy special stabilization.

Table 11. Equilibrium Constants for the Reaction in Equation 2

Compound	Keq
$CpCp^{CF_3}TiMeCl$	1.12
$Cp^{Cl}_2TiMeCl$	1.03
$CpCp^{Cl}TiMeCl$	0.40
$Cp_2TiMeCl$	0.08
$Cp'_2TiMeCl$	0.03
$Cp*CpTiMeCl$	<0.01

Since the electron withdrawing ligands stabilize the metallacycles (ground state), the electron donating ligands should destabilize the ground

state. Therefore, electron donating ligands should speed the cleavage reactions if ground state effects were solely operable. It has been shown however, that electron donating ligands slow the cleavage reaction due to destabilizing the transition state. Thus, there are two opposing effects to increasing the rate of metallacycle cleavage.

A qualitative difference in stabilization and destabilization of the metallacycles can be gained from Table 11. When two chlorines are substituted on the cyclopentadienyl ligands, the K_{eq} increases by a factor of 12.8. When two methyl groups are substituted on the cyclopentadienyl ligands, the K_{eq} decreases only by a factor of 2.7. Thus, the chlorines induce a larger ground state stabilization then the methyl groups induce a ground state destabilization. In Table 9, 1 cleaves 2.2 times faster than 10, whereas 1 cleaves 7.0 times faster than 11. Thus, since the ground state is not as sensitive to two methyl groups as it is to two chlorines, yet 11 still cleaves much slower than 10, the methyl groups must induce a larger transition state destabilization than the chlorines induce a transition state stabilization.

SUMMARY

The work presented lends insight into the manner in which titanocene metallacyclobutanes cleave to form a titanocene methylidene intermediate. Competition trapping experiments strongly implicate an olefin-titanocene methylidene as an intermediate. The fundamental conclusions can be summarized as follows: 1) the latent olefin of the metallacycle slides toward the titanium to coordinate to an empty orbital in the rate determining step; 2) this complex can then rapidly react by an Sn2 process where the olefin is displaced by another Lewis base. It is not rigorously ruled out that the olefin can also dissociate in an Sn1 manner to yield uncoordinated titanocene methylidene which also reacts rapidly with traps. The nature of the movement of the olefin lends itself to steric and electronic manipulation. In the reactions of ring substituted titanacyclobutanes with trapping reagents, the sterics play only a small role in determining the relative rates observed; electronic effects seem to dominate. The electronic effects can be understood from the fact that increasing the electron-donating ability of the substituted-rings causes a destabilization of the transition state between metallacycle and carbene olefin. This destabilization arises from the "reductive" nature of the conversion of metallacycle to carbene-olefin. Electron withdrawing ligands also slow the rate of cleavage by stabilizing the ground state. This ground state stabilization is further demonstrated by the equilibrium constant studies between titanocene methyl chlorides and dimethyltitanocenes which show electron withdrawing ligands stabilize titanium carbon sigma bonds.

The Ti[47,49] NMR spectra of these complexes was not a reliable measure of the electron density at the Ti center. The UV/vis and methyl $C-H$ coupling constants, however, did provide an accurate measure (with one exception in the UV/vis) of the Ti electron density.

The mechanistic results contrast the theoretical results of Rappé and Upton.[11] This study presented evidence for the existence of an olefin-titanocene methylidene complex, whereas the theoretical Generalized Valence Bond Method found no such intermediate in an energy well for the $Cl_2Ti=CH_2(CH_2=CH_2)$ system. The other experimental results are consistent with the theoretical treatment by Rappé and Upton.[11] The reaction most likely proceeds in the manner they present by the Orbital Phase Continuity Principle, except that there exists a small energy well for olefin coordination preceding the $2+2$ reaction.

Kinetics studies on titanocene methylidene phosphine adducts demonstrate that the reaction proceeds by a rate determining loss of phosphine followed by a rapid trapping of titanocene methylidene. The rate of trapping by acetylenes is approximately one-tenth the rate of trapping by phosphine and thus saturation is never observed.

EXPERIMENTAL

General Considerations. All manipulations were performed by using glove box or standard Schlenk line techniques. Argon was purified by passage through Chemalog R3-11 and activated Linde 4A molecular sieves. Deuterated solvents were purchased from Cambridge Isotope Laboratories and purified by vacuum transfer from sodium benzophenone ketyl. All acetylenes and phosphines were purchased from Aldrich Chemical Company and used as supplied.

Synthesis of all titanocene metallacyclobutanes,[23] titanocene methylidene phosphine adducts[16,24] and of Tebbe's reagent[25] were from literature preparations. Deuterated metallacycles were synthesized from selectively labeled olefins. Tebbe's-d_8 reagent was synthesized as of a modified literature preparation[26], and deuterated neohexene was synthesized by hydrozirconation using Cp_2ZrHCl,[27] monodeuterated t butylacetylene and quenching with D_2O.

^{1}H NMR spectra were recorded on a JEOL FX-90Q and/or JEOL GX-400. Spectra were taken in benzene -d_6 or toluene -d_8 solutions and referenced to residual protons on the solvent. All kinetics were followed by an automated kinetic routine which took spectra at programmable intervals.[28] All reactions were followed to at least 3 half-lives. The temperatures reported for the NMR probe were determined by the chemical shift difference of methanol.[29] Reactant and product concentrations and/or ratios were determined by integration of the cyclopentadienyl resonances.

All sample weighing and preparation was done in a VAC Dri-Train MO 40-1 dry box using either a Sartorius pan loader with a precision of 1 mg or an Sartorius Analytical balance with a precision of 0.1 mg. The 5 mm NMR samples were capped with a septum and then the septa wrapped with parafilm. This allowed for easy syringing of solvents and reactants. The NMR solvents were loaded in volumetic flasks in the dry box and then capped with a septum and wrapped with parafilm. This allowed for easy transport of small amounts of deuterated solvents to the NMR spectrometer where the final combination of reactants and solvents took place. The time required for equilibration of the sample in the NMR probe was determined to be three minutes.

In all kinetic runs, 10 mg of the metallacycle or phosphine adduct were used. If the trapping reagent was solid, it was weighed into the 5 mm NMR tube prior to transfer into the dry box. If the trapping reagent was a liquid, it was syringed into the NMR tube immediately after the solvent was added and immediately before putting the sample in the NMR probe. If saturation kinetics was being tested for, a solution was made such that 0.4 mL of the solution contained 10 mg of metallacycle or phosphine adduct. The NMR probe was always stabilized at the reaction temperature for at least five minutes before starting an experiment. Tables 12 through 17 summarize the kinetic results and conditions for data presented in sections A, B and C.

The ^{49,47}Ti NMR spectra were recorded on the JEOL GX-400 at 22.52 MHz. The 90° pulse length, 40 μsec, was determined from a sample of neat $TiCl_4$ sealed in a 5 mm tube held concentrically in a 10 mm NMR tube filled with 2 mL of $CDCl_3$ as a lock solvent. ^{49,47}Ti spectra of the ring-substituted

titanium compounds were obtained from saturated solutions of the titanium compounds in 2 mL of $CDCl_3$ held in 10 mm NMR tubes. Deuterium locking was used. The FID data were collected using 90° pulses and an acquisition time of 0.272 sec. The pulse delay between the end of acquisition and the beginning of the next pulse was 1 sec. The spectral window was 30 KHz wide, and 16 k data points were collected yielding a digital resolution of 3.7 Hz. An exponential line broadening factor of 10 Hz was applied to the raw FID, which was then Fourier transformed to yield the spectrum. Both ^{49}Ti and ^{47}Ti resonances appear in a single spectrum separated by 268.1 ppm with the ^{49}Ti resonance downfield relative to the ^{47}Ti resonance. Chemical shifts were referenced relative to external neat $TiCl_4$ using the convention that positive δ values are downfield. The reported linewidths include the 10 Hz of line-broadening. No proton decoupling was used as its use produced no effect on the line-shape of the resonances.

The uv/vis absorption spectra of the ring-substituted titanocene dichlorides were obtained on an HP 8451A diode array spectrophotometer. Solutions (3.3×10^{-3} M) of the titanocene dichlorides in spectra grade chloroform were prepared in air. The solutions were transferred to 1 cm pathlength cuvettes, and the absorption spectra were recorded in air. The λ_{max} of the lowest energy transition was located at the point where the first derivative of the spectrum was zero.

The solvents used in organometallic syntheses were purified as follows. Toluene, benzene, diethyl ether and THF (predried with CaH_2) were transferred onto sodium benzophenone ketyl and later distilled into solvent flasks equipped with teflon screw valves.

All infrared spectra were obtained on a Shimadzu IR-435 in the expanded slow scan mode. Frequencies were recorded relative to a polystyrene film.

Competition kinetics versus temperature on 2, 3, 7 and Tebbe reagent. Five NMR tubes were loaded with 10 mg Tebbé reagent. Four NMR tubes were loaded with 10 mg of **3**. Three NMR tubes were loaded with 10 mg of **2**. Four NMR tubes were loaded with 10 mg of **7**. 1.14 g (10eq.) of diphenylacetylene was put in a 10 mL round bottom and covered with a septum. The round bottom was then purged with Ar. Toluene (6.8 mL) was added along with 835 µl (10eq.) of neohexene. This mixture was stirred to dissolve the acetylene. Constant temperature baths at -10°C, 0.0°C, 15°C, 25°C and 40°C were prepared.[29] The trap solution (0.4 mL) was syringed onto **2**, **3** and Tebbe's reagent (along with 10 µl pyridine) at -20°C and shaken vigorously. The NMR tubes were then put in the 0.0°C bath for 10 hrs. The trap solution (0.4 mL) was syringed into **2**, **3**, **7** and Tebbe's reagent (along with 10 µl pyridine) at -20°C and shaken vigorously. The four NMR tubes were then put in the 15°C bath for 5 hours. The trap solution (0.4 mL) was syringed into **2**, **3**, **7** and Tebbe reagent (along with 10 µl pyridine) at -20°C and shaken vigorously. The four NMR tubes were then put into the 25°C bath for 1 hour. The trap solution (0.4 mL) was syringed onto **2**, **7** and Tebbe reagent (along with 10 µl pyridine) at -20°C and shaken vigorously. The three NMR tubes were then put in the 40°C bath for 15 minutes. After the allotted time period for each experiment, the solvent was removed in vacuo and the NMR tubes taken into a dry box where 0.4 mL C_6D_6 was syringed in. The

cyclopentadienyl ^{1}H NMR resonances of the products were integrated to determine the product ratios.

Deuterium isotope effects on 1. Two NMR tubes were loaded with 10 mg 1. Two NMR tubes were loaded with 10 mg d-2 1. Two NMR tubes were loaded with 10 mg d-4 1. In a 5 mL round bottom was loaded 20.3 mg (1.1 eq.) diphenylacetylene, 1.6 mL C_6D_6 and 12 μl toluene (as internal standard). In another 5 mL round bottom was loaded 180 mg diphenylacetylene (6.5eq.), 1.6 mL C_6D_6 and 12 μl toluene (as internal standard). The NMR spectrometer was stabilized at 55°C. Immediately before each experiment, 0.4 mL of one trapping solutions was added to one NMR tube of each of the three sets of compounds at room temperature. The other trap solution (0.4 mL) was then added to the other NMR tube of the three sets at room temperature. The NMR tubes were shaken vigorously and immediately put in the NMR probe. The determined reaction rates for equivalent protio and deuterio reactions were ratioed to give the isotope effect.

Deuterium isotope effects on 4. Two NMR tubes were loaded with 10 mg 4. Two NMR tubes were loaded with 10 mg d-2 4. In a 5 mL round bottom was added 22.5 mg diphenylacetylene (1.1eq.), 1.2 mL C_6D_6 and 9 μl toluene (as internal standard). In another 5 mL round bottom was added 136 mg diphenylacetylene (6.5eq.), 1.2 mL C_6D_6 and 9 μl toluene. The NMR spectrometer was stabilized at 50°C. Directly before each experiment 0.4 mL of one of the trapping solutions was added to one NMR tube of each of the two sets of compounds at room temperature, then 0.4 mL of the other trap solution

was added to the other NMR tube of the two sets at room temperature. The NMR tubes were shaken vigorously and immediately put in the NMR probe. The determined reaction rates for equivalent protio and deuterio reactions were ratioed to give the isotope effect.

Competitive isotope effect. A NMR tube was charged with 10 mg d-2 1, 45 mg diphenylacetylene and 4 mL C_6D_6. The tube was sealed and warmed to 55°C for 4 hours. The reaction was cooled to room temperature and the α hydrogens of the metallacyclobutene and the methylene hydrogens of the neohexene integrated by NMR. The procedure was repeated in C_6H_6 and the deuterium incorporation also determined by ^2H NMR.

Competitively trapping Tebbe's reagent with trimethylphosphine and 3 hexyne. A NMR tube was charged with 10 mg Tebbe reagent. A solution of 0.2 mL C_6D_6, 100 μl 3-hexyne and 70 μl trimethylphosphine was made up in a 2 mL volumetric flask. The NMR spectrometer was stabilized at 25°C. C_6D_6 (0.2 mL) was syringed onto the Tebbe reagent. The NMR tube was shaken to dissolve the Tebbe reagent. Then 0.2 mL of the trap solution was syringed into the NMR tube. At the same time that a stop watch was started. The reaction was then followed by an automated kinetic routine. At the time of addition of the traps, the Tebbe was completely converted to 8 and metallacyclobutene. 8 then reacted with 3-hexyne to form more of the metallacyclobutene. The pseudo first order rate constant was $1.24\text{-}10^{-3}s^{-1}$. At the time that t=0, the logarithm intercept was .1215. Using this intercept and the first order logarithm expression, it can be calculated that the ratio of

products from trimethylphosphine and 3-hexyne is 10.9. When the kinetic expression for mechanism 7 is factored as shown below, then the terms that cause the expression to saturate are in parenthesis.

$$rate = k[R]\left(\frac{k_2[T]}{k_{-1}[O]+k_2[T]} \right)$$

If now [O] is taken to be 1 and the [T] to be 27.9 (as is in the case of a 27.9 fold excess of 3-hexyne) and the [O] rate constants to be 1 compared to the 10.9 (as found above) for the [T] rate constants, then the following expression results.

$$rate = k_1[R]\left(\frac{1 \cdot 2\,7.9}{10.9 \cdot 1+1 \cdot 27.9} \right) \Rightarrow rate = .71.9 k_1[R]$$

This expression equals 71.9. Therefore, 71.9 percent of the rate determining k_1 should have been reached when the 3-hexyne is in a 27.9 fold excess.

Competition trapping experiments. Three 10 mg samples of compounds 2, 3, 7, 8, 9 and Tebbe reagent were measured into individual NMR tubes. Into a 10 mL round bottom was measured out 364 μl (10eq.) neohexene, 50 mg diphenylacetylene (10eq.) and 3 mL toluene. Into another 10 mL round bottom 252 μl cyclopentene (10eq.), 500 mg diphenylacetylene (10 eq.) and 3 mL toluene was measured out. Into a third 10 mL round bottom 399 μl 4-octyne (10eq.), 500 mg diphenylacetylene (10eq.) and 3 mL toluene was measured out. Each solution (0.4 mL) was syringed onto each of the compounds 2, 3, 7, 8, 9 and Tebbe reagent (along with 10 μl pyridine) in individual NMR tubes at 25°C. The reactions were then shaken vigorously

and allowed to stand for 1 hour. The solvent was then removed in vacuo and each NMR sample taken into the dry box where 0.4 mL C_6D_6 was added. The product ratios were determined by integrating the cyclopentadienyls resonances.

Synthesis of $Cp_2TiCD_2(Cl)Al(CD_3)_2$. A 300 mL three neck flask was equipped with a reflux condensor and a dropping funnel and flamed out under vacuum and charged with 100 mL ether and 4.6 g Mg(0.190 mols). To the solution, 25 g (10 mL, 0.173 mols) CD_3I was added dropwise over a 1 hr period to keep up a gentle reflux. Once the Grignard reagent was completely formed, 23.5 g $HgCl_2$ (0.087 mols) was added slowly down the reflux condensor. The reaction was then refluxed for 24 hrs. The reaction was then quenched with 100 mL H_2O. The reaction underwent a normal organic ether/water extraction workup. The ether solution was dryed with $MgSO_4$ and filtered. The ether was distilled off and the $(CH_3)_2Hg$ was distilled through a vigreaux column. A fraction between 86 and 96° C was collected. Yield $\approx$ 60 percent 11.5 g.

Dimethyl mercury (11.5 g, 0.049 mols) was added to 2.4 g Al powder (0.15 mols, 3 eq) under Ar in a sealable pressure container. The reaction was heated to 90° C for 18 hrs and then cooled to room temperature. The $Al(CD_3)_3$ was dynamic vacuum transferred off all of the Al powder and Hg metal into a flask equipped with a Kontes valve. Yield 95 percent 2.2 g $Al(CD_3)_3$.

In 15 mL toluene was suspended 3.5 g ($1.41 \cdot 10^{-2}$ mols) Cp_2TiCl_2 in a medium Schlenk flask. $Al(CD_3)_3$ (2.2 g, $3.1 \cdot 10^{-2}$ mols) and the suspension was heated to 55° C for 36 hours. The reaction was cooled to room temperature

and 5 mL pentane laid on the top. The reaction was cooled to -20° C, and the crystals formed were isolated by cannula filtration. Yield d_8 Tebbe's reagent 1.3 g; 35 percent.

Preparation of $Cp^{Cl}_2TiMeCl$. This procedure is analogous to the method[45] used to prepare $Cp_2TiMeCl$. $AlMe_3$ (7 mL of 2 M $AlMe_3$ in toluene, 14 mmol) was added *via* syringe to an Ar-flushed flask containing a solution of $Cp^{Cl}_2TiCl_2$ (3.27 g, 12.4 mmol) in 30 mL CH_2Cl_2 at 0°C. The reaction mixture immediately became a very dark brown-red. The reaction mixture was stirred for 2.5 h at 0°C. Diethyl ether (15 mL) was then added at 0°C; the solution immediately changed color from dark brown-red to orange. The solution was warmed to room temperature and all volatiles were removed *in vacuo*. The resulting oily residue was dissolved in 6 mL CH_2Cl_2 and 10 mL of diethyl ether was carefully layered on top of the solution. The mixture was slowly cooled to -50°C and orange-red crystals formed. The mother liquor was decanted off, and the crystals were washed with two 5 mL aliquots of diethyl ether and dried *in vacuo*. Yield was 46%. ^{1}NMR (C_6D_6): δ 5.80 (m, 2H, $C_5\underline{H}_4Cl$), 5.58 (m, 2H, $C_5\underline{H}_4Cl$), 5.44 (m, 2H, C_5H_4Cl), 5.23 (m, 2H, $C_5\underline{H}_4Cl$), 1.01 (s, 3H, Ti-$\underline{Me}$), ^{13}C {H^1} NMR (C_6D_6): 117.7, 116.2, 112.9, 112.1, 109.5 ($\underline{C}_5H_4Cl$), 53.6 (Ti-$\underline{Me}$). Anal. Calcd for $C_{11}H_{11}Cl_3Ti$: C, 44.40; H, 3.73. Found: C, 44.16; H, 4.04.

Preparation of $<Cp>_2TiMeCl$. The compound was prepared as for $Cp_2^{Cl}TiMeCl$.. Yield was 72%. ^{1}H NMR (C_6D_6): δ (d, 2H, $C_5H_2Me_3$), 5.44 (d, 2H, $C_5\underline{H}_2Me_3$), 1.85 (s, 3H, $C_5H_2\underline{Me}_3$), 1.68 (s, 3H, $C_5H_2Me_3$), 1.54 (s, 3H,

$C_5H_2Me_3$), 0.70 (s, 3H, Ti-$\underline{Me}$). ^{13}C {^1H} NMR (C_6D_6): δ 128.3, 120.1, 120, 119.5, 118.8 ($\underline{C}_5H_2Me_3$), 16.3, 13.8, 15.4, ($C_5H_2\underline{Me}_3$), 57.6 (Ti-$\underline{Me}$).

Preparation of CpCp^{CF_3}TiMeCl. This compound was successfully synthesized only on an NMR tube scale since it decomposes slowly. CpCp^{CF_3}TiCl$_2$ (10 mg) was dissolved in a 5 mm NMR tube in 0.4 mL C_6D_6 under N_2 and 3.5 µl AlMe$_3$ was syringed in. The reaction turned dark orange. Yield was quantitative by NMR. ^1H NMR (C_6D_6): δ 6.27 (m, 2H, $C_5\underline{H}_4CF_3$), 6.18 (m, 2H, $C_5\underline{H}_4CF_3$), 5.85 (s, 5H, $C_5\underline{H}_5$), 1.73 (s, 3H, Ti-$\underline{Me}$). ^{13}C {^1H} NMR (C_6D_6): δ 118.9 ($\underline{C}_5H_5$), 113.5, 116.9, 121.2, 123.2, 131.7 ($\underline{C}_5H_4CF_3$), 128.7 (q, $C_5H_4\underline{C}F_3$), 82.5 (Ti-$\underline{Me}$).

Preparation of Cp$^{Cl}_2$TiCH$_2$Al(Me)$_2$Cl. A medium schlenk tube was charged with 2.12 g (6.7·10^{-3} mols) Cp$^{Cl}_2$TiCl$_2$, and the Cp$^{Cl}_2$TiCl$_2$ suspended in 60 mL toluene under Ar at room temperature. A 2 M AlMe$_3$ in toluene solution (8.5 mL, 1.7·10^{-7} mols) was syringed in, and the reaction heated at 50°C for 26 hrs. The volatiles were moved by vacuum at room temperature for 12 hrs. The resulting moist solid was extract with 3 x 10 mL pentane, and the pentane extracted pumped dry under vacuum for 12 hrs. The resulting red solid was dissolved in 10 mL pentane and slowly cooled to -50°C yielding 1.1 g of product as a red powder. (Yield 46%). ^1H NMR (C_6D_6): δ 5.63, 5.52, 5.46, 5.32 (all m, 8H tot, $C_5\underline{H}_4Cl$), 8.59 (s, 2H, µ-CH$_2$), 0.34 (s, 6H, Al-$\underline{Me}$). ^{13}C {^1H} NMR (C_6D_6): 119.7, 113.0, 112.1, 111.8, 111.5 ($\underline{C}_5H_4Cl$), 199.2 (µ$^-\underline{C}H_2$).

Preparation of $Cp^{Cl}{}_2TiCH_2CH(tBu)CH_2$. A medium Schlenk tube was charged with 1 g $Cp^{Cl}{}_2TiCH_2Al(Me)_2Cl$ ($2.8 \cdot 10^{-3}$ mols) and then 3 mL CH_2Cl_2 syringed in at -30°C. Another medium Schlenk tube was charged with 0.38 g ($3.1 \cdot 10^{-3}$ mols) dimethylaminopyridine (DMAP) and 3 mL CH_2Cl was syringed -30°C. Neohexene (1.5 mL, $1.1 \cdot 10^{-2}$ mols) was added to the DMAP solution and then this solution was syringed onto the $Cp^{Cl}{}_2TiCH_2Al(Me)_2$ solution. The reaction was stirred for 15 minutes at -30 and then warmed to -10°C over 15 minutes. The reaction was cooled back down to -30°C and slowly cannulated into 50 mL pentane at -30°C. A light orange precipitate formed and the red mother liquor was filtered off by Schlenk filtration. The precipitate was then washed with 10 mL pentane and the combined pentane solution pumped to dryness under vacuum. The resulting red powder was dissolved in 3 mL toluene and slowly cooled to -50°C. The resulting red powder was isolated by filtration. (Yield 220 mg, 24%.) ^1H NMR (C_6D_6): δ 5.44, 5.39, 5.24, 5.15 (m, 2H each, $C_5\underline{H}_4Cl$), 22.17 (t, $J = 10$ Hz, H_α), 2.47 (t, $J = 10$ Hz, H_α), -0.11 (t, $J = 10$ Hz, H_β), 0.92 (s, 9H, t-C$\underline{Me}_3$). C^{13} $\{^1H\}$ NMR (C_6D_6): δ 113.1, 110.9, 109.9, 109.0, 108.3 ($\underline{C}_5H_4Cl$), 76.9 (αC), 30.2 (-$\underline{C}Me_3$), 29.2 (-C$\underline{Me}_3$), 20.1 (βC).

Equilibration of $CpCpTiMeCl$ and $CpCpTiMe_2$. A typical experiment involved loading 10 mg of the $CpCpTiMeCl$ in an NMR tube and dissolving it in 0.4 mL C_6D_6. One half of an equivalent of neat $AlMe_3$ (usually approximately 2 µl) was syringed in and the NMR tube shaken. The equilibrias were established immediately. The product and reactant ratios were determined by ^1H NMR integration. The K_{eq} was calculated. Another 1

or 2 μl of neat AlMe$_3$ was added and the product ratios and K$_{eq}$ determined again. The value reported is an average of the two experimental equilibrium constants. The two values were always within 20% of one another.

β-1-Chloro-endocyclopentadiene. A 100 mL 3 neck round bottom equipped with an argon inlet was charged with 10 g (67.5 mmols) of α-1-hydroxyendodicyclopentadiene.[4] The flask was purged with Ar and 30 mL CCl$_4$ (distilled from P$_2$O$_5$) was added via syringe. PØ$_3$ (19.7 g, 75.2 mmols) was added. The reaction was then stirred under Ar at 60°C for 9 hrs. The clear solution formed a white precipitate of Ø$_3$PO. The reaction was cooled to room temperature and 50 mL pentane was added to precipitate the remaining Ø$_3$PO. The solution was filtered through a 7 cm coarse frit with a 1 cm layer of silica gel. The precipitate was then washed with 3 X 40 mL of ether. The organic layer was then reduced in volume to a light yellow oil. The oil was vacuum distilled at 35°C and 5 torr. Yield 8.5 g (75%). ^{1}H NMR (CDCl$_3$) (400 MHz JEOL GX-400) 5.92, 5.84, 5.74, 5.51 (each 1 H, m, olefinic), 1.36, 1.54 (each 1 H, d, CH$_2$ bridge), 2.82, 3.07 (each 1 H, s, bridgeheads), 2.97, 3.44 (each 1 H, m, fused bridgeheads), 4.27 (1 H, s, CHCl); ^{13}C NMR (CDCl$_3$), 137.2, 137.8, 133.3, 131.3, 66.1, 54.8. 54.2, 51.1, 45.1, 45.0. Anal., Calcd: C, 72.07: H, 6.65. Found: C, 72.32: H, 6.48.

Lithium Chlorocyclopentadienide. Two medium Schlenk tubes were connected by a Kontes valve stopcock to a glass bead filled 2 cm X 50 cm glass tube equipped with a vacuum attachment. 3-chlorodicyclopentadiene (18.7 g, 112.6 mmols) was syringed into the Schlenk tube and degassed twice. The

chlorodicyclopentadiene was frozen and the entire apparatus evacuated to 0.002 torr. The tube was heated under vacuum to 450°C in an oven. The chlorodicyclopentadiene was thawed and heated to 90°C. The volatiles were collected in the second Schlenk tube cooled in liquid nitrogen. The pyrolysis took about an hour. The tube was filled with Ar and warmed to 0°C. The volatiles were kept at 0°C and used immediately. (The volatiles can be stored at -50°C for weeks with only slight decomposition.) Yield 18.0 g (96%). The solution (all 18 g) of the cyclopentadiene and chlorocyclopentadiene was cannulated into 180 mL THF (distilled from Na benzophenone ketal) at 0°C. The yield of chlorocyclopentadiene is calculated by assuming a 1:1 ratio of cyclopentadiene to chlorocyclopentadiene after pyrolysis. In this case, 44.4 mL (0.9 eq., 97.2 mmols) of 2.2 M nBuLi in hexane was added dropwise to the THF solution over a 5 minute period. The reaction was then stirred at room temperature for $\frac{1}{2}$ hr and the volume reduced by half with vacuum. The THF solution was then cannulated in to 500 mL of vigorously stirred pentane (distilled from Na benzophenone ketyl) at -78°C. A pink precipitate was formed and was collected by filtration at -78°C. The pink solid was washed twice with 30 mL pentane at -78°C, dried in vacuo, and tranferred in a dry box. Yield 9.5 g (80% based on chloroendodicyclopentadiene) ^{1}H NMR d8 THF, 5.47 s; ^{13}C NMR, 102.5 and 102.0.

Bischlorocyclopentadienyl Titanium Dichloride. A 500 mL Schlenk round bottom was charged with lithium chlorocyclopentadienide (8.12 g, 76.6 mmols) in a dry box. Ether, 200 mL (distilled from Na benzophenone ketyl) was added via syringe and the salt suspended by stirring. The reaction

mixture was cooled to 0°C and 4.2 mL (38.3 mmols) TiCl$_4$ was added via syringe. Immediately, the color turned dark red and the mixture was stirred for one half hour at room temperature. Aqueous HCl (40 mL, 3M) was syringed in and the reaction vigorously stirred for 5 minutes. A red precipitate formed. The reaction was filtered in air through a coarse frit and the red brick solid washed with 4 x 20 mL EtOH then 4 x 20 mL ether. The precipitate was dried under vacuum. Yield 8.2 g (67%). An analytical sample can be prepared by sublimation at 220°C at (0.005 torr). The ^{1}H NMR was identical to the literature.[1] Anal. Calcd: C, 37.78: H, 2.54. Found: C, 37.44: H, 2.51.

Table 12: Reaction Order Studies

Metalla-cycle	Trap	mg or µl Trap	eq. Trap	Sol-vent	C°	Order	$k_{obs}s^{-1}$	Additional Comments
1	A	7.0	1.1	Ben	55	1st	$4.33 \cdot 10^{-4}$	
3	A	6.5	1.1	Tol	4	2nd	$2.47 \cdot 10^{-3} m^{-1}$	
1	A	7.0	1.1	Ben	55	2nd	$2.53 \cdot 10^{-4} m^{-1}$	20µl neohexene

A = diphenylacetylene, Ben = C$_6$D$_6$, Tol = D^8-toluene

Table 13: Saturation Kinetics on 2

Metalla-cycle	Trap	mg or µl Trap	eq. Trap	Sol-vent	C°	Order	$k_{obs}s^{-1}$
2	A	10.0	1.4	Tol	5	1st	$1.00 \cdot 10^{-3}$
2	A	21.7	3.5	Tol	5	1st	$1.29 \cdot 10^{-3}$
2	A	40.5	6.6	Tol	5	1st	$1.43 \cdot 10^{-3}$
2	A	59.3	9.7	Tol	5	1st	$1.36 \cdot 10^{-3}$
2	B	2.0	0.7	Tol	5	1st	$1.25 \cdot 10^{-3}$
2	B	4.0	1.5	Tol	5	1st	$1.22 \cdot 10^{-3}$
2	B	10.0	3.7	Tol	5	1st	$1.22 \cdot 10^{-3}$
2	B	20.0	7.4	Tol	5	1st	$1.12 \cdot 10^{-3}$
2	B	45.0	16.3	Tol	5	1st	$1.09 \cdot 10^{-3}$
2	C	4.0	0.9	Tol	5	1st	$6.98 \cdot 10^{-4}$
2	C	8.0	1.8	Tol	5	1st	$9.10 \cdot 10^{-4}$
2	C	16.0	3.6	Tol	5	1st	$1.14 \cdot 10^{-3}$
2	C	30.0	7.2	Tol	5	1st	$1.11 \cdot 10^{-3}$
2	C	60.0	14.3	Tol	5	1st	$1.18 \cdot 10^{-3}$

A = diphenylacetylene, b = dimethylacetylene, C = neohene, Tol = D^8-toluene

Table 14: Saturation Kinetics on 3

Metalla-cycle	Trap	mg or µl Trap	eq. Trap	Sol-vent	C°	Order	k_{obs} s^{-1}
3	A	4.0	0.77	Tol	0	1st	$1.3 \cdot 10^{-4}$
3	A	20.0	4.1	Tol	0	1st	$2.80 \cdot 10^{-4}$
3	A	40.0	8.4	Tol	0	1st	$3.45 \cdot 10^{-4}$
3	A	80.0	16.8	Tol	0	1st	$3.56 \cdot 10^{-4}$
3	A	6.0	0.84	Tol	0	1st	$1.7 \cdot 10^{-4}$
3	A	15.0	1.6	Tol	0	1st	$2.45 \cdot 10^{-4}$
3	A	31.4	4.4	Tol	0	1st	$2.98 \cdot 10^{-4}$
3	A	50.0	7.0	Tol	0	1st	$3.15 \cdot 10^{-4}$
3	B	4.0	1.27	Tol	0	1st	$3.72 \cdot 10^{-4}$
3	B	20.0	6.4	Tol	0	1st	$3.78 \cdot 10^{-4}$
3	B	40.0	12.7	Tol	0	1st	$3.52 \cdot 10^{-4}$
3	B	60.0	19.2	Tol	0	1st	$3.72 \cdot 10^{-4}$

A = diphenylacetylene, B = dimethylacetylene, Tol = D^8-toluene

Table 15: Pseudo First Order on 8

Metalla-cycle	Trap	mg or µl Trap	eq. Trap	Sol-vent	C°	Order	$k_{obs}s^{-1}$
8	D	10.0	1.8	Ben	25	1st	$1.45 \cdot 10^{-3}$
8	D	25.0	4.6	Ben	25	1st	$2.32 \cdot 10^{-3}$
8	D	50.0	9.2	Ben	25	1st	$3.12 \cdot 10^{-3}$
8	D	100.0	18.3	Ben	25	1st	$4.28 \cdot 10^{-3}$
8	D	150.0	27.4	Ben	25	1st	$5.73 \cdot 10^{-3}$
8	E	5.0	1.2	Ben	25	1st	$9.52 \cdot 10^{-4}$
8	E	20.0	5.2	Ben	25	1st	$3.58 \cdot 10^{-3}$
8	E	40.0	9.4	Ben	25	1st	$4.28 \cdot 10^{-3}$
8	E	80.0	18.8	Ben	25	1st	$5.43 \cdot 10^{-3}$
8	E	120.0	28.0	Ben	25	1st	$6.67 \cdot 10^{-3}$
8	A	15.2	2.3	Ben	25	1st	$2.95 \cdot 10^{-4}$
8	A	31.6	4.8	Ben	25	1st	$4.78 \cdot 10^{-4}$
8	A	46.7	7.0	Ben	25	1st	$6.76 \cdot 10^{-4}$
8	C	6.0	1.2	Ben	25	1st	$1.8 \cdot 10^{-4}$
8	C	20.0	4.2	Ben	25	1st	$3.38 \cdot 10^{-4}$
8	C	40.0	8.3	Ben	25	1st	$5.27 \cdot 10^{-4}$
8	C	80.0	16.1	Ben	25	1st	$7.75 \cdot 10^{-4}$
8	C	120.0	24.7	Ben	25	1st	$1.23 \cdot 10^{-3}$

D = 4-octyne, E = 3-hexyne, A = diphenylacetylene, C = neohene, Ben = C_6D_6

Table 16: Phosphine Equilibration

Phosphine Adduct	Phosphine	µl Phosphine	eq. Phosphine	Solvent	C°	Order	$k_{obs}s^{-1}$
8	A	2	0.45	Tol	0	1st	$4.11 \cdot 10^{-5}$
8	A	4	0.91	Tol	0	1st	$9.40 \cdot 10^{-5}$
8	A	8	1.80	Tol	0	1st	$1.26 \cdot 10^{-4}$
8	A	16	3.64	Tol	0	1st	$1.45 \cdot 10^{-4}$
8	A	32	7.27	Tol	0	1st	$1,58 \cdot 10^{-4}$
8	A	64	14,5	Tol	0	1st	$1.63 \cdot 10^{-4}$
9	B	2	0.93	Tol	0	1st	$4.45 \cdot 10^{-3}$
9	B	4	1.86	Tol	0	1st	$6.59 \cdot 10^{-3}$
9	B	8	3.72	Tol	0	1st	$8.14 \cdot 10^{-3}$
9	B	16	7.45	Tol	0	1st	$8.67 \cdot 10^{-3}$
9	B	32	14.9	Tol	0	1st	$8.92 \cdot 10^{-3}$
9	B	64	29.8	Tol	0	1st	$9.10 \cdot 10^{-3}$

$A = PMe_2\phi$, $Tol = d_8$-toluene, $B = PMe_3$,

Table 17: $1/k_{obs}$ Kinetics

Phosphine Adduct	Trap	μl Trap	μl PMe$_3$	Solvent	C°	Order	k_{obs}s^{-1}
8	A	40	20	Ben	25	1st	$1.39 \cdot 10^{-3}$
8	A	40	30	Ben	25	1st	$9.65 \cdot 10^{-4}$
8	A	40	40	Ben	25	1st	$8.17 \cdot 10^{-4}$
8	A	40	50	Ben	25	1st	$6.15 \cdot 10^{-4}$

A = 3-hexyne, Ben = C_6D_6

REFERENCES

(1) Lee, J.B.; Gajda, G.J.; Schaefer, W.P.; Howard, T.R.; Ikariga, T.; Straus, D.A.; Grubbs, R.H. *J. Am. Chem. Soc.* **1981**, *103*, 7358.

(2) (a) Clawson, L.E.; Buchwald, S.L.; Grubbs, R.H. *Tetrahedron Lett.* **1984**, *50*, 5733; (b) Brown-Wensley, K.A. Ph.D. Thesis, California Institute of Technology, Pasadena, California, 1981; (c) Pine, S.H.; Yahler, R.; Evans, D.A.; Grubbs, R.H. *J. Am. Chem. Soc.* **1980**, *102*, 3270; (d) Pine, S.H.; Pettit, R.J.; Geib, G.D.; Cruz, S.G.; Gallego, C.H.; Tijerina, T.; Pine, R.D. *J. Org. Chem.* **1985**, *50*, 2316; (e) Cannizzo, L.F.; Grubbs, R.H. *J. Org. Chem.* **1985**, *50*, 2316; (f) Stille, J.R.; Grubbs, R.H. *J. Am. Chem. Soc.* **1986**, *108*, 855; (g) For review see: Brown-Wensley, K.A.; Buchwald, S.L.; Cannizzo, L.F.; Clawson, L.E.; Ho, S.; Meinhart, J.D.; Stille, J.R.; Strauss, D.; Grubbs, R.H. *Pure Appl. Chem.* **1986**, *108*, 855.

(3) (a) Stille, J.R.; Grubbs, R.H. *J. Am. Chem. Soc.* **1983**, *105*, 1664; (b) Chou, T.; Huang, S. *Bull. Inst. Chem. Academia Sinica* **1984**, *31*, 41.

(4) Buchwald, S.L.; Anslyn, E.V.; Grubbs, R.H. *J. Am. Chem. Soc.* **1985**, *107*, 1766.

(5) (a) Tebbe, F.N.; Parshall, G.W.; Overall, D.W. *J. Am. Chem. Soc.* **1979**, *101*, 5074; (b) Klabunde, U.; Tebbe, F.N.; Parshall, G.W.; Harlow, R.L. *J. Mol. Catal.* **1980**, *8*, 37; (c) Howard, T.R.; Lee, J.B.; Grubbs, R.H. *J. Am. Chem. Soc.* **1980**, *102*, 6876; (d) Lee, J.B.; Ott, K.C.; Grubbs, R.H. *J. Am. Chem. Soc.* **1982**, *104*, 7491; (e) Straus, D.A.; Grubbs, R.H. *J. Mol. Catal.* **1985**, *28*, 9.

(6) (a) Gilliom, L.R.; Grubbs, R.H. *J. Am. Chem. Soc.* **1986**, *108*, 733; (b) For a review on ring opening polymerization, Calderon, J.J. *Macromol. Sci.*

Revs. **1972**, *C7(1)*, 105 and Katz, J.J.; Lee, S.J.; Shippey, M.A. *J. Mol. Catal.* **1980**, *8*, 219.

(7)　(a) Mackenzie, P.B.; Ott, K.C.; Grubbs, R.H. *Pure and Appl. Chem.* **1984**, *56*, 59; (b) Park, J.W.; Mackenzie, P.B.; Schaefer, W.P.; Grubbs, R.H. *J. Am. Chem. Soc.* **1986**, *108*, 6402-6404.

(8)　(a) Thoi, H.H.; Ivin, K.J.; Rooney, J.J. *J. Mol. Catal.* **1982**, *15*, 245; (b) Leconte, M.; Basset, J.M. *J. Am. Chem. Soc.* **1979**, *202*, 7296; (c) Calderon, N.; Lawerence, J.P.; Ofstead, E.A. *Adv. Organomet. Chem.* **1979**, *17*, 449.

(9)　Bobrowicz, F.W.; Goddard, W.A., III in <u>Modern Theoretical Chemistry: Methods of Electronic Structure Theory</u>, Schaefer, H.F., III, Ed., Plenum Press:New York, 1977, Vol. 3, Chapter 4, pp. 79-127.

(10)　(a) Nelson, C.W., Jr.; Goddard, W.A., III *J. Chem. Phys.* **1969**, *51*, 716; (b) Steigerwald, M.L.; Goddard, W.A., III *J. Am. Chem. Soc.* **1984**, *106*, 308.

(11)　Upton, T.H.; Rappé, A.K. *J. Am. Chem. Soc.* **1985**, *107*, 1206.

(12)　Eisenstein, O.; Hoffmann, R.; Rossi, A.R. *J. Am. Chem. Soc.* **1981**, *103*, 5582.

(13)　(a) Francl, M.M.; Hout, R.F.; Hehre, W.J. *Organometallics* **1983**, *2*, 815; (b) Gregory, A.P.; Mintz, E.A. *J. Am. Chem. Soc.* **1985**, *107*, 2179; (c) Rappé, A.K.; Goddard, W.A., III *J. Am. Chem. Soc.* **1982**, *104*, 297.

(14)　Lauder, J.W.; Hoffmann, R. *J. Am. Chem. Soc.* **1976**, *98*, 1729.

(15)　(a) Hughes, W.B. *J. Am. Chem. Soc.* **1970**, *92*, 532; (b) Grubbs, R.H. *Prog. Inorg. Chem.* **1978**, *24*, 1; (c) Calderon, N.; Lawerence, J.P.; Olstead, E.A. *Adv. Organomet. Chem.* **1979**, *17*, 449.

(16)　Hartner, Jr., F.W.; Schwartz, J.; Cleft, S.M. *J. Am. Chem. Soc.* **1983**, *105*, 601.

(17)   (a) Tebbe, F.N.; Harlow, R.L. *J. Am. Chem. Soc.* 1980, *102*, 6149; (b) McKinney, R.J.; Tulip, T.H.; Thorn, D.L.; Coolbaugh, T.S.; Tebbe, F.N. *ibid* 1981, *103*, 5584; (c) Howard, T.R.; Lee, J.B.; Grubbs, R.H. *ibid* 1980, *102*, 6876; (d) Meinhart, J.D.; Santarsiero, B.D.; Grubbs, R.H. *ibid* 1986, *108*, 3318.

(18)   The simplifications are extensions of reasoning presented in first year physical chemistry books such as Moore, W.J. Physical Chemistry 4th Ed., Prentice Hall, Inc.:New Jersey, 1964, Chapter 9, pp.324.

(19)   Comprehensive Organometallic Chemistry Wilkinson, G.; Stone, F.G.A.; Abel, E.W., Oxford, Perganon Press, Vol. 3, pp.324.

(20)   Stryer, L. Biochemistry, W.H. Freeman and Company: San Francisco, 1975, Chapter 1, pp.124.

(21)   Collins, C.J.; Bowman, N.S. Isotope Effects in Chemical Reactions Van Nostrand Reinhold Company: New York, 1970.

(22)   Finch, W.C.; Anslyn, E.V.; Grubbs, R.H. unpublished results.

(23)   Straus, D.A.; Grubbs, R. H. *Organometallics*, 1982, *1*, 1658.

(24)   Meinhart, J.D.; Grubbs, R.H. unpublished results.

(25)   Yoshida, T.; Negishi, E.I.; *J. Amer. Chem. Soc.* 1981, *103*, 1276.

(26)   Ott, K.C.; de Boer, E.J.M.; Grubbs, R.H. *Organometallics*, 1984, *3*, 223.

(27)   Hart, D.W.; Blackburn, T.F.; Schwartz, J. *J. Am. Chem. Soc.*, 1975, *97*, 679.

(28)   Supplied as part of the JOEL FX-90Q Operator Software.

(29)   Gordon, A.J. The Chemists' Companion: A Handbook of Practical Data, Techniques and References. Wiley: New York, 1972.

(30)   (a) Foley, H.C.; Strubinger, L.M.; Fargos, T.S.; Geoffroy, G.L. *J. Amer. Chem. Soc.* **1983**, *105*, 3064; (b) Casey, C.P.; Shusterman, A.J.; Vollendorf, N.W., Haller, K.J. *J. Amer. Chem. Soc.* **1982**, *104*, 2417 and references therein.

(31)   Swager, T.M.; Cannizzo, L.F.; Novak, B.M.; Virgil, S.; Grubbs, R.H. unpulished results.

(32)   Herzberg, G. Molecular Spectra and Molecular Structure, Van Nostrand Reinhold Com.: New York, 1945.

(33)   Finch, W.C., Ph.D. Thesis, California Institute of Technology, 1986.

(34)   Chien, J.C.W. *J. Phys. Chem.* **1963**, *67*, 2477.

(35)   Ott, K.C.; Grubbs, R.H. *Organometallics* **1984**, *3*, 223.

(36)   Gassman, P.G.; Macomber, D.W.; Hershberger, J.W. *Organometallics* **1983**, *2*, 1470.

(37)   Gassman, P.G.; Campbell, W.H.; Macomber, D.W. *Organometallics* **1984**, *3*, 385.

(38)   Levy, G.C.; Nelson, G.L. Carbon-13 Nuclear Magnetic Resonance for Organic Chemists, Wiley, New York:1972, pp. 25-28.

(39)   Hammond, G.S. *J. Am. Chem. Soc.* **1955**, *77*, 334.

(40)   For a discussion of bonding in these systems see Rappé, A.K.; Goddard, W.A. *J. Am. Chem. Soc.* **1982**, *104*, 297.

(41)   Conway, B.G.; Rausch, M.D. *Organometallics* **1985**, *4*, 688.

(42)   Gassman, P.G.; Winter, C.H. *J. Am. Chem. Soc.* **1986**, *108*, 4228.

(43)   Heydlauf *Eur. J. Pharmacol.* **1969**, *6*, 340.

(44)   Woodward, R.B.; Katz, T.J. *Tetrahedron* **1959**, *5*, 70.

(45)   "Chem. Abstracts" *54*, 18546f, 1960.

CHAPTER 2

THE RING OPENING METATHESIS POLYMERIZATIONS OF CYCLOHEPTENE AND CYCLOOCTENE

ABSTRACT

The ring opening metathesis polymerizations of cyclooctene and cycloheptene were studied as a function of the polymer molecular weights and the kinetics of the reactions. It was found that the molecular weights of the polymers depended only slightly upon the reaction time and monomer concentration. The first order kinetic plots of the polymerization reactions showed rapid catalyst decomposition and a significant kinetic order in olefin. These results are discussed in an attempt to better understand the mechanism and relative rates of polymerization of highly strained and slightly strained olefins.

INTRODUCTION

Polymerization of olefins is an industrially important process.[1] Several polymers including trans-polyoctenamer,[2] polynorbornene,[3] polyethylene,[4] and polyproplyene[5] are produced industrially. The polymerization reactions are catalyzed by transition metal complexes and can be classified either as addition (Zeigler-Natta) or ring opening polymerizations.

The Zeigler-Natta polymers[6] are formed by alkene insertion into an early metal- carbon σ bond to form a new metal-carbon σ bond (Eq. 1). The metal center is usually a Ti or Zr halide, and the reaction requires a Lewis acid co-catalyst such as $AlEtCl_2$.
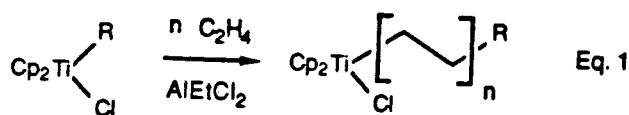
The ring opening metathesis polymerization[7] (ROMP) of cyclic olefins was first found by Natta as a competing reaction to the Zeigler-Natta polymerizations.[8] Mechanistic studies have now firmly established the intermediacy of alternating chain-propagating metal carbenes and metallacycles[9](Eq.2).
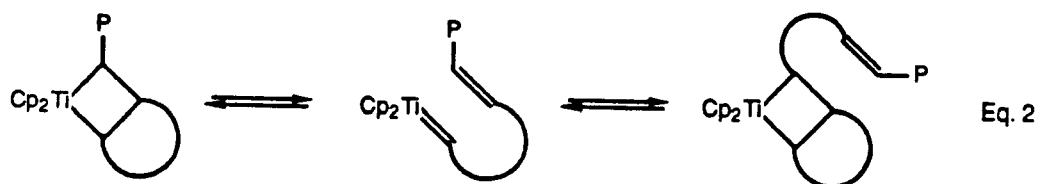
In this chapter, the ring opening metathesis polymerizations of cyclooctene and cycloheptene by titanocene metallacyclobutanes are presented. In addition,

the kinetics of polymerization of slightly strained cyclic olefins is discussed in light of new and old results.

RESULTS AND DISCUSSION

a. Cyclooctene and Cycloheptene Polymerizations

Metallacycle **1** produces exclusively the substituted carbene at 23 °C and polymerizes norbornene at 65 °C to give narrow-dispersed polynorbornene.[10] In addition, **1** polymerizes cyclopentene at 35 °C when a large excess of cyclopentene is employed.[11] The polymerization of cyclopentene with **1** is initiated by the consumption of two equivalents of cyclopentene to give metallacycle **2**. The successful polymerization of cyclopentene prompted the investigation of cyclohexene, cycloheptene and cyclooctene polymerizations.
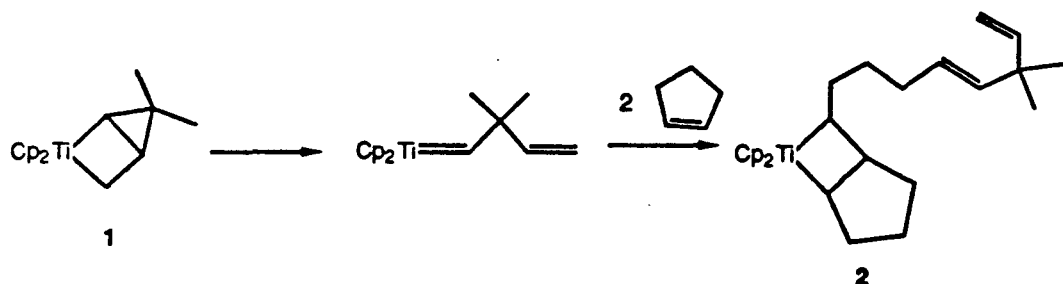
The reaction of metallacycle **1** with 2 equivalents of cyclohexene, cycloheptene or cyclooctene resulted in decomposition of the metallacycle. Thus, metallacycles analogous to **2** formed from cyclohexene, cycloheptene and cyclooctene are unstable at room temperature. This does not demonstrate that polymerization of these olefins will not occur at high olefin concentration due to more efficient trapping of the alkylidene formed. Polymerization of these strained cyclic alkenes is driven by an enthalpy change due to loss of ring strain. In contrast, the entropy term favors several monomers versus a polymer. Table 1 shows the ring strain of the C_3 to C_8 cyclic olefins. The ring strain of cyclohexene is not large enough at room temperature to cause polymerization. Indeed, the reaction of **1** with 100

equivalents of cyclohexene only resulted in catalyst decomposition. Polymerizations of cycloheptene and cyclooctene were, however, achieved with 20-100 equivalents of olefin using 1 as the catalyst.

Table 1: Ring Strain

Olefin	$H^{\circ}_{f,298}$ Correction[17]
▷	53.7
☐	29.8
⬠	5.9
⬡	1.4
heptagon	5.4
octagon	6.0

In order to show that the metallacycles formed by the reaction of 1 with cycloheptene and cyclooctene are viable species, the photochemical reaction of 1 with these cyclic alkenes was investigated. Upon photolysis of 1 in the presence of one equivalent of olefin, the expected trisubstituted metallacycles shown in Figure 1 were formed. These metallacycles also polymerize the cyclic olefins when a large excess of olefin is used and yield roughly the same polydispersities as 1.

The polymerization results are summarized in Table 2. The resulting polymers were isolated by end-capping with acetone[11] and precipitation into MeOH. The polymers were then characterized by ^{1}H and ^{13}C NMR and GPC. The NMR spectra were consistent with those previously reported for polyoctenamer and polyheptenamer.[12] The number of monomers per chain was determined by integration of the olefinic resonances of the polymer versus the olefinic resonances of
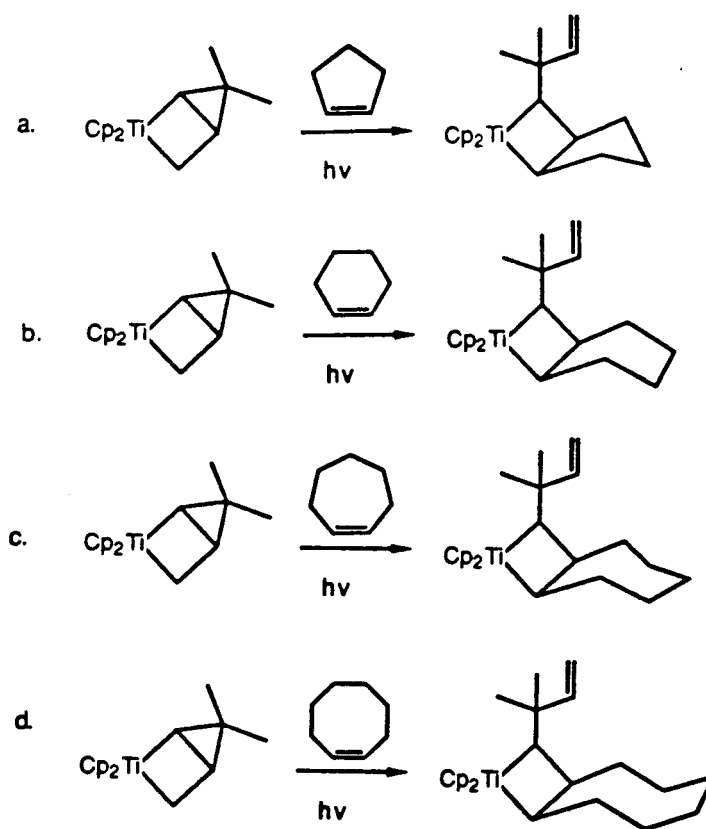
Figure 1: Photochemical reactions of **1** with cyclic olefins.

the end group -C(CH$_3$)$_2$CH=CH$_2$ derived from the catalyst. The molecular weights determined by ^{1}H NMR spectra integration were lower than those found by GPC (versus polystyrene standards), and a conversion factor of approximately 1.7 is suggested. The polydispersities (M$_w$/M$_n$) were not as low as those previously measured for norbornene polymerization,[10a] but are similar to those measured in cyclopentene polymerizations[11] and are in the range of living systems. The increase in dispersities with longer reaction times is indicative of both secondary metathesis of the carbon-carbon double bonds of the polymer and catalyst decomposition. The ratio of cis to trans double bonds was consistently one for both polycyclooctene and polycycloheptene. As the polymerizations proceed, the reactions darken and

Table 2: Polymer Molecular Weights

Run #	Olefin	[Olefin] M	Total Time(hr)	MW[a] (NMR)	Mn (GPC)	Mw (GPC)	n[b] (GPC)	Correction Factor
1	cycloheptene	4.27	6	no polymer isolated				
2	cycloheptene	4.27	21	960	2211	2920	1.32	2.3
3	cycloheptene	4.27	27	1152	1990	2511	1.26	1.7
4	cycloheptene	2.13	21	1056	1772	2126	1.19	1.7
5	cycloheptene	6.41	21	1152	2201	2613	1.18	1.9
6	cyclooctene	3.86	6	9460	15677	29678	1.89	1.7
7	cyclooctene	3.86	13	12908	21944	52735	2.40	1.7
8	cyclooctene	3.86	27	11770	19588	33940	1.73	1.7
9	cyclooctene	1.93	13	9130	10934	18934	1.81	1.2
10	cyclooctene	5.79	13	13255	19693	34649	1.76	1.5

a. Determined by ^1H NMR: ((methylene protons of the end group) --- (vinyl protons of polymer)
   X (MW of alkene))

b. Polydispersity

eventually turn black at prolonged reaction times (36 hours).

Examination of Table 2 reveals several trends. The molecular weights of poly-cycloheptene slightly increase as a function of reaction time. After 6 hours, no polymer is isolated, whereas after a reaction time of 27 hours, a polymer of molecular weight 1152 was isolated. The molecular weights, however, remained between 960 and 1152 regardless of cycloheptene concentration. In contrast, the molecular weights of polycyclooctene increased as a function of increasing concentration of cyclooctene, whereas there was little dependence on the reaction time. At a low concentration of 1.93 M cyclooctene, a polymer of molecular weight 9130 was formed. At a concentration of 5.79 M cyclooctene, a polymer of molecular weight 13255 was formed. At a constant molarity of 3.86 and varied reaction times, the polymer molecular weights remained between 9460 and 12908. This data leads one to conclude that the reaction is zero order in cycloheptene and has a small order in cyclooctene. This conclusion however, is false as is explained in the next section. Since the molecular weight of cyclooctene has little dependence on the reaction time, the catalyst must be decomposing early in the reaction and polymerization stops. The small dependence of polymer molecular weights on time or monomer concentration makes these polymerizations hard to control.

The polymerization of cycloheptene is much less efficient than the polymerization of cyclooctene due to its much lower strain energy. In 13 hours, a cyclooctene polymer of molecular weight 12908 was formed, whereas in 21 hours, a cycloheptene polymer of molecular weight 960 was formed. Also, the polymerization of cyclooctene is more efficient than of cyclopentene. In 24 hours, a cyclooctene polymer of approximately 9000 molecular weight was formed. A cyclopentene polymer of molecular weight 4000 took 98 hours to form.[11]

The major drawback to cyclooctene and cycloheptene polymerization compared to cyclopentene is the much more rapid catalyst decomposition. This rapid decomposition must be due to the instabilty of the resultant trisubstituted metallacycle. This is supported by two results. First, the cyclopentene metallacycle **3** cleaves at room temperature, whereas the cyclohexene metallacycle **4** cleaves near 0 °C. Thus, the larger fused ring metallacycles are less stable. Second, metallacycle **2** is isolable, whereas the analogous larger ring metallacycles are not isolable. Both these results indicate that the trisubsituted metallacycle cleavage is occurring at a rapid rate at room temperature, and the cyclic olefins are not efficient traps for the titanocene alkylidene formed. In order to observe polymerization, the rate of trapping of the titanocene alkylidene must be faster than the decomposition routes available. This only occurs for very high concentrations of monomer. Even at high monomer concentrations, catalyst decompostion occurs, limiting the usefulness of this polymerization method.
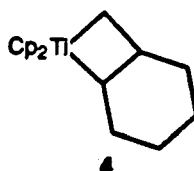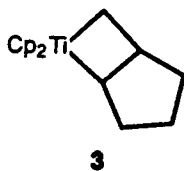
b. *Kinetics of Polymerization of Cyclooctene and Cycloheptene*

The overlap of signals in the ^{1}H NMR spectra of the cyclic olefins and poly(1-alkylidene) precluded use of ^{1}H NMR for kinetic studies. No attempt was made to follow the kinetics by VPC, even though qualitatively, the general trend of increasing rates of cyclic olefin consumption with higher concentrations of olefin was observed.

Quantitative kinetic data was obtained by following the ^{13}C resonances of the olefin. ^{13}C NMR has been employed to determine the kinetics of polymerization of ethylene by a scandium catalyst[13] and the polymerization of cyclopentene[11] by 1. Utilizing this method, the polymerizations of cyclooctene and cycloheptene at 27 °C for several concentrations of monomer were studied. The kinetic data are presented in Table 3. These rates are initial rates measured over the first twenty percent of the reaction. A typical first order plot of the reaction of 1 with cyclooctene is shown in Figure 2. It can be observed from Figure 2 that the rate drops off dramatically after a certain point. The rate drop off at the end of the reaction is a consequence of the catalyst decomposing as it runs out of free olefin. The ^{13}C resonances of the cyclopentadienyl ligands can be observed to disappear toward the end of the polymerization also, due to slow decomposition of the metallacycle.

Table 3: Kinetic Data

Run #	Monomer	[M] M	Rate
1	Cyclooctene	1.54	1.38 E-4 s^{-1}
2	Cyclooctene	3.85	1.77 E-4 s^{-1}
3	Cyclooctene	6.18	2.83 E-4 s^{-1}
4	Cycloheptene	1.71	3.02 E-5 s^{-1}
5	Cycloheptene	4.27	4.27 E-5 s^{-1}
6	Cycloheptene	6.80	5.73 E-5 s^{-1}

Prior to catalyst decomposition, the rate of olefin consumption is first order in catalyst and has a small order in olefin. The kinetic order is dependent upon the olefin and is 0.31 for cyclooctene, 0.25 for cyclopentene[16] and 0.21 for cyclohep-
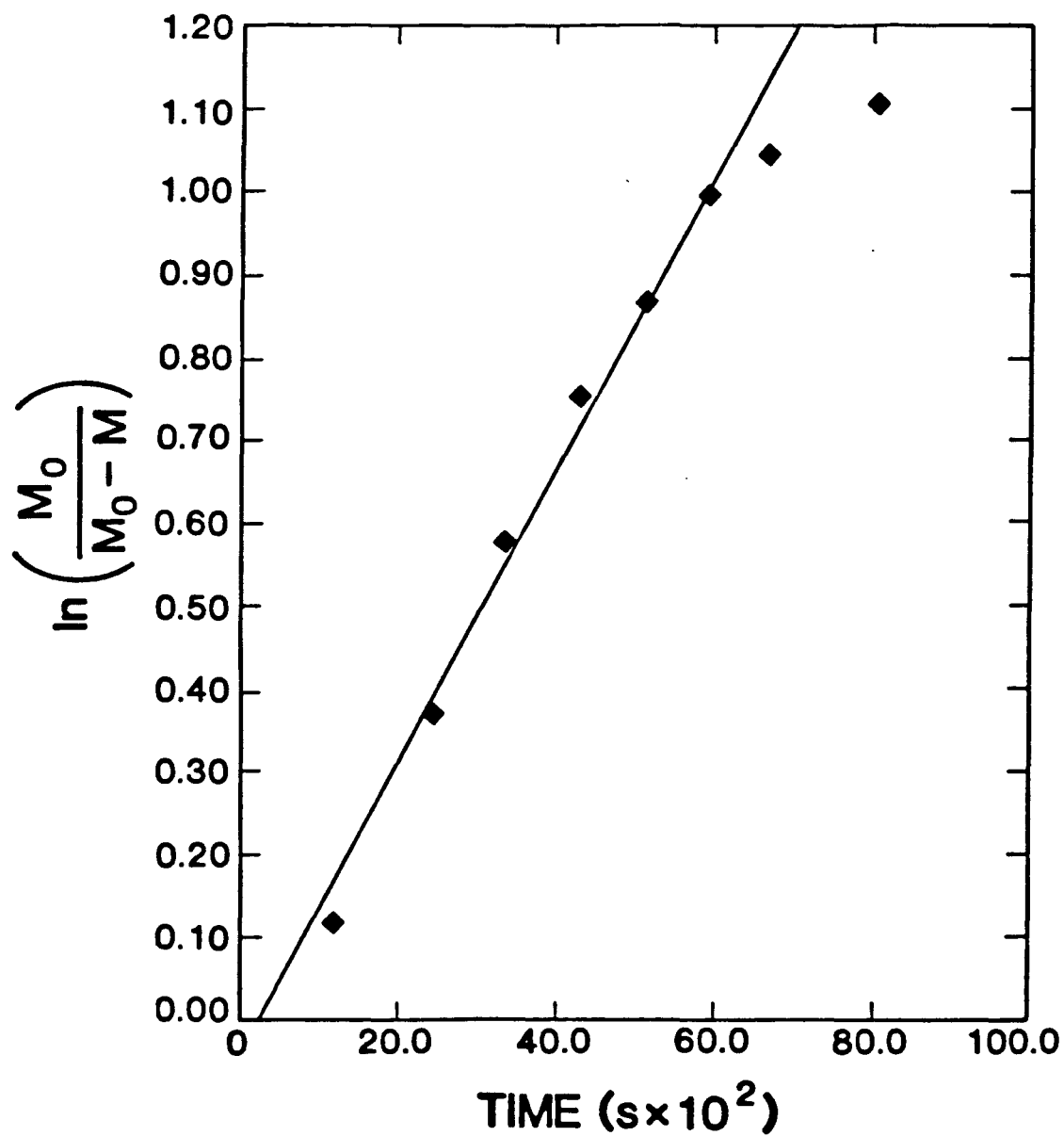
Figure 2: First order plot for kinetic run number 2: Table 3, rho =0.997, Sdv. y

$= 0.387 \times 10^{-1}$
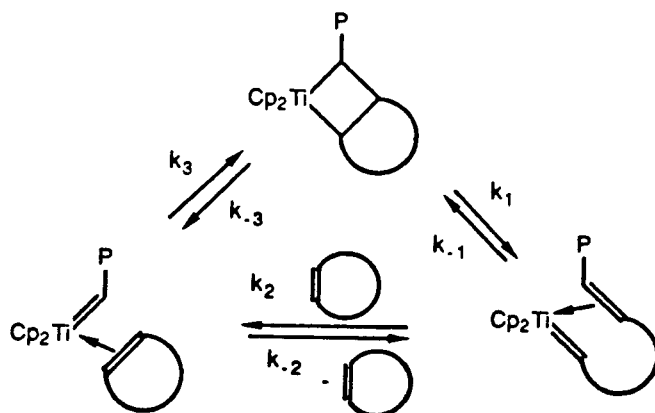
Scheme 1: ROMP mechanism for titanocene metallacyclobutanes.
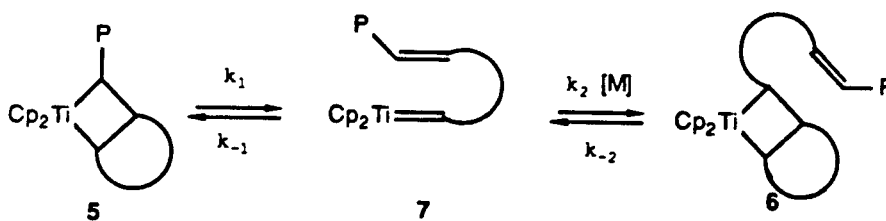
$$\frac{-d\,[M]}{dt} = \frac{(\,k_1 + k_{-2})\,k_2\,[C]\,[M]}{k_{-1} + k_2\,[M]} - k_{-2}\,[C]$$

$$= \frac{k_1\,k_2\,[C]\,[M]}{k_{-1} + k_2\,[M]} + \frac{k_{-2}\,k_2\,[C]\,[M]}{k_{-1} + k_2\,[M]} - k_{-2}\,[C]$$

1st Term   2nd Term   3rd Term

C = Catalyst
M = Monomer

Scheme 2: Simplified ROMP mechanism.

tene. The kinetic orders are similar, but the rate of polymerization of cyclooctene is greater than the rate for cyclopentene, which is greater than the rate for cyclo-heptene. All this data can be explained by analysis of the kinetic expression for olefin polymerization using 1.

Based on concepts presented in Chapter 1, a mechanism such as that shown in Scheme 1 probably best describes the polymerization reaction. Following the complexes in a clockwise direction represents polymerization, whereas the counterclockwise direction represents depolymerization. The kinetic expression for this mechanism is large and lends little insight into interpreting the experimental data. Furthermore, none of the rate constants can be obviously neglected since polymerization and depolymerization reactions are both probable for the slightly strained olefins studied. Thus, a simplification is shown in Scheme 2 along with its kinetic expression.

In Scheme 2, the propagating metallacycles 5 and 6 are indistinguishable during the polymerization, thus their concentrations can be assumed to be the same. The rate expression (derived using the steady state approximation for 7) is dependent upon both catalyst and olefin. This is the same expression as previously found in the polymerization of cyclopentene.[11] It is presented here in a nonsimplified form for easier analysis. The first term represents productive metathesis and olefin polymerization, whereas the third term represents depolymerization. In the cases studied, the monomer concentration remains constant (due to the large excess of monomer and the measurement of initial rates), and $k_{OBS} = k_1 k_2 [M] / (k_{-1} + k_2 [M])$. Thus, based on the type of reasoning presented in Chapter 1, the ratio of k_{-1} to $k_2 [M]$ determines the olefin dependence. In the polymerization of cyclopentene, cycloheptene and cyclooctene, the rate of self trapping (k_{-1}) is comparable

to the rate of free olefin trapping ($k_2[M]$), and thus, there is an olefin dependence. This dependence is similar for cyclopentene, cycloheptene and cyclooctene. Thus, the ratio of self trapping and free olefin trapping for each cyclic olefin is approximately the same. This is a reflection of the differential strain and steric interaction introduced into the transition state for trapping by free and pendant olefin being roughly the same for each olefin. The absolute rates of free and pendant olefin trapping for each olefin, however, could be very different.

The ratio of the first term to the third term determines the rate of polymerization. The rate determining steps for polymerization and depolymerization are k_1 and k_{-2}, respectively. In the polymerization of cycloheptene, the strain energy in the olefin is small and the terms dependent upon k_1 and k_{-2} are roughly the same. Therefore, the polymerization rate is slow since the terms dependent upon k_1 and k_{-2} do not cancel one another. In the case where strain makes k_1 (productive cleavage) much faster than k_{-2}, polymerization occurs and the first term is dominating.

The kinetics of polymerization of these simple cyclic olefins can be contrasted to the kinetics of polymerization of olefins with greater strain. The same mechanism and kinetic expression presented here can be used to examine the norbornene polymerization. In the polymerization of norbornene, the kinetic dependence on olefin was found to be zero.[10] In order to observe zero order dependence on norbornene, the rate of self trapping must be negligible compared to that of trapping by norbornene (k_{-1} much less than $k_2[M]$). It is not necessary to assume that depolymerization (k_{-2}) is negligible to observe zero order dependence on monomer. It is safe, however, to assume that depolymerization is negligible for highly strained rings and that the cleavage rate k_1 determines the observed rate of reaction. In

the polymerization of slightly strained rings, however, the rate is dependent on both the rate of polymerization and the rate of depolymerization. These relative rates are dependent on the strain in the cyclic olefin, with strain driving productive metathesis. In the first approximation, the greater the strain, the larger k_1 will be. Thus, the polymerization of norbornene could be predicted to be more rapid than the polymerization of the simple monocyclic C_5, C_7 and C_8 olefins due to its higher strain. This discussion, however, ignores any electronic, geometrical or steric differences introduced into the metallacycle due to the different olefin structures. The bicyclic structure of norbornene causes the metallacycle ring to be puckered and the transition state leading to metathesis to be sterically encumbered. The kinetic barrier to polymerization of norbornene is greater than for the simple cyclic olefins, even though the thermodynamic driving force (strain) is greater. In the case of comparable olefins, such as cyclopentene, cycloheptene and cyclooctene, the rate of polymerization parallels the strain energy.

The effect of transition state destabilization due to steric crowding is best demonstrated by the rate of cleavage of 1 and the tetramethyl cyclobutene metallacycle 8. These metallacycles cleave at approximately room temperature, even though it has been shown that cyclopropene[14] and cyclobutene[14] polymerize at -60 °C.

Cp₂Ti

8
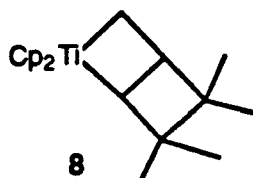
SUMMARY

Ring opening metathesis polymerizations of cycloheptene and cyclooctene can be performed at high monomer concentrations. The polymers obtained have low, but not excellent, polydispersities. The polydispersities and ability to control molecular weights are not ideal due to the fast rate of catalyst decomposition. Kinetics of the polymerization of cycloheptene and cyclooctene reveal a small dependence upon olefin. In constrast, the molecular weight (GPC) analysis showed little or no dependence upon olefin concentration. This is due to decomposition of the catalyst ending polymerization. The kinetic dependence upon monomer is due to the relative rates of trapping of the titanocene alkylidene by free monomer or pendant olefin being comparable. This kinetic order in monomer does not give any information on the rates of polymerization versus depolymerization. The rate of consumption of monomer reflects the relative rates of polymerization and depolymerization. These reactions are dependent upon both the catalyst's steric and electronic environment and the strain in the cyclic olefins.

EXPERIMENTAL

General Procedures

All work involving air and/or moisture sensitive compounds was performed using standard high vacuum or Schlenk techniques. Argon was purified by passage through columns of BASF RS-11 (Chemlog) and Linde 4A molecular sieves. All sample weighing of air and/or moisture sensitive compounds was performed in a Vacuum Atmosphere dry box under nitrogen. ^{1}H and ^{13}C NMR spectra were recorded on a JEOL FX-90Q (89.6 MHz ^{1}H, 22.53MHz ^{13}C) and a JEOL GX-400 (399.65 MHz ^{1}H, 100.67 MHz ^{13}C). Chemical shifts are referenced to residual protons on the deuterated solvents. Analytical gas chromatographic analyses (VPC) were performed on a Shimadzu GC-Mini 2 flame ionization instrument modified for capillary use and equipped with a Hewlett-Packard Model 339A integrator (column:0.24 mm X 15m DBI).

Gel permeation chromatographic (GPC) analyses utilized Shodex KF-803, 804, 805 and 805.5 columns, a spectroflow 757 absorbance detector (λ= 254nm), and a Knauer differential refractometer. GPC analyses were performed on 0.20-0.40 percent w/v solutions of polymer in CH_2Cl_2. Typically, an injection volume of 0.100-0.200 ml and a flow rate of 1.5ml/min were used. Calibration was based on narrow dispersity polystyrene standards (Polysciences) ranging from MW 450 to 19,600. The molecular weight averages and distribution were calculated by standard procedures[15] from the refractive index trace and were not corrected for peak broadening. Polymerization was carried out under N_2 in a heavy walled glass tube equipped with a stir bar, female 14/20 joint and a Teflon valve.

All metallacycles were prepared as previously described.[10,11,18] The olefin 3,3-dimethylcyclopropene was kindly provided by S.C. Virgil.

The monomers used in the polymerizations were prepared and purified as follows. Norbornene was purchased from Aldrich, refluxed over sodium, distilled into a thick walled tube equipped with a Teflon valve and kept in the dry box. Cyclopentene, cyclohexene, cycloheptene and cyclooctene were purchased from Aldrich, filtered through alumina (neutral grade, EM Sciences) and distilled from Na metal. All monomers were deoxygenated by two freeze-pump-thaw cycles and stored in the dry box. The toluene used in polymerizations and the d_8-toluene or d_6-benzene used for NMR studies were purified by distillation from sodium benzophenone ketyl into solvent flasks equipped with Teflon valves.

Photolysis was accomplished with either a 450 watt medium pressure mercury vapor Honovia lamp with pyrex filter or an Oriel 1000 watt Hg(Xe) arc lamp with UV and IR filtering.

NMR tube scale reactions were prepared in the dry box and capped with a rubber septum. All arc lamp photolysis experiments were prepared in sealable NMR tubes and were sealed under vacuum.

Reaction of 1 with Cycloalkenes: A 5mm NMR tube was charged with 10 mg 1 (3.8×10^{-5} mols), 0.4 mL d_8-toluene and 3.5 ul C_5H_8, or 4.5 ul C_6H_{10}, or 5.5 ulC_7H_{12}, or 6.5 ul C_8H_{14} (all 7.6×10^{-5} mols) were added via syringe at -100 °C. The reaction was photolyzed for three 15 minute intervals. After each 15 minute interval, the solution was recooled to -100 °C. Conversion was approximately 60 percent by ^{1}H NMR. If the reaction was photolyzed with an arc lamp for 15 minutes at -100°C, the conversion was approximately 95 percent by ^{1}H NMR. Spectral data is displayed in Table 4 for each product. The ^{1}H and ^{13}C resonances are assigned by comparison to the resonances of metallacycle 3 which were identified by the COSY and C-H correlated spectra shown in Figure 3.

Table 4: ^{1}NMR and ^{13}C NMR Resonances

Compound	^{1}NMR	^{13}C
	Cp: 5.42 (s,5H), 5.35 (s,5H) Me: 1.16 (s,3H), 1.12 (s,3H) olefin: 5.05 (q,2H), 6.02 (q,1H) alpha C: 2.70 (d,1H), 4.78 (m,1H) beta C's: 0.28 (m, 1H), 0.02 (m,1H) ring : 2.35 (m,2H), 2.17 (m,2H) 1.91 (m,1H), 1.65(m,2H)	109.5, 107.6 148.7, 137.2 115.8, 109.8 11.2, 19.8 45.8, 41.3, 39.9, 36.6 32.9, 29.8
	Cp: 5.76 (s,5H), 5.94 (s,5H) Me: 1.14 (s,3H), 1.18(s,3H) olefin: 6.05 (q,1H), 5.02 (q,3H) alpha: 2.66 (q, 1H), 2.83 (d,1H) beta: 0.42 (q,1H), -0.03 (q,1H) ring: 1.90(m,2H), 2.00(m,2H) 1.80(m,2H), 1.54(m,2H)	110.3, 108.5 150.0, 137.4 109.4, 107.9 11.8 96.6, 22.5, 31.0, 32.5 36.0, 46.7, 63.2
	Cp: 5.42 (s,5H), 5.55 (s,5H) Me: 1.04 (s,3H),1.07 (s,3H) olefin: 4.95 (q,2H), 6.00(q,1H) alpha: 2.95 (d,1H), 3.51 (t,1H) beta: 0.09 (q,1H), 0.55 (d,1H) ring: 2.04 (m,2H), 1.43(m,2H) 1.93 (m, 2H), 1.23(m,2H) 2.22 (m,1H)	109.2, 110.4 150.5, 137.1 108.0, 110.6 15.4 96.3, 29.6, 31.8, 33.1 34.4, 36.1, 38.9, 45.9
	Cp: 5.40 (s,5H), 5.43(s,5H) Me: 1.05 (s,3H), 1.85 (s,3H) olefin: 5.00 (q, 2H), 6.00 (q,1H) alpha: 3.60 (d,1H), 3.21 (t,1H) beta: -0.35 (m,1H), 0.05(m,1H) ring: 1.05 (m,2H), 1.85 (m,2H) 1.42 (m,2H), 1.63 (m,2H) 2.03 (m,2H)	108.8, 109.9 137.1, 149.3 111.2, 113.3 10.3 97.6, 26.8, 27.0, 29.7 32.8, 34.1, 36.5, 37.0 47.4
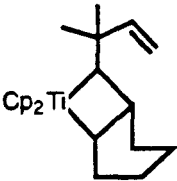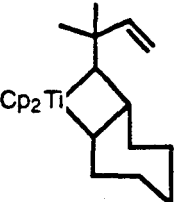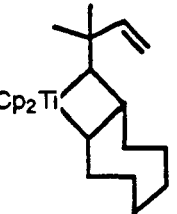
Figure 3: a) COSY spectra of **3**. b) C-H correlated spectra of **3**.
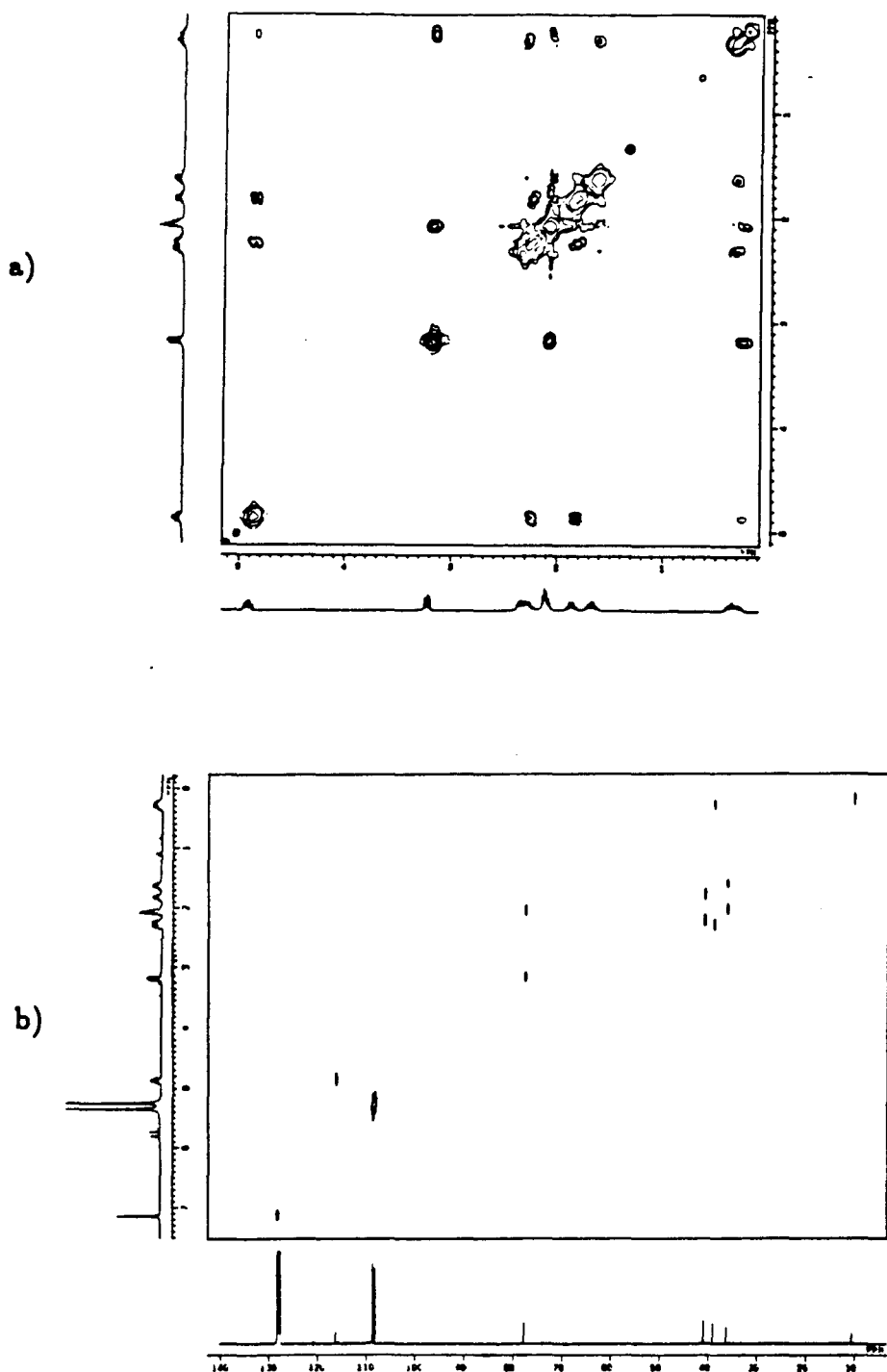
The COSY spectrum was recorded with a 90° pulse width (15 us) and a frequency window of 2640 Hz. 1024 points were collected in the f_2 domain and 256 slices were taken. The f_1 domain was then zero filled to 512 points. The C-H correlated spectrum was recorded with 4092 points, a 90° pulse width (7.5 us) and a spectral window of 14000Hz in the f_2 domain. An f_1 domain of 3100 Hz was used with 128 slices zero filled to 256. A pulse delay of 2.5 s was used.

Polymerization of Cycloheptene and Cyclooctene: In the polymerizations several different concentrations of **1** and cyclic olefins were employed (see Table 2). A typical procedure is given below.

A heavy walled tube equipped with a 14/20 female joint and a Teflon valve was charged with 25 mg **1** (9.6×10^{-5} mols) in the dry box. Toluene and the allotted amount of cyclic olefin were added via syringe at 23° C in the dry box. The solution was briefly stirred, capped, removed from the dry box and stirred at 23° C for the allotted time period. The solutions darkened with time and became black after approximately 48 hrs. The solution was then pipetted (in air) into 2 mL of acetone and allowed to stand for 30 minutes. A yellow precipitate appeared. Toluene was added to redissolve any precipitated polymer and the solution filtered through a 0.5 inch plug of silica gel. The silica gel was then washed with 2x5 mL toluene. The combined toluene solution was dried *in vacuo* to yield a light yellow oil. The oil was dissolved in the minimum amount of toluene and pipetted into rapidly stirred MeOH (5 mL) in a thick-walled centrifuge tube. The solution immediately turned cloudy and a precipitate was formed. The solution was centrifuged for 15 minutes and the mother liquor decanted off. The resultant oil was dried by blowing Ar over its surface and stored under an inert atmosphere.

^{13}C NMR Kinetics: Three 5 mm NMR tubes were charged with 20 mg **1**

(7.7x10^{-5} mols). Each NMR tube was cooled to 0 °C and the volume of solvent and cyclic olefin shown in Table 5 syringed into the tube. To run the kinetic experiments, each tube was placed in the NMR probe and allowed to equilibrate at 26.7 °C for 5 minutes. ^{13}C NMR spectra were recorded with a pulse width of 2.5 ms, pulse delay of 0.7 s, spectral window of 4000 Hz (centered between benzene and the olefin carbon resonance of the monomer) and 32K points. Integration of the olefinic carbon versus benzene (δ128.2, δ128.0, δ127.8) of the NMR solvent gave the concentration of olefin remaining. Spectral peak heights were used for integration since the cis and trans polymers peaks slightly overlapped those of the monomer. After 1.5hrs, approximately 50 to 80 percent of the monomer was consumed, and the data accumulation was ended. Least squares analysis of a first order logarithmic expression yielded the rates given in Table 3.

Table 5: Kinetic Conditions

Run #	Monomer	mL Monomer	mL d$_6$-benzene
1	Cyclooctene	0.10	0.40
2	Cyclooctene	0.25	0.25
3	Cyclooctene	0.40	0.10
4	Cycloheptene	0.10	0.40
5	Cycloheptene	0.25	0.25
6	Cycloheptene	0.40	0.10

REFERENCES

1. (a) Gates,B.C.; Katzer,J.R.; Schuit,G.C. Chemistry of Catalytic Processes; McGraw-Hill, New York, **1979**. (b) Pino,P.; Mulhaupt,R. *Angew. Chem., Int. Ed. Eng.*, **1980**, *19*, 857.

5. (a) Sinn,H.; Kaminsky,W. *Adv. Organomet. Chem.*, **1980**, *18*, 99. (b) Ewen,J.A. *J. Am. Chem. Soc.*, **1984**, *106*, 6355.

2. Streck,R. *Chemtech*, **1983**, *13*, 758.

3. Ohm.R.; Shein,C. Encyclopedia of Chemical Techonology, 3rd Ed.; Wiley Interscience, New York, **1982**; Vol.18, pp436-442.

4. Parshall,G. Homogenous Catalysis; Wiley Interscience, New York, **1980**.

6. Boor,J. Zeigler-Natta Catalysis and Polymerizations; Academic Press, New York, **1979**.

7. (a) Schrock,R.R. *J. Organomet. Chem.*, **1986**, *300*, 249. (b) Greene,R.M.E.; Hamilton,J.G.; Ivin,K.J.; Rooney,J.J. *Makromol. Chem.*, **1986**, *187*, 619. (c) Kress,J.; Aquero,A.; Osborn,J. *J. Mol. Catal.*, **1986**, *36*, 1. (d) Katz,T.J.; Lee,S.J.; Shippey,M.A. *J. Mol. Catal.*, **1980**, *8*, 219. (e) Feast,W.J.; Harper,K. *J. Mol. Catal.*, **1985**, *28*, 293. (f) Patton,P.A.; McCarthy,T. *J. Macromolecules*, **1987**, *20*, 778. (g) Bencze,L.; Kraut-Vass,A. *J. Mol. Catal.*, **1985**, *28*, 369.

8. Natta,G.; Dall'Asta,G.; Mazzanti,G. *Angew. Chem.*, **1964**, *76*, 765.

9. (a) Katz,T.J. *Adv. Organomet. Chem.*, **1977**, *16*, 283. (b) Grubbs,R.H. *Prog. Inorg. Chem.*, **1978**, *24*, 1.

10. Gilliom,L.R.; Grubbs,R.H. *J. Am. Chem. Soc.*, **1986**, *108*, 733.

11. Cannizzo,L.F.; Ph.D. Thesis, 1987, California Institute of Technology

12. Ivin,K.J. Olefin Metathesis; Academic Press, London, **1983**.

13. Burger,B.J.; Ph.D. Thesis, 1987, California Institute of Technology

14. Virgil,S.C.; Grubbs,R.H., Unpublished Results

15. Yau,W.W.; Kirkland,J.J.; Bly,D.D. Modern Size-Exclusion Liquid Chromatography; Wiley Interscience, New York, **1979**.

16. The olefin dependence for cyclopentene was obtained by examination of the kinetics data presented the Ph.D. thesis of L.F. Cannizzo[11].

17. (a) Benson,S.W. Thermochemical Kinetics; John Wiley and Sons, New York, **1976**, p273. (b) Schleyer,P.v.R.; Williams,J.E.; Blanchard,K.R. *J. Am. Chem. Soc.*, **1970**, *92*, 2377. (b) Dempsey,R. *Isr. J.Chem.*, **1983**, *23*, 85.

18. Straus,D.A.; Grubbs,R.H. *Organometallics*, **1982**, *1*, 1658.

CHAPTER 3

MOLYBDENUM ALKYLIDENE AND IMIDO COMPLEXES:

STUDIES OF STRUCTURE AND REACTIVITY

ABSTRACT

The reactivity of Mo alkylidenes and carbene imido complexes with olefins was studied by GVB (Generalized Valence Bond) ab initio electronic structure calculations. We illustrate an approach using molecular fragments for predicting electronic structures for alkylidene and metallacycle complexes. The analysis is presented with an emphasis on understanding how the bonding influences reactivity. The reaction of the cationic complex $Cl_3MoCH_2^+$ with ethylene was found to be favorable due to the geometry of the coordination sphere. The reaction of Cl_4MoCH_2 with ethylene was found to be exothermic but the coordination sphere is sterically crowded. A chlorine in $Cl_3MoCH_2^+$ was replaced with hydroxide to probe the influence of alkoxides. There was no significant energy difference between $Cl_2(OH)MoCH_2^+$ or $Cl_3MoCH_2^+$ for the reaction with ethylene. The reaction of the carbene imido complex $Cl_2Mo(NH)CH_2$ with ethylene was found to be energetically favorable. The high reactivity of carbene imido complexes in olefin metathesis is due to a spectator imido effect which stabilizes the metallacycle by a donor-acceptor interaction. In addition, the coordination sphere of the carbene imido complex is favorable for metathesis.

INTRODUCTION

Transition metal alkylidenes form a versatile set of catalysts with potential to perform both olefin metathesis[1] and ring opening metathesis polymerizations.[2] Olefin metathesis involves the simultaneous cleavage of two olefin double bonds followed by the formation of alternate double bonds.(A)

Ring opening metathesis polymerization is essentially the same as olefin metathesis, except that the double bond is incorporated in a ring.(B)
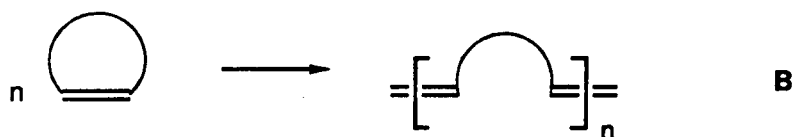
The carbene catalysts can either be of the alkylidene type[3] (high valent,d^o) 1, Fischer type[4] (low valent,d^n) 2, alkylidene oxo type[5] (high valent,d^o) 3 or alkylidene imido type[6] (high valent,d^o) 4.
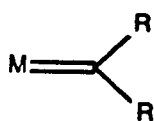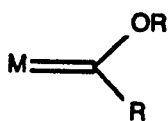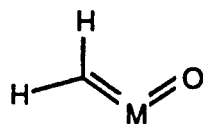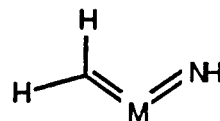
The wide variety of these catalysts emphasize the importance of a metal-carbon double bond for catalytic activity, and yet, the catalytic activity strongly depends upon the metal and its ligands. Several metals spanning the d block ele-

ments from Ti to Ir catalyze the metathesis reaction. In fact, ring opening metathesis polymerization can be catalyzed by the so-called classical systems[7] such as $RuCl_3$ and $OsCl_3$. It is proposed that these compounds react with cyclic olefins to form very reactive alkylidenes. These catalysts, however, give high polydispersities[8] due to slow initiation rates relative to propagation rates.

The most effective metathesis catalysts known involve high valent (generally d^o) complexes of Groups IVB and VIB. The Group IVB catalysts are based on the titanocene metallacyclobutanes developed by Grubbs.[9] These catalysts have been extensively studied mechanistically[10] and theoretically.[11] The group VIB catalysts are based upon tungsten alkylidenes developed by Osborn[12] and Basset[13] and imido alkylidenes developed by Schrock.[14] Due to their recent development, these catalysts have not been extensively studied either mechanistically or theoretically.

The Osborn catalyst 5 and the Basset catalyst 6 require the labilization of a halide ligand for high catalytic activity.[12,13] This is normally accomplished by the addition of a Lewis acid such as $AlCl_3$ or $GaBr_3$.(C)

The essential difference in reactivities between 5 and 7 or 6 and 8 is not completely understood but most likely depends upon the oxidation state of the metal and its coordination environment.

The Schrock catalyst 9 does not require a Lewis acid.[14] The resulting advantages include ease of synthetic workup and the possibility of metathesis of olefins with basic functionalities.[15]

The reason for the high activity of 9 is not completely clear. The original investigators[14,15] suggest an analogy to the Osborn systems[12] since both catalysts are pseudotetrahedral in their active forms. The electronics involved in the coordination sphere, as well as the coordination geometry, however, are probably

5

7

C

6

8

9
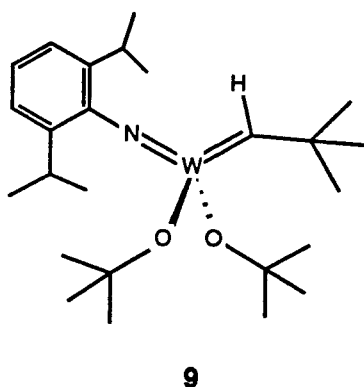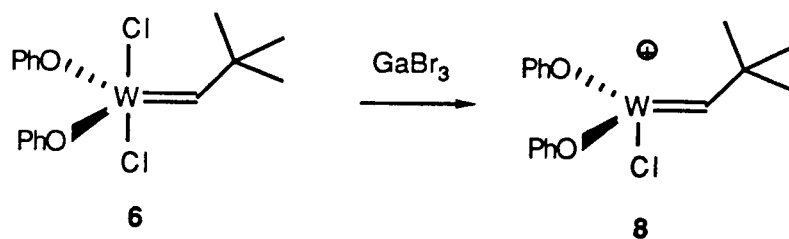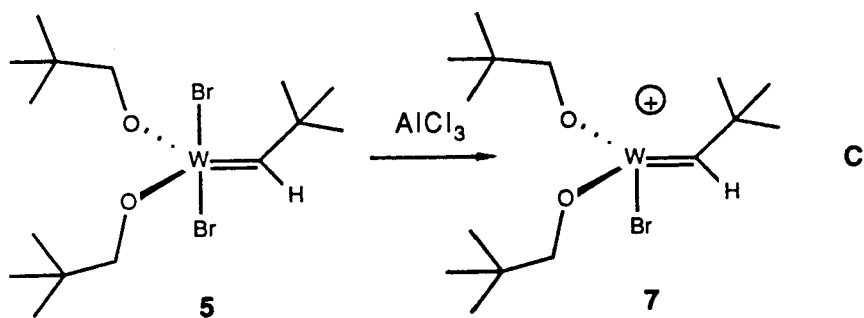
responsible for the high activity of **9**. Due to the recent interest in ring open-ing metathesis polymerizations for making industrially useful polymers (rubbers,[16] block copolymers,[17] conductive polymers[18]), an investigation of the activity of **5** and **9** by ab initio methods was undertaken to determine the essential differences and similarities between them.

Olefin metathesis has been studied previously by the Extended Huckel method[19] and by the Generalized Valence Bond method.[20] The GVB study revealed

that the reaction of Cl_4MoCH_2 with ethylene was unfavorable by +15 kcal/mol. The reaction was found to be favorable by -21 kcal/mol, however, when $Cl_2Mo(O)CH_2$ reacts with ethylene. The reactivity reversal was interpreted in terms of an increase in the Mo-O bond order upon formation of the metallacycle. This stabilizing "Spectator Oxo" effect was also found to play a role in hydrocarbon oxidation by high-valent Group VI oxides.[21] It was suggested that spectator imido ligands would lead to similar but smaller effects. In the present study, the role of spectator imidos and spectator alkoxides are also probed using GVB ab initio methods.

CALCULATIONAL DETAILS

A. Basis Sets and Effective Potentials

In all the complexes studied, we explicitly considered all electrons for C, N, and H, but effective potentials were used to replace core electrons of Cl and Mo. For Cl, the Ne core was replaced with the SHC effective potential[22] (treating neutral Cl with seven explicit electrons). For Mo, a relativistic effective potential[23] was used for the Zn core (treating neutral Mo with 12 explicit electrons). All calculations used Cartesian Gaussian basis sets. For carbon[24] and nitrogen,[24] the (9s5p) primitive Gaussian basis was contracted to valence double zeta[3s,2p]. For hydrogen,[22] the (3s) primitive basis was scaled ($\zeta=1.2$) and contracted to (2s). For Mo,[23] the basis set was contracted to [3s,4p,2d] from the primitive (3s,5p,3d). For Cl,[22] the (3s,2p) primitive basis was contracted to [1s,1p] based on $TiCl_4$.

B. Wave functions

Two types of wave functions were utilized:

A) HF (Hartree Fock)[25]

In this wave function, the singlet state has all orbitals doubly occupied and optimized self-consistently. This leads to a good description of bonds involving highly overlapping orbitals but a poor description of bonds involving low overlap such as Mo-C and Mo-N π bonds.

B) GVB-PP(Generalized Valence Bond with perfect pairing restriction).[26]

In this wave function, doubly occupied orbitals of the HF wave function are replaced with correlated pairs of electrons described as a spin singlet state.

$$\Psi_{HF} = (\psi_1\psi_1)(\alpha\beta - \beta\alpha)$$

$$\Psi_{GVB} = (\psi_r\psi_l + \psi_l\psi_r)(\alpha\beta - \beta\alpha)$$

The GVB wavefunction introduces electron correlation effects by allowing each electron to have its own orbital, which is then optimized self-consistently. GVB calculations often only correlate a portion of the bond pairs. These are chosen to be the pairs that change significantly during a reaction sequence and would otherwise have large correlation errors. To indicate the level of correlation, the GVB wavefunction is denoted as GVB(n/m), where n is the number of electron pairs being correlated and m is the number of orbitals used for the correlated pairs (generally 2n). In the calculations, all Mo-C, Mo-N and N-H bonds were correlated.

C. Geometry Optimizations and Energetic Comparisons

Geometry optimizations were carried out with the GRADIENT[27] program developed by Anthony Rappé which uses analytic gradients to optimize geometries for GVB-PP wavefunctions. All geometries containing Mo (except $Cl_2(OH)MoCH_2^+$ and $Cl_2(OH)MoC_3H_6^+$) were fully optimized. As discussed previously,[28] the following scheme for determining energetics for chemical processes was utilized. Using the GVB-PP method, we calculated the energy differences for reactions where the number and type of bonds are as similar as possible. To calculate enthalpy changes above 0 K for these processes, one must add the differential zero-point corrections to the calculated energy differences. The resulting $\Delta H_{f,0}$ are combined with previously obtained $\Delta H_{f,0}$ for the other species in the idealized reactions to calculate $\Delta H_{f,0}$ for the molecule of interest. These $\Delta H_{f,0}$ are combined with vibrational frequencies (experimental, calculated or estimated) and moments of inertia to obtain $\Delta H_{f,300}$ and ΔS_{300}. Finally, the $\Delta G_{r,300}$ for the reactions are calculated. The program FRCMAN developed by Anthony Rappé was used to calculate these correction

factors based on the Janaf thermodynamic tables.[29]

To determine the quantitative energy change between the alkylidene complexes and the metallacycle complexes, we needed the total energy of ethylene at a comparable geometry optimization level and correlation level. Therefore, ethylene was geometry optimized at the GVB(2/4) level where both the C-C σ and π bonds were correlated. The total energy for ethylene was then added to the total energy of an alkylidene complex. This sum was then compared to the corresponding metallacycle total energy to determine the free energy of reaction. The metallacycle complex and the corresponding alkylidene complex were correlated at comparable levels. Thus, if the alkylidene complex was described with GVB(x/y) and ethylene with GVB(2/4), then the metallacycle was always correlated at the GVB(x+2,y+4) level. This allows for a consistent energy evaluation between the alkylidene plus ethylene and the metallacycle.

D. Structural Simplifications

Several simplifications of the experimental catalysts were made for calculational convenience. The studies presented are meant to probe the energetics of the bonding breaking and bond forming reactions and are not meant to model the large steric interactions in the experimental catalysts. Therefore, the Osborn and Basset catalysts **5** and **6** are modeled by **10**. The alkyl groups are replaced by hydrogen and the alkoxide or bromide ligands are replaced by chlorine. To investigate the difference between halides and alkoxides, one chlorine ligand in the cationic complexes **11** and **15** was replaced by OH. Thus, structure **13** is also a model for **5** and **6**. Complexes **13** and **17**, however, were not fully geometry optimized. The structures of the $Cl_2MoC_3H_6$ or Cl_2MoCH_2 fragments of **13** and **17** were the same as the fully optimized structures **11** and **15**. The OH ligand replaced the third chlorine ligand.

A typical Mo-O bond distance of 1.79Å was used. The Mo-O-H bond angle was constrained to 180° to probe the donor capabilities of the alkoxide.

Mo was used in place of W for calculational convenience. It was felt that the close correspondence in the reactivities and structures of W and Mo alkylidenes[30] implied that this substitution would not significantly affect the reactivity trends calculated. Furthermore, the covalent and ionic radii for Mo and W are similar [31] so that the results of geometry optimizations can be compared to crystal structure data for both Mo and W alkylidene complexes. In support of this assumption, Table 1 compares the X-ray crystal structure data for a benzylidene analog of **9** and the fully optimized structure **12**.

Experimental Bond Lenghts and Angles		Calculated Bond Lenghts and Angles	
W-C	1.86	Mo-C	1.86
W-N	1.71	Mo-N	1.67
W-N-C	175.6	Mo-N-H	164.5
C-W-N	100.9	C-Mo-N	105.2

Table 1: Comparison of experimental and calculated bond angles and bond lengths.

RESULTS AND DISCUSSION

First, the GVB description of the bonding and charge distribution in the H_2CMoCl_4 (10) complex will be contrasted with the $H_2CMoCl_3^+$ (11) cationic complex. It will be shown that the charge distribution and the coordination sphere of these two complexes control their relative reactivity toward ethylene and make the cationic complex $H_2CMoCl_3^+$ more reactive kinetically, even though the reaction is more exothermic for H_2CMoCl_4. Next, an examination of the bonding and charge distribution in the methylidene imido complex $H_2C(HN)MoCl_2$ (12) is compared to the H_2CMoCl_4 and $H_2CMoCl_3^+$ complexes. It will be shown that the imido ligand is intimately involved in the reactivity of the methylidene ligand. Finally, a Cl in $H_2CMoCl_3^+$ is replaced with OH to probe the influence of alkoxide ligands on the metathesis reaction. The reactivity of $H_2CMo(OH)Cl_2^+$ (13) is found to be similar to that of 11. The discussions are presented with an emphasis on understanding the bonding and its relationship to reactivity.

A. Bonding in H_2CMoCl_4 and $H_2CMoCl_3^+$ and the corresponding metallacycles $H_6C_3MoCl_4$ and $H_6C_3MoCl_3^+$.

The goal of this study is to extract a quantitative and conceptual understanding of the bonding in 10, 11, 12 and 13 and a quantitative understanding of their reactivity with olefins. Thus, the geometries of 10 and 11 were fully optimized at the GVB (4/8) perfect pairing level where both the C-H and the Mo-C bonds were correlated. The corresponding metallacycles 14 and 15 were also optimized at the GVB (4/8) perfect pairing level where both the C-Mo and the C-C bonds were correlated.

The fully optimized structures are presented schematically in Figure 1. Complexes 10, 11 and 13 are models of the Osborn[12] and Basset[13] catalytic systems
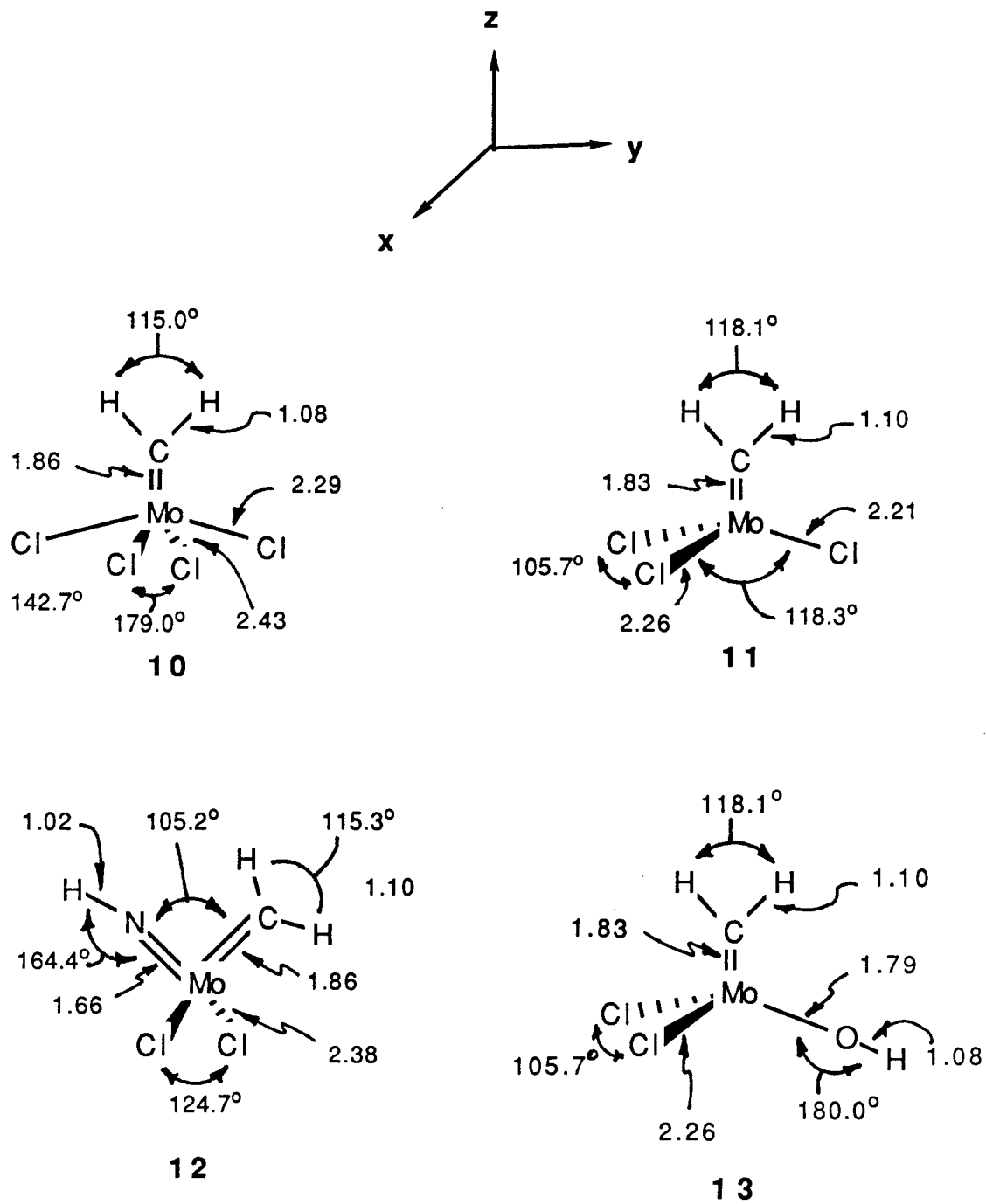
Figure 1: Fully optomized structures. Bond lengths in Angstroms.
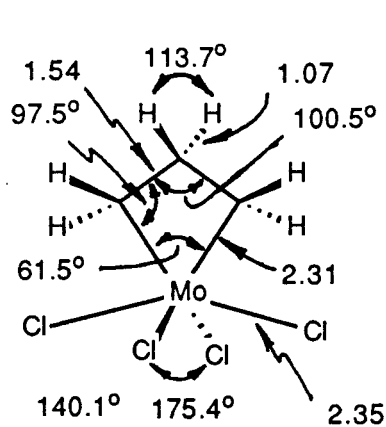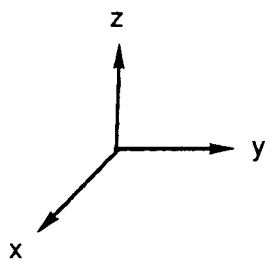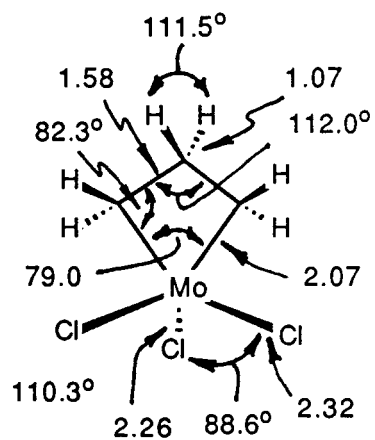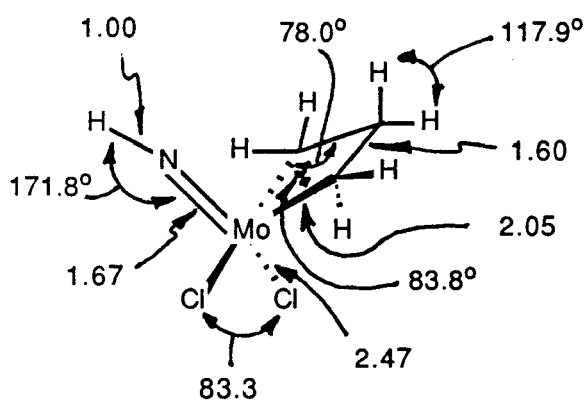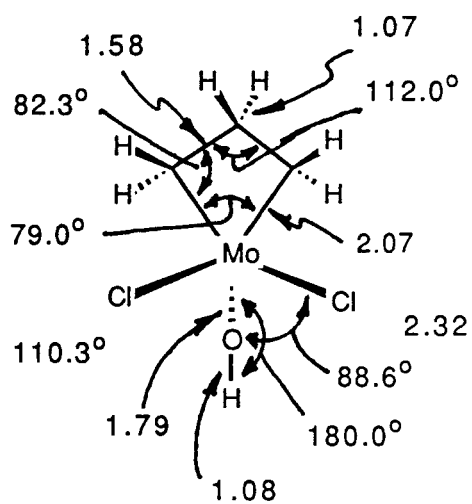
Figure 1 cont.: Fully optomized structures. Bond lengths in Angstroms.

based on **5** and **6**. For the alkylidenes (**10** and **11**) and metallacycles (**14** and **15**), the systems were constrained to have Cs symmetry. This forced both the Mo-C and the C-C bonds of the metallacycle geometries to be identical across the xz plane in Figure 1. This constraint of Cs symmetry did not force the metallacycle ring to be planar and, in fact, both geometries displayed a puckered four-membered ring.

Comparison of the geometries of **10** to **11** and **14** to **15** revealed that all the Mo-C and Mo-Cl bonds are significantly shorter in the cationic complexes. The Mo-C σ bonds are $0.24\overset{\circ}{A}$ shorter in the **15** than in the **14**, while the Mo-Cl σ bonds are on an average $0.06\overset{\circ}{A}$ shorter in **15** than in **14**. A similar trend is also observed in the methylidene complexes **10** and **11**. In **11**, however, the Mo=C bond is only $0.03\overset{\circ}{A}$ shorter, while the Mo-Cl bond is $0.12\overset{\circ}{A}$ shorter than in **10**. These shorter bonds are due to the ligands being drawn closer to the Mo in the cationic metallacycle and alkylidene due to their higher electrophilicity.

The metallacycles, **14** and **15** are puckered by $15.24°$ and $18.15°$, respectively. The puckering in the cationic complex is larger due to less steric interaction with the chlorines. Metallacycle ring puckering has been invoked to explain the stereochemistry of olefin metathesis.[32]

As a starting point for examining the bonding in the methylidene complexes and the metallacycle complexes, we chose to study the molybdenum chloride fragments. The spacial arrangement of the singly occupied orbitals of the triplet states of the molybdenum chloride fragments will dictate the lowest energy geometry of the alkylidenes and metallacycles. In $MoCl_4$ and $MoCl_3^+$, four or three electrons on Mo, respectively, are used for partially ionic bonds to the chloride ligands. The chlorines remove s electron density from the metal due to the high electronegativity of the chlorines. The s electrons, not the d electrons, are preferentially removed due

to their lower ionization potential. This leaves two electrons on the Mo for bonding to the other ligands. There is the choice of $d\sigma$, $d\pi y$, $d\pi x$, $d\delta x^2$-y^2, and $d\delta xy$.

To determine which orbitals are used to bond to CH_2, the triplet states of $MoCl_3^+$ and $MoCl_4$ were calculated. For $MoCl_4$, trans chlorine angles of $180°$ and $140°$ were used since these correspond to the Cl-Mo-Cl angles in the final geometry **10**. The high spin orbitals are displayed in Figure 2. They are essentially pure Mo $d\sigma$ and Mo $d\pi$ orbitals.
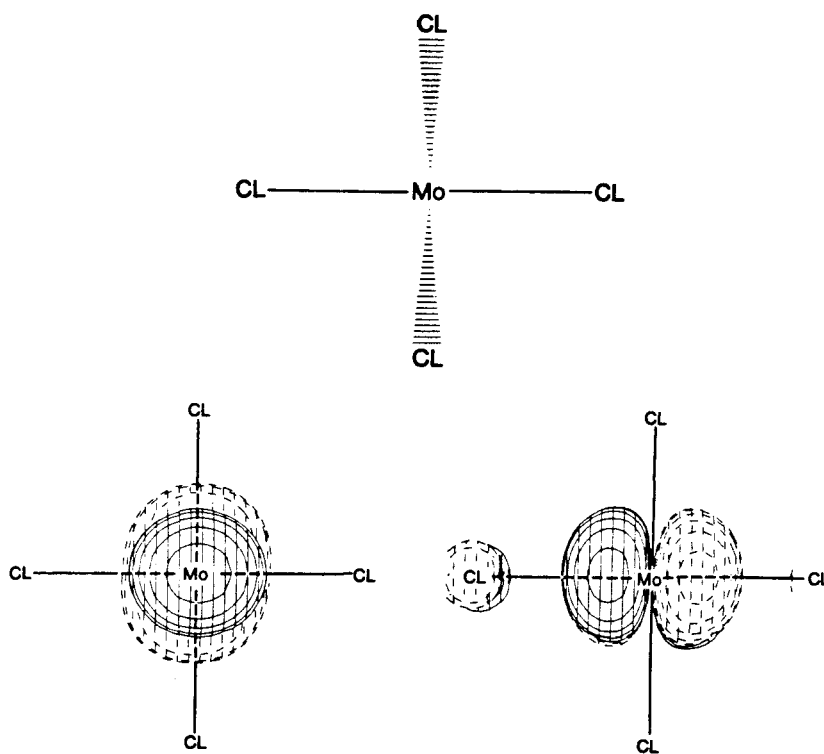
Figure 2: High spin orbitals for the triplet state of $MoCl_4$.

In order for the high spin orbitals to be orthogonal to the Mo-Cl bonds, one would predict that the lowest energy configuration would be one in which the Mo-Cl

bonds lie along the nodal planes of the singly occupied orbitals. In other words, the placement of the Mo-Cl bonds and the singly occupied orbitals are interrelated with both the singly occupied orbitals and the Mo-Cl bonding orbitals preferring to lie in each other's angular nodes. The calculated configurations of the singly occupied orbitals are exactly those predicted by this reasoning. The chlorines at 180° from one another have their Mo-Cl bonds along a $d\pi$ orbital angular node. This allows the Mo-Cl bonds to remain orthogonal to the high spin $d\pi$ orbital. The chlorines at 140° from one another have their Mo-Cl bonds along a $d\pi$ orbital angular node also, but in addition, these Mo-Cl bonds lie in an angular node of the $d\sigma$ orbital. The angular node in the $d\sigma$ orbital dictates a bent Cl-Mo-Cl angle. When the high spin $^3B_2$ state[33] of CH_2 bonds to $MoCl_4$, the high spin orbitals of the $MoCl_4$ fragment dictate that the H-C bonds are eclipsed with the chlorines that are 140° from one another (1). Thus, the bending of the chlorines away from the alkylidene substituents in the yz plane (Figure 1) is not due to sterics between R groups on the alkylidene carbon and the chlorines but instead is rooted in the electronics of the $MoCl_4$ fragment. In fact, we find the barrier to rotation of the methylene group to be 9 kcal/mol favoring the predicted geometry (1).

(1)
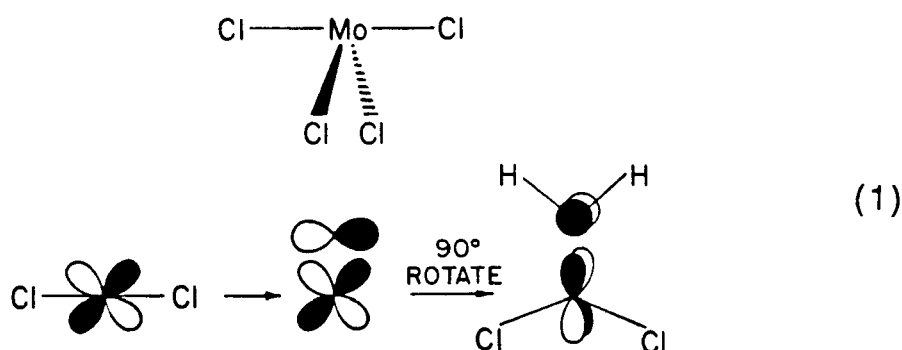
Figure 3 shows the orbital interaction diagram for the triplet state of $MoCl_4$ (no energy scale implied). To form the four bonds to Mo, the molybdenum uses one

s and three d orbitals. These orbitals are high in s character and polarized toward the Cl's due to the high electronegativity of Cl. This yields the two high spin $d\sigma$ and $d\pi$ orbitals on Mo and the three low-lying empty orbitals on Mo. These empty orbitals are slightly antibonding with respect to the Mo-Cl bonds and are basically Mo $d\pi y$, $d\delta x^2\text{-}y^2$ and $d\delta xy$ in character. These empty orbitals are shown in Figure 17 and are discussed in the reactivity section. The orbital interaction diagram of Figure 3 is a schematic simplification of the bonding in the $MoCl_4$ fragment since, in reality, all five d orbitals on Mo are used to a small extent to form the Mo-Cl bonds.
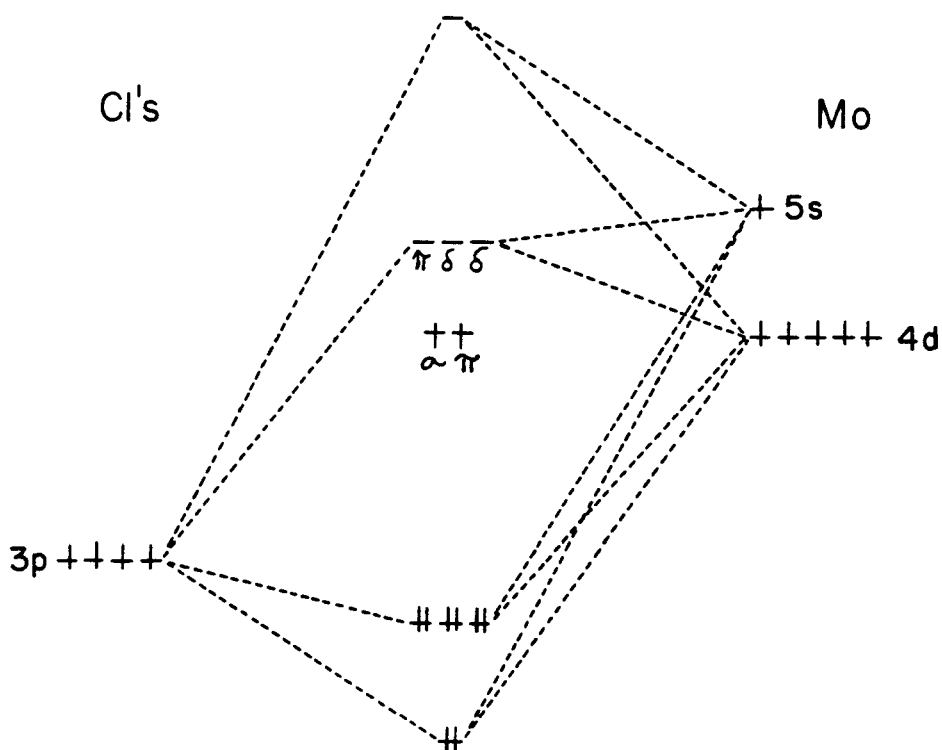
Figure 3: Orbital interaction diagram for $MoCl_4$ showing the high spin and empty orbitals on Mo.

To further develop the fragmental approach to predicting the lowest energy

geometry of the alkylidenes, we calculated the triplet state of $MoCl_3^+$. As previously shown, the high spin orbitals of the quartet $MoCl_3$ fragment also lie along the Mo-Cl bond's angular nodes.[34] Similarly, in triplet $MoCl_3^+$ the high spin orbitals are $d\sigma$ and $d\pi + d\delta$ in character and lie along the Mo-Cl angular nodes. This consequently places the $d\pi + d\delta$ orbital tilting over two Cl's (2).

(2)
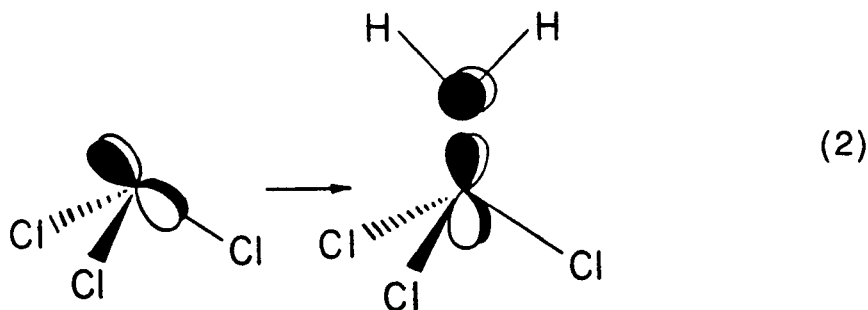
Thus, this dictates that the CH_2 group would bond with the plane formed by CH_2 in the same plane as a Mo-Cl bond. In fact, we find the barrier to rotation of the methylene group to be 5.7 kcal/mol favoring the geometry predicted by examining the interrelationship of the nodal planes of the Mo-Cl bonds and the singly occupied orbitals.

The contour plots of the GVB orbitals of the methylidene complex 11 are presented in Figure 4. As discussed in the calculational details, each GVB orbital has one electron, but the two orbitals of a pair are allowed to overlap. The contour plots of the GVB orbitals of 10 appear approximately the same as those for 11.

As indicated in Figure 4, the methylidene complexes have covalent Mo-C σ and π bonds. The orbitals are typical for Mo-C double bonds and consist of a $d\pi$ and $d\sigma$ orbital on the Mo and a p and sp^2 orbital on the carbon.

The metallacycles, however, present several interesting features. The contour plots of the GVB orbitals of the metallacycles 14 and 15 are presented in Figure
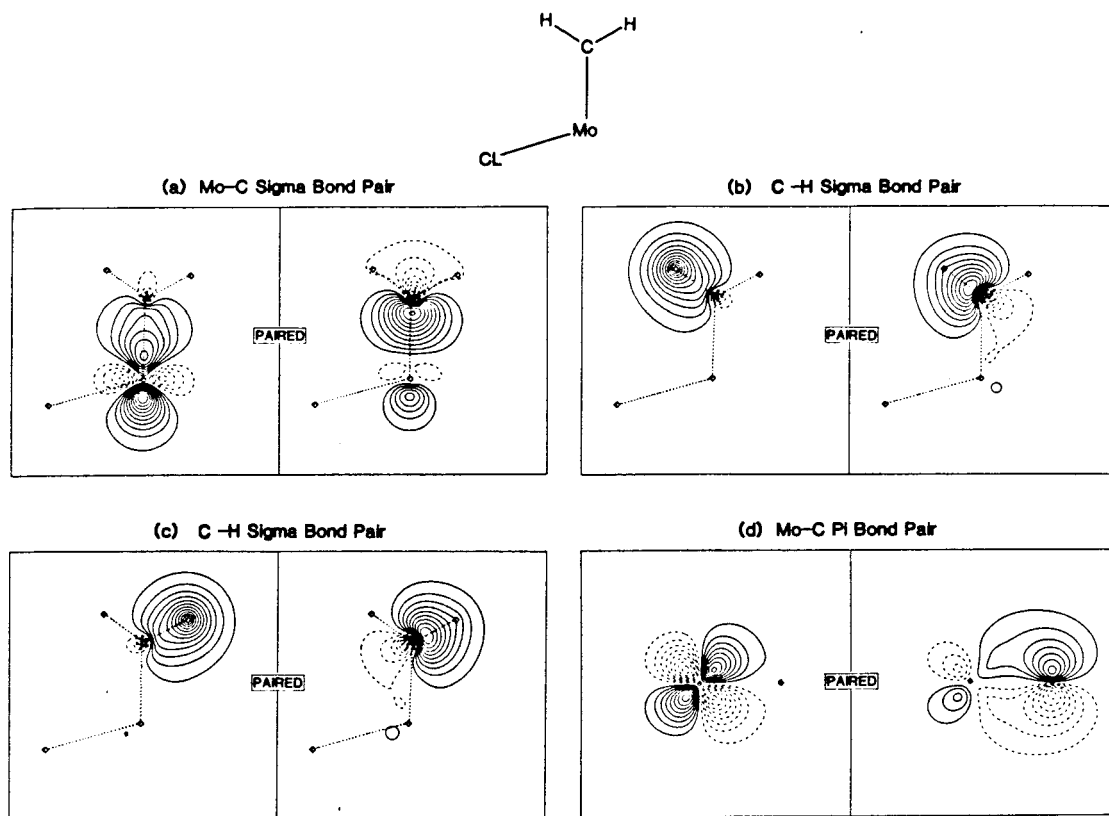
Figure 4: Contour plots of the GVB orbitals for $Cl_3MoCH_2^+$. Spacing between contours is 0.05 a.u.; solid lines are positive and dashed lines are negative. Figure d is plotted in a plane formed from a 90° rotation along the Mo-C bond vector.

5. The C_3H_6 framework has a central angle of 100.5° and 112.0° in **14** and **15**, respectively, and the C-C bond pairs are unstrained and well directed along the bond axis. Only the C-C contour plots for **15** are displayed since those for **14** appear almost identical (Figure 5c and d). The carbon-centered Mo-C GVB pair orbitals have high p character (Figure 5a, b, e and f). This is a reflection of the high positive charge on Mo due to the cationic charge of **15** or the influence of four electron-withdrawing chlorines on **14**. The Mo consequently acts very electronegative. The
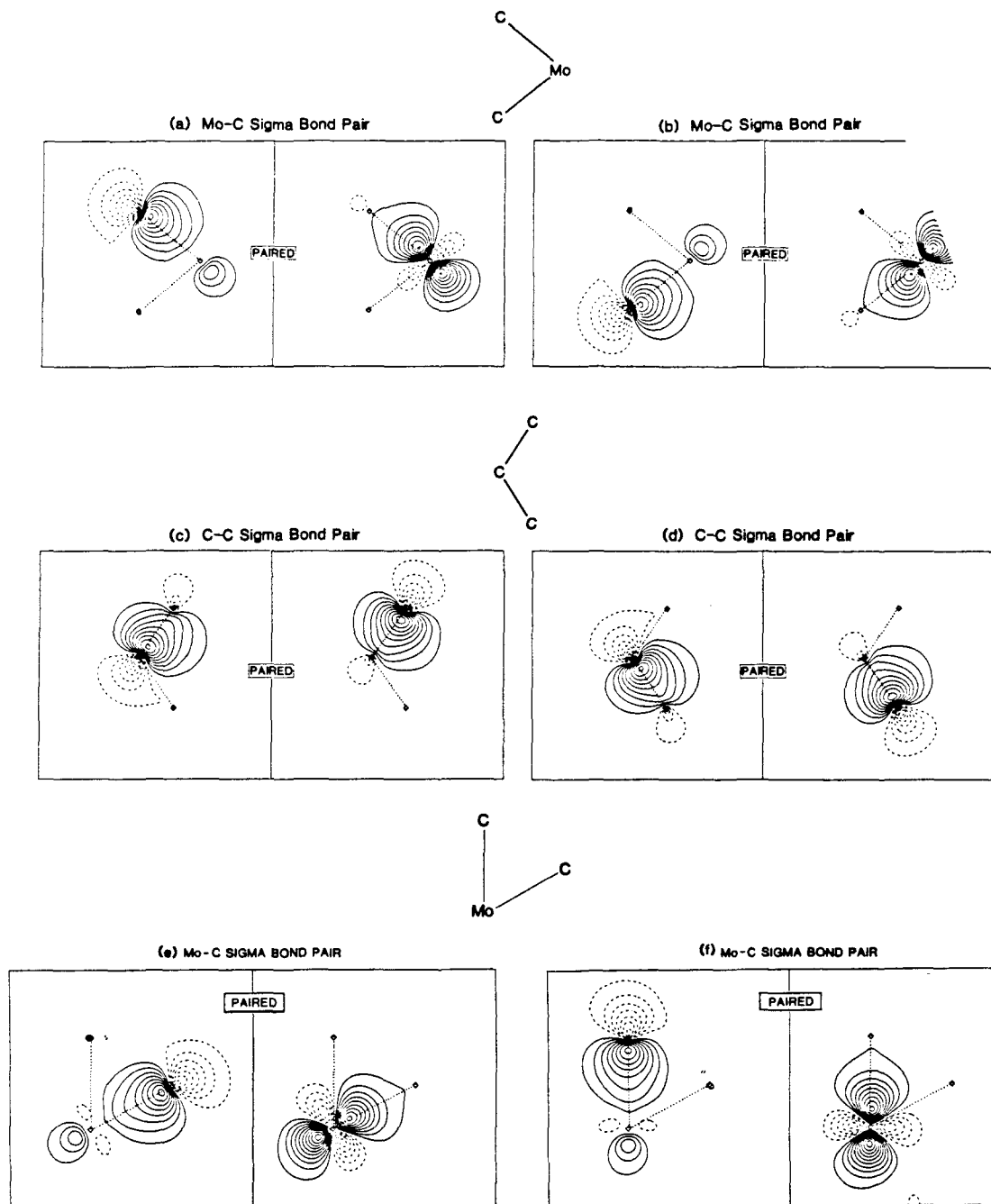
Figure 5: Contour plots of the GVB orbitals for $Cl_3MoC_3H_6^+$ and $Cl_4MoC_3H_6$. Figures a, b, c and d are for **15** and Figures e and f are for **14**. The C-C contour plots for **14** are not shown since they are almost identical to those for **15**.

C-Mo-C angles are 61.5° and 79° in **14** and **15**, respectively. The much smaller angle of **14** relative to that of **15** is due to the much longer Mo-C bond distance in **14**. The Mo-C single bonds are slightly strained. In **14**, the GVB orbitals that are centered on Mo are $d\sigma$ in character and are directed 4 degrees off of the Mo-C vector. The two d orbitals on Mo that bond to the carbons are 55° from one another. Rappé and Goddard[35] showed that for two pure d orbitals to be symmetric about their respective bond axes, they must be separated by either 54.7° or 125.3°. Therefore, **14** makes covalent sigma bonds to the carbons at precisely the expected angle. On the other hand, electron repulsion effects favor a $d\sigma$, $d\delta$ ground state configuration which favors a 90° bond angle.[35] The competition between these effects usually results in metallacycles with a bond angle between 70° and 80°.

The small C-Mo-C angle in $Cl_4MoC_3H_6$ is due to the necessity of making four coplanar bonds to Mo. The metal must form two covalent bonds to C and two ionic bonds to Cl. There are only three d orbitals with density in the yz plane. They are $d\sigma$, $d\pi yz$, and $d\delta x^2$-y^2 in character. If a linear combination of $d\pi$ and $d\delta$ orbitals is taken, two additional $d\sigma$ character orbitals are formed in this plane. All three $d\sigma$ orbitals are shown in Figure 6.

These orbitals are the ones previously shown by Rappé and Goddard to be 54.7° from one another.[35] If two of these $d\sigma$ orbitals (a and b, Figure 6) are used to form the Mo-C σ bonds in **14**, then the d orbital left over for bonding to the Cl's is c in Figure 6. This orbital mixes in s character and would tend to form two Mo-Cl bonds at an angle of 180° to each other. The optimized geometry, however, has a bond angle of 140.1°, and therefore, these Mo-Cl bonds are slightly strained. The decreased Cl-Mo-Cl bond angle is due to steric interactions between the coplanar C's and Cl's. A recalculation of the wavefunction with these Cl's at an angle of 180°

Figure 6: Three coplanar dσ orbitals at 54.7° from one another.

(3) was performed on the $Cl_4MoC_3H_6$ geometry. It was found to be 40 kcal/mol higher in energy than **14**.

(3)

Therefore, the small C-Mo-C bond angle of 61° is due to the constraint of forming 4 bonds from Mo to coplanar ligands. Since two of these bonds are to

chlorine (which withdraws s electron density), the remaining bonds to C are forced to be high in d character and would prefer an angle of 54°.

To further investigate this effect, the Mo-Cl bonds of the $MoCl_4$ fragment were correlated. The GVB pair orbitals are shown in Figure 7. The high spin π orbital lies in the same plane as orbitals c and d. These orbitals can be seen to be high in s character when contrasted with the orbitals in Figure 5. Furthermore, these Mo-centered GVB orbitals in Figure 7c and d are linear with respect to one another since they are combinations of an s orbital and the d orbital in Figure 6c. Thus, the metal uses sd hybrids to form the Mo-Cl bonds in the yz plane. This forces almost pure d orbitals on Mo to bond to the carbons. A small Mo-C bond angle and a large Mo-C bond length result from this compromise in Mo-C versus Mo-Cl bonding requirements.

Complex 15, however, has a much wider C-Mo-C angle of 79°. This is due to the much shorter Mo-C bond distances. The two $d\sigma$ orbitals that bond to the two carbons are at an angle of 99°. These orbitals are 10° off the Mo-C bond vectors (Figure 5a and b). The Mo in 15 is not as constrained to use pure d orbitals to bond to the carbons since the Mo only has to form the two Mo-C bonds in the same plane. Hence, the $d\sigma$ orbitals have more s character because they do not have to compete with Cl's in the same plane. This allows the orbital angle to open up to form the Mo-C bonds. Thus, the Mo-C bond distance is shorter in $Cl_3MoC_3H_6^+$ than in $Cl_4MoC_3H_6$ for two reasons. The first is the larger positive charge on Mo which draws the carbons closer in the cationic complex, and second, the Mo uses hybrids with more s character. In Table 2, the GVB bond overlaps for the complexes studied are tabulated. The Mo-C sigma bond overlap for both 14 and 15 are the same. Thus these bonds are energetically similar. This further demonstrates that

Complex	Bond	Overlap
A. Cl_4MoCH_2	Mo-C Sigma	0.75
10	Mo-C Pi	0.52
B. $Cl_3MoCH_2^+$	Mo-C Sigma	0.76
11	Mo-C Pi	0.57
C. $Cl_4MoC_3H_6$	Mo-C Sigma	0.55
14	C-C Sigma	0.83
D. $Cl_3MoC_3H_6^+$	Mo-C Sigma	0.55
15	C-C Sigma	0.83
E. $Cl_2Mo(NH)CH_2$	Mo-C Sigma	0.78
12	Mo-C Pi	0.52
	Mo-N Pi	0.64
	Mo-N Pi	0.64
	N-Lone pair	0.93
F. $Cl_2Mo(NH)C_3H_6$	Mo-C Sigma	0.65
16	C-C Sigma	0.83
	Mo-N Pi	0.61
	Mo-N Pi	0.68
	N-Lone Pair	0.88
G. $Cl_2Mo(OH)CH_2^+$	Mo-C Sigma	0.75
13	Mo-C Pi	0.56
	Mo-O	0.82
	Mo-O	0.82
	Mo-O	0.82
H. $Cl_2Mo(OH)C_3H_6^+$	Mo-C	0.60
17	C-C	0.83
	O-H	0.81
	Mo-O	0.85
	Mo-O	0.85
	Mo-O	0.81

Table 2: GVB bond overlaps.
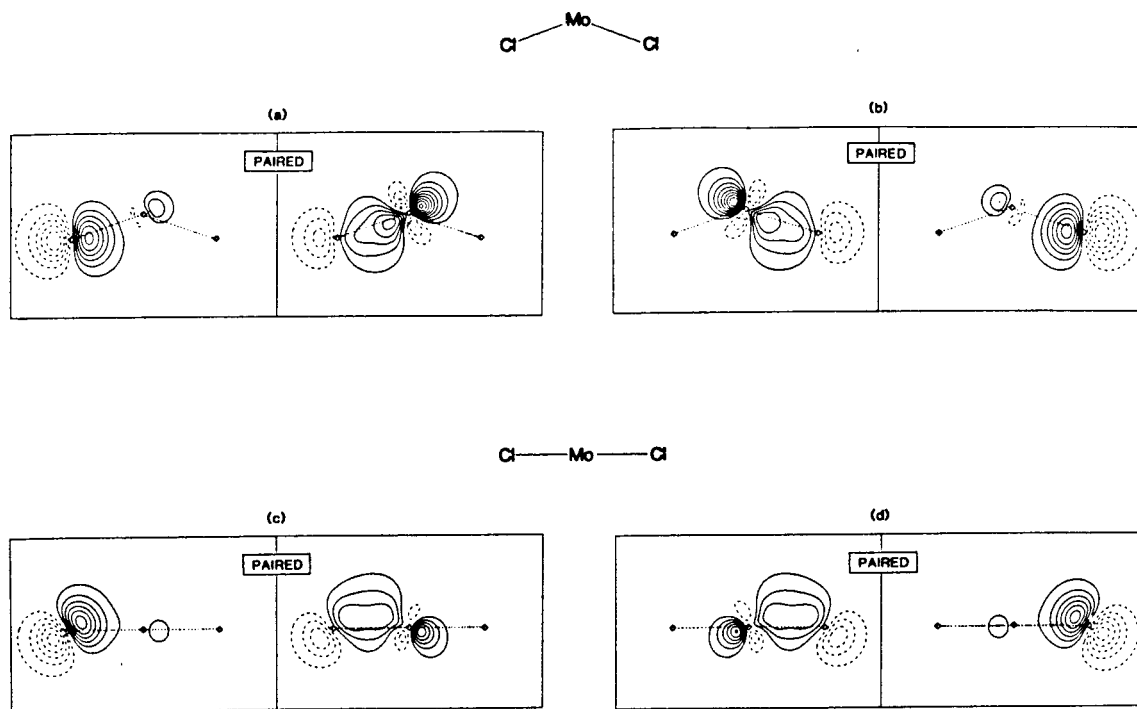
Figure 7: Contour plots of the GVB orbitals for $MoCl_4$.

the C-Mo-C bond angle is dependent upon the Mo-Cl bonds since the only difference between the complexes is the placement of the chlorines.

B. Bonding in $Cl_2Mo(NH)CH_2$ and the corresponding metallacycle $H_6C_3Mo(NH)Cl_2$

The carbene imido complex **12** was fully geometry optimized at the GVB(8/16) perfect pairing level where all the Mo-C, Mo-N, N-H and C-H bonds were correlated. The corresponding metallacycle **16** was fully geometry optimized at the GVB(8/16) perfect pairing level also. All the Mo-C, Mo-N, C-C, and N-H bonds were correlated. Both **12** and **16** were constrained to have Cs symmetry. This forced both Mo-C and C-C bonds of **16** to be the same across the xz plane in
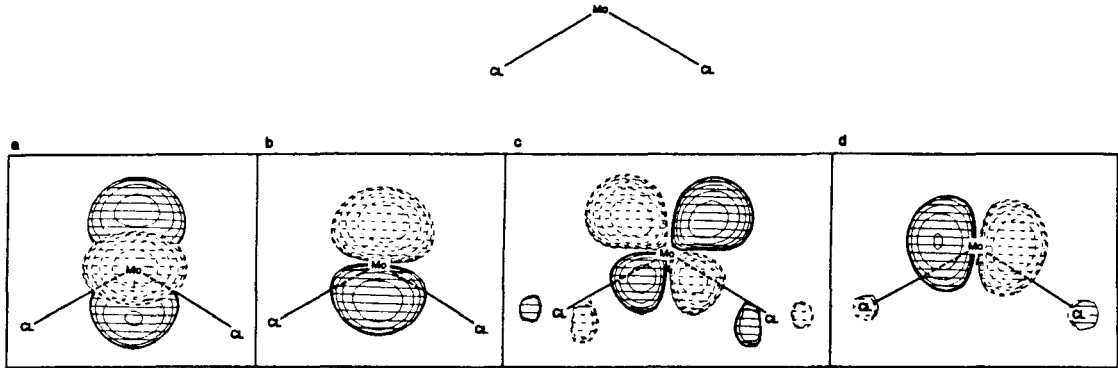
Figure 8: High spin orbitals of the quintet state of $MoCl_2$.
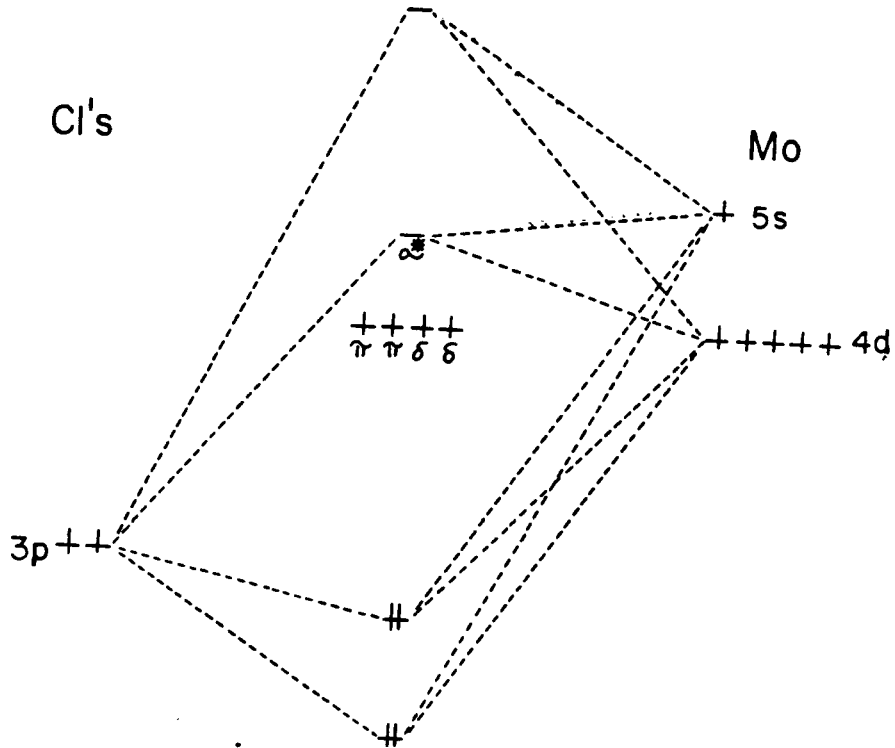
Figure 9: Orbital interaction diagram for $MoCl_2$ showing the high spin and empty orbitals on Mo.

Figure 1. The metallacycle ring was allowed to pucker and did so to an extent of 9°.

Examination of the bonding in the imido carbene complex **12** was first approached by calculating the quintet state of $MoCl_2$. In $MoCl_2$, two of the six valence electrons on the Mo are used for partially ionic bonds to the two Cl ligands. This leaves four electrons on the Mo for bonding to the other ligands. There is a choice of $d\sigma$, $d\pi yz$, $d\pi xz$, $d\delta xy$, $d\delta x^2\text{-}y^2$ orbitals for the electrons to occupy. To determine the lowest energy configuration of the four electrons in the five d orbitals, a calculation was performed on the quintet state of $MoCl_2$. A Cl-Mo-Cl angle of 110° was used since this corresponds to the Cl-Mo-Cl angle in complex **12**. These high spin orbitals are presented in Figure 8. They are essentially pure d-like and are the Mo $d\delta x^2\text{-}y^2$, $d\pi yz$, $d\pi xz$, and $d\delta xy$ orbitals. The empty orbital is dz^2 in character. The orbital interaction diagram for $MoCl_2$ is shown in Figure 9. To bond to the two chlorines, the Mo uses two sd hybrids. The d orbital used is $d\sigma z^2$ (Figure 9). The molecular Mo-Cl orbitals, however, are essentially localized on the chlorines and, thus, the empty $d\sigma z^2$ orbital is σ in character and is slightly Mo-Cl antibonding. This orbital remains empty when the quintet state of $MoCl_2$ bonds to an imido and an alkylidene ligand.

The high spin orbitals of Figure 8 form the covalent bonds to the NH and CH_2 fragments. The orbitals in Figure 8a and 8b mix to form a σ bond and a π bond. The orbitals in 8c and 8d mix to form two other π bonds (Figure 10). From these orbitals, one observes that the lowest energy π bonds are not in the same plane, nor perpendicular to one another, but are linear combinations of $d\pi$ and $d\delta$ orbitals. This leads to a CH_2 group that is in the same plane with the MoNH group. In fact, a 90° rotation along the Mo-C bond axis leads to complete loss of a π bond.
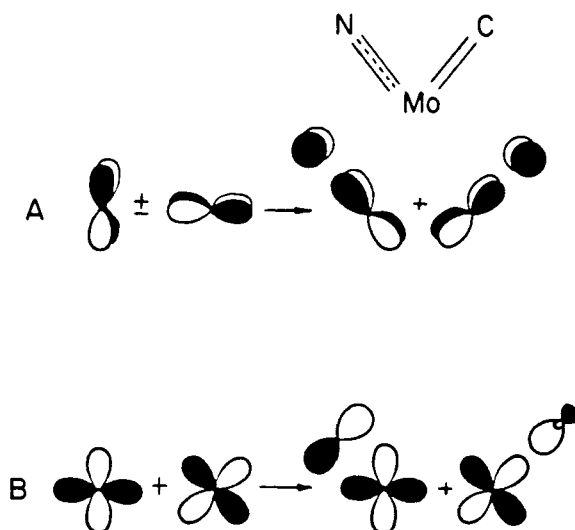
Figure 10: Orbital mixing to form the Mo-C and Mo-N bonds of $Cl_2Mo(NH)CH_2$. These orbitals are schematic representations of those shown in Figure 8.

The ground state of the NH fragment is $2s^2, px^1, py^1$. One would expect a double bond with the Mo and a lone pair on NH. A weaker donor interaction can also occur between the N lone pair and an empty Mo d orbital. If the NH fragment does not gain any extra bonding by mixing in the excited $2s^1, px^1, py^2$ configuration, the $2s^2$ lone pair would best delocalize toward an empty $d\sigma$ orbital. This is the bonding found in Cl_4MoNH[36] complexes and explains the near linear Mo-N-R angle in all mono-imido complexes.[37] In the $MoCl_2$ complex, however, the empty orbital is not of sigma or pi symmetry with respect to the NH fragment. In addition, this empty orbital is higher in energy than the bonding Mo d orbitals since it has significant antibonding character with the chlorine ligands. Thus, its acceptor capabilities are low. The NH fragment does take advantage of some donor interaction with this Mo empty orbital, but the extent of donation is low. This is seen in Figure 11f. The lone pair orbital appears s like and mostly centered on the N. The NH fragment

Figure 11: Contour plots of the GVB orbitals for $Cl_2Mo(NH)CH_2$. Figures g and h are plotted in the plane of the Mo-C and Mo-N π bonds respectively.

does not mix in significant s^1, px^1, py^2 character and thus it forms two strong π bonds with the metal and a very weak donor-acceptor bond. The Mo-N-H angle is 165° instead of the 180° expected for a good donor interaction.

The other covalent Mo-N and Mo-C σ and π bonds in **12** are conventional (Figures 11a, b, c, g and h). They are essentially covalent with no large charge polarization toward C and N. The Mo-N π bonds in Figure 11b and h are more polarized toward N than the Mo-C π bond (Figure 11g) due to the higher electronegativity of N.

When forming the metallacycle, the Mo-C π bond is broken and a new Mo-C sigma bond is formed. The rehybridization is similar to that previously discussed for **14**. In order to form a strong covalent bond with the second carbon, the metal mixes both the $d\sigma$ and $d\pi$ orbital of the original Mo-C double bond but, in addition, needs to mix in the empty $d\sigma$ orbital. Thus, the metal uses three d orbitals to form 2 Mo-C sigma bonds. This leaves a third empty d orbital. This d orbital is also now $d\sigma$ is character and is lower in energy than the empty $d\sigma$ orbital in Figure 9. Consequently, a hybrid d orbital of lower energy has been created which is of better symmetry to form a good donor interaction with the NH lone s electron pair. The donation is seen in Figure 12a. This donation causes a stabilizing effect and has been termed the spectator imido effect (see the reactivity section).

The Mo-C and Mo-N σ and π bonds, respectively are quite normal and covalent in character. These orbitals are displayed in Figures 12b, d, e and f. The Mo-C bonds are slightly strained, with the Mo d hybrids at an angle of approximately 130° with respect to each other. The d hybrids are approximately 23° off the Mo-C bond vectors.

The Mo-Cl bond distances have significantly increased by 0.09$\overset{\circ}{A}$ in the inter-

Mo≡≡≡N—H

(a) N - Mo DONOR ACCEPTOR BOND

PAIRED

(b) Mo - N Pi BOND

PAIRED

(c) N - H SIGMA BOND

PAIRED

(d) Mo - N Pi BOND

PAIRED

C
|
Mo———C

(e) Mo - C SIGMA BOND

PAIRED

(f) Mo - C SIGMA BOND

PAIRED
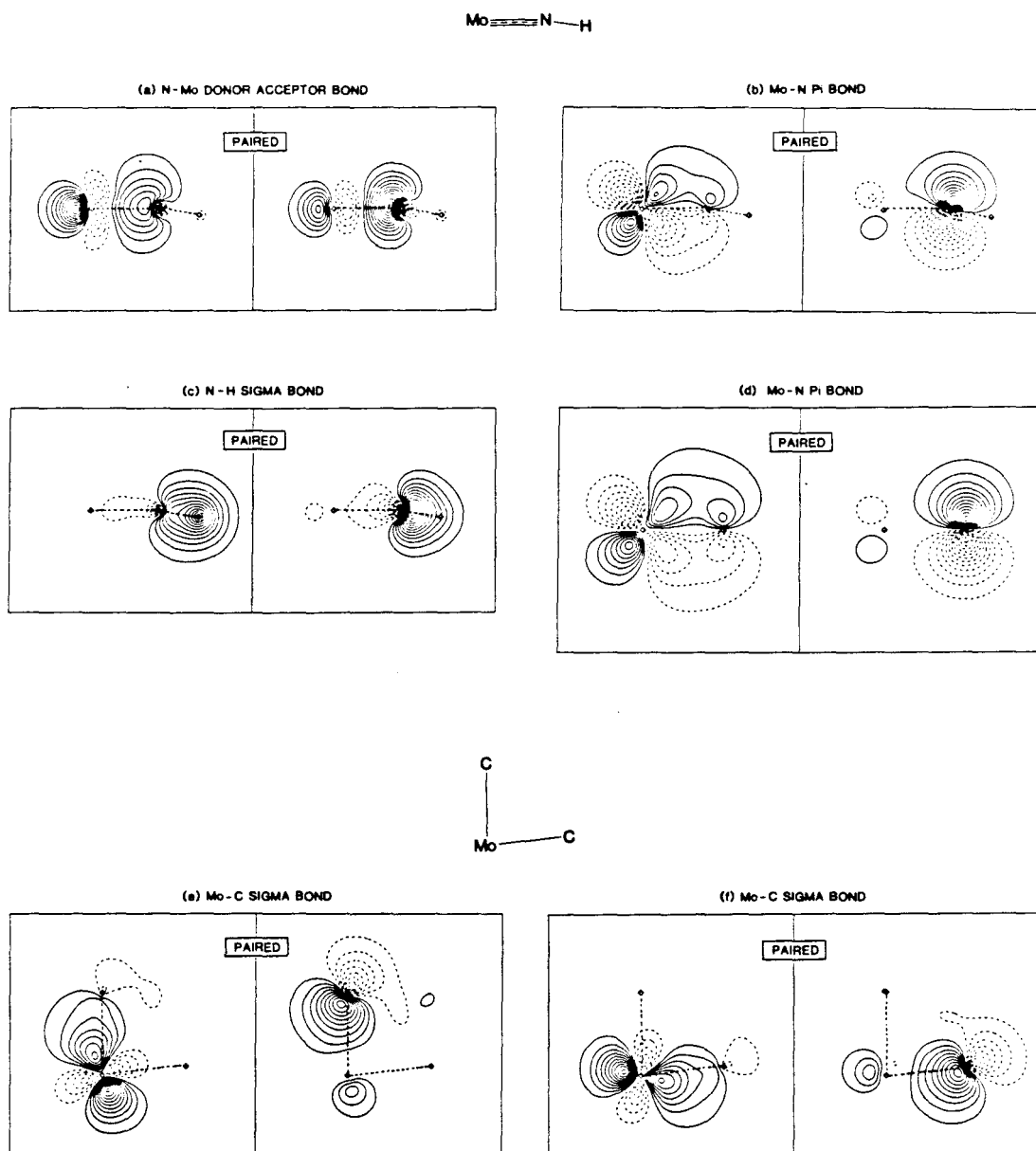
Figure 12: Contour plots of the GVB orbitals for $Cl_2Mo(NH)C_3H_6$. Figure d is plotted in a plane formed by a 90° rotation along the Mo-N bond vector.

conversion of **12** to **16**. In contrast, in the interconversion of **10** to **14**, the Mo-Cl bond lengths only increased by 0.04Å. The Mo-Cl bond distance increase in **14** is due to increased steric crowding in the metallacycle. The longer Mo-Cl bonds in **16**, however, is also due to population of the slightly antibonding Mo-Cl orbital by the nitrogen donor lone pair.

C. Bonding in $Cl_2Mo(OH)CH_2^+$ and the corresponding metallacycle $Cl_2Mo(OH)C_3H_6^+$

Examination of the bonding in $Cl_2Mo(OH)CH_2$ was accomplished by calculating the wavefunction at the GVB(6/12) level where all the Mo-C, Mo-O and O-H bonds were correlated. The Mo-C bonds appear exactly like those shown in Figure 4a and 4d for **11**. These bonds are essentially covalent with no large charge transfer from Mo to C.

The ground state of the OH fragment is s^2, px^2, py^1. Thus, two modes of bonding can be envisioned. The first is a 90° Mo-O-H bond angle with a sigma bond and with the possibility for donation by a p orbital to Mo. The second bonding mode would yield a 180° Mo-O-H bond angle. This bonding mode would involve a donor sigma bond from oxygen to molybdenum and a covalent Mo-O π bond. In addition, the possibility for a Mo-O donor-acceptor π bond exists. Due to the high valent nature and high electrophilicity of the $Cl_2Mo(OH)CH_2$ complex, a bond angle of 180° degrees was chosen in order to fully probe the donor capability of the OH ligand. Various degrees of mixing of these bonding modes have been observed.[38] Any increase in the electrophilicity of the metal induces a larger donation by O and, consequently, the M-O-R bond angle becomes larger.

The contour plots of the Mo-O and O-H GVB orbitals of **13** are displayed in Figure 13. The O-H bond is highly polarized toward O due to the large elec-

tronegativity difference. The Mo-O bonds are all similar. Instead of forming one donor σ bond, a covalent π bond and a weak donor π bond, the metal formed three equivalent Mo-O bonds. Each of these bonds are polarized toward O, due to the lone pair oxygen nature of the bonds. The oxygen formed three sp^3 hybrids with a population of 5 electrons. Thus, all three Mo-O bonds are two thirds lone pair O donor bonds and one third Mo-O covalent bonds. In order to accomodate this bonding arrangement, the Mo has used three d orbitals and an s orbital to form three equivalent hybrid orbitals for the O bonds. The orbitals shown in Figures 13c and 13d are plotted in planes formed by a 120° rotation along the Mo-O bond vector of Figure 13b.
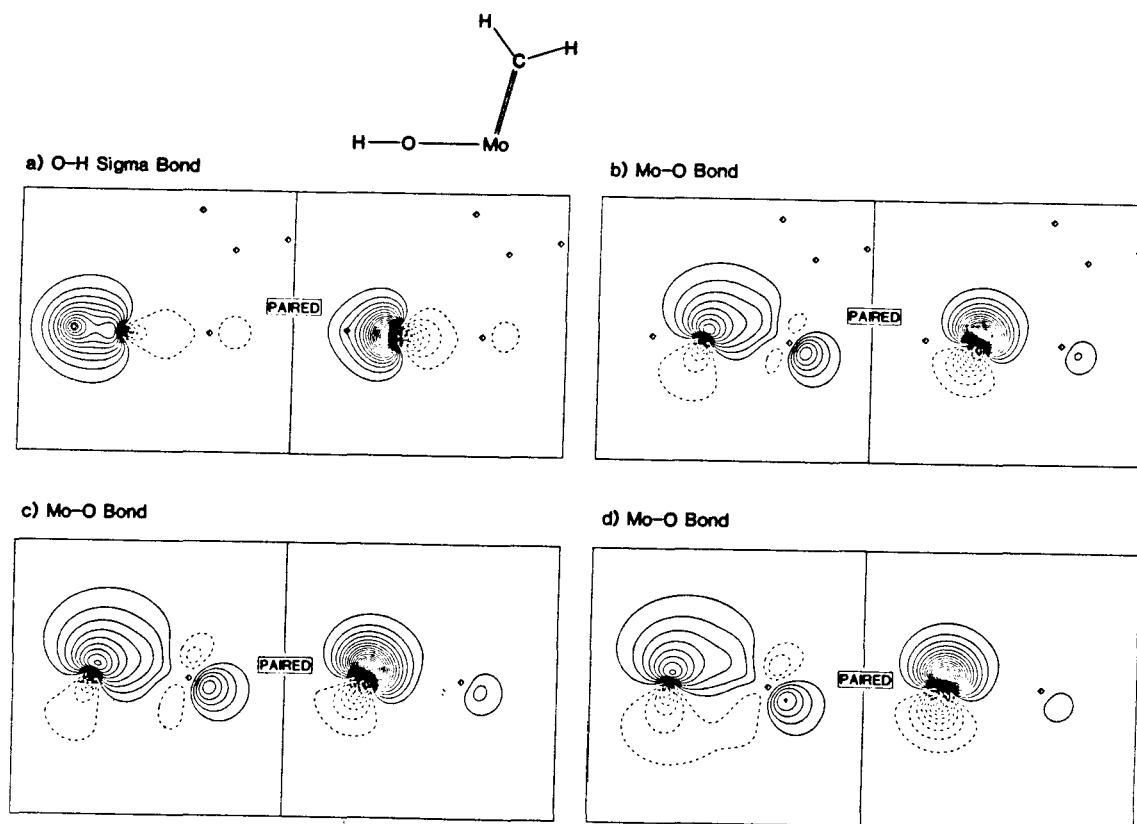
Figure 13: Contour plots of the GVB orbitals of the Mo-O bonds of $Cl_2Mo(OH)CH_2$. Figures c and d are plotted in planes formed by a 120° rotation along the Mo-O bond vector.

The contour plots of the Mo-O GVB orbitals in the metallacycle **17** appear essentially identical to those presented for the methylidene complex **13**. The molybdenum forms three equivalent bonds to the oxygen with a mixture of oxygen lone pair donor and Mo-O covalent character. There is no increase in donation of the oxygen lone pairs upon formation of the metallacycle. The lack of increase in the Mo-O bond order is due to the symmetry of the orbitals that molybdenum uses to bond to the oxygen remaining essentially the same upon metallacycle formation. In **13**, the molybdenum already possesses empty orbitals that the OH ligand can use to back donate. Thus, the full stabilization possible by donation of the oxygen lone pairs is already developed in **13**. There is no extra donation gained upon metallacycle formation.

D. Bonding in $Cl_2Mo(O)CH_2$ versus $Cl_2Mo(NH)O$

The electronic structure of $Cl_2Mo(NH)O$ and Cl_2MoO_2 has previously been studied by the Goddard group.[36] In these complexes, both the NH and O fragments possess a lone s electron pair which can be donated to the metal. In fact, there is a competition between the donor ligands for donation into the empty d orbital on Mo. Therefore, both covalently bonded ligands possess a ligand-Mo bond order greater than two. In an analogous manner to the work presented here, the donation increases upon breaking of one of the metal-ligand π bonds to form a metallacycle. In the $Cl_2Mo(NH)O$ fragment, an optimized Mo-N-H angle of 142° was found. This is due to the donor acceptor Mo-N interaction possessing large p character on the N. This donation is of π symmetry, unlike the σ donation found for $Cl_2Mo(NH)CH_2$.

The empty orbital that both the NH and O ligands compete for in $Cl_2Mo(NH)O$ cannot be σ in symmetry with respect to both ligands. A π symmetry orbital, however, can be π in symmetry with respect to both ligands. Thus,

the NH and O fragments donate electron density to Mo in a π fashion rather than a σ fashion (4).

(4)
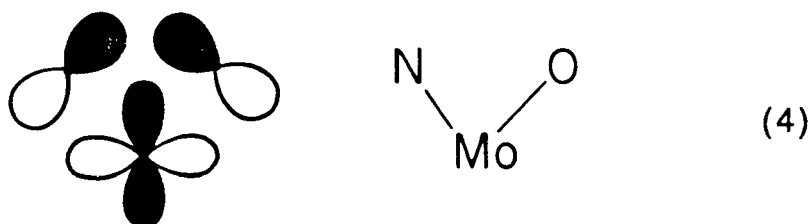
Upon formation of a metallacycle across the N-Mo bond, the N no longer acts as a donor ligand. Thus, the oxygen no longer competes for the empty orbital and can make a donor σ interaction with the metal. This donor sigma interaction stabilizes the metallacycle.

In a $Cl_2Mo(O)CH_2$ complex, the oxo ligand has no competition as a donor to the metal. Thus, a full sigma oxygen donation interaction to the metal is possible. This possibility was tested by calculating the wavefunction for $Cl_2Mo(O)CH_2$ at the GVB(6/12) level, where all Mo-C and Mo-O bonds were correlated.[39] The contour plots of the GVB orbitals are displayed in Figure 14. Since oxygen is a better donor than nitrogen and forms stronger, shorter π bonds to Mo than N, the oxygen donation is more pronounced. This is seen in Figure 14b. All the other Mo-ligand bonds appear typical.

E. Charge Distribution

The Mullikan populations for compounds studied are shown in Figure 15. The charge distributions between the Mo and C atoms represent covalent interactions. The negative charges on the carbons are due to the positive charges on the hydrogens and are not due to electron withdrawal from the Mo. These covalent interactions
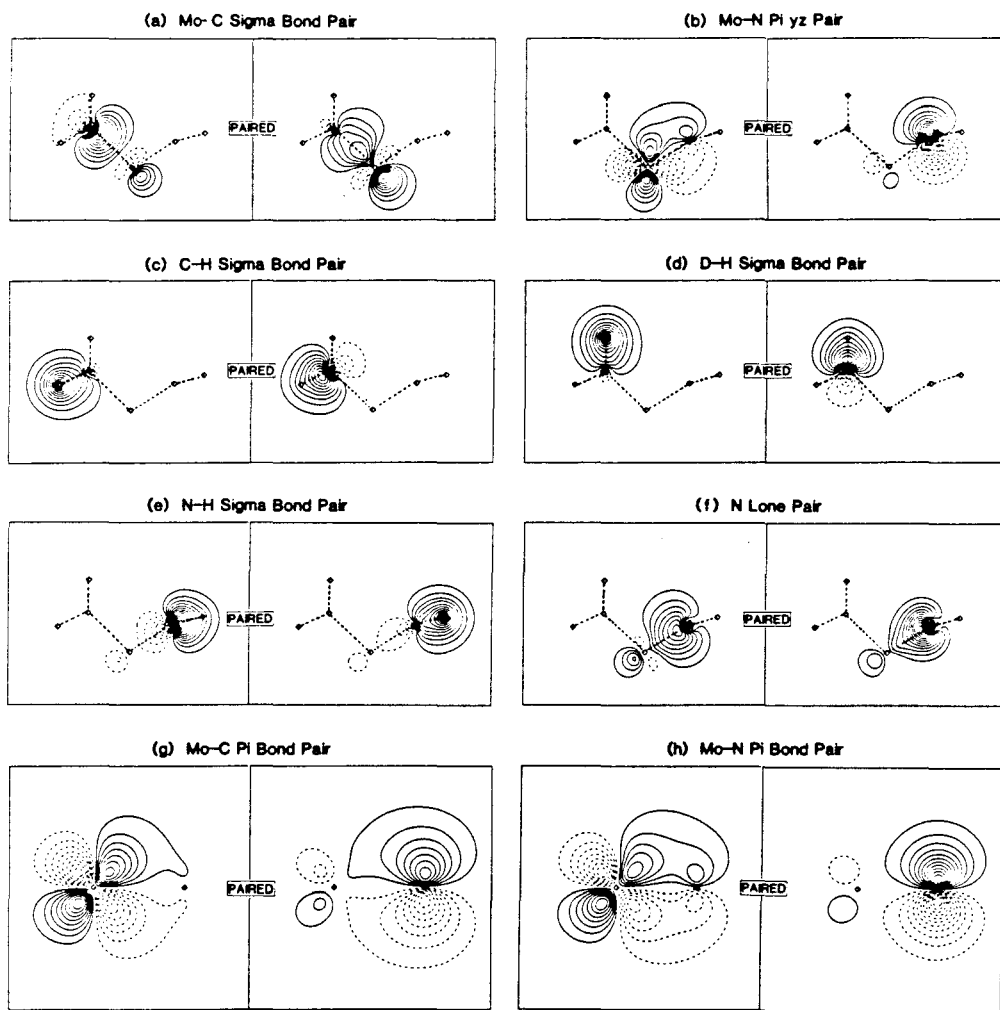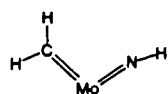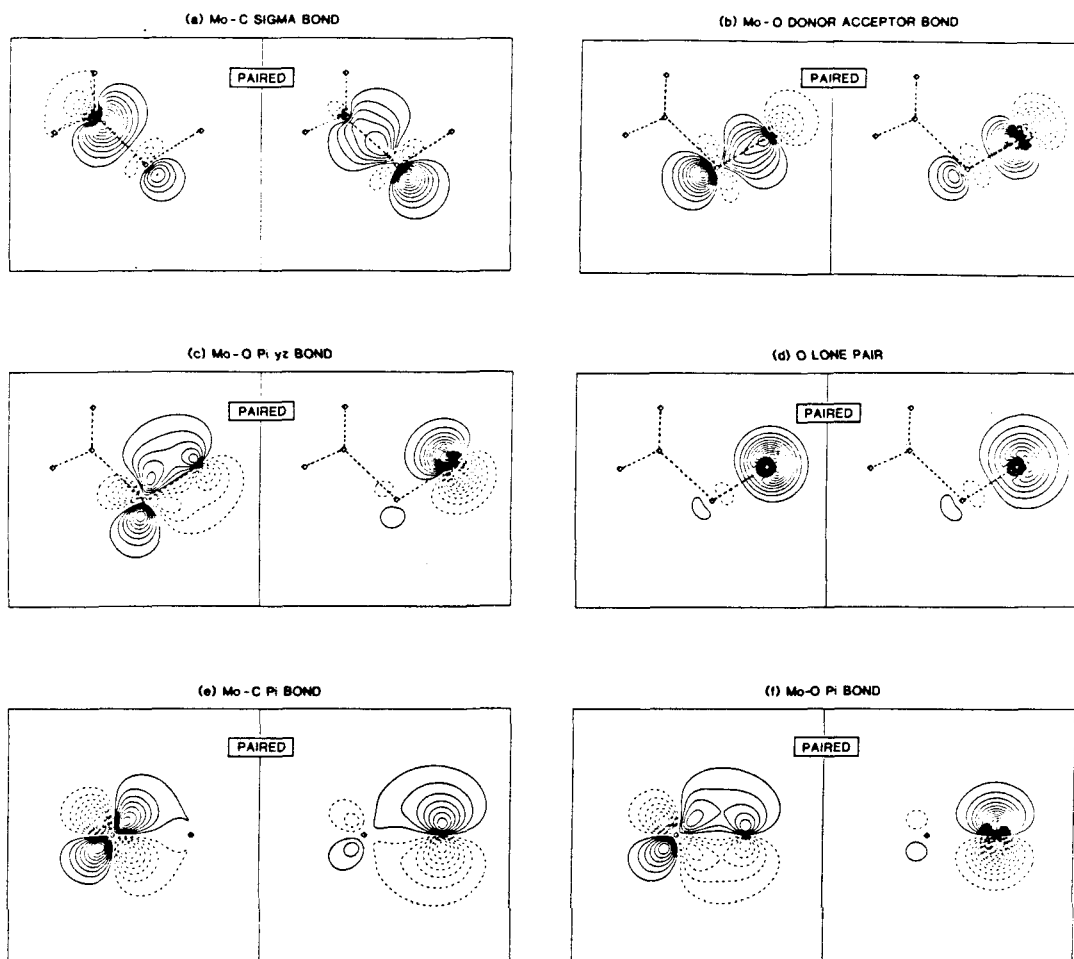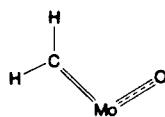
Figure 14: Contour plots of the GVB orbitals for $Cl_2Mo(O)CH_2$. Figures e and f are plotted in the planes of the Mo-C and Mo-O π bonds respectively.

157
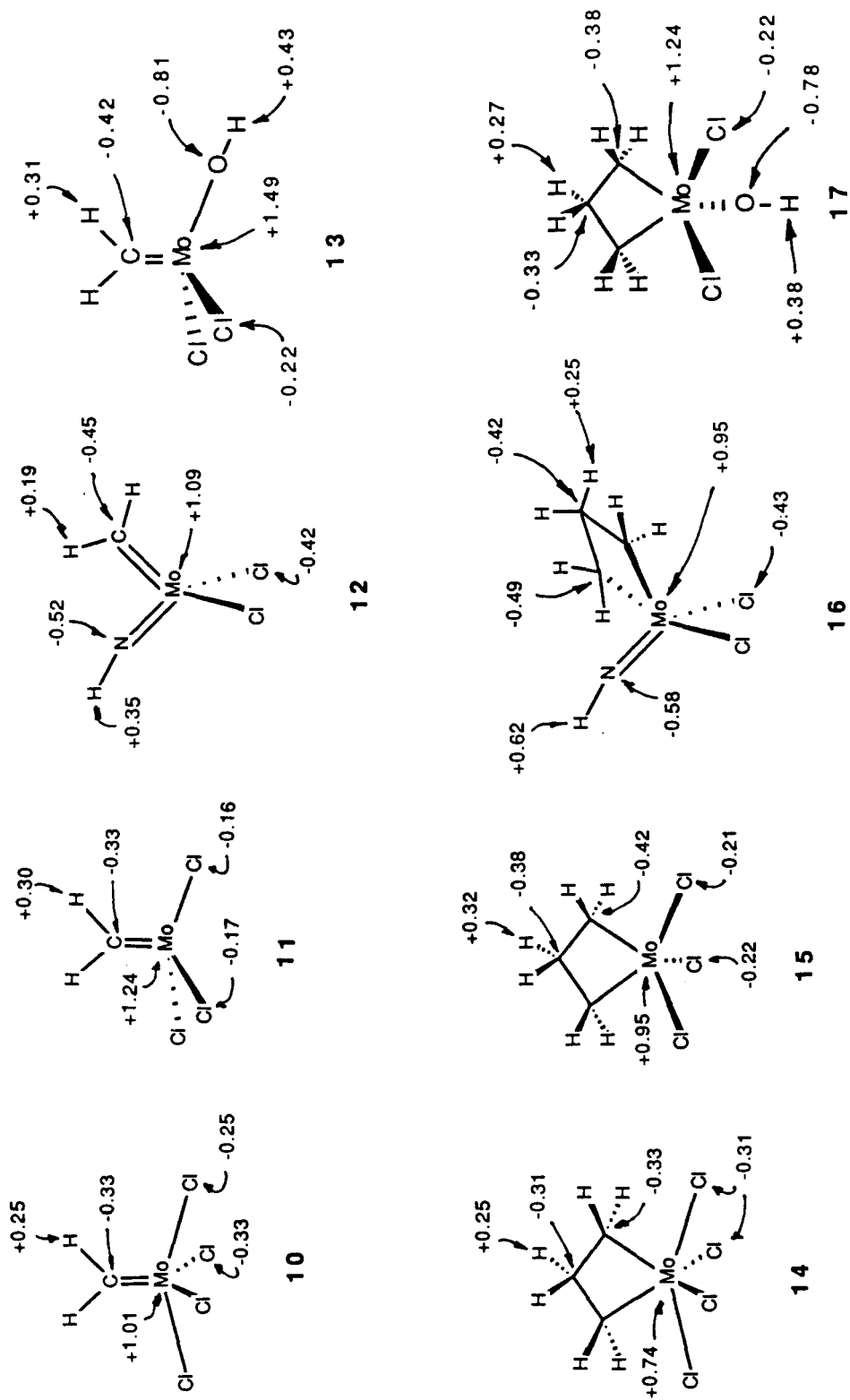
Figure 15: Mullikan populations.

are also supported by the GVB contour plots of the Mo-C and Mo-N bonds of all the complexes studied. There is no large charge polarization toward C or N in these contour plots. In the cation **15**, the charge on Mo is +0.21 higher than in **14**. The charge on Mo in the cation **11** is +0.23 higher than in **10**. Thus, in both geometries **11** and **15**, the full positive charge is not completely isolated on the Mo center but is distributed among the chlorines and carbons. The chlorines are not as negatively charged in the cations since an s electron has been already removed due to the positive charge. Therefore, the chlorines compete more with the carbons for the d electron density.

F. Reactivity

The 2+2 reaction of metal alkylidenes with ethylene was studied. This is the first step in the well-accepted Herrison-Chauvin mechanism for olefin metathesis.[40] The simplest catalyst studied was Cl_4MoCH_2 **10**. As indicated in Figure 16, this reaction is favorable, with $\Delta G_{300} = $ -11 kcal/mol.[41] The bonding in the metallacycle is strong enough to compensate for the loss of the π bonding in the metallacycle and the olefin. The analogous reaction for the cationic complex $Cl_3MoCH_2^+$ was found to be unfavorable, with $\Delta G_{300} = $ +3 kcal/mol. In this case, the bonding in the metallacycle is not strong enough to compensate for the loss of the π bonding. The reactivity reversal is due to the stronger π bond in **11** than in **10**. The π bond is stronger in the cationic complex due to the shorter Mo-C bond distance. The π bond overlap increases at a greater rate than σ bond overlap as the Mo-C bond distance decreases. In Table 2, the GVB bond overlaps for **10** and **11** are tabulated. The overlap is 0.05 greater in **11** than in **10**.

To further investigate the relative Mo-C double bond strengths in **10** and **11**, the snap bond energies of the Mo-C double bonds were calculated. The Mo-C double
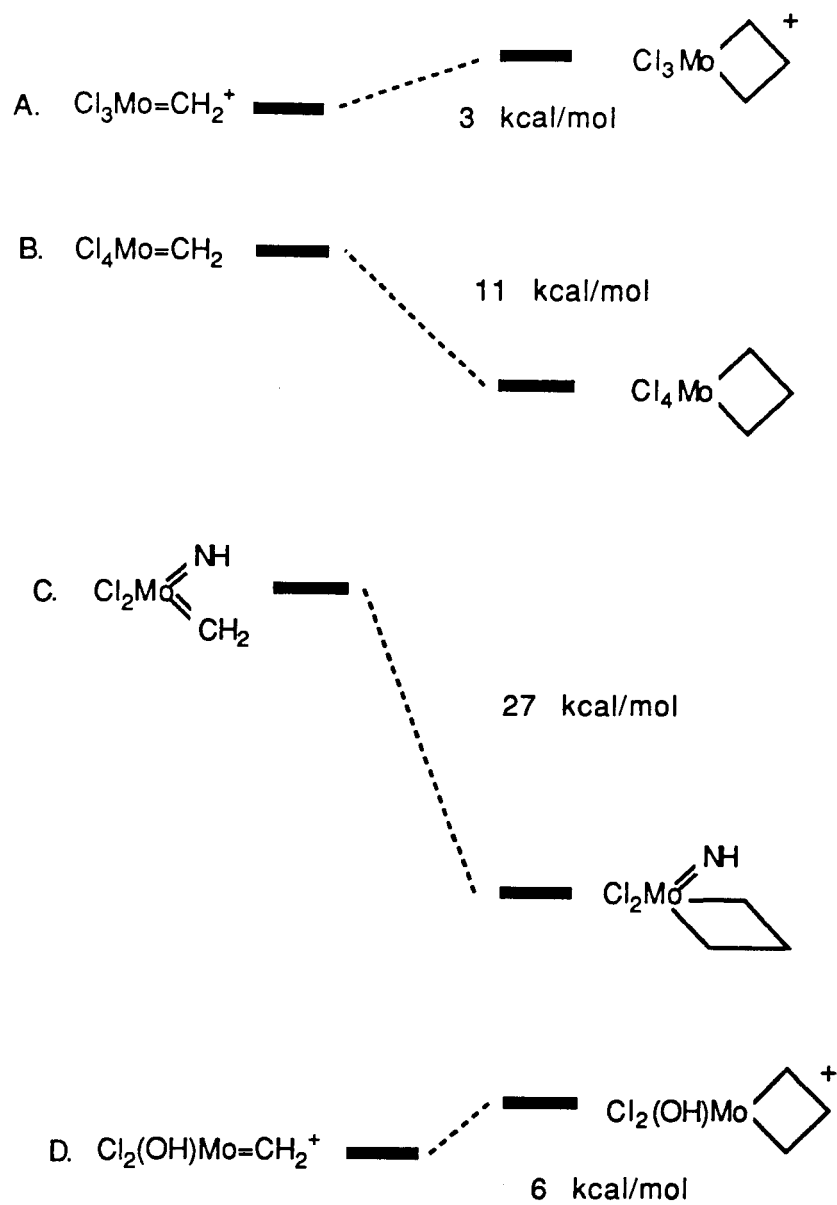
Figure 16: Schematic reaction coordinates for the metallacycle formation reactions.

bond strengths in **10** and **11** were found to be 53.8 and 75.2 kcal/mol, respectively. The bond strength of **11** is 21.4 kcal/mol greater than that in **10**. This difference is similar to the 14 kcal/mol difference in free energies of reaction of **10** and **11** with ethylene. Therefore, the stronger Mo-C double bond of **11** considerably raises the energy of reaction of **11** with ethylene versus the same reaction for **10**. Thus, the concept of the greater electrophilicity making **11** more reactive than **10** is only partially correct. The greater electrophilicity makes the Mo-C π bond stronger. The σ bond strength in **14** and **15** remains roughly the same since their overlaps are not different (Table 2). Consequently, the reactivity difference that favors **11** must be based on a kinetic preference. To probe the kinetic difference between the complexes, a calculation was performed to find the empty orbitals available for coordination of an olefin.

The empty orbitals for both **10** and **11** are shown in Figure 17. There are three empty orbitals as previously discussed for the $MoCl_3^+$ and $MoCl_4$ fragments (Figure 3). These orbitals are in the yz and xy planes. These orbitals can allow for olefin coordination along three different directions in both **10** and **11**. The only productive coordination is along the +x or −x axis (Figure 17c). This coordination would lead to metallacycle formation.

In Cl_4MoCH_2, however, the empty orbital along the +x and −x direction is blocked by the trans chlorines which are 180° from one another. Therefore, olefin coordination along this axis is sterically encumbered and the reaction is predicted to be energetically unfeasible. In $Cl_3MoCH_2^+$, however, the coordination sites along the x and −x directions are open due to the wide Cl-Mo-Cl angle of 118.3°. This allows for olefin coordination and subsequent reaction. The reaction free energy of +3 kcal/mol confirms that this reaction is feasible. In addition, due to
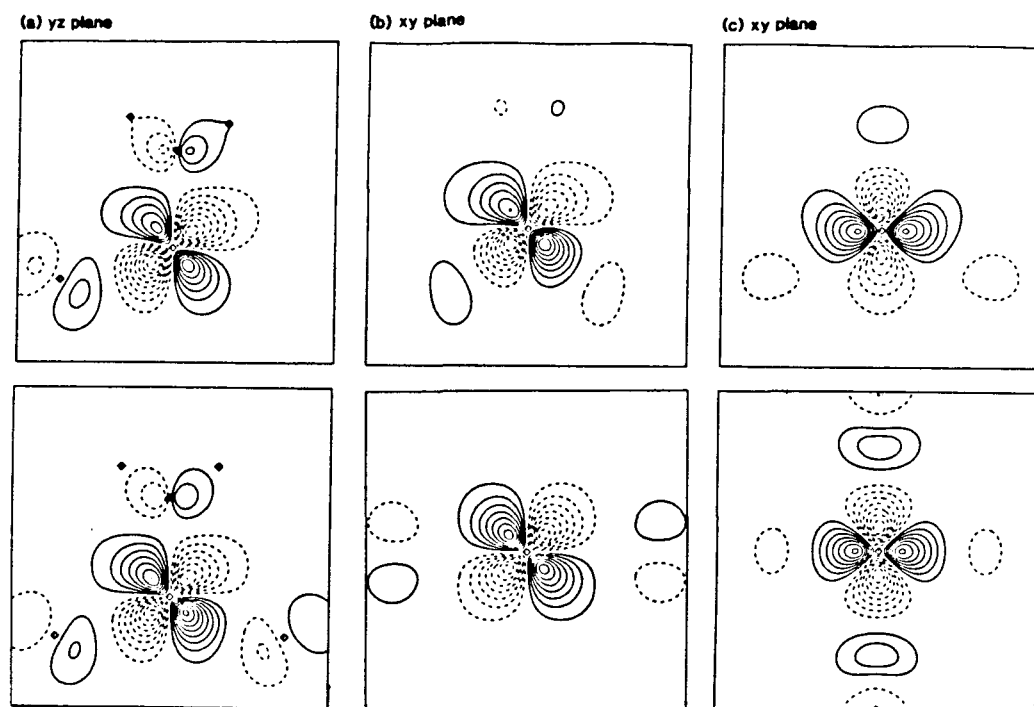
Figure 17: Empty orbitals centered on Mo for $Cl_3MoCH_2^+$ and Cl_4MoCH_2. The top row are the empty orbitals for $Cl_3MoCH_2^+$ and the bottom row are the empty orbitals for Cl_4MoCH_2. The planes refered to are those given in Figure 1.

the greater electrophilicity of the cationic $Cl_3MoCH_2^+$ complex, the donor-acceptor olefin-methylidene complex should be lower in energy than the analogous olefin complex with Cl_4MoCH_2, further lowering the kinetic barrier to reaction.

The reaction of the carbene imido complex **12** with ethylene was found to be favorable by a ΔG_{300} of -27 kcal/mol. This stabilization in comparison to the reaction of **10** with ethylene (about 16 kcal/mol), must come from an electronic difference between the Mo-N and Mo-Cl bonds. As discussed in the structural and bonding section *B*, the Mo-N bond has a bond order greater than two in both the imido carbene **12** and imido metallacycle **16**. In the imido metallacycle complex, however, the donation of the N lone pair to the Mo is significantly greater than in

the imido carbene complex due to a rehybridization of the d orbitals to form two Mo-C σ bonds. This lowers the energy of the empty orbital and also changes its $d\sigma$ character such that the N s lone pair can more efficiently donate. Thus, the imido group is intimately involved in the reaction of the alkylidene with olefins.

To further investigate the spectator imido effect, a calculation was performed to determine the snap bond energy of the Mo-N triple bond in both **12** and **16**. The bond strengths were found to be 80.6 and 97.9 kcal/mol for **12** and **16**, respectively. The Mo-N bond strength of **16** is stronger by 17.3 kcal/mol. This energy difference is similar to the 16 kcal/mol stabilization gained upon forming a metallacycle from **12** versus **10**. Thus, the majority of the stabilization in the reaction of the complex **12** with ethylene arises from the increased Mo-N bond strength.

In addition to a spectator imido effect stabilizing the 2+2 reaction with olefins, this reaction is favorable kinetically since the only empty orbital for olefin coordination is along the x axis and leads to metallacycle formation. This direction for coordination is not very sterically encumbered since the chlorines are bent down from the x axis by 28°. Thus, the imido carbene complex **12** is efficient in the metathesis reaction due to two effects. The first is a stabilization of the metallacycle complex by increased donation by the spectator imido, and the second effect is the open coordination site which leads to metathesis.

The reaction of the carbene complex **13** was found to be endothermic by 6 kcal/mol. The endothermic nature of this reaction versus that for **10** is again due to a larger Mo-C bond strength in complex **13** versus **10**. There is no increase in donation from the alkoxide to the Mo upon formation of the metallacycle as was observed for the imido ligand in **12**. Thus, there is no stabilizing effect from the spectator alkoxide, and the reaction coordinate is similar to that for **11**. The lack

of an increase in donation from O to Mo upon metallacycle formation is due to the low donating ability of an alkoxide. In addition, complex **13** has an empty dπ symmetry orbital already available for donation from the alkoxide ligand and the alkoxide consequently donates to the Mo slightly. Upon formation of metallacycle **17**, the hybridization and symmetry of this orbital are not perturbed, and thus, no increase in Mo-O bond order occurs.

SUMMARY

The geometry of bonding of triplet methylene to $MoCl_3^+$ and $MoCl_4$ is dictated by the geometry of the high spin orbitals of $MoCl_3^+$ and $MoCl_4$. The lowest energy configuration for the high spin orbitals of the $MoCl_3^+$ and $MoCl_4$ fragments occurs when the angular nodes of the high spin orbitals are placed along the Mo-Cl bonds. In a similar manner, the CH_2 and NH fragments bond to $MoCl_2$ in a manner predicted by the high spin orbitals on $MoCl_2$. These high spin orbitals dictate that the atoms of the moieties Mo, NH and CH_2 are coplanar.

The bonds from Mo to N and C are essentially covalent, whereas those to Cl are polarized toward the Cl's and are of high s character on the Mo. The d orbitals not used to make bonds to the carbons and nitrogens are empty and are slightly antibonding with respect to the Mo-Cl bonds. These empty orbitals dictate the direction of coordination of olefins.

The metallacycle $C_3H_6MoCl_4$ has an unusually small C-Mo-C bond angle and a long Mo-C bond length of 2.31Å. The small angle is due to the necessity of making four coplanar bonds to Mo. Two of these bonds are to chlorine and are high in s character. Thus, the bonds to carbon are higher in d character than usual. This high d character induces a bond angle close to $54°$, as previously shown by Rappé and Goddard.

The reactivity of $Cl_3MoCH_2^+$ with ethylene was found to be endothermic by 3 kcal/mol, but the empty d orbitals on Mo facilitate olefin coordination and metathesis. Conversely, the reaction of Cl_4MoCH_2 with ethylene was found to be exothermic by 11 kcal/mol. The empty orbitals on Mo, however, are all blocked by the chlorine ligands, and thus, coordination of an olefin is sterically encumbered. The thermodynamics of the reaction of $Cl_3MoCH_2^+$ are less favorable than those of the reaction

of Cl_4MoCH_2, due to the stronger Mo-C bond strength in $Cl_3MoCH_2^+$.

The reaction of $Cl_2Mo(NH)CH_2$ with ethylene is exothermic by 27 kcal/mol. The high reactivity is due to a stabililization of the metallacycle by the spectator imido. Upon formation of the metallacycle, an extra $d\sigma$ orbital is formed and a $d\pi$ orbital is lost. This rehybridization creates an empty orbital with the correct symmetry for donation by the lone s pair on nitrogen.

In dioxo or oxo imido Group VIB complexes, both ligands compete for donation to the empty orbitals. The empty orbital cannot be σ in character with respect to both ligands, and thus, the ligands donate into a π symmetry orbital. Upon breaking one of the Mo-N or Mo-O π bonds, one donor ligand can no longer donate, and thus, the other ligand donates in a sigma fashion to the metal. In the complex $Cl_2Mo(O)CH_2$, the methylene ligand does not compete with the oxo to donate, and thus, the oxo can form two π bonds and a full donor sigma bond to Mo.

The reaction of $Cl_2Mo(OH)CH_2^+$ **13** with ethylene is endothermic by 6 kcal/mol. This is similar to the endothermicity of the reaction of **11** with ethylene and is due to a strong Mo-C double bond. In complex **13**, the alkoxide can donate into an empty $d\pi$ orbital on Mo. Upon metallacycle formation, the hybridiation and symmetry of this orbital is not perturbed, and there is no increase in donation. Thus, there is no stabilization from a spectator alkoxide.

REFERENCES AND NOTES

1. (a) Dragutan,V.; Balaban,A.; Dimone,M. Olefin Metathesis and Ring Opening Polymerizations of Cyclo-Olefins; Wiley-Interscience, Chichester, **1985**. (b) Ivin,K.J. Olefin Metathesis; Academic Press, London, **1983**. (c) Mol,J.C. *CHEMTECH*, **1983**, *13*, 250. (d) Grubbs,R.H. Comprehensive Organometallic Chemistry; Wilkinson,G. Ed.; Pergamon Press, Ltd., Oxford, 1982., Vol.8, pp499-551. (e) Banks,R.L. *Catalysis*, **1981**, *4*, 100.

2. (a) Calderon,J.J. *Macromol. Sci.*, **1972**, *C7(1)*, 105. (b) Katz,T.J.; Lee,S.J.; Shippey,M.A. *J. Mol. Catal.*, **1980**, *8*, 219.

3. (a) Howard,T.R.; Lee,J.B.; Grubbs,R.H. *J. Am. Chem. Soc.*, **1980**, *102*, 6876. (b) Straus,D.A.; Grubbs,R.H. *J. Mol. Catal.*, **1985**, *28*, 9. (c) McLain,S.J.; Wood,C.D.; Schrock,R.R. *J. Am. Chem. Soc.*, **1979**, *101*, 4458. (d) Smith,G.; McLain,S.; Sancho,J. *Pure Appl. Chem.*, **1980**, *52*, 729.

4. (a) Katz,T.J.; Ho,T.H.; Shih,N.Y.; Ying,Y.C.; Stuart,V.W. *J. Am. Chem. Soc.*, **1984**, *106*, 2659. (b) Katz,T.J.; Hacker,S.M.; Kendrick,R.D.; Yammoni,C.S. *J. Am. Chem. Soc.*, **1985**, *107*, 2182. (c) Fischer,E.O. *Adv. Organomet. Chem.*, **1976**, *14*, 1.

5. (a) Schrock,R.R.; Rocklage,S.; Wengrovious,J.; Rupprecht,G.; Fellmannn,J. *J. Mol. Catal.*, **1980**, *8*, 73. (b) Wengrovious,J.; Schrock,R.R.; Churchill,M.R.; Missert,J.R.; Youngs,W.J. *J. Am. Chem. Soc.*, **1980**, *102*, 4515.

6. Schaverien,C.J.; Dewan,J.C.; Schrock,R.R. *J. Am. Chem. Soc.*, **1986**, *108*, 2771.

7. (a) Porri,L.; Diversi,P.; Lucherini,A.; Rossi,R. *Die. Makro. Chemie*, **1975**, *176*, 3121. (b) Porri,L.; Rossi,R.; Diversi,P.; Lucherini,A. *Die. Makro. Chemie*, 1974, *175*, 3097.

8. Thoi,H.H.; Ivin,K.J.; Rooney,J.J. *J. Mol. Catal.*, **1982**, *15*, 245.

9. Straus,D.A.; Grubbs,R.H. *Organometallics*, **1982**, *1*, 1658.

10. (a) Anslyn,E.V., Grubbs,R.H. *J. Am. Chem. Soc.*, **1987**, *109*, 4880. (b) Lee,J.B.; Ott,K.C.; Grubbs,R.H. *J. Am. Chem. Soc.*, **1982**, *104*, 7491.

11. Upton,T.H.; Rappé,A.K. *J. Am. Chem. Soc.*, **1985**, *107*, 1206.

12. (a) Kress,J.; Osborn,J.A.; Greene,R.M.; Ivin,K.J.; Ronney,J.J. *J. Am. Chem. Soc.*, **1987**, *109*, 899. (b) Kress,J.; Aguero,A.; Osborn,J.A. *J. Mol. Catal.*, **1986**, *36*, 1.

13. (a) Quignard,F.; Leconte,M.; Basset,J.M. *J. Mol. Cat.*, **1986**, *36*, 13. (b) Quignard,F.; Leconte,M.; Basset,J.M. *J. Chem. Soc., Chem. Comm.*, **1985**, *23*, 1816.

14. (a) Schrock,R.R. *J. Organomet. Chem.*, **1986**, *300*, 249. (b) Schrock,R.R.; Feldman,J.; Cannizzo,L.F.; Grubbs,R.H. *Macromolecules*, **1987**, *20*, 1172.

15. Schrock,R.R.; DePue,R.T.; Feldman,J.; Schaverien,C.T.; Dewan,T.C.; Liu,A.H. *J. Am. Chem. Soc.*, **1987**, *109*, 0000.

16. Streck,R. *CHEMTECH*, **1983**, *13*, 758.

17. (a) Ohm,R., Stein,I. Encyclopedia of Chemical Technology; 3rd Ed., Grayson,M., Ed., Wiley Interscience, New York, **1982**, Vol.18, p436. (b) Cannizzo,L.F.; Grubbs,R.H. *Macromolecules*, **1987**, *20*, 0000.

18. Swager,T.M.; Grubbs,R.H. *J. Am. Chem. Soc.*, **1987**, *109*, 894.

19. (a) Kertesy,M.; Hoffmann,R. *Solid State Commun.*, **1982**, *47*, 97. (b) Eisenstien,O.; Hoffmann,R.; Rossi,A.R. *J. Am. Chem. Soc.*, **1981**, *103*, 5582.

20. Rappé,A.K.; Goddard III,W.A. *J. Am. Chem. Soc.*, **1982**, *104*, 448.

21. Rappé,A.K.; Goddard III,W.A. *J. Am. Chem. Soc.*, **1982**, *104*, 3287.

22. Huzinaga,S. *J. Chem. Phys.*, **1965**, *42*, 1293.

23. Hay,P.J. Personal communication to William A. Goddard III.

24. Dunning Jr,T.H.*J. Chem. Phys.*, **1970**, *53*, 2823.

25. Szabo,A.; Ostlund,N.S. Modern Quantum Chemistry; MacMillan Pub. Co. Inc., New York, 1982.

26. Bobrowicz,F.W.; Goddard III, W.A. Modern Theoretical Chemistry, Methods of Electronic Structure Theory; Schaefer,H.F., Ed. Plenum Press, New York, 1977, Vol. 3, Chapter 44, pp79-127.

27. Rappé,A.K.; Personal Communication to Goddard III, W.A.

28. Rappé,A.K.; Goddard III,W.A. Potential Energy Surfaces and Dynamics Calculations; Truhlar,D.G., Ed., Plenum Press, New York, **1981**, pp661-684.

29. Stull,D.R.; Prophet,H. Janaf Thermochemical Tables, 2nd Ed.; NSRDS, Washington D.C., 1971.

30. (a) Strutz,H.; Dewan,J.C.; Schrock,R.R. *J. Am. Chem. Soc.*, **1985**, *107*, 5999.
    (b) Kauffmann,T.; Ennen,B.; Sander,J.; Wieschollek,R. *Angew. Chem., Int. Ed. Eng.*, **1983**, *22*, 244.

31. Weast,R.C. CRC Handbook of Chemistry and Physics; CRC Press, Boca Raton, **1980**.

32. (a) Katz,T.J., McGinnis,J. *J. Am. Chem. Soc.*, **1975**, *97*, 1592.   (b) Casey,C.P.; Albin,L.D.;, Burkhardt,T.J. *J. Am. Chem. Soc.*, **1977**, *99*, 2533.
    (c) Tinland,B.; Quignard,F.; Leconte,M., Basset,J.M. *J. Am. Chem. Soc.*, **1983**, *105*, 2924.

33. Hay,P.J.; Hunt,W.J.; Goddard III,W.A. *Chem. Phys. Lett.*, **1972**, *13*, 1.

34. Anslyn,E.V.; Brusich,M.J.; Goddard III,W.A. *Organometallics*, **1987**, *6*, 0000.

35. Rappé,A.K.; Goddard III,W.A. *J. Am. Chem. Soc.*, **1982**, *104*, 297.

36. Allison,A., Ph.D. Thesis, 1984, California Institute of Technology

37. Nugent,W.A., Haymore,J.K. *Coord. Chem. Rev.*, **1980**, *31*, 123.

38. Collman,J.P.; Hegedus,L.S.; Norton,J.R.; Finke,R.G. "Principles and Applications of Organotransition Metal Chemistry"; University Science Books, Mill Valley, Ca., **1987**.

39. This reaction has been previously found to be endothermic by +15 kcal/mol[20]. The discrepancy between the two results is probably due to different levels of electron correlation and the fact that complexes **10** and **15** are fully geometry optimized.

40. (a) Herrison,J.L.; Chavin,Y. *Makromol. Chem.*, **1970**, *141*, 161. (b) Soufflet,P.; Commereuc,D.; Chauvin,Y. *Compt. Rend. Acad. Sci., Ser. C*, **1973**, *276*, 169.

41. This complex has been previously studied at the GVB(4/8) level, and no donor interaction was found.[20] The discrepancy between that result and those presented here are probably due to different levels of electron correlation.

The Reaction of $Cp_2Ti = CH_2$ With Organic Halides:

Evidence for a Radical Mechanism

ABSTRACT

Sources of "$Cp_2Ti=CH_2$" react with organic halides RX to yield $Cp_2Ti(X)CH_2$-R. Benzyl and allyl halides react more rapidly than 1° or 3° halides. Tertiary butyl chloride reacts to yield isobutylene and titanocene methyl chloride. Substituents have little effect on the rate of benzyl halides ($RC_6H_4CH_2Cl$, R = C_6H_5, OCH_3, CH_3 Cl) reacting with $Cp_2Ti=CH_2$. Optically active C_6H_5-CHDCl reacts with complete scrambling of stereochemistry. A mechanism involving initial electron transfer is proposed to account for these observations.

INTRODUCTION

Metal carbenes have been demonstrated in such important catalytic processes as olefin metathesis[1] and Fischer-Tropsch CO[2] reduction and suggested as intermediates in Ziegler-Natta polymerization[3] and hydrocarbon cracking.[4] The reactivity patterns exhibited by isolated metal carbenes are divided into two classes: electrophilic carbenes (A),[5] which add nucleophiles at the carbene carbon, and nucleophilic carbenes (B),[6] which add electrophiles at the carbene carbon. This chapter demonstrates a different type of reactivity pattern for a metal carbene; reaction by electron transfer.

A   **B**
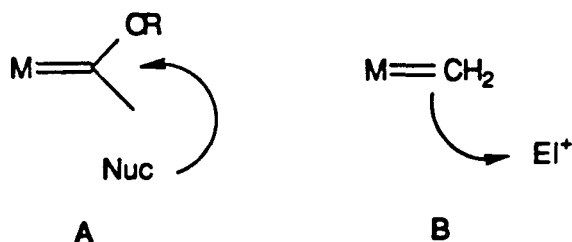
Titanocene metallacyclobutanes such as **1** can function as a reagent for a variety of synthetically useful transformations, presumably through the carbene **2**.[7] To further characterize the reactivity of **2**, its reactions with alkyl halides were explored.

RESULTS AND DISCUSSION

Treatment of 1 with allylic chloride (1.1 equiv, RT, C_6D_6, 12 h) produced a quantitative yield (^{1}H NMR) of titanocene butenyl chloride instead of a stable metallacycle resulting from reaction with the olefin. Further study of reactions of 1 with alkyl halides gave the results shown in Figure 1. Most interesting, while 1 reacts readily with activated alkyl halides, and slowly with t-butylchloride, no reaction is observed with excess methyl iodide, even after prolonged reaction times. Such a reactivity pattern is contrary to that expected for a S_N2 type displacement, the pathway that 2 would be expected to follow in reactions with alkyl halides.[6,8] Since nucleophilic displacement did not explain the observed reactivity, it was decided to study this reaction in detail, choosing benzyl chloride as substrate.

Figure 1:
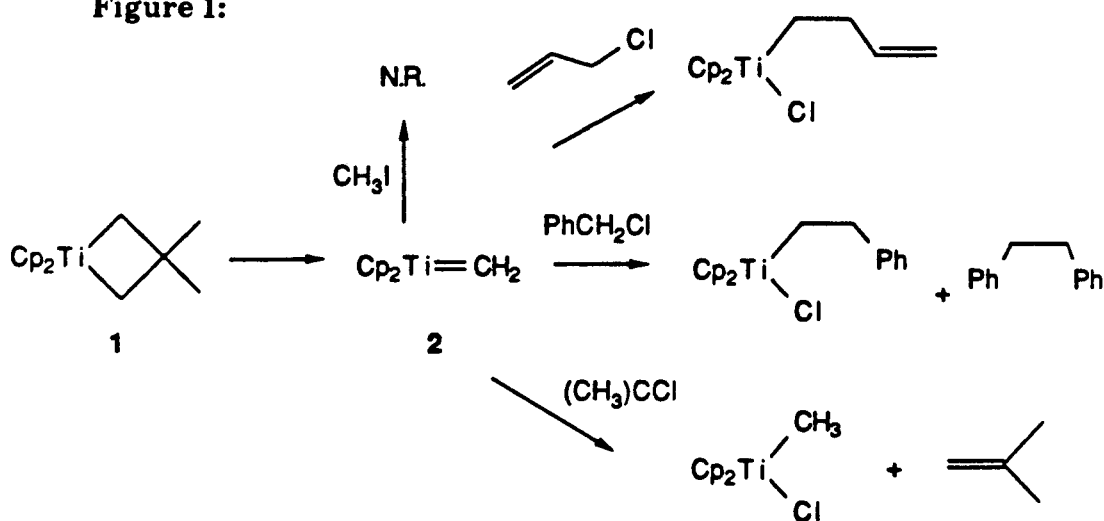
Figure 2:
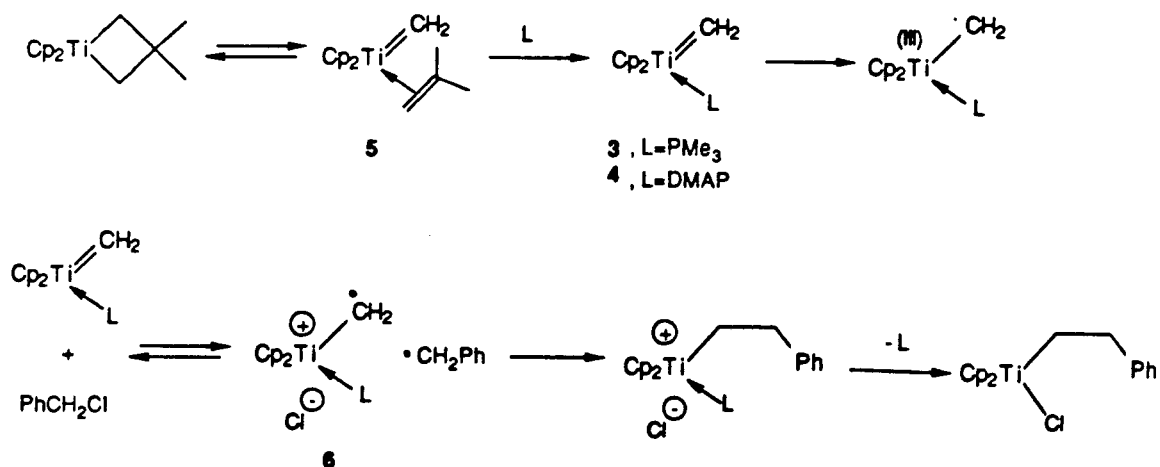
The reaction of **1** with benzyl chloride (1.2 equiv) gave the known titanocene phenethyl chloride[8a] and bibenzyl in a ratio of 90:10. The reaction exhibited second order kinetics in C_6D_6 ($k = 9.3$ x 10^{-4} M^{-1} s^{-1}, $\tau_{\frac{1}{2}} = \sim 59$ min, RT, first order in both **1** and ϕCH_2Cl) and showed little sensitivity to para substitution of the aromatic ring. For example, relative rates of *p*-methoxy benzyl, *p*-phenyl benzyl, *p*-chloro benzyl, *p*-methyl benzyl and benzyl chloride were 2.64, 2.99, 2.45, 1.22, and 1.0.[8b] Seeking to support the assumption that **2** was actually an intermediate in this reaction, the crystalline trimethyl phosphine[9] adduct **3** was exposed to benzyl chloride (Scheme 2). This reaction gave a 95:5 ratio of titanocene phenethyl chloride and bibenzyl and was essentially instantaneous. This suggested that the ligated carbene was more reactive than free carbene. In confirmation, addition of 10 mol percent dimethylaminopyridine (DMAP) to the reaction mixture containing **1** and benzyl chloride (1.0 equiv)[5] revealed a significant rate enhancement ($\tau_{\frac{1}{2}} = 8$ min, RT) over the reaction without added DMAP.[10] Moreover, essentially no

bibenzyl ($<5\%$) was formed in the reaction. In addition, the reaction of 1 with benzyl chloride showed a linear dependence on DMAP concentration and the reaction became zeroth order in benzyl chloride concentration, consistent with the reaction proceeding *via* 4 (Figure 2).

The details of the carbon-carbon bond forming process in the reaction of 4 (and 3) with ϕCH$_2$Cl, were investigated by examining the stereochemical course of this process. Treatment of 1 in the presence of 10 mol percent DMAP with an excess of optically active ϕCHDCl (80% *e.e.*)[11] gave, after (CH$_3$)$_3$C-OOH oxidation[12] and Na$_2$SO$_3$ workup, a quantitative yield of the β-chiral 2-phenethyl alcohol (eq. 1). Determination of the stereochemistry at the β-carbon was achieved using ^{1}H NMR at 400 MHz and confirmed with ^{2}H NMR at 77.6 MHz (proton decoupled) in the presence of 50 mol percent Eu (dcm)$_2$[13] in a method similar to that of Stille.[11] The results shown in Figure 3 indicate that a complete loss of stereochemistry has occurred in the carbon-carbon bond forming event.[14] Racemization occurred during product formation since recovered unreacted benzyl chloride showed complete retention of optical activity after conversion to the benzyl alcohol (Figure 4).
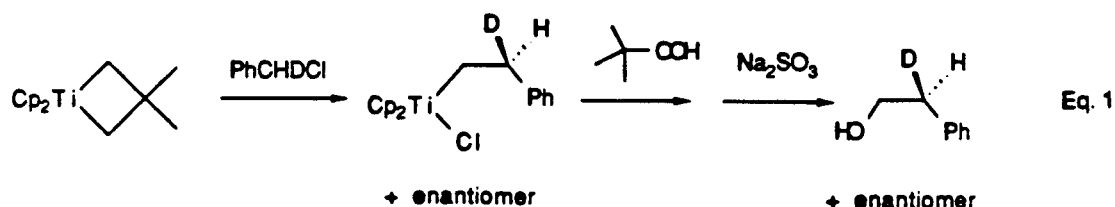
Taken together, the results are most readily explained by the mechanism shown in Figure 2. In the proposed mechanism, L traps out the carbene-olefin complex 5 to form a carbon ligand complex. This complex either induces
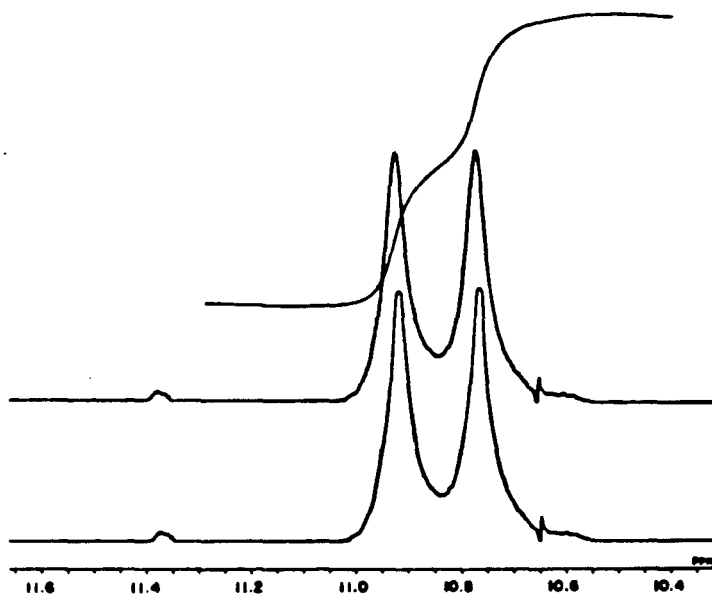
Figure 3: 400 MHz ^{1}H NMR (α carbon protons decoupled) showing ratio of enantiomers of PhCHDCH$_2$OH to be 1:1.
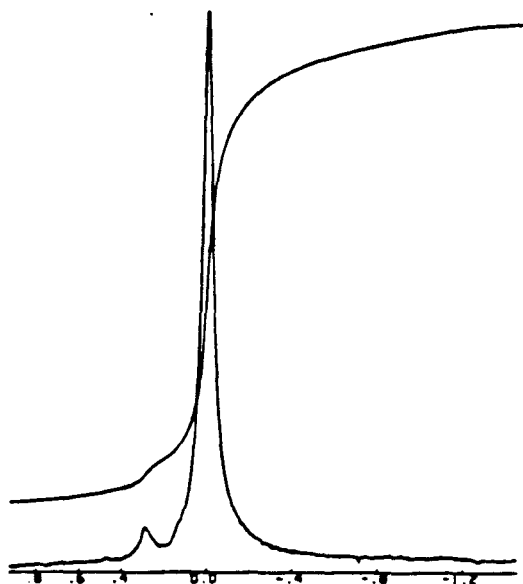
Figure 4: 500 MHz ^{1} NMR showing the *e.e.* of PhCHDOH to be greater than 80 percent.

radical character on the carbene carbon, making it more reactive, or at least increases the lifetime of the methylidene, increasing its chance to react with a benzyl chloride. At this point, the complex transfers an electron to the substrate (*e.g.*, benzyl chloride) to give **6**, which, by radical coupling and ligand exchange, yields titanocene phenethyl chloride. Bibenzyl is produced by benzyl radicals escaping from the cage and dimerizing.

In short, the reaction of titanocene methylene (**2**) with alkyl halides exhibits behavior contrary to that expected for either of the two previously defined classes of metal carbenes and to that predicted from on reactions with olefins or organic carbonyls. The results presented are best explained by invoking one electron steps for both the cleavage of the carbon-halogen bond and the formation of the carbon-carbon bond and suggest that instead of two distinct classes of metal carbenes, metal carbenes manifesting a contiuum of reactivity behavior may exist. The pathway followed in a particular reaction is dictated by the combination of the characteristics of the metal carbene and the nature of the substrate.

With evidence of an electron transfer reaction for titanocene methylidene, other titanocene methylidene reactions could be reformulated to proceed by an electron transfer mechanism. The reaction of **1** with acid chlorides has been shown to yield titanocene methyl enolates.[17] The reaction has been postulated to proceed by oxametallacycle formation and β-chloride elimination as presented in Figure 5. In light of the electron transfer mechanism proposed for allyl and benzyl chloride, an alternative mechanism for the reaction of **1** with acid chlorides can be envisioned. The electron transfer reaction does not involve the highly reactive oxametallacycle which

would most likely retro 2 + 2 faster than β-chloride eliminate. Alternatively, electron transfer could occur and radical coupling and ligand exchange would yield the titanocene enolate chloride (Figure 5).

Figure 5:
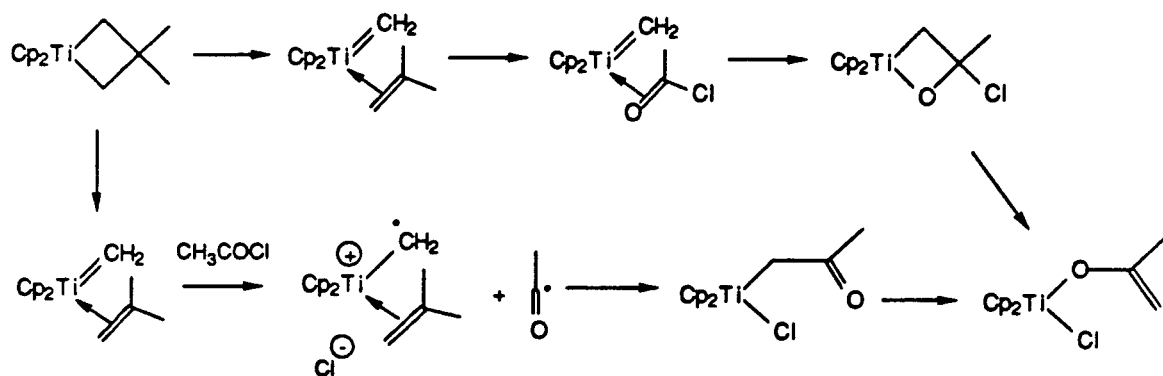
EXPERIMENTAL

General Considerations. All manipulations of air and/or moisture sensitive compounds were carried out using standard Schlenk vacuum line and dry box techniques. Argon used in Schlenk work was purified by passage through columns of BASF-RS-II (Chemalog) and Linde 4Å molecular sieves.

Routine [1] H and ^{13}C spectra were recorded on JEOL FX-90Q or JEOL GX-400 spectrometers. All chemical shifts are reported relative to residual protons on the deuterated solvents. The C_6D_6 was purified by vacuum distillation from sodium benzophenone ketyl.

The reaction of **1** with CH_3I and $(CH_3)_3CCl$ were performed by Steve Buchwald.[15] The kinetics of **1** and **3** with $PhCH_2Cl$ were also performed by Steve Buchwald.[15] Optically active Ph/CHDCl and **1**[16] were prepared by literature preparations. Identification of titanocene phenethyl chloride was done by spectral comparison with published data.[8a]

Reaction of 1 with Allyl Chloride. A 5 mm NMR tube was charged with 38 mg ($1.53 \cdot 10^{-4}$ mols) of **1** and 0.4 ml C_6D_6. The NMR tube was cooled to 0° and 15 µl ($1.68 \cdot 10^{-4}$ mols) allyl chloride was syringed in. The reaction was warmed to R.T. for 12 hrs. The volatiles were removed with vacuum and another 0.4 ml C_6D_6 was added. Yield quantitative by ^{1}H NMR. ^{1}H NMR (90 MHz, C_6D_6): δ 5.77 (s, 10 H), 5.60 (m, 1 H), 4.95 (m, 2 H), 2.20 (m, 2 H), 1.54 (m, 2 H). [13]C{[1]H} (22.3 MHz, C_6D_6): δ 41.83, 68.53, 111.75, 115.65, 143.01.

Preparation of Racemized Phenethylalcohol. A medium schlenk tube was charged with 250 mg (1 mmol) of 1 and 7 ml benzene. Chiral benzyl chloride (460 µl, 2 mmol) was syringed into the solution and the reaction was stirred at R.T. for 12 hrs. The solution was then cannulated onto 20 ml of rapidly stirred pentane at -50° C. An orange precipitate formed which was collected by filtration and dried with vacuum. The pentane solution was saved. The orange titanocene phenethyl chloride was redissolved in 10 ml benzene and 1.3 ml of 70 percent *t*-butyl hydroperoxide was added via syringe. The reaction was stirred vigorously for 15 minutes. Heat was evolved. The solution was then extracted with ether and the ether layer saved. The ether was removed by a rotoevaporator to yield a clear oil. The oil was purified by preparative gas chromatography on a 5 ft, 5 percent SE 30 column. NMR analysis was done by 400 MHz ^{1}H NMR and 77 MHz ^{2}H NMR in the presence of 50 mol percent Eu(dcm)$_2$ (Figure 3).

Analysis of Unreacted Benzyl Chloride. The filtered pentane solution from above was dried on a rotoevaporator to yield a clear oil (yield 95 mg, 0.75 mmols). The oil was dissolved in 10 ml MeOH (purified by distillation from CaH$_2$). A three neck 25 ml round bottom was equipped with a reflux condensor and the MeOH solution added. Sodium acetate (2.8 g) was added and the reaction was refluxed for 24 hr. The reaction was cooled to R.T., 1 g K$_2$CO$_3$ was added, and the reaction refluxed for 1 hr. The solution was cooled to 0° C. and filtered through a medium glass frit. The MeOH was removed by a rotoevaporator to yield a moist paste. The paste was spread on a preparative TLC plate and eluted with a 2:1 pentane:ether mixture. The major band with

a R_f of 0.5 was collected. Yield 40 mg. The benzyl alcohol was analyzed by 500 MHz and 90 MHz ^{1}H NMR and 77 MHz ^{2}H NMR in the presence of 50 mol percent Eu(dcm)$_2$. Figure 4 shows complete retention of optical activity.

Substituent Effects. A 5 ml round bottom was charged with 0.5 ml benzene, 10 mg 1 ($4.0 \cdot 10^{-5}$ mols) and 56 mg benzyl ($3.2 \cdot 10^{-4}$ mols) and $3.2 \cdot 10^{-4}$ mols of the para substituted benzyl chloride. The round bottom was septa capped and the solution stirred at room temperature for 12 hrs. The reaction was quenched by HCl gas and the solution filtered through basic alumina. Analysis of the ethyl benzenes was done by analytical gas chromatography on a 1 meter SE 30 capillary column.

REFERENCES

(1)   Grubbs, R.H. <u>Comprehensive Organometallic Chemistry</u>; Wilkinson, G.; Stone, F.G.A.; Abels, E.V., Eds. Chapter 54 (1982).

(2)   Brady, R.C. III; Pettit, R. *J. Am. Chem. Soc.* **1980**, *102*, 6181.

(3)   Green, M.L.H. *Pure & Appl. Chem.* **1978**, *50*, 27-35.

(4)   Foger, K.; Anderson, J.R. *J. Catalysis* **1978**, *54*, 318.

(5)   Fischer, E.O.; Maasbol, A. *Angew. Chem. Int. Ed., Engl.* **1964**, *3*, 580.

(6)   Schrock, R.R. *Accts. Chem. Res.* **1979**, *12*, 98 and references therein. contrast this behavior with that observed for $Cp_2Ta(CH_3)=CH_2$ which reacts cleanly with CH_3I at RT but not with ϕCH_2Cl under the conditions. Schrock, R.R.; Sharp, P.R. *J. Am. Chem. Soc.* **1978**, *100*, 2389.

(7)   Buchwald, S.L.; Cannizzo, L.; Clawson, L.; Ho, S.; Meinhart, D.; Stille, J.R.; Straus, D.; Grubbs, R.H. *Pure & Appl. Chem.* **1984**, *56*, 1733.

(8)   (a) Waters, J.A.; Mrtimer, G.A. *J. Organomet. Chem.* **1970**, *22*, 417. (b) Benzyl toslylate does not perform the same chemistry under these conditions.

(9)   Hartner, Jr., F.W.; Schwartz, J.; Cleft, S.M. *J. Am. Chem. Soc.* **1983**, *105*, 601.

(10)   The reaction of ϕCH_2Cl and DMAP is very slow under the conditions of the reaction.

(11)   Lau, K.S.Y.; Wong, P.K.; Stille, J.K. *J. Am. Chem. Soc.* **1976**, *98*, 5832.

(12)   Blackburn, T.F.; Labinger, J.A.; Schwartz, J. *Tetrahedron Lett.* **1975**, 3041.

(13) McCreary, M.D.; Lewis, D.W.; Wernick, D.L.; Whitesides, G.M. *J. Am. Chem. Soc.* **1974**, *96*, 1038.

(14) Identical results were obtained in the reaction of **3** with optically active ϕCH_2Cl. No exchange between styrene and $Cp_2Ti(Cl)CH_2\text{-}CD_2\text{-}\phi$ was observed under the raction conditions.

(15) Steve Buchwald Notebooks I and II. R.H. Grubbs Group, California Institute of Technology.

(16) Stauss, D.A.; Grubbs, R.H. *Organometallics* **1982**, *1*, 1658.

(17) Stille, J.R.; Grubbs, R.H. *J. Am. Chem. Soc.* **1983**, *105*, 1664.

CHAPTER 5

SYNTHESIS AND STRUCTURES OF BIMETALLIC
TITANIUM AND CHROMIUM CARBENE COMPLEXES
OF THE TYPE $Cp_2Ti(Cl)O(CH_3)CCr(CO)_5$.

Abstract

β,β-dimethyltitanocene metallacyclobutane 1 reacts with $M(CO)_6$ (M = Cr, Mo) in toluene to yield a titanocene ketene adduct and $M(CO)_5$. This reaction produces two intermediates, 3 and 4, with the formula $Cp_2Ti(O)CH_2CM(CO)_5$. Independent synthesis of 3 and 4 (M = Cr) was achieved by the reaction of $Cp_2Ti(Cl)O(CH_3)CCr(CO)_5$ 9 and $NaN(TMS)_2$. Complexes 3 and 4 are formed in a 1 to 1 ratio, with this ratio changing to 1.3 to 1 when the methylene group is deuterated. The fluxional behavior of intermediates 3 and 4 was studied using variable temperature ^1H NMR. The reaction of $NaN(TMS)_2$ and $Cp^*_2Ti(Cl)O(CH_3)CCr(CO)_5$ ($Cp^* = C_5Me_5$) does not yield complexes analogous to 3 and 4, but instead yields $Cp^*_2Ti(Cl)O(CH_2)CCr(CO)_5Na$. $Cp^*_2Ti(Cl)O(CH_3)CCr(CO)_5$ exists as two rotational isomers, 11 and 12. The X-ray crystal structure of 11 reveals that the methyl group is wedged between the two permethylcyclopentadienyl ligands. Crystals of 11 are monoclinic, $P2_1/c$, with $a = 12.490(2)$Å, $b = 13.472(3)$Å, $c = 17.791(4)$Å, $\beta = 109.83(2)°$ and $Z = 4$. The reaction of $Cp^*_2TiCl_2$ and $2LiO(CH_3)CCr(CO)_5$ yields $Cp^*_2Ti(O(CH_3)CCr(CO)_5)_2$, 13. The X-ray crystal structure of 13 reveals that the methyl group of each Fischer carbene moiety is wedged between the permethylcyclopentadienyl ligands. Crystals of 13 are monoclinic, $P2_1/n$, with $a = 9.958(2)$Å, $b = 32.226(8)$Å, $c = 11.998(3)$Å, $\beta = 108.21(2)°$ and $Z = 4$.

Introduction

Insertion reactions are some of the most common and important reactions in organometallic chemistry.[1] They are mechanistically interesting, used in organic synthesis and postulated in catalysis. A subset of the broad group of insertion reactions is the insertion of carbon monoxides of group VIB metal carbonyl complexes into early transition metal alkyl, aryl and hydride bonds.[2] Several different examples are shown in Figure 1. These reactions are often viewed as the nucleophilic attack of an alkyl, aryl or hydride on the electrophilic carbon of a coordinated carbon monoxide. Furthermore, the reactions are strikingly similar to the preparative reactions for generating Fischer carbene[3] complexes from alkyl or aryl lithium reagents and metal carbonyls. In the past several years, several new routes to Fischer carbenes have been reported. Specifically, Erker[4] has used η^2 bound olefins of early transition metals to effect the synthesis of metallocyclic carbenes and Petz has reported the insertion of metal carbonyls into the Ti $-$ N bond of Ti(N(CH$_3$)$_2$)$_4$ to give Fischer carbenes.[5]

These insertion reactions form carbon-carbon and/or metal carbon bonds and thus can be viewed as one of the primary steps in building small organic fragments from carbon monoxide. In addition, synthetic utility can be envisioned by using the metal-carbon bonds for other insertion reactions or by taking advantage of the Fischer carbene moiety for Diels Alder reactions,[6] quinone formation,[7] or several other recently developed synthetic methods using Fischer carbenes as synthons.[8,9]

To our knowledge, there are no examples of metal-bound carbon monoxide inserting into early transition metal alkylidenes. Furthermore, the reaction of metal alkylidenes with carbonyl complexes is surprisingly rare, even

$Cp_2^*ZrH_2$ + $Mo(CO)_6$ ⟶ [structure: Cp_2^*Zr—O—C(=$Mo(CO)_5$) with H H]

Cp_2^*Ti [cyclopropane] + $Cr(CO)_6$ ⟶ [structure: Cp_2^*Ti—O—C(=$Cr(CO)_5$) ring]

Cp_2^*ScR + Cp_2MoCO ⟶ [structure: Cp_2^*Sc—O—C(R)(=$MoCp_2$)]

[structure: Cp_2Zr benzocyclopropene] + $Mo(CO)_6$ ⟶ [structure: Cp_2Zr—O—C(=$Mo(CO)_5$) fused benzo ring]
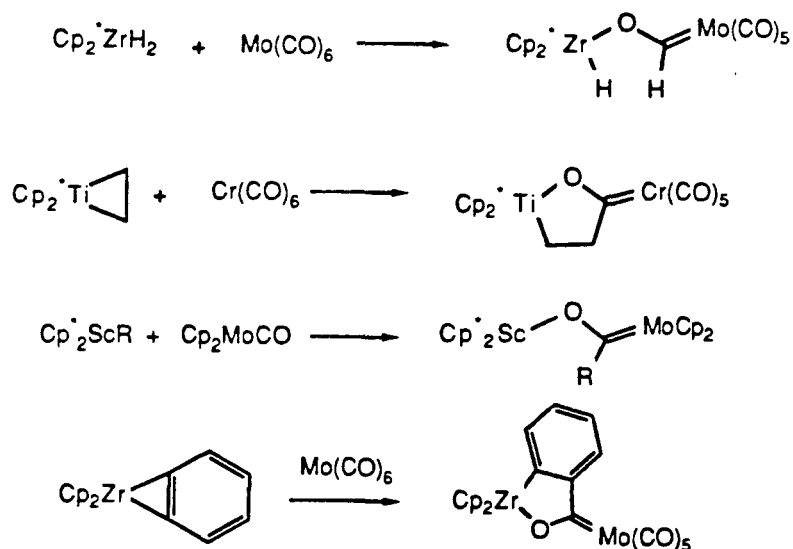
Figure 1: Early transition metal insertions of bound carbon monoxide.

though other organic and inorganic carbonyls do react with organic and inorganic carbenes. Hermann has extensively studied the addition of organic carbenes to inorganic carbonyl complexes[10] and the reactions of carbon monoxide with inorganic alkylidene complexes.[11]

Only one metal alkylidene has been documented to attack a metal carbonyl. This reaction involves the insertion of a carbon monoxide ligand of $CpMn(CO)_3$ into an uranium alkylidene.[12] (1). The bonding in the product can be described by two canonical forms: an enolate and a Fischer carbene.

Cp_3U=$CHPMe_2Ph$ + $Cp(CO)_3Mn$ ⟶ [structure: $Cp(CO)Mn$—C(—$OUCp_3$)=C(H)(Me_2PhP)]

⟶ [structure: $Cp(CO)Mn$=C(—$OUCp_3$)—C(H)(Me_2PhP)] (1)
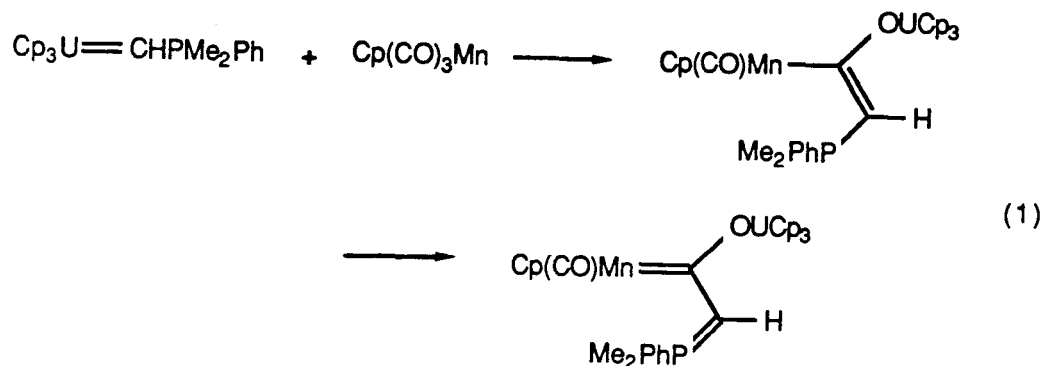
Although the coupling of metal alkylidenes with metal carbonyl complexes is rare in monometallic systems, such coupling is frequently postulated in heterogeneous Fischer-Tropsch systems[13] to yield surface bound ketene fragments. The formation of bound ketene in bimetallic and cluster complexes has been documented,[14] and herein we report the coupling of titanocene methylidene with $Cr(CO)_6$ to yield a titanocene ketene complex.

Results and Discussion

The reaction of titanocene metallacyclobutanes with group VIB metal carbonyls proceeds at a rate proportional to the rate of cleavage of the titanocene metallacyclobutane to titanocene methylidene. The reaction proceeds at 5 °C when the metallacycle is β,β-dimethyl titanocene metallacyclobutane 1. At this temperature, this reaction produces two intermediates which rearrange to form titanocene ketene 5 (Figure 2). These intermediates are formulated to be a β-exoalkylidene, α-oxatitanocene metallacyclobutane 3 and a titanocene-group VIB metal bridged ketene adduct 4. The rearrangement of 3 and 4 to 5 proceeds before total consumption of the titanocene metallacyclobutane.

Figure 2: Reaction of "Cp2Ti = CH2" with M(CO)6 (M = Cr, Mo).

Figure 3 shows the ^{1}H NMR spectra for the reaction of 1 and Mo(CO)6. Initially, 1 cleaves to form titanocene methylidene and isobutylene. The titanocene methylidene then reacts with Mo(CO)6 to form 3 and 4. The intermediates 3 and 4 are formed in a 1:1 equilibrium mixture over the

Figure 3: ¹H NMR spectra of the reaction of 1 with Mo(CO)$_6$. Spectrum 1 is labeled to indicate the resonances of compound 1. Spectrum 2 is labeled to indicate the resonances of compound 3. Spectrum 3 is labeled to indicate the resonances due to compound 4. Spectrum 4 is labeled to indicate the resonances of compound 5 and isobutylene (‡).

temperature range $-50\,°C$ to $15\,°C$ (the cyclopentadienyl ligand resonances of 3 and 4 have the same intensity, Figure 3). This one to one ratio of cyclopentadienyl ligand resonances indicates that the intermediate could be one structure with diastereotopic cyclopentadienyl ligands or the two intermediates shown in Figure 2. The ^1H NMR spectrum suggests the presence of a methylene group with a chemical shift in the correct region for an α methylene of a titanocene metallacyclobutane, but this shift is also indicative of a Fischer carbene moiety. The resonance for 3a was at $\delta 3.17$ (Figure 3, Spectrum 2), which is at slightly lower field than normally found for titanocene metallacyclobutanes[15] (typically in the range of $\delta 1.8$ to $\delta 2.7$). The small downfield shift is due to the methylene also being α to the double bond of the Fischer carbene. For example, the chemical shift of the methyl group bound to the carbene carbon of $(CO)_5CrCC(CH_3)OCH_3$ is $\delta 3.05$.[16]

The ^1H NMR spectra are also suggestive of a ketene adduct due to geminal coupling ($J_{HH} = 1.5$), but the olefin resonances possess a large high field chemical shift. While olefin resonances of titanocene and zirconocene ketene adducts are typically in the range of 4 to 5 ppm,[17] the resonances found for 4a are $\delta 2.97$ and $\delta 4.13$. (Figure 3, Spectrum 3).

The insertion of a carbon monoxide ligand of $Mo(CO)_6$ into the titanocene methylidene Ti$-$C double bond is presumed to proceed by initial coordination of the carbonyl oxygen to the titanium, followed by nucleophilic attack of the methylidene on the electrophilic carbonyl carbon. Evidence for this insertion mechanism is the analogous oxygen coordinated complex isolated by Stucky[18] et al. (2).

This analogous complex $Cp^*_2Ti(CH_3)(OC)_3MoCp$, was isolated from the reaction of $CpMo(CO)_3H$ with $Cp^*[C_5(CH_3)_4=CH_2]Ti(CH_3)$. This complex exhibits a donor-acceptor interaction between one of the carbonyl oxygens and

CpMo(CO)$_3$H + Cp*[C$_5$(CH$_3$)$_4$=CH$_2$]Ti(CH$_3$) $\longrightarrow$

$$Cp_2^* \, Ti \overset{\displaystyle /CH_3}{\underset{\displaystyle \diagdown O=C=Mo(CO)_2Cp}{}} \qquad (2)$$
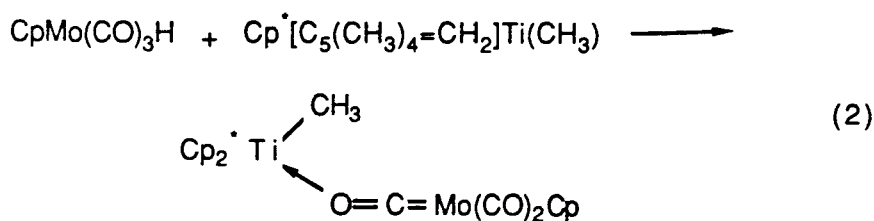
the titanium center, and this interaction increases the C-O bond length of the coordinated carbonyl.[18] Thus, the donor-acceptor interaction from an oxygen of Mo(CO)$_6$ to the titanium of Cp$_2$TiCH$_2$ should also increase the electrophilicity of the carbonyl carbon and promote attack by the titanocene methylidene. Similar interactions have been observed between molecular Lewis acids and metal coordinated carbon monoxide. Shriver has extensively studied the Lewis acid promoted migration of alkyl and aryl moieties to coordinated CO.[19] The initial coordination of the CO ligand of Mo(CO)$_6$ to the titanium center can be viewed as Lewis acid promoted migration of the methylidene to the carbonyl.

Complex 4 possesses a μ_2-η_2 ketene ligand. An analogous oxycarbene complex, Cp$_2$Zr(Ac)Mo(CO)$_2$Cp, has been isolated following carbon monoxide loss from Cp$_2$Zr(η^2-Ac)Mo(CO)$_3$Cp (3). The oxycarbene complex was found to

$$\underset{\displaystyle Cp_2Zr \rule[0.5ex]{1.2cm}{0.4pt} Mo(CO)_3Cp}{\overset{\displaystyle O\!-\!\!\!\overset{\displaystyle O}{\diagup}}{}} \quad \longrightarrow \quad \underset{\displaystyle Cp_2Zr \rule[0.5ex]{1.2cm}{0.4pt} Mo(CO)Cp}{\overset{\displaystyle O\!-\!\!\!\overset{\displaystyle O}{\diagup}}{}} \qquad (3)$$
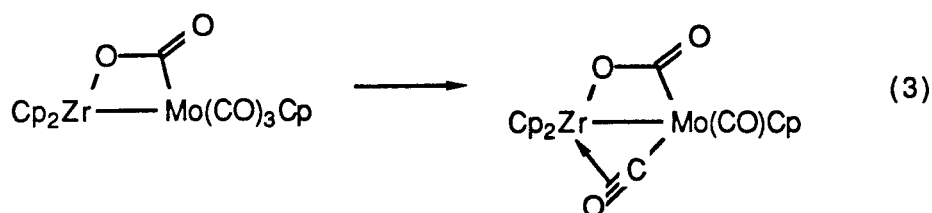
contain a bridging carbonyl ligand, and 4 may also possess a similar bridging carbonyl ligand.

In order to more fully address the question of whether 3 and 4 were actually one complex with diastereotopic cyclopentadienyl ligands or two separate complexes, several studies were commenced to perturb the equilibrium between 3 and 4 away from a value of unity. In the first attempt, the group VIB metal carbonyl was substituted with triphenylphosphine and triphenylphosphite. The reaction of 1 with $Mo(CO)_5PPh_3$ yielded only the titanocene ketene complex 5 (Figure 4a) without any detectable intermediates. In contrast, the reaction of 1 with $Mo(CO)_5P(OPh)_3$ did result in formation of intermediates 6 and 7 in a *trans* to *cis* ratio of 1.6 to 1 (Figure 4b). However, the equilibrium between oxametallacycle 6 and bridging ketene adduct 7 was still approximately unity for both the *cis* and *trans* complexes. The ^{31}P NMR shows three signals (one peak is twice as large and presumably is two overlapping signals) with the correct integrated intensities for the four intermediates.

Further attempts at perturbing the equilibrium away from unity by reacting 1 with non-Group VIB carbonyl complexes failed. Facile addition of titanocene methylidene is observed only when carbonyl complexes of group VIB are the electrophilic complexes. Using other carbonyl complexes as the electrophiles results in decomposition of the titanocene methylidene. This lack of reactivity with late metal carbonyl complexes is probably due to the decreased electrophilicity of the bound carbon monoxide. In fact, attempts to form Fischer carbenes from late transition metal complexes is difficult, as these complexes do not react efficiently with alkyl or aryl lithium reagents.

Independent synthesis of the proposed intermediates 3 and 4 provided additional structural proof and a facile method for shifting the equilibrium of 3 and 4 away from a value of unity. The reaction of titanocene dichloride with the Fischer carbene salt 8 forms compound 9[21] (Figure 5). Deprotonation of 9
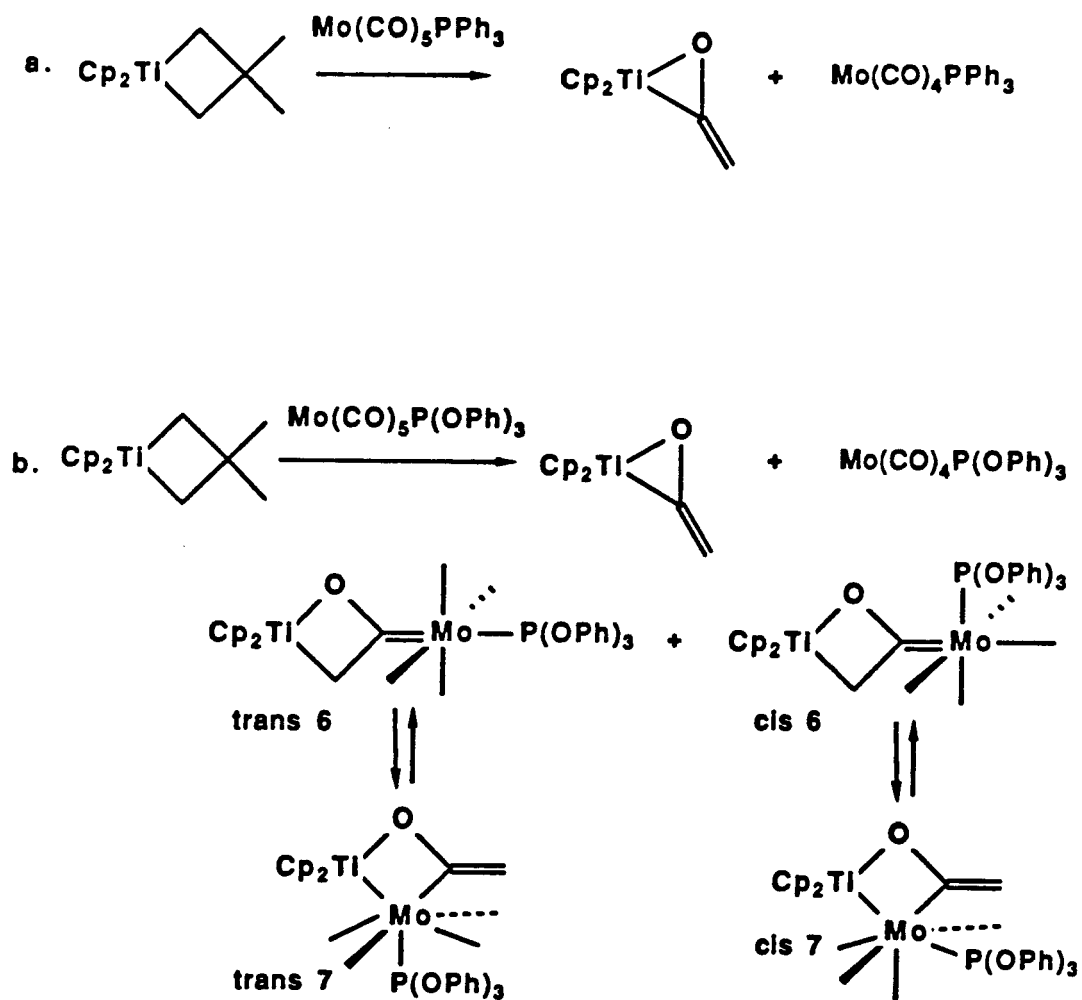
Figure 4: a) Reaction of "$Cp_2Ti=CH_2$" with $Mo(CO)_4PPh_3$

b) Reaction of "$Cp_2Ti=CH_2$" with $Mo(CO)_4P(OPh)_3$

at low temperature with sodium hexamethyldisilamide yields the same intermediates formed in the reaction of 1 and $Cr(CO)_6$. This intramolecular alkylation and oxametallacyclobutane formation can be accomplished at -50 °C. At temperatures below -10 °C, the intermediates do not rearrange to titanocene ketene at a perceptible rate.

The synthetic route shown in Figure 5 allowed facile isotopic enrichment of the methylene group of **3b** and **4b**. Thus, ^{13}C labeled **9** $Cp_2Ti(Cl)O(*CH_3)CCr(CO)_5$ was synthesized and allowed to react with $NaN(TMS)_2$. The proton coupled ^{13}C NMR spectrum is displayed in Figure 6. The CH coupling constant for the methylene group of **3b** was found to be 133.1 Hz, well within the range normally observed for the α carbons of titanocene metallacyclobutanes, typically a J_{CH} of 130 to 140 Hz, is found. Two coupling constants for the methylene group of **4** were found with values of 160.4 Hz and 150.4 Hz. These values are typical of sp^2 hybridized carbons (normally 150 to 170 Hz).[22] Thus, compound **4** does contain olefinic protons, even though the ^{1}H NMR chemical shifts are slightly higher field than usual.

Compound **9** was also synthesized deuterium enriched $(Cp_2Ti(Cl)O(CD_3)CCr(CO)_5)$ and allowed to react with $NaN(TMS)_2$. The reaction afforded the intermediates **3** and **4** in a 1.3 to 1 ratio favoring the oxametallacycle over the bridging ketene complex and finally broke the degeneracy of the equilibrium ratio. This result substantiated the existence of two intermediates with the structures displayed in Figure 2.

The interconversion of **3** and **4** presumably occurs through a zwitterionic form analogous to $Cp_2Zr(CH_3)OCMo(CO)_2Cp$.[23] This zwitterionic form is stabilized through delocalization of the anionic charge[24] and the donation from oxygen to titanium (**4**). This resonance stabilization is evident from the
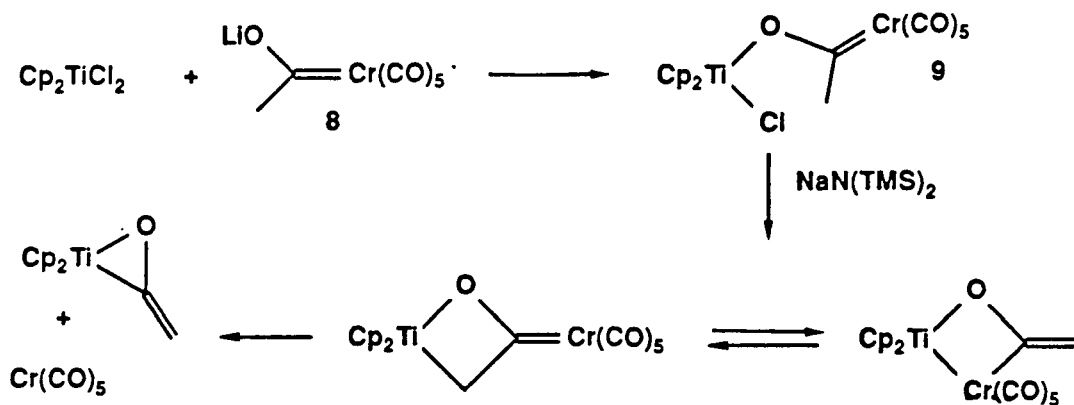
Figure 5: Alternative synthesis of **3b** and **4b**.
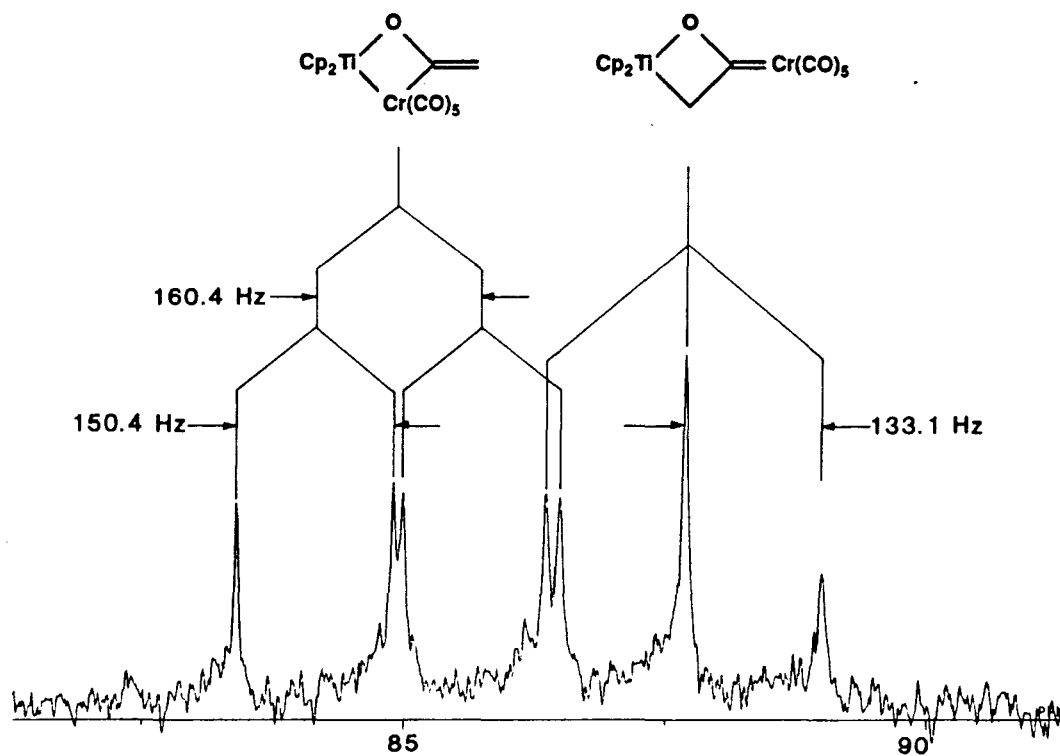
Figure 6: ^{13}C (^1H coupled) spectra of ^{13}C enriched **3b** and **4b**.

low pK$_a$ of typical Fischer carbenes. The aqueous pK$_a$ of the methyl group
bound to the carbene carbon of (CO)$_5$CrC(Me)OMe is 8.0.[25]

$$\text{Cp}_2\text{Ti} \text{---} \text{O} \underset{\ominus}{\overset{\oplus}{\diagdown}} \text{---} \text{Cr(CO)}_5 \tag{4}$$
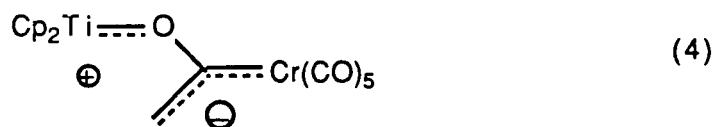
Variable-temperature ^{1}H NMR spectra of intermediates **3b** and **4b**
revealed a fluxional process similar to other oxametallacyclobutanes and
metallacyclopentenes (Figure 7).[26] At -40 °C, a 400 MHz ^{1}H NMR spectrum
shows initial broadening of the resonance attributed to the methylene group
of **3b**. Further cooling of the toluene solution to -80 °C results in complete
collapse of the methylene resonance of **3b**. Concurrent with this
decoalescence, the cyclopentadienyl ligand resonance of **3b** begins to broaden.
Finally at -100 °C, both the methylene and cyclopentadienyl ligand
resonances sharpen into two separate peaks apiece. The low temperature
limit was never reached due to freezing of the solvent. All attempts at
attaining the slow exchange limit in freon solvents were unsuccessful due to
the insolubility of compounds **3b** and **4b**. The fluxional processes observed are
attributed to a puckering of the ring of the oxametallacyclobutane **3b** in order
to allow π donation of either the oxygen or the β exo-double bonds to the
titanium. The extent of π donation by either of these mechanisms is the
subject of current theoretical debate.[27] At 0 °C, the rate of interconversion of
the two ring puckered structures shown in Figure 7 is rapid, and thus, the
methylene and cyclopentadienyl resonances appear as singlets. Upon cooling,
the interconversion rate decreases, and correspondingly, the ^{1}H NMR
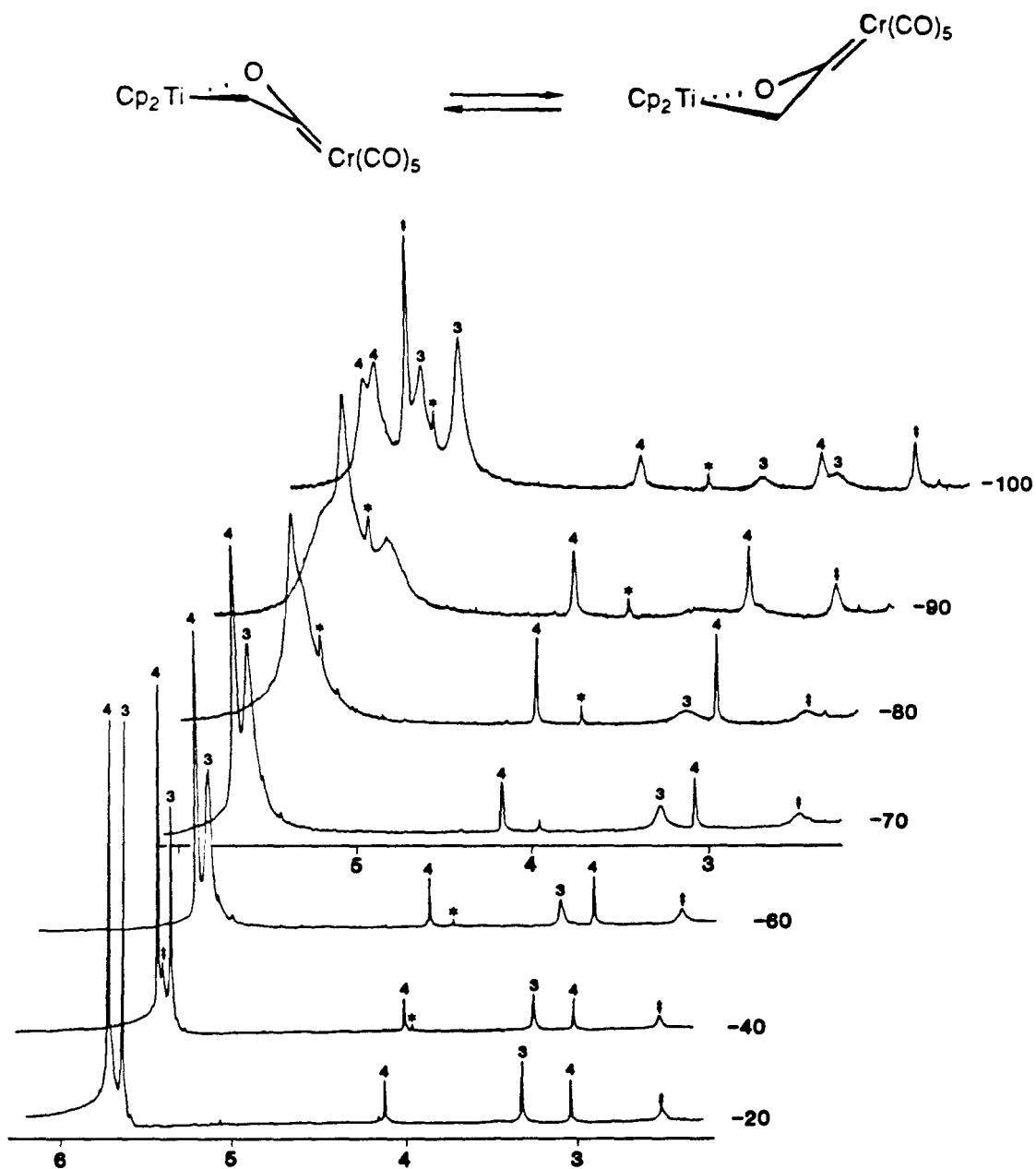
Figure 7: Variable temperature ^{1}H spectra of **3b** and **4b**. All resonances are labeled according to their compound number. ★ = impurity, ‡ = starting material (9)..

resonances broaden. This puckering is also possible for **4b**, and thus, the cyclopentadienyl ligand resonances of **4b** are also observed to broaden and then refocus into two separate signals at -100 °C (Figure 7).

Extension of the deprotonation and intramolecular alkylation reaction of Figure 5 resulted in limited success. Although Cp$_2$Zr(ketene) is a known compound[17], the zirconocene complex **10** does not cleanly undergo intramolecular alkylation in toluene to form analogs to **3** and **4** (Figure 8a). The ethyl complex **11** can be synthesized from EtLi, Cr(CO)$_6$ and Cp$_2$TiCl$_2$, but it also does not intramolecularly alkylate (Figure 8b). Reaction of **9** with nBuLi resulted in alkylation at titanium instead of deprotonation. Both the Fischer carbene moiety and the chloride were displaced (Figure 8c). These products were identified by independent synthesis. The reaction of **8** with Cp*$_2$TiCl$_2$ forms rotomers **12** and **13**. Neither **12** nor **13** react with NaN(TMS)$_2$ to form analogs to **3** or **4**; instead, these reactions produce stable anions (Figure 8d). The anion formed from **11** is soluble in toluene, whereas the anion formed from **13** immediately precipitates as its sodium salt. These results are consistent with the anionic charge being highly delocalized and a sterically encumbered closure reaction to form analogs to **3** and **4**.

The two rotomers (**12** and **13**, Figure 9) cannot be interconverted by heating in toluene to 110 °C. Instead, the complexes begin to decompose at about 90 °C, probably by loss of CO. Interconversion is restricted because the permethylcyclopentadienyl wedge sterically inhibits rotation. Compounds **12** and **13** can also exist in two isomeric forms due to inversion at oxygen (**12a** and **b**, **13a** and **b**). This inversion at oxygen does not interconvert rotomers **12** and **13**; instead, the inversion forces either the methyl groups or the Cr(CO)$_5$ fragment into the wedge formed by the permethylcyclopentadienyl ligands.
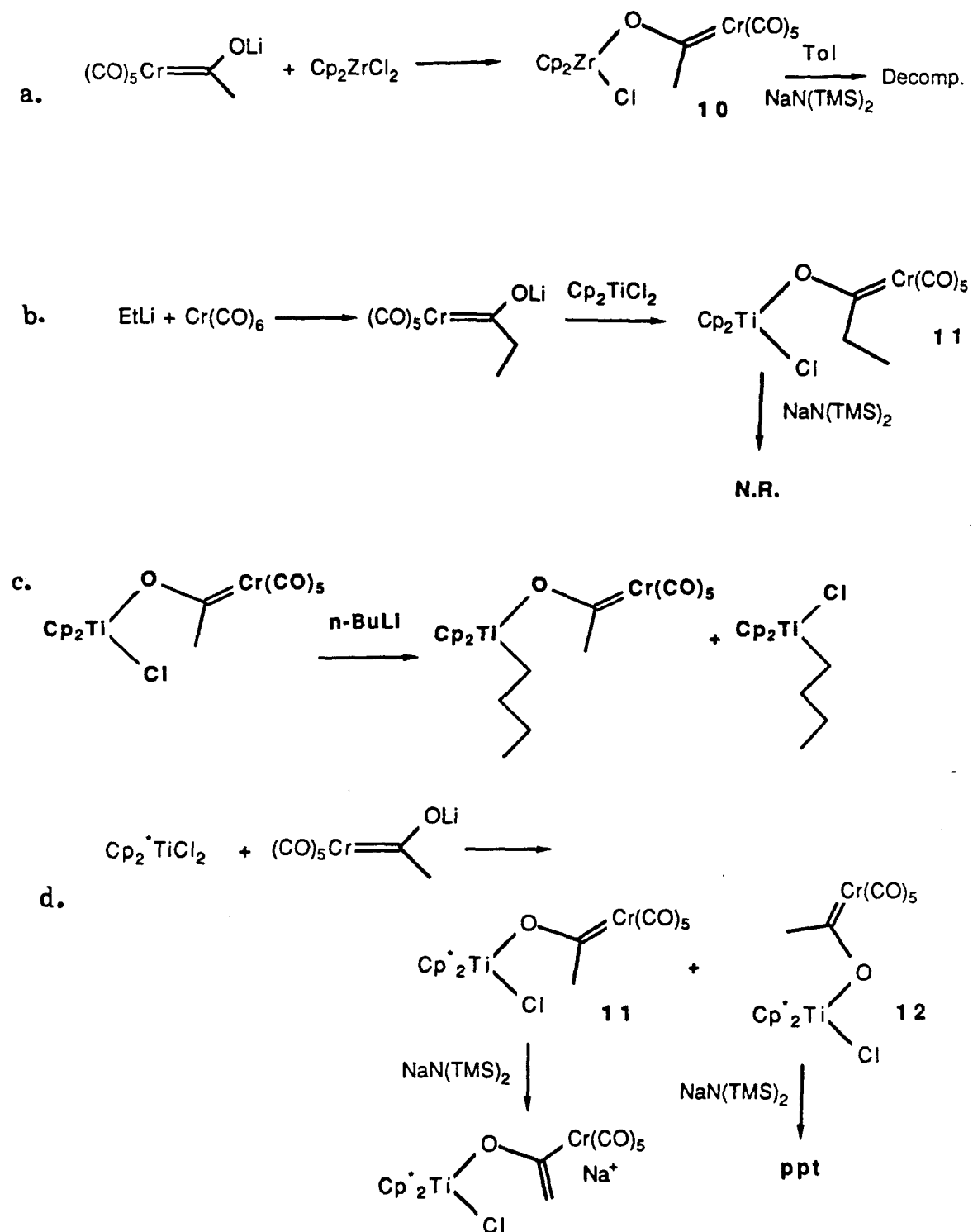
Figure 8: Attempted extension of the deprotonation and intramolecular alkylation presented in Figure 5.
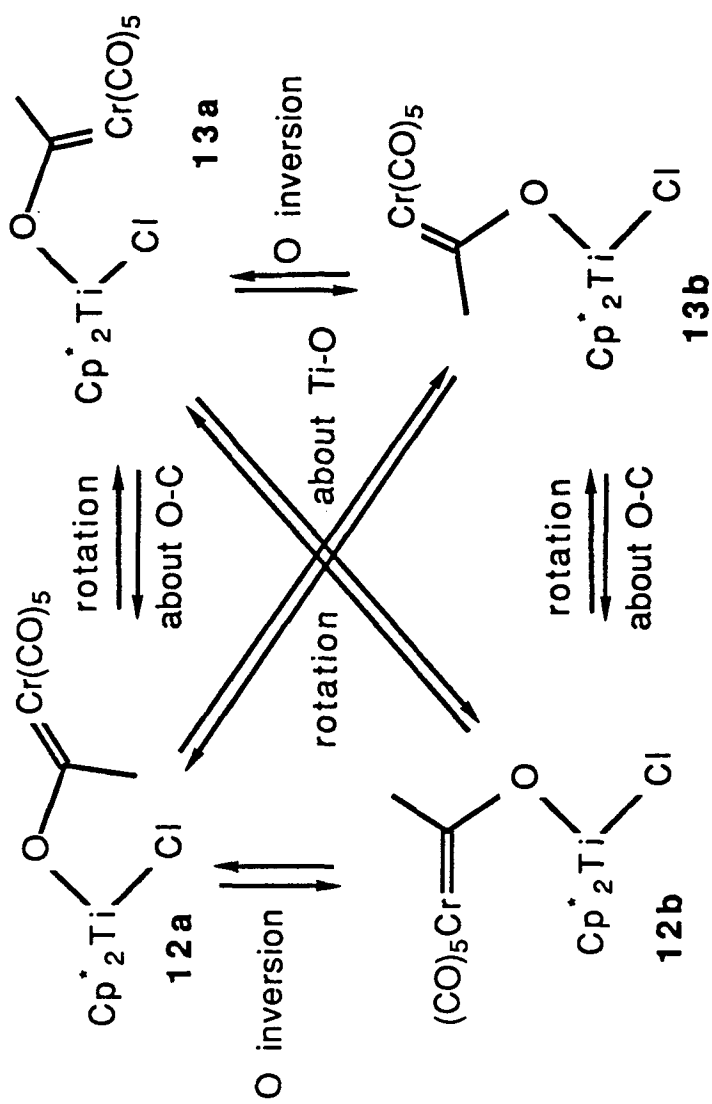
Figure 9: Interconversion of 12 and 13.

These isomers most likely exist predominately as **12a** and **13b** due to the large steric bulk of the Cr(CO)$_5$ fragment.

The reaction of the anion generated from either **12** or **13** with one equivalent of HCl yields both **12** and **13** in a ratio of approximately 2 to 1. Thus, the anions generated from either **12** or **13** must be capable of interconverting.

The X-ray crystal structure of **12** was determined, and an ORTEP diagram is shown in Figure 10. There are several unique features about the structure of **12**. The Ti$-$O$-$C angle is 158.3(4)° and the O$-$Ti$-$Cl angle is 97.2(1)°. In a similar compound Cp*$_2$TiCl$_2$,[28] the Cl$-$Ti$-$Cl angle was found to be 92.9°. The larger angle of 97.2° in **12** is most likely due to steric nonbonded interactions between the Cl and the Fischer carbene methyl group. The proximity of these two groups in the permethylcyclopentadienyl wedge induces an increase in the bond angle separating the Cl and the O substituents. For comparison, a similar complex [Cp$_2$ZrOC(Ph)Mo(CO)$_5$]$_2$O, with two Fischer-type molybdenum zirconoxyphenylcarbene moieties has been structurally characterized.[2d] The O$-$Zr$-$O bond angle in [Cp$_2$ZrOC(Ph)Mo(CO)$_5$]$_2$O was found to be 99.4(1)°. This angle is similar to the observed Cl$-$Ti$-$O angle of **12** and again results from large steric interactions within the cyclopentadienyl wedge. In addition, the Ti$-$O$-$C angle of 158.3(4)° in **12** is larger than that found in an analogous alkoxy titanocene chloride complex Cp$_2$Ti(OC$_2$H$_5$)Cl.[29] In this complex, the Ti$-$O$-$C angle was found to be 133.2(2)°. Therefore, the larger Ti$-$O$-$C bond angle in **12** is due to steric interactions and is not the result of increased O lone-pair donation to the Ti center. Further evidence of the steric crowding in the permethylcyclopentadienyl wedge is provided by the near planarity of Cl, Ti, O, C, Cr and Me moieties. The slight displacement of the Me group
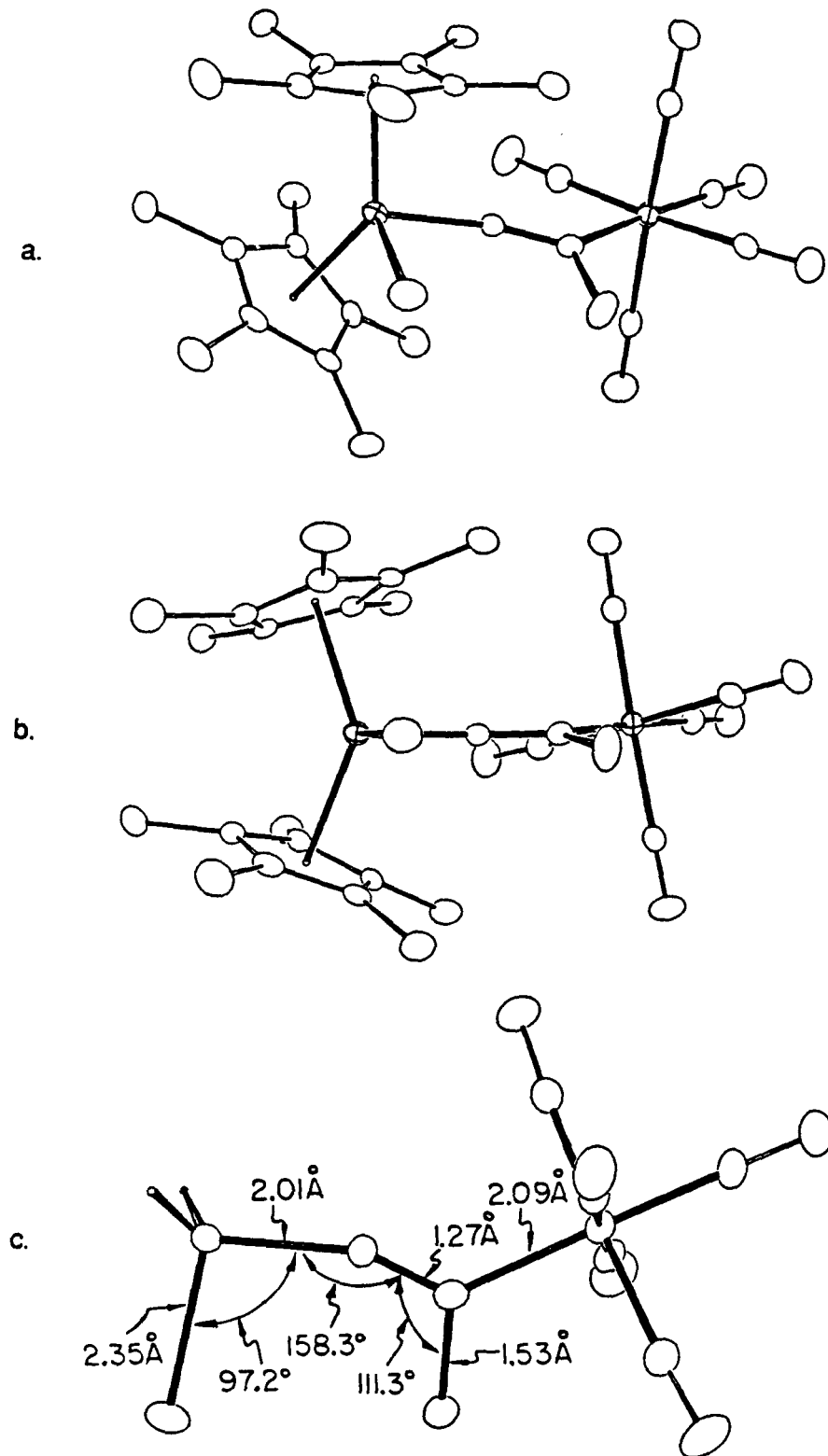
Figure 10:   ORTEP diagrams of compound 12.

from the plane by 7° is again most likely due to steric repulsion between Cl and Me. If the Me group were locked symmetrically between the permethylcyclopentadienyl ligands and felt no steric repulsion from the Cl, then all the atoms and groups would be expected to lie in the same plane. Appendix I gives the structural data for **12**.

In order to determine if isomer **13** is a rotomer of **12** (with the methyl group wedged along one side of the titanium center), as depicted in Figure 9, an X-ray crystal structure was desired. Suitable crystals of **13** were not obtained; instead, compound **14** was prepared by treatment of Cp*$_2$TiCl$_2$ and two equivalents of **8** (5).

$$Cp_2^* TiCl_2 \quad + \quad 2 \quad \overset{LiO}{\underset{}{\diagdown}}{=}Cr(CO)_5 \quad \longrightarrow \quad \text{(structure 14)} \qquad (5)$$

14
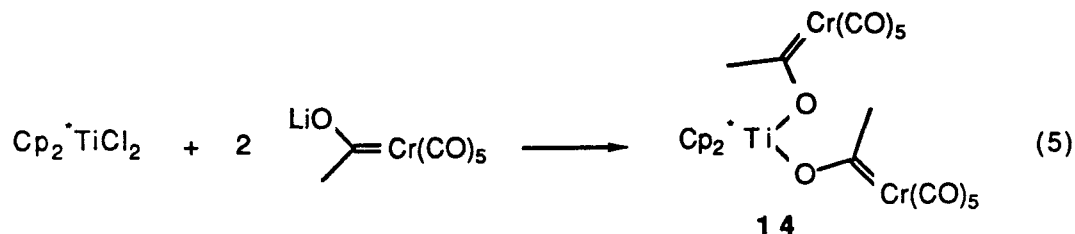
The ^{1}H NMR spectrum of **13** revealed two different methyl resonances at δ 2.28 and 3.48, indicating that the two Fischer carbene moieties are not bonded symmetrically to Cp*$_2$Ti.

Figure 11 shows an ORTEP diagram of **14**. The same general features evident in the X-ray structure of **12** are present, and the second Fischer carbene unit also has its methyl group located in between the wedge of the permethylcyclopentadienyl ligands. This methyl group resides along the side of the permethylcyclopentadienyl wedge and not in the face of the wedge, as does the other Fischer carbene unit. An additional interesting feature of the structure of **14** is the orientation of the carbene π bonds with respect to the carbonyls. The Fischer carbene moiety which has its methyl group along the
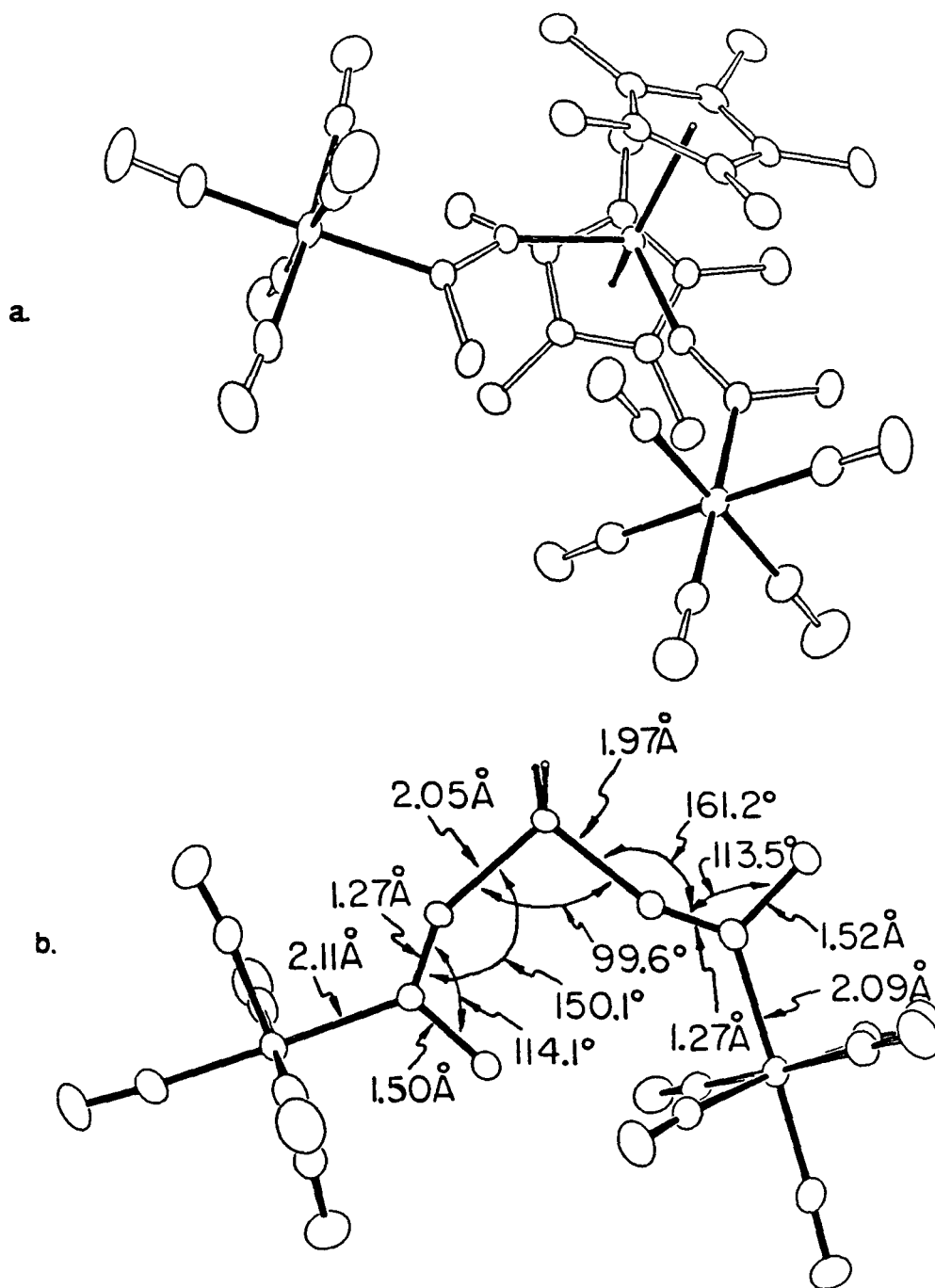
Figure 11: ORTEP diagrams of compound 14.

side of the permethylcyclopentadienyl wedge, has its Cr−C π bond between two different carbonyl groups. This is one of the few examples of a metal carbene π-bond that is positioned between two donor-acceptor ligands.[30] This arrangement results from the methyl group steric demand of the other Fischer carbene forcing the rotation of the carbonyls away from their normal positions. Appendix II gives the structural data for **14**.

Fischer-type carbenes are often viewed as singlet carbenes donating a pair of electrons via an sp^2-hybrid orbital to an empty metal acceptor orbital and a filled metal d orbital back donating into an empty p orbital on carbon. This type of bonding description was found by both a Hartree-Fock and generalized molecular orbital theory calculation.[31] It has been shown, however, that such calculations tend to lead to donor (or ionic) descriptions to the wavefunction since the two orbitals used in the bond pair must have unit overlap.[32] The generalized valence bond method has found that the singlet donor carbene state of $RuCH_2{}^+$ lies 12.9 kcal/mole above a covalent alkylidene metal carbon σ and π bond.[33] The introduction of a heteroatom substituent, however, has been found to stabilize the donor singlet carbene state.[34] A resonance structure with significant C-O double bond character and an anionic metal is often invoked to explain the electrophilicity of these carbenes[35] and the observed low barriers to rotation.[31] In either of the two bonding descriptions (donor carbene versus covalent alkylidene), a p orbital on carbon interacts with a dπ orbital on chromium. A dπ symmetric orbital can be built at any angle with respect to the carbonyl ligands by a linear combination of dxz and dyz orbitals (taking the Cr=C axis as the z axis). Thus, rotation along the Cr-C bond axis only slightly perturbs the Cr-C double bond. In fact, the Cr-C bond distance in the rotated Fischer carbene moiety of **14** is 0.02 Å shorter than the Cr-C bond distance of the other Fischer carbene moiety.

Complex **9** reacts with trimethylaluminum to metathesize the chlorine for a methyl and yields **15**. The methyl derivative reacts with NaN(TMS)$_2$ to form a stabile anion **16** (Figure 12a).

The reaction of **12** or **13** with trimethylaluminum yields the same two products **17** and **18** in a 1.2 to 1 ratio, respectively. (Figure 12b). The transmetallation reaction can proceed by three possible mechanisms. (Figure 13). The first is a chloride abstraction to form a positively charged titanium center (13a). Delivery of the methyl group from AlMe$_4$$^-$ could then proceed in a stereochemical random fashion. Conversely, the reaction could proceed by a stereochemically specific transmetallation of a chloride for a methyl group. Then the two products could transmetallate the Fischer carbene moieties to scramble the stereochemistry (Figure 13b). Finally, the Fischer carbene unit could be transmetallated to the AlMe$_3$ (Figure 13c). To test these possibilities, compound **19** was synthesized from the hydroxy Fischer carbene **20** and AlMe$_3$ (Figure 14). When **19** reacts with Cp$_2$*TiMeCl, **17** and **18** are again formed in a 1.2 to 1 ratio. Therefore, mechanistic possibility c in Figure 13 is supported.

The reaction of **9** with NaN(TMS)$_2$ in THF was significantly different than in toluene (Figure 15a). The first product formed at -50 °C was the bridging enolate sodium salt **21**. This anion intramolecularly closed to yield **3** and **4** at −20 °C. The ratio of **3** to **4** in THF was 1.2 to 1, respectively. Compound **10** also reacted at -50 °C with KOtBu to yield the corresponding potassium salt **22** (Figure 15b). At -50 °C, the potassium salt **22** is stable, but when the temperature was raised to 0 °C, products **23** and **24** were formed in a ratio of 2 to 1, respectively. Over a period of several hours, products **23** and **24** reacted with HOtBu to form **25** (Figure 15c). The reaction of **10** with two equivalents of KOtBu at -50 °C initially formed the anion again, but upon warming, the
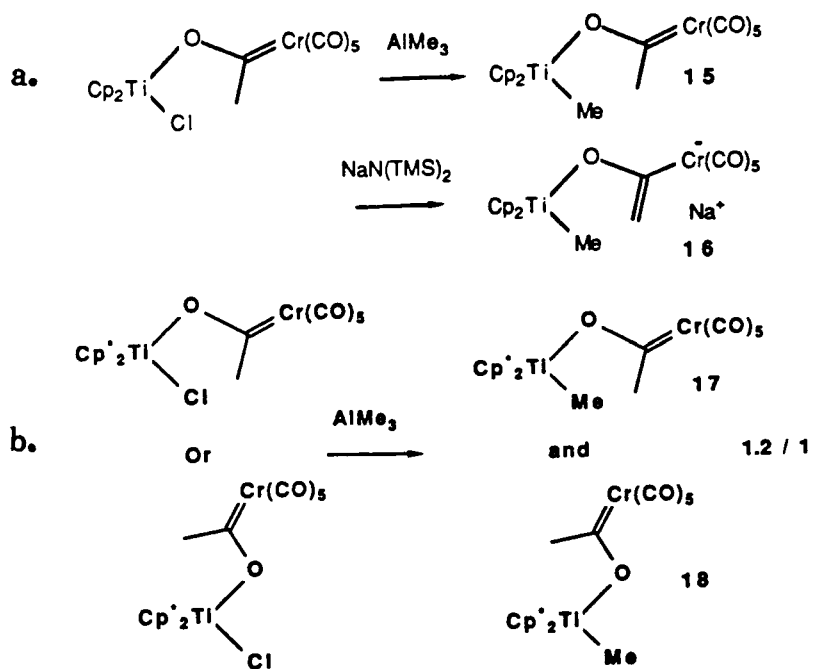
Figure 12. Reactions of AlMe₃ with 9, 12, and 13.
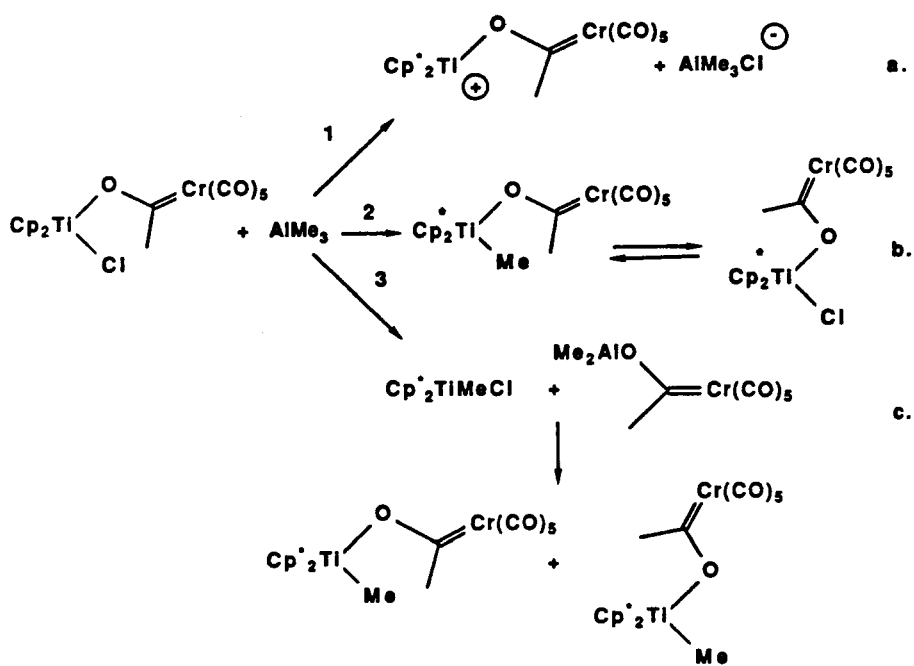
Figure 13: Transmetallation mechanisms.

extra equivalent of KOtBu effectively competed with the intramolecular alkylation at the zirconium center (Figure 15d). The intermolecular alkylation by KOtBu competed with the intramolecular alkylation by Cr due to the extreme unreactive nature of the Fischer carbene enolate. The enolate anion is delocalized throughout the $Cr(CO)_5$ fragment, and thus, the intramolecular closure is relatively slow.
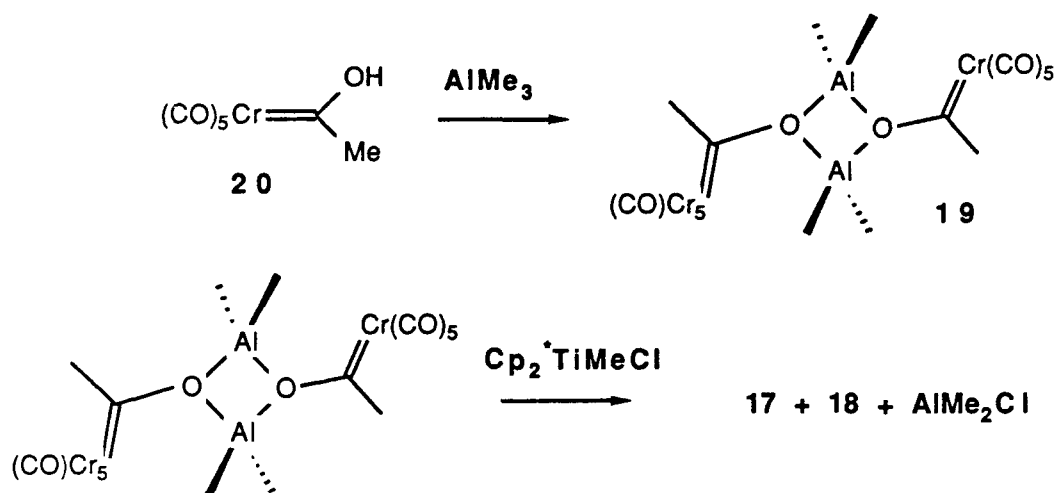
Figure 14: Reaction of **19** with Cp*$_2$TiMeCl.

Figure 15: Reactions of **9** and **10** with bases in THF.
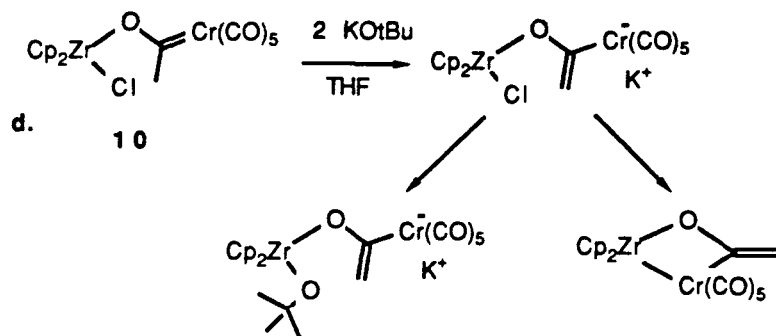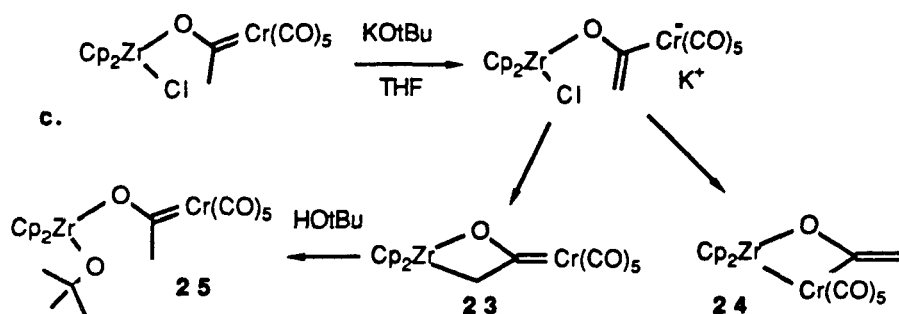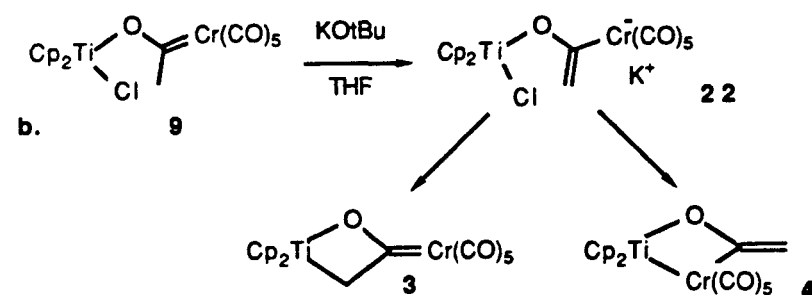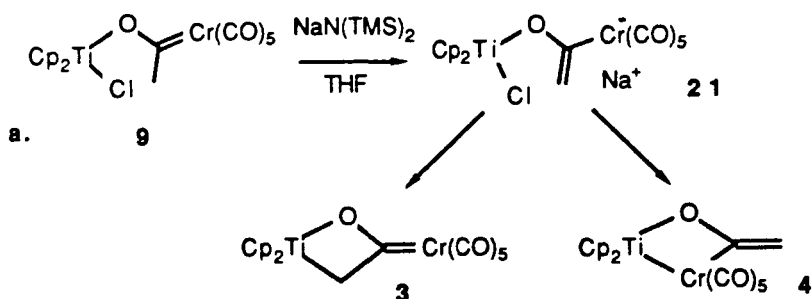
Summary

The reaction of titanocene methylidene with either $Mo(CO)_6$ or $Cr(CO)_6$ forms two complexes in a 1:1 equilibrium ratio. The complexes are formulated as a β-exo Fischer carbene oxametallacyclobutane 3 and a bimetallic bridged ketene adduct 4. The intermediates thermally rearrange to form titanocene ketene 5. Independent synthesis of 3 and 4 from $Cp_2Ti(Cl)O(CH_3)CCr(CO)_5$ 9 and $NaN(TMS)_2$ allowed for structural proof. The structural proof is based on isotopic labeling and the observation of fluxional behavior. The complex $Cp^*_2Ti(Cl)O(CH_3)CCr(CO)_5$ exists as two rotomers. These rotomers are identified by X-ray structural analysis and are found to possess a rigid conformation of the Fischer carbene moieties with respect to the permethylcyclopentadienyl wedge.

Experimental

General Considerations. All manipulations were performed using glovebox or standard Schlenk line techniques. Argon was purified by passage through Chemalog R3-11 and activated 4Å molecular sieves. Deuterated solvents were purchased from Cambridge Isotope Laboratories and purified by vacuum transfer from sodium benzophenone ketyl. CH_2Cl_2 was purified by vacuum distillation from CaH_2. THF was predried over CaH_2 and then vacuum distilled from sodium benzophenone ketyl. Preparative chromoatography was performed using the method of Still.[38] $Cr(CO)_6$ and $Mo(CO)_6$ were purchased from Alfa and used as received.

Metallacyclobutanes,[15] titanocene ketene,[17] $Cp_2Ti(Cl)O(CH_3)CCr(CO)_5$,[21] $LiO(CH_3)CCr(CO)_5$,[21] $Mo(CO)_5PPh_3$,[36] $Mo(CO)_5P(OPh)_3$,[36] $Cp_2^*TiCl_2$,[37] and $(CO)_5CrC(CH_3)OH$,[39] were synthesized as previously described. Deuterated or ^{13}C enriched **9** was synthesized from the deuterated or ^{13}C enriched CH_3I.

^{1}H NMR spectra were recorded on a JEOL FX-90Q (89.6 MHz ^{1}H, 13.76 MHz ^{2}H, 36.2 MHz ^{31}P, 22.5 MHz ^{13}C) and/or JEOL GX-400 (3.99.65 MHz ^{1}H, 100.67 MHz ^{13}C). Spectra were taken in benzene-d_6 or toluene-d_8 solutions, and resonances were referenced to residual protons on the solvent. All NMR tube experiments were prepared in a dry box and the NMR tube capped with a rubber septum.

Crystal Structure Determination of $Cp_2^*Ti(Cl)O(CH_3)CCr(CO)_5$. A single crystal of $Cp_2^*Ti(Cl)O(CH_3)CCr(CO)_5$ was obtained from slow cooling of a solution of pet ether/$CHCl_3$ (1/2) and was mounted in air. The crystal was then optically centered on an Enraf-Nonius CAD 4 diffractometer equipped with a graphite monochromator and a Mo $K\alpha$ radiation. The space group was $P2_1/c$. A total of 11168 reflections were collected. After merging equivalent

(2/m-symmetry) reflections, 4942 remained, of which 4101 had $F_0{}^2 > 0$ and 1827 had $F_0{}^2 > 3\sigma(F_0{}^2)$. These reflections, $1 \leqq \theta \leqq 25°$, were collected in the hemisphere ($\pm h$, $\pm k$, $+l$). Crystal decay was monitored by three check reflections, and the intensities did not significantly decrease over two days of exposure to X-rays.

The positions of the titanium and chromium atoms were determined from a Patterson map, and the Fourier map phased on the two heavy atoms revealed the remainder of the structure. All hydrogen atoms were placed at idealized positions with fixed coordinates and isotropic Gaussian amplitudes. All other atoms were refined with anisotropic U_{ij} parameters.

All calculations were performed on a VAX 11/750, computer using the CRYM system of programs.

Crystal Structure Determination of Cp$_2$*Ti(O(CH$_3$)CCr(CO)$_5$)$_2$. A single crystal of Cp$_2$*Ti(O(CH$_3$)CCr(CO)$_5$)$_2$ was obtained from slow cooling of a 1:2 solution of pet ether/CHCl$_3$ and was mounted in air. The crystal was then optically centered on an Enraf-Nonius CAD 4 diffractometer equipped with a graphite monochromator and Mo $K\alpha$ radiation. The space group was P2$_1$/n. A total of approximately 14000 reflection were collected. After deleting space group absences and merging duplicates, 6401 reflections remained, of which 5860 had $F_0{}^2 > 0$ and 4309 had $F_0{}^2 > 3\sigma(F_0{}^2)$. The data was collected in the hemisphere ($\pm h$, $\pm k$, $+l$), $\theta = 2°$ to $50°$, and in the quadrant ($\pm h$, $+k$, $+l$), $\theta = 50°$ to $55°$. Crystal decay was monitored by three check reflections, whose intensities decreased negligibly over the approximate 3 days of exposure.

The position of the titanium and the two chromium atoms were determined from a Patterson map, and a Fourier map phased on these heavy atoms revealed the remainder of the structure. All hydrogen atoms were placed at

idealized positions with fixed coordinates and isotropic Gaussian amplitudes. All other atoms were refined with anisotropic U_{ij} parameters.

All calculations were performed on a VAX 11/750 computer using the CRYM system of programs.

Reaction of 1 with M(CO)$_6$, M = Cr, Mo. In a dry box, a 5 mm NMR tube was loaded with 10 mg (4.0·10^5 mols) of 1 and 1 equivalent of M(CO)$_6$. A small flask was filled with 0.6 mL d_8 toluene and capped with a rubber septum. The solvent and NMR tube were cooled to -10 °C. The NMR probe was precooled to 5 °C, and 0.4 ml of cooled d_8 toluene was syringed into the NMR tube. The reaction was monitored by ^{1}H NMR. Identification of the final product, titanocene ketene, was done by comparison of published ^{1}H and ^{13}C NMR data.[30] [1]H (90 MHz, toluene-d_8). Intermediate **3a** (M = Mo): δ 5.68 (s, 10 H), 3.17 (s, 2 H). Intermediate **4a** (M = Mo): 5.75 (s, 10 H), 2.97 (d, 1 H, J_{HH} = 1.5), 4.13 (d, 1 H, J_{HH} = 1.5). Intermediate **3b** (M = Cr): 5.67 (s, 10 H), 3.35 (s, 2 H). Intermediate **4b** (M = Cr): 5.75 (s, 10 H), 3.04 (d, 1 H, J_{HH} = 1.5), 4.11 (d, 1 H, J_{HH} = 1.5).

Reaction of 1 with Mo(¹³CO)$_5$P(O∅)$_3$. A 5 mm NMR tube was charged with 18 mg 1 (7.26·10^{-5} mols) and 46 mg Mo(CO)$_5$P(O∅)$_3$ (8.42·10^{-5} mols). A small flask was loaded with 0.6 mL toluene-d_8. The solvent and the NMR probe was cooled to 0 °C, and the solvent was syringed into the tube. The reaction was monitored by ^{1}H NMR. *Trans* **6;** ^{1}H NMR (90 MHz, toluene-d_8) δ 5.69 (s, 10 H), 3.29 (s, 2 H), ^{13}C NMR (22.5 MHz, toluene-d_8) δ 338.6 (J_{CP} = 29.3 Hz); *Cis* **6,** ^{1}H NMR (90 MHz, toluene-d_8), δ 5.81 (s, 10 H), 3.47 (s, 2 H), ^{13}C NMR (22.5 MHz, toluene-d_8) δ 342.5 (J_{CP} = 12.2); *Trans* **7,** ^{1}H NMR

(90 MHz, toluene-d_8), δ 5.79 (s, 10 H), 3.02 (s, 1 H), 4.18 (s, 1 H); *Cis* 7, 5.92 (s, 10 H), 3.09 (s, 1 H), 4.23 (s, 1 H).

Reaction of Cp$_2$Ti(Cl)O(CH$_3$)CCr(CO)$_5$ (9) and NaN(TMS)$_2$. A 5 mm NMR tube was loaded with 20 mg of 9 (4.5·10^{-5} mols) and 7 mg (3.8·10^{-5} mols) NaN(TMS)$_2$. A small flask was loaded with 0.6 mL toluene-d_8. The solvent was cooled to -50 °C along with the NMR probe. The solvent was added to the NMR tube at -50 °C. The reaction yielded intermediates 3 and 4 instantaneously. The reaction was slowly warmed to room temperature in the NMR probe, and isomerization to the titanocene ketene adduct 5 was observed.

Reaction of Cp$_2$Ti(Cl)O(^{13}CH$_3$)CCr(CO)$_5$ and NaN(TMS)$_2$. A 5 mm NMR tube was loaded with 10 mg (2.2·10^{-5} mols) Cp$_2$Ti(Cl)O(^{13}CH$_3$)CCr(CO)$_5$ and 4 mg (2.1·10^{-5} mols) NaN(TMS)$_2$. A small flask was loaded with 0.6 mL toluene-d_8. The solvent and the NMR probe were cooled to -50 °C. Toluene (0.4 mL) was syringed into the NMR tube at -50 C°. **3b:** (^{13}C, d_8-toluene), δ 87.3 (t, $J_{CH} = 133.1$ Hz), **4b:** (^{13}C, d_8-toluene), δ 90.1 (dd, $J_{CH} = 150.4$ and 160.4 Hz).

Reaction of Cp$_2$Ti(Cl)O(CD$_3$)CCr(CO)$_5$ and NaN(TMS)$_2$. Two 5 mm NMR tubes were loaded with 10 mg (2.2·10^{-5} mols) Cp$_2$Ti(Cl)O(CD$_3$)-CCr(CO)$_5$ and 4 mg (2.1·10^{-5} mols) NaN(TMS)$_2$. A small flask was loaded with 0.6 mL d_8 toluene and another small flask loaded with 0.6 mL protio toluene. The solvent flasks were cooled to -50 °C, and 0.4 mL of each solvent was syringed into one of the NMR tubes. A ^{2}H NMR spectra was recorded for the sample in the protio solvent, and a ^{1}H NMR spectra was recorded for the sample in the

deuterio solvent. Integration of the ^{2}H or ^{1}H resonances revealed a 1.3 to 1 ratio of **3b** to **4b**.

Synthesis of Cp$_2$Zr(Cl)O(CH$_3$)CCr(CO)$_5$. A 250-mL three-necked flask was charged with 2.5 g (1.02·10^{-2} mols) LiO(CH)$_3$CCr(CO)$_5$, 3 g (1.03·10^{-2} mols) Cp$_2$ZrCl$_2$ and 100 mL CH$_2$Cl$_2$. The reaction was stirred for 1 hr. A fine white suspension of LiCl precipitated and the solution turned orange. The solution was filtered through a 1 inch plug of celite on a glass frit. The CH$_2$Cl$_2$ solvent was removed under vacuum until an orange precipitate started to form. The solution was then cooled to -50 C° for 24 hrs. Yellow orange crystals were collected by filtration and washed with -50 C° pentane. The crystals were then dried *in vacuo*. Yield 3.1 g, 60% ^{1}H NMR (90 MHz, C$_6$D$_6$) δ 5.87 (s, 10 H), 2.52 (s, 3 H); ^{13}C {^{1}H} (22.5 MHz, C$_6$D$_6$) δ 367.3, 224.4, 218.1, 115.3, 52.3: Anal. Calcd for C$_{17}$H$_{13}$O$_6$ZrCrCl: C, 41.51; H, 2.66. Found: C, 41.27; H, 2.66.

Synthesis of Cp*$_2$Ti(Cl)OC(CH$_3$)Cr(CO)$_5$ (12 and 13). A 300-mL three-necked flask was equipped with refluxed condenser and charged with 2.7 g (4.5·10^{-3} mols) Cp$_2$*TiCl$_2$, 1.6 g LiO(CH$_3$)CCr(CO)$_5$ (6.6·10^{-3} mols) and 100 ml CH$_2$Cl$_2$. The reaction was refluxed for 7 hrs and cooled to room temperature. The solution was then filtered through a 1 inch plug of celite on a glass frit. The solvent was removed on a rotary evaporator and the red solid dissolved in the minimum amount of CH$_2$Cl$_2$. A preparative column was run with 200 g silica gel with a 2/1 pentane/CH$_2$Cl$_2$ eluent. The first red band **11** (R_f=0.53), second red band **13** (R_f=0.35) and third red band **12** (R_f=0.12) were collected. Each fraction was dried by a rotary evaporator and was recrystallized from a 2/1 pet ether/CHCl$_3$ solution. Compound **12** yield 0.92 g,

22 %: ^{1}H NMR (400 MHz, C$_6$D$_6$), δ 1.72 (s, 30 H); δ 2.87 (s, 3 H); C^{13}: (100.1 MHz, C$_6$D$_6$) δ 352.2, 223.8, 219.4, 128.5, 50.9, 12.69. Anal. Calcd for C$_{26}$H$_{33}$O$_6$CrTi: C, 55.07; H, 5.64. Found: C, 54.90; H, 5.59. Compound 13 yield 0.42 g, 11 %; ^{1}H NMR (400 MHz, C$_6$D$_6$), δ 1.64 (s, 30 H), 2.58 (s, 3 H); C^{13} (100.1 MHz, C$_6$D$_6$): δ 344.7, 224.2, 219.9, 125.3, 50.5, 11.7.

Synthesis of Cp*$_2$Ti(O(CH$_3$)CCr(CO)$_5$)$_2$. A medium Schlenk tube was loaded with 500 mg (1.2·10^{-3} mols) Cp$_2$*TiCl$_2$ and 615 mg (2.5·10^{-3} mols) LiO(CH$_3$)CCr(CO)$_5$. The reactants were suspended in 10 ml THF and stirred at room temperature for 72 hrs. The solvent was removed under vacuum and the red solid dissolved in CH$_2$Cl$_2$ and filtered through a 1 inch plug of celite on a glass frit. The red solution was chromatographed on silica gel with a 2/1 pentane/CH$_2$Cl$_2$ eluent. The major product 13 (R_f=0.35) was collected and dried on a rotary evaporator. Yield 270 mg, 35%. ^{1}H (90 MHz, C$_6$D$_6$), δ 1.51 (s, 30 H), 2.28 (s, 3 H), 3.48 (s, 3 H); ^{13}C (100.1 MHz, C$_6$D$_6$) δ 223.32, 223.42, 218.93, 219.17, 346.47, 350.56, 58.39, 57.41, 129.59, 12.84.

Reaction of 12 or 13 with NaN(TMS)$_2$. A 5 mm NMR tube was charged with 10 mg (1.7·10^{-5} mols) 11 or 12, 3 mg NaN (TMS)$_2$ (1.6·10^{-5} mols) and 0.4 mL toluene-d_8. The NMR tube was shaken and allowed to stand for 4 hrs. A ^{1}H NMR spectra showed formation of an anion from 12, but a precipitate from 13 was formed. Anion from 12: ^{1}H (90 MHz, toluene-d_8) δ 1.68 (s, 30 H), 5.72 (s, 1 H), 5.02 (s, 1 H); ^{13}C (100.1 MHz, toluene-d_8) δ 129.4, 105.6, 182.7, 11.6.

Synthesis of Cp$_2$TiClO(Et)CCr(CO)$_5$. A 100 mL three-necked flask was charged with 1 g (0.14 mols) of Li wire and equipped with a dropping funnel

and a reflux condenser. The Li was washed with pentane and dried under vacuum. Pentane (20 ml) was added to the reaction vessel and 4.48 ml EtBr (0.075 mols, dissolved in 20 ml pentane) was added dropwise over a 2 hr. period. The solution turned cloudy. The reaction was cooled to room temperature and 50 ml of ether was added and the solution stirred vigorously. The solution was filtered and dried *in vacuo*. The LiEt was titrated with a standardized solution of diphenylacetic acid until a pink color persisted. Activity was 0.13 (130 mg/1 g).

A medium Schlenk tube was charged with 1 g ($3.6 \cdot 10^{-3}$ mols) of the EtLi/LiBr mixture and dissolved in 20 ml ether. A 300 mL three-necked flask was equipped with a reflux condenser and charged with 900 mg ($4.0 \cdot 10^{-3}$ mols) $Cr(CO)_6$. The EtLi/LiBr solution was slowly cannulated into the $Cr(CO)_6$ solution over a half hour period. The reaction turned dark red and was stirred for $\frac{1}{2}$ hr. Another 100 ml three-necked flask was charged with 850 mg ($3.4 \cdot 10^{-3}$ mols) of Cp_2TiCl_2 and 40 ml CH_2Cl_2. The $LiO(Et)CCr(CO)_5$ solution was cannulated into the Cp_2TiCl_2 solution. The solution turned deep red, and a fine white precipitate appeared. The solvent was removed *in vacuo*. The red solid was dissolved in CH_2Cl_2 and filtered through a 1 inch plug of celite on a glass frit. The solution was then chromatographed on silica gel with a 3:1 CH_2Cl_2/pentane eluent. The major red band ($R_f = 0.45$) was collected and the solvent removed by a rotoevaporator. Yield 470 mg, 30% (based on Cp_2TiCl_2).. ^1H NMR (90 MHz, C_6D_6), δ 5.87 (s, 10 H), 2.90 (q, 2 H), 0.99 (t, 3 H); ^{13}C NMR (22.5 MHz, C_6D_6), δ 218.4, 224.1, 363.3, 54.7, 109.3, 118.0.

Synthesis of $Cp_2TiCl(nBu)$ and $Cp_2Ti(nBu)O(CH_3)CCr(CO)_5$. A medium Schlenk tube was charged with 0.560 g ($2.3 \cdot 10^{-3}$ mols)

$Cp_2Ti(Cl)O(CH_3)Cr(CO)_5$. CH_2Cl_2 30 mL was syringed in and the reaction was cooled to -50 °C. A solution of nBuLi (1.02 mL of 2.2 M nBuLi, ($2.2 \cdot 10^{-3}$ mols)) was added dropwise over 20 minutes. The reaction was then warmed to room temperature and filtered through a 1 inch plug of celite on a glass frit. The solvent was removed under vacuum, and the dark red oil washed twice with 10 ml 0 °C pentane. The red solid was dried *in vacuo*. $Cpp_2Ti(nBu)Cl$ ^{1}H NMR (400 MHz, C_6D_6) δ 5.79(s, 10 H), δ 1.65 (t, 2 H), δ 1.40 (q, 2 H), δ 1.19 (sx, 2 H), δ 0.90 (t, 3 H); ^{13}C NMR (100.1 MHz, C_6D_6) δ 115.7, 72.9, 40.7, 28.9, 14.6: $Cp_2Ti(nBu)O(CH_3)CCr(CO)_5$ ^{1}H NMR (400 MHz, C_6D_6), δ 5.53 (s, 10 H), δ 2.18 (s, 3 H), δ 1.98 (t, 2 H), δ 1.42 (q, 2 H), δ 1.41 (sx, 2 H), δ 0.94 (t, 3 H). ^{13}C NMR (100.1 MHz, C_6D_6) δ 144.2, 352.7. 224.5, 218.7, 65.5, 38.3, 28.3, 13.9.

Reaction of $Cp_2^*Ti(Cl)O(CH_2)CCr(CO)_5 \cdot Na$ with HCl. A 5 mm NMR tube was loaded with 10 mg $Cp^*_2Ti(Cl)O(CH_2)CCr(CO)_5 \cdot Na$ ($1.6 \cdot 10^{-5}$ mols) and 0.4 mL toluene-d_8. The solution was cooled to -30° C, and 0.4 ml ($1.8 \cdot 10^{-5}$ mols) HCl was added in via gas tight syringe. A ^{1}H NMR showed formation of both **12** and **13**.

Synthesis of $Cp_2Ti(Me)O(CH_3)CCr(CO)_5$. A medium Schlenk tube was charged with 500 mg ($1.1 \cdot 10^{-3}$ mols) $Cp_2Ti(Cl)O(CH_3)CCr(CO)_5$ and 20 mL C_6H_6. At room temperature, 0.65 mL of a 2 M $AlMe_3$ solution (in toluene) ($1.3 \cdot 10^{-3}$ mols) was cannulated into the Schlenk tube. The reaction turned orange and was stirred for 30 min and 10 ml ether was added. The solvent was removed under vacuum, and the resultant orange paste was dried *in vacxuo* for 12 h. The orange paste was then dissolved in 5 ml toluene and slowly cooled to -50 °C. Orange crystals were collected by filtration. Yield 310 mg, 66% [1]H (90 MHz, C_6D_6) δ 5.47 (s, 10 H), 2.18 (s, 3 H), 0.78 (s, 3 H); [13]C (100.1

MHz, C_6D_6) δ 352.6, 224.6, 218.7, 113.9, 42.7, 51.6: Anal. Calcd for $C_{18}H_{16}O_6TiCr$: C, 50.49; H, 3.77. Found: C, 50.45; H, 3.80.

Reaction of 12 or 13 with $AlMe_3$. A 5 ml NMR tube was charged with either 10 mg of 12 or 13. C_6D_6 (0.4 mL) was added along with 2 μl $AlMe_3$. The reaction was complete in one minute. Both isomers 13 and 14 were formed in a 1.2 to 1 ratio. The individual isomers were identified by NOE difference spectra. Irradiation of the δ 2.35 resonance enhanced the δ 0.19 resonance. Irradiation of the δ 2.43 resonance gave no enhancement of the δ 0.67 resonance. Isomer 17: ^1H (400 MHz, C_6D_6) δ 1.62 (s, 30 H), 2.35 (s, 3 H), 0.19 (s, 3 H); Isomer 18: ^1H (400 MHz, C_6D_6) δ 1.52 (s, 30 H), 2.43 (s, 3 H), 0.67 (s, 3 H);

Synthesis of $Cp_2Ti(Me)O(CH_2)CCr(CO)_5 \cdot Na$. A medium Schlenk tube was charged with 250 mg ($5.9 \cdot 10^{-4}$ mols) $Cp_2Ti(Me)O(CH_3)CCr(CO)_5$ and 10 mL THF. The solution was cooled to -50° C. In a second medium Schlenk tube, 110 mg ($6.0 \cdot 10^{-4}$ mols) $NaN(TMS)_2$ was dissolved in 5 ml THF and cooled to −50 °C. The $NaN(TMS)_2$ solution was slowly cannulated into the $Cp_2Ti(Me)O(CH_3)CCr(CO)_5$ solution. The solution was warmed to room temperature for 20 min. The orange solution precipitated a yellow solid. The yellow solid was filtered under Ar and washed with 0 °C toluene. The yellow solid was dried *in vacuo*. Yield 120 mg, 45%. ^1H (400 MHz, $-d_8$ THF) δ 5.86 (s, 10 H), 4.05 (d, 1H, $J_{HH} = 3.4$), 3.56 (d, 1H, $J_{HH} = 3.4$), 0.43 (s, 3 H); ^{13}C (100.1 MHz, $-d_8$ THF) δ 225.5, 223.8, 219.2, 111.3, 103.8, 29.1.

Synthesis of $((Me_2Al)O(CH_3)CCr(CO)_5)_2$. A medium Schlenk tube was charged with 500 mg ($2.1 \cdot 10^{-3}$ mols) $HO(CH_3)CCr(CO)_5$ and 40 ml toluene.

The solution was cooled to 0 °C and 1.2 mL ($2.3 \cdot 10^{-3}$ mols) of a 2.0 M AlMe$_3$ solution (in toluene) was added dropwise. Gas was evolved and the solution turned deep red. The reaction was stirred at room temperature for one half hour and the solvent removed *in vacuo*. The red paste was dried *in vacuo* for 18 h, redissolved in the minimum amount of toluene and cooled to -50° C. Yield 246 mg, 20 % collected by filtration. ^{1}H NMR (90 MHz, toluene-d_8), δ 2.75 (s, 6 H), δ -0.26 (s, 12 H).

Reaction of (Me$_2$AlO(CH$_3$)CCr(CO)$_5$)$_2$ and Cp*$_2$TiMeCl. A 5 mm NMR tube was charged with 10 mg Cp*$_2$TiMeCl ($2.7 \cdot 10^{-5}$ mols), 16 mg ($2.7 \cdot 10^{-5}$ mols) (Me$_2$AlO(CH$_3$)CCr(CO)$_5$)$_2$ and 0.4 mL toluene-d_8. The reaction was allowed to stand for 1 hr. A ^{1}H NMR spectrum showed complete conversion to **17** and **18**.

Reaction of Cp$_2$Ti(Cl)O(CH$_3$)CCr(CO)$_5$ and NaN(TMS)$_2$ in THF. A 5 mm NMR tube was charged with 20 mg ($4.5 \cdot 10^{-5}$ mols) Cp$_2$Ti(Cl)O(CH$_3$)CCr(CO)$_5$ and 8 mg ($4.3 \cdot 10^{-5}$ mols) NaN(TMS)$_2$. A 1 mL volummetric flask was filled with 0.6 ml THF-d_8 and cooled to -50 °C. 0.4 mL of solvent was added to the NMR tube. There was immediate formation of anion **20**. ^{1}H NMR (90 MHz, D^8 THF) δ 6.27 (s, 10 H), δ 4.33 (d, 1 H, $J_{HH} = 2.4$), δ 3.69 (d, 1 H, $J_{HH} = 2.4$). When the reaction was warmed to -20 °C to 0 °C, products **3** and **4** were formed. Product **3** ^{1}H NMR (90 MHz, THF-d_8), δ 6.42 (s, 10 H), 2.77 (s, 2 H); Product **4**, δ 6.31 (s, 10 H), 4.12 (d, 1 H, $J_{HH} = 2.4$), 3.78 (d, 1 H, $J_{HH} = 2.4$).

Reaction of Cp$_2$Ti(Cl)O(CH$_3$)CCr(CO)$_5$ and KOtBu in THF. A 5 mm NMR tube was charged with 20 mg ($4.5 \cdot 10^{-5}$ mols)

$Cp_2Ti(Cl)O(CH_3)CCr(CO)_5$ and 9 mg KOtBu ($9.0 \cdot 10^{-5}$ mols). A 1 mL volummetric flask was filled with 0.6 ml THF-d_8 and cooled to -50 °C. 0.4 ml of solvent was added to the NMR tube. There was immediate formation of anion 21. ^{1}H NMR (90 MHz, THF-d_8) δ 6.30 (s, 10 H), 4.35 (d, 1 H, $J_{HH} = 2.4$ Hz), 3.78 (d, 1 H, $J_{HH} = 2.4$). When the reaction was warmed to 0 °C, products 3 and 4 were formed.

Reaction of $Cp_2Zr(Cl)O(CH_3)CCr(CO)_5$ and 1 eq KOtBu in THF. A 5 mm NMR tube was charged with 20 mg ($4.1 \cdot 10^{-3}$ mols) $Cp_2Zr(Cl)O(CH_3)CCr(CO)_5$ and 5 mg ($4.5 \cdot 10^{-3}$ mols) KOtBu. A 1 ml volummetric flask was filled with 0.6 ml THF-d_8 and cooled to -50° C. 0.4 ml of solvent was added to the NMR tube. There was immediate formation of anion 22 ^{1}H NMR (90 MHz, THF-d_8), δ 6.31 (s, 10 H), 4.40 (d, 1 H, $J_{HH} = 2.5$), δ 3.77 (d, 1 H, $J_{HH} = 2.5$). Products 23 and 24 formed at room temperature. Product 23: δ 6.31 (s, 10 H) 4.62 (d, 1 H, $J_{HH} = 2.4$), 3.90 (d, 1 H, $J_{HH} = 2.4$) and product 24, δ 6.46 (s, 10 H), 2.68 (s, 2 H or 3 H).

Reaction of $Cp_2Zr(Cl)O(CH_3)CCr(CO)_5$ and 2 eq. KOtBu in THF. A 5 mm NMR tube was charged with 20 mg ($4.1 \cdot 10^{-5}$ mols) $Cp_2Zr(Cl)O(CH_3)CCr(CO)_5$ and 9 mg KOtBu ($9.0 \cdot 10^{-5}$ mols). A 1 ml volummetric flask was filled with 0.6 ml THF-d_8 and cooled to -50 °C. 0.4 ml of solvent was added to the NMR tube. There was immediate formation of anion 22. When the reaction was warmed to 0 °C, products 24 and 25 were formed: Compound 25 ^{1}H NMR (90 MHz, THF-d_8), δ 6.18 (s, 10 H), δ 4.41 (d, 1 H, $J_{HH} = 2.5$), 3.72 (d, 1 H, $J_{HH} = 2.5$) 1.15 (s, 9 H).

References

1. Collman, J. P.; Hegedus, L. S.; Norton, J. R.; Finke, R. G. "Principles and Applications of Organotransition Metal Chemistry," University Science Books, Mill Valley California, 1987, Chapter 6.

2. a) Wolcyanski, P.T.; Threlkel, R.S.; Bercaw, J.E. *J. Am. Chem. Soc.* **1979**, *101*, 218. b) Mashima, K.; Jyodoi, K.; Ohyoshi, A.; Tokaya, H. *Chem. Comm.* **1986**, *15*, 1145. c) St. Clair, M.; Bercaw, J.E. unpublished results. d) Erker, G.; Dorf, U.; Krüger, C.; Tsay, Y.H. *Organometallics* **1987**, *6*, 680.

3. Fischer, E.O. *Chem. Ber.* **1979**, *109*, 1128.63.

4. Erker, G.; Dorf, V.; Benn, R.; Reinhardt, R. *J. Am. Chem. Soc.* **1984**, *106*, 7649.

5. Petz, W. *J. Organomet. Chem.* **1974m** *72*, 369.

6. a) Chan, K.S.; Wulff, W.D. *J. Am. Chem. Soc.* **1986**, *108*, 5229. b) Wulff, W.D.; Yang, D.C. *J. Am. Chem. Soc.* **1983**, *105*, 6726; Wulff, W.D.; Yang, D.C. *J. Am. Chem. Soc.* **1984**, *106*, 7565.

7. a) Liebeskind, L.S.; Jewell, C.F. *J. Organomet. Chem.* **1985**, *285*, 305. b) Jewell, C.F.; Liebeskind, L.S.; Williamson, M. *J. Am. Chem. Soc.* **1985**, *107*, 6715.

8. a) Dötz, K.; Kuhn, *J. Organomet. Chem.* **1985**, *285*, C23. b) Döty, K. *Angew. Chem. Int. Ed. Engl.* **1975**, *14*, 644. c) Semmelhack, M.F.; Boyell, T.J.; Sato, T.; Wulff, W.D.; Spies, E.; Yask, A. *J. Am. Chem. Soc.* **1982**, *104*, 5850. d) Dötz, K. *Pure & Appl. Chem.* **1983**, *11*, 1689. e) Hegedus, L.S.; McGuire, M.A.; Schultze, L.M.; Yyun, C.; Anderson, O.P. *J. Am. Chem. Soc.* **1984**, *106*, 2680.

9. Semmelhack, M.F.; Park, J. *Organometallics* **1986**, *5*, 2550, and references therein.

10. Ziegler, M.L.; Weidenhammer, K.; Hermann, W.A. *Angew. Chem. Int. Ed. Engl.* **1977**, *16*, 555.

11. Hermann, W.A.; Plank, J. *Angew. Chem. Int. Ed. Engl.* **1978**, *17*, 525.

12. Cramer, R.E.; Higa, K.T.; Gilje, J.W. *J. Am. Chem. Soc.* **1984**, *106*, 7245.

13. Collman, J.P.; Hegedus, L.S.; Norton, J.R.; Finke, R.G. "Principles and Applications of Organotransition Metal Chemistry," University Science Books: Mill Valley, CA, 1987, pp 653-656 and references therein.

14. a) Keim, W.; Röper, W.R.; Strutz, H. *J. Organomet. Chem.* **1981**, *219*, C5. b) Bassner, S.L.; Morrison, E.D.; Geoffroy, G.L. *J. Am. Chem. Soc.* **1986**, *108*, 5358 and references therein.

15. Straus, D.A.; Grubbs, R.H. *Organometallics* **1982**, *1*, 1658.

16. Casey, C.P. *React. Intermediates* **1985**, *3*, 109.

17. Straus, D.A.; Grubbs, R.H. *J. Am. Chem. Soc.* **1982**, *104*, 5499.

18. Hamilton, D.W.; Willis, W.S.; Stucky, G.D. *J. Am. Chem. Soc.* **1981**, *103*, 4255.

19. a) Butts, S.B.; Strauss, S.H.; Holt, E.M.; Stinson, R.F.; Alcock, N.W.; Shriver, D.F. *J. Am. Chem. Soc.* **1980**, *102*, 5093. b) Porter, R.H.; Shriver, D.F. *Organomet. Chem.* **1975**, *90*, 41. c) Stinson, R.E.,; Shriver, D.F. *Inorg. Chem.* **1980**, *19*, 1141.

20. Longato, B.; Norton, J. R.; Huffman, J. C.; Marsella, J. A.; Caulton, K. G. *J. Am. Chem. Soc.* **1981**, *103*, 209.

21. Fischer, E.O.; Fontana, S. *J. Organomet. Chem.* **1972**, *40*, 159.

22. Gordon, A. J.; Ford, R. A. "The Chemists Companion" Wiley-Interscience: New York, 1972, p. 286.

23. Martin, B.D.; Matchett, S.A.; Norton, J.R.; Anderson, O.P. *J. Am. Chem. Soc.* **1985**, *107*, 7952, and references therein.

24. Casey, C.P.; Anderson, R.L. *J. Am. Chem. Soc.* **1973**, *56*, C37.

25. Casey, C. P.; Anderson, R. L. *J. Am. Chem. Soc.* **1974**, *96*, 1230.

26. a) Ho, S.C.; Hentges, S.; Grubbs, R.H., unpublished results. b) Erker, G.; Wicker, J.; Engel, KI.; Rosenfeldt, F.; Dietrich, W.; Krüger, C. *J. Am. Chem. Soc.* **1980**, *102*, 6344. c) Erker, G.; Engel, K.; Krüger, C.; Müller, G. *Organometallics* **1984**, *3*, 128.

27. a) Tatsumi, K.; Yasuda, H.; Nakamura, A. *Isr. J. Chem.* **1983**, *23*, 145. b) Hofmann, P. Frede, M.; Stauffert, P. Lasser, W.; Thewalt, U. *Angew. Chem., Int. Ed. Engl.* **1985**, *24*, 712.

28. McKenzie, T.C.; Sanner, R.D.; Bercaw, J.E. *J. Organomet. Chem.* **1975**, *102*, 457.

29. Hoffmann, J.C.; Moloy, K.G; Marsella, J.A.; Caulton, K.G. *J. Am. Chem. Soc.* **1980**, *102*, 3009.

30. Shubert, U. "Transition Metal Carbene Complexes," Verlag Chemie: West Germany, 1983.

31. Taylor, T. E.; Hall, M. B. *J. Am. Chem. Soc.* **1984**, *106*, 1576.

32. Carter, E. A.; Goddard, W. A. *J. Phys. Chem.* **1984**, *88*, 1485.

33. Carter, E. A.; Goddard, W. A. *J. Am. Chem. Soc.* **1986**, *108*, 2180.

34. a) Baird, N. C.; Taylor, T. F. *J. Am. Chem. Soc.* **1978**, *100*, 1333. b) Staemmler, V. *Theor. Chim. Acta* **1974**, *35*, 309.

35. Collman, J. P.; Hegedus, L. S.; Norton, J. R.; Finke, R. G. "Principles and Applications of Organotransition Metal Chemistry" University Science Books: Mill Valley, CA, 1987, p. 127.

36. Covey, W.D.; Brown, T.L. *Inorg. Chem.* **1973**, *12*, 2820, and references therein.

37. Bercaw, J.E.; Marvich, R.H.; Bell, L.G.; Brintzinger, H.H. *J. Am. Chem. Soc.* **1972**, *94*, 1219.

38. Still, W. C.; Kahn, M.; Mitra, A. *J. Org. Chem.* **1978**, *43*, 2923.

39. Buhro, W. E.; Wong, A.; Merrifield, J. H.; Lin, G. Y.; Constable, A. C.; Gladysy, J. A. *Organometallics* **1983**, *2*, 1852.

CHAPTER 6

METALLACYCLOBUTADIENE VERSUS METALLATETRAHEDRANE

STRUCTURES FOR Cl$_3$MoC$_3$H$_3$ COMPLEXES

ABSTRACT: The bonding and energetics in the $Cl_3MoC_3H_3$ metallacyclobutadiene are contrasted with those in the metallatetrahedrane. The complexes are found to be within 20 kcal/mol of one another, with the metallatetrahedrane being the lower in energy. The Mo-C bonds are essentially covalent in both structures, and the metallacyclobutadiene possesses resonance stabilization. Charge distribution in the carbon fragments reveals no cyclopropenium character in the C_3H_3 ring of the metallatetrahedrane. Bonding, energetics, and charge distributions are all discussed with an emphasis on structure and reactivity.

I. INTRODUCTION

Metallacyclobutadienes **A** are believed to play the same role in acetylene metathesis[1] [eq (1)] as metallacyclobutanes **B** play in olefin metathesis[2] [eq (2)]. Strong evidence for the role of **A** in acetylene metathesis is provided by the isolation and crystal structures of the following complexes: **1.** $W[C(CMe_3)(CMe)_2]Cl_3$,[3] **2.** $W(C_3Et_3)[O-2,6-C_6H_3(iPr)_2]_3$,[4] and **3.** $W(C_3Et_3)[OCH(CF_3)_2]_3$.[5] Unfortunately, not all of the metallacyclobutadienes isolated are active catalysts.[5-7] Species **2** and **3** are, however, isolated as end products from catalytically active systems.[4,5] Despite the experimental observation of these species, there remain a number of questions concerning the bonding in these complexes. Are the complexes best viewed as metallacyclobutadienes, and, if so, is there resonance stabilization or destabilization in the π system? The x-ray structures of **1**, **2**, and **3** reveal a particularly short W-βC distance ranging from 2.093 to 2.159 Å, only about 0.2 Å longer than the W-αC bond.[3-5] This naturally led to speculation that there might be a bonding interaction between W and the β carbon, and that **1**, **2**, and **3** might be structurally or electronically different from the metallacycles presumed to form in the catalytically active systems. Further studies of dialkylacetylene metathesis involved varying the steric bulk of the alkyl groups on the metallacycle carbons and of the axial-equatorial ligands. The conclusion reached was that sterics are the overriding factor influencing the rate of metathesis, and thus, the stability of the metallacycle.[4-7]

The fate of **1** in the presence of excess diethylacetylene is not that of metathesis but of cyclopentadienyl formation. Surprisingly, two cyclopentadienyl complexes (**4** and **5**) are formed.[7] The simplest mechanism which would give rise to a cyclopentadienyl complex is one in which the alkyne coordinates and then in-

$$LnM \equiv CR \atop + \atop RC \equiv CR \rightleftharpoons \underset{A}{\begin{array}{c} LnM = CR \\ | \quad | \\ RC = CR \end{array}} \rightleftharpoons \underset{RC}{LnM} \; + \; \underset{CR}{CR} \qquad 1$$

$$LnM = CR \atop + \atop RC = CR \rightleftharpoons \underset{B}{\begin{array}{c} LnM - CR \\ | \quad | \\ RC - CR \end{array}} \rightleftharpoons \underset{RC}{LnM} \; + \; \underset{CR}{CR} \qquad 2$$

Cl_3W **1**

$[C_6H_3(i\text{-}Pr)_2\text{-}O\text{-}]_3W$ **2**

$[(CF_3)_2CHO]W$ **3**

WCl_3 **4**

WCl_3 **5**

6
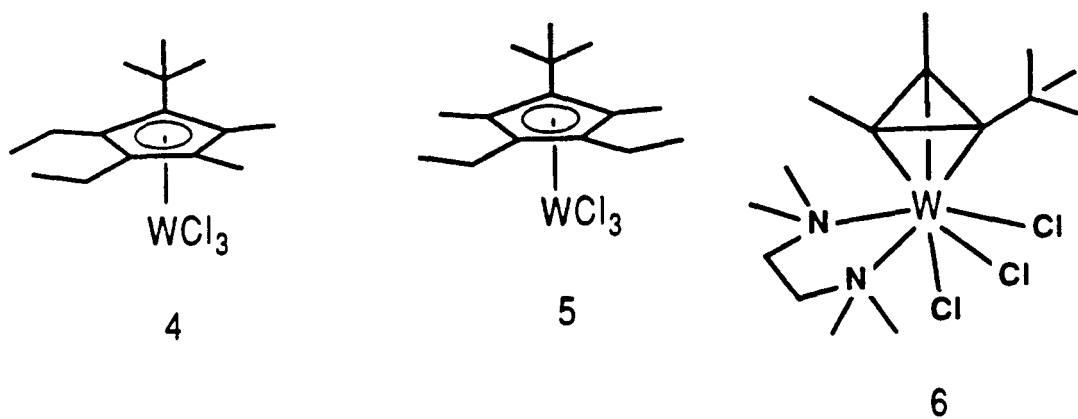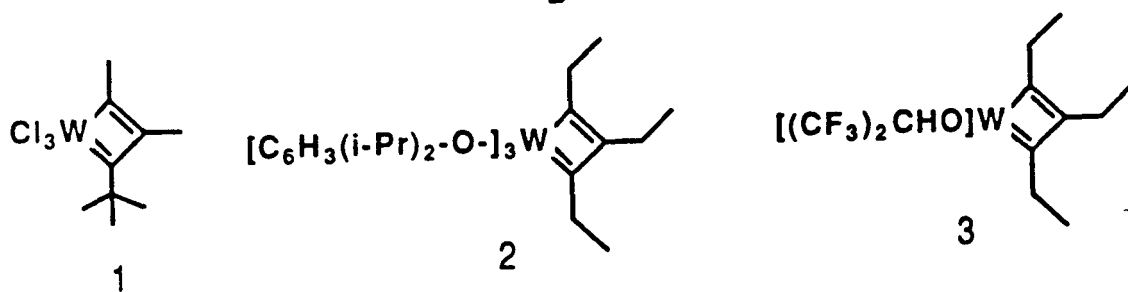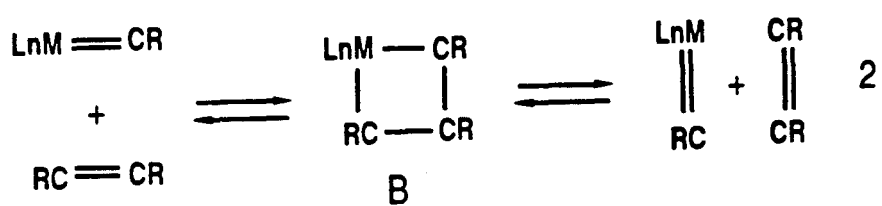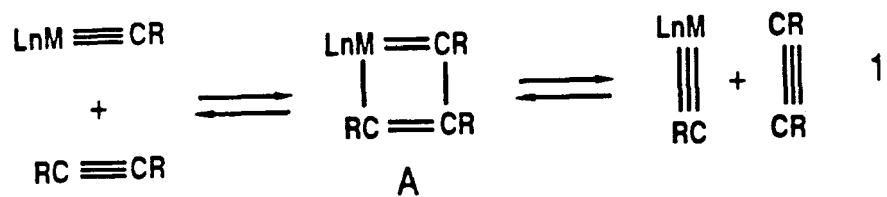
serts into a W-alpha C bond to yield a tungstenabenzene intermediate, which then collapses to a cyclopentadienyl complex. Such a route should yield only 4. A possible answer to this problem[7] was suggested following the isolation of 6 $W[C_3Me_2(CMe_3)][TMEDA]Cl_3$ from the reaction of 1 and TMEDA (tetramethylethylenediamine). The complex is pseudo-octahedral and contains a *symmetrically bound* η_3-cyclopropenyl ligand. This interconversion between a metallacyclobutadiene and a metallatetrahedrane allows for the formation of the two cyclopentadienyl complexes by rotation of the η_3 ring, and thus, isomerization of the alkyl groups in the metallacyclobutadiene.

The structure of 6 revealed that the ring substitutents all bend up out of the plane of the carbon ring.[7] The original investigators[7] explain this in terms of steric interactions between the ring groups and the W ligands. The origin of this interaction is presumably due to the carbon ring being drawn close to the metal due to the latter's electron deficiency. These investigators[7] proposed W(IV) and $(C_3R_3)^-$ but did not rule out that the tungstenatetrahedrane is W(VI) with a $(C_3R_3)^{3-}$ ligand. They suggested that $(C_3R_3)^+$ with W (II) seemed least satisfactory.

The interconversion between metallatetrahedrane and metallacyclobutadiene has been treated theoretically for the general case where an ML_n fragment cleaves a C-C bond of the metallatetrahedrane to give a metallacyclobutadiene.[8] Equilbrium geometries for several ML_n and C_3R_3 fragments were predicted, but detailed analyses of bonding and energetics were not presented.

The experimental studies suggest several questions which lend themselves to detailed theoretical analysis. What is the nature of the W-C bonding interaction in the metallacyclobutadiene and the metallatetrahedrane? Is it mostly covalent or ionic? Is there resonance stabilization or destabilization in the metallacyclobutadi-

ene? What are the charges on the carbon fragments, and how large is the electron deficiency of each species? Is there any W-βC bonding interaction in the metallacyclobutadiene? What are the relative energetics between the two structures, and why do they interconvert so readily? Is there any barrier to rotation of the C_3R_3 ring in the metallatetrahedrane species? What role do the electron-withdrawing ligands play in the energetics of the species?

II. CALCULATIONAL DETAILS

A. Basis Sets and Effective Potentials

All electrons were considered explicitly for C and H, but effective potentials were used to replace core electrons of Cl and Mo. For Cl, the Ne core was replaced with the SHC effective potential[9] (treating neutral Cl with seven explicit electrons), and for Mo, a relativistic effective potential[10] was used for the Zn core (treating neutral Mo with 12 explicit electrons). All calculations used Cartesian Gaussian basis sets. For carbon,[9] the (9s5p) primitive Gaussian basis was contracted to valence double zeta [3s, 2p].[11] For hydrogen,[9] the (3s) primitive basis was scaled ($\zeta = 1.2$) and contracted to (2s).[11] For Mo,[10] the basis set was contracted to [3s, 4p, 2d] from the primitive (3s, 5p, 3d). For Cl,[9] the (3s, 2p) primitive basis was contracted to [1s, 1p] based on $TiCl_4$.

B. Wavefunctions

Wavefunctions were calculated at the Hartree-Fock (HF), generalized valence bond (GVB) and generalized valence bond configuration interaction (GVB-CI) levels. For HF, the singlet state has all orbitals doubly-occupied,

$$\Phi^{HF} = \phi(1)\phi(2)(\alpha\beta - \beta\alpha), \tag{3}$$

but optimized self-consistently. This leads to a good description of bonds constructed from highly overlapping orbitals but a poor description of bonds involving low overlap (e.g., M-C pi bonds). The GVB wavefunction introduces electron correlation effects by allowing each electron to have its own orbital, which is then optimized self-consistently. For a typical two-electron bond, the GVB wavefunction has the form

$$\Phi^{GVB} = [\phi_\ell(1)\phi_r(2) + \phi_r(1)\phi_\ell(2)](\alpha\beta - \beta\alpha), \tag{4}$$

where ϕ_r and ϕ_ℓ are, in general, fairly localized on opposite atoms in the bond.

Because some electron pairs are well treated in HF [as in (1)], while others require correlation [as in (3)], GVB calculations often correlate only a portion of the bond pairs.[12] Generally, the pairs that change significantly during a reaction sequence are correlated to those that have large correlation errors. To indicate the level of correlation, the GVB wavefunction is denoted as GVB (n/m), where n is the number of electron pairs being correlated and m is the number of orbitals used for the correlated pairs (generally 2n). In the various $Cl_3Mo(C_3H_3)$ complexes, the 12 electrons involved in Mo-C and C-C bonding are correlated since these electrons change dramatically as the structure is changed from **7** to **8**. Therefore, GVB (6/12) level calculations are carried out. The shape of the self-consistent GVB orbitals is used to interpret the bonding characteristics of the wavefunction. It is found that these six bond pairs have the following character: the metallacyclobutadiene **7** has two metallacycle π bonds, two Mo-C σ bonds, and two C-C σ bonds (leaving the other orbitals as self-consistent doubly-occupied orbitals). The metallatetratrahedrane involves three Mo-C bonds and three C-C bonds.

The self-consistent GVB calculations were restricted (perfect pairing) such that each correlated pair is constrained to have the form in Eq. (4). This leads to an excellent description of systems that are well described in term of one bonding structure (e.g., **8**) but not of systems involving strong resonance effects (as in **7**).
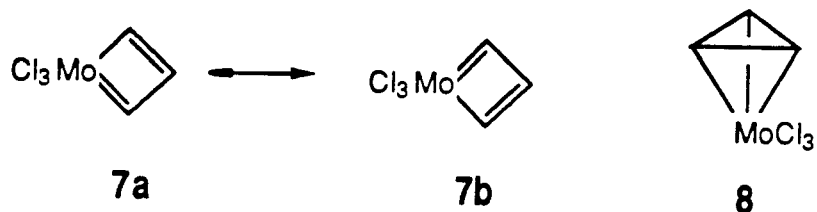
One approach to handling resonance in the GVB description is to optimize the orbitals for the resonating structures (**7a** and **7b**) self-consistently, while allowing dif-

ferent orbitals for the two structures.[13] This is termed GRVB (generalized resonating valence bond) and has been applied to similar systems (e.g., cyclobutadiene).[14] An alternative approach is to start with the GVB orbitals for one bonding structure, say (7a), and then to carry out a configuration interaction calculation in which the occupation of the orbitals is allowed to change, permitting the orbitals to describe other resonance structures (e.g., 7b). The latter approach was used for the metallacyclobutadiene. Thus for, (a), the Mo-C and C-C sigma bonds were allowed to have all spin pairings within each set of natural orbitals in a given bond pair [not just the one in (4)]; this is termed GVB-RCI. All excitations were allowed within the four natural orbitals representing the GVB π bonds (GVB-CI). In addition, to allow readjustments in the shapes of the various orbitals in the presence of resonance, all excitations were allowed out of the dominant configurations into the entire valence space (GVB-RCI-S) for the Mo-C bonds in order to allow resonance. For the metallatetrahedrane, the C-C bonds were described with GVB-RCI and the Mo-C bonds with GVB-CI.

III. RESULTS AND DISCUSSION

First, the GVB description of the bonding in both the metallacyclobutadiene and the metallatetrahedrane is examined with an emphasis on qualitative aspects. Next, an examination of the charge distribution and a comparison of relative energetics between the two complexes is presented. This will all be done with an emphasis on reactivity.

A. Geometries

The structures for the two geometries are presented schematically in Figure 1. Mo was used in place of W for calculational convenience. It is felt that because of the close correspondence of reactivity and structures for W and Mo, that this substitution will not significantly affect the trends calculated. In fact, similar alkylidyne,[15] metallatetrahedrane[16] and metallacyclobutadiene[15d] chemistry for Mo is already emerging and exhibits acetylene metathesis and polymerization activity. In addition, several acetylene metathesis systems based on Mo are known.[17] Furthermore, the covalent and ionic radii for Mo and W are similar,[18] so that no adjustment of the bond lengths and angles from the W crystal structure are expected.

In support of this assumption, a recent crystal structure of a less oxidized metallatetrahedrane, $CpMo(CO)_2(C_3Ph_3)$, showed bond lengths of approximately 0.1 Å longer than used in our calculation. This is as would be expected for a less oxidized species where the electron-rich C_3R_3 fragment is not held as close to the metal.

The goal of this study is to extract a conceptual understanding of **7** and **8** and of the relative bonding characteristics and relative energetics. Consequently, the geometries are based solely on crystal structure information. In cases where the crystal structure information could not be used to place the atoms, several
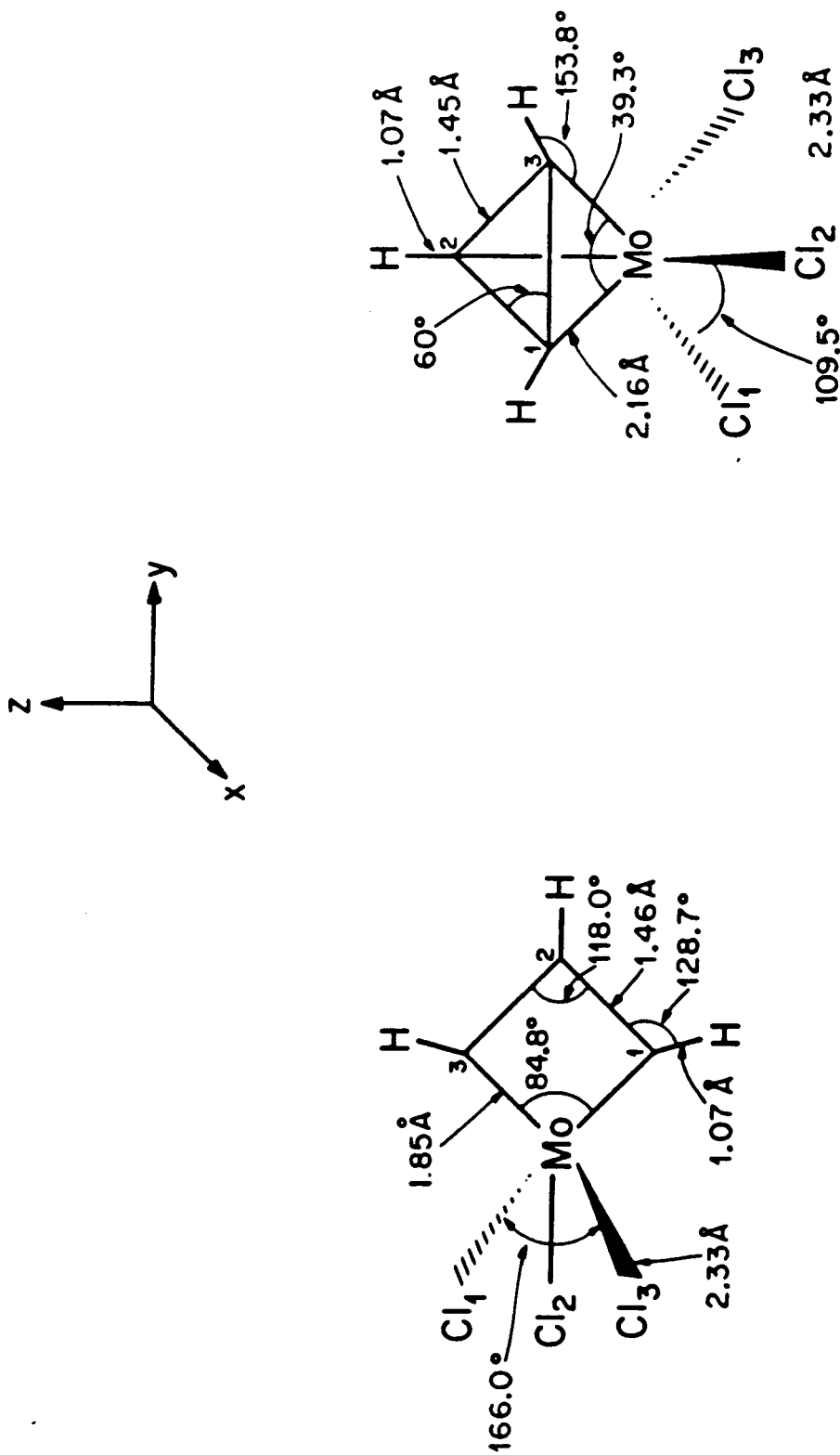
Figure 1: Calculated structures for the metallatetrahedrane and the metallacyclobutadiene.

geometries were calculated. For complex **8**, the system was constrained to have equal Mo-C distances and equal C-C distances, leading to C_{2v} symmetry in the $Cl_3Mo (C_3H_3)$ complex. In complex **8**, however, the chlorines are not totally placed from crystal structure information, and the TMEDA ligand was omitted. The Mo-Cl bond distances were derived from the crystal structure, but the Cl positions relative to the cyclopropenyl fragment were placed in several arrangements, always retaining C_{3v} symmetry. The TMEDA ligand was deleted so that the two complexes have the same number of ligands and electrons, allowing a fair comparison of the relative energetics for these bonding types.

B. Orbitals

The contour plots of the GVB orbitals for the metallacyclobutadiene are presented in Figure 2 and the GVB orbitals for a metallatetrahedrane in Figure 3. As discussed in Section II.B, each GVB orbital has **one** electron, but the two orbitals of a bond pair are allowed to overlap, forming a wavefunction as presented in Eq. (2).

1. Bonding in the Metallacyclobutadiene

As indicated in Figure 2, the metallacyclobutadiene has covalent Mo-C_1, $C_1 - C_2$, $C_2 - C_3$, and Mo-C_3 σ bonds and covalent $C_1 - C_2$ and Mo-C_3 π bonds. Thus, the name metallacyclobutadiene is appropriate. Considering both resonance structures (**7a** and **7b**), the bond order is $1\frac{1}{2}$ for each (Mo-C) and (C-C) bond. The result is that three d orbitals on the Mo are involved in the bond to the C_3H_3 fragment. The other three valence electrons initially on Mo are involved in partially ionic bonds to the three Cl atoms.

The C_3H_3 framework has a central bond angle of 118.1°, and the C-C bond pairs are well directed along the bond axes (unstrained). However, Figures 2a and

2b show that the Mo-C single bonds are strained. The center of the C lobe of the GVB bond is at an angle of 120° with respect to the $C_1 - C_2$ axis (as if it were going to point at the H of planar allyl), leading to an angle of 42° off the line joining Mo and C_1. Similarly, the d-like bonding orbital on the Mo points about 22° off of the Mo-C_1 vector, leading to a bent bond. The net result is that the two Mo d-like orbitals form Mo-C bonds lying at an angle of 129° with each other. This is quite consistent with the prediction of Rappé and Goddard[19], who showed that in order for two pure d orbitals to each be symmetric about their respective bond axes, the angle must be 125.3°.

The C-C π bond (Figure 2h) is conventional, involving px orbitals on each carbon. The Mo-C π bond (Figure 2g) is quite covalent, involving one orbital that is Mo d-like ($d_{xy} + d_{yz}$) and one that is Cp_x. A cross section through these π bonds in a plane parallel to the MoC_3H_3 plane (xz) but displaced 0.5 Å (in the y direction) reveals some bonding delocalization of the C-C π bond onto the Mo-C π bond (in Figures 2e and 2f) and some delocalization of the Mo-C π bond onto the C-C π bond. In fact, this delocalization from the Mo-C π bond to the C-C π bond is about equal on each carbon. In addition, the delocalization of the C-C π bond to the Mo-C π bond is about equal on both the C and the Mo. Thus, neither of these bonds has any significant interaction between Mo and the βC but only delocalization stemming from a resonance contribution. The contour plots (Figure 2) show that there is no significant bonding interaction between the Mo and the βC. The C-C σ framework is sp^2 (Figures 2c and 2d) with a C-C-C and H-C-C bond angle of ~120°. The combination of a C-C-C bond angle of 118° with bent Mo-C single bond leads to a short Mo-beta-C distance. The geometry, thus, is a balance struck between the small C-Mo-C angle and the restraint of forming two good C-C
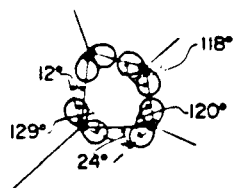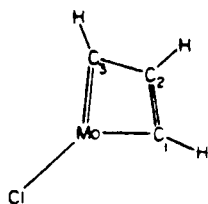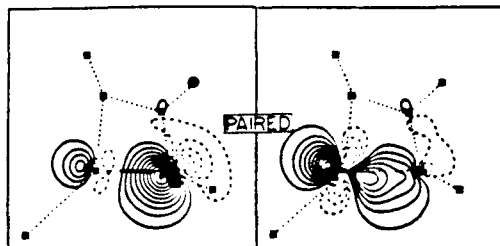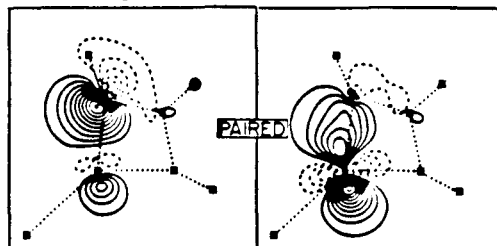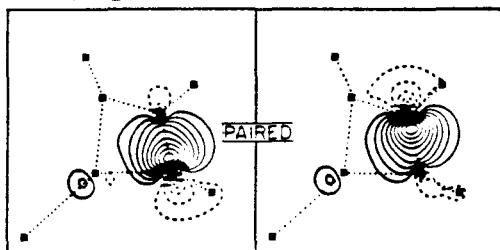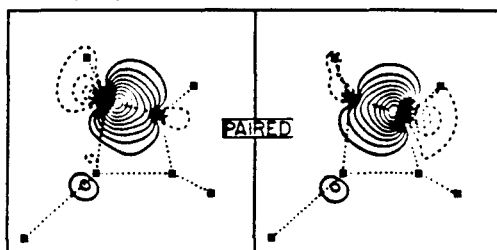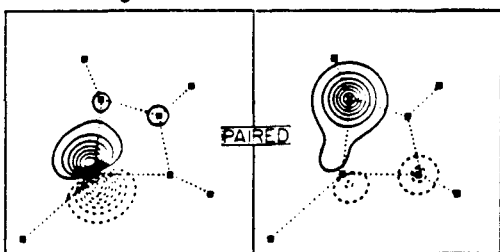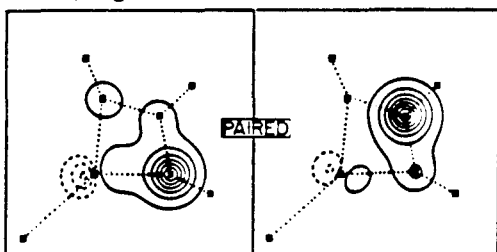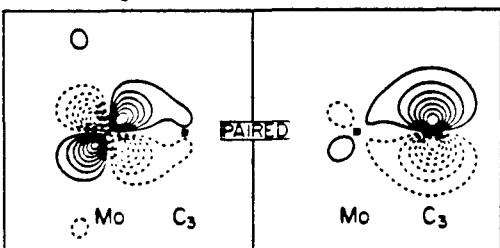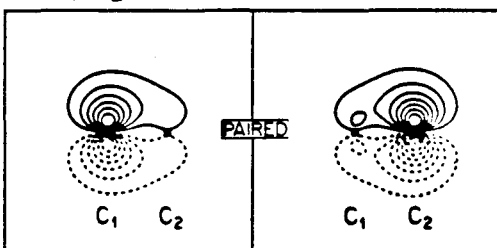
Figure 2: Contour plots for the GVB-PP orbital of metallacyclobutadiene. Spacing between contours is 0.05 a,u.; solid lines are positive and dashed lines are negative.

bonds with a bond order of 1.5. There is no a Mo-βC bonding interaction.

A contrasting view is presented by Bursten,[20] who performed Fenske-Hall[21] molecular orbital calculations and found a significant W-β carbon interaction in the butadienoid core $[WC_3H_3]^{3+}$. Bursten's results are best portrayed by using perturbational molecular orbital theory (PMOT). The interaction of the two occupied orbitals (A_2, B_2) of allyl radical with the two $d\pi$ orbitals on W produce the two bonding orbitals presented below.

b_2 $\qquad$ a_2
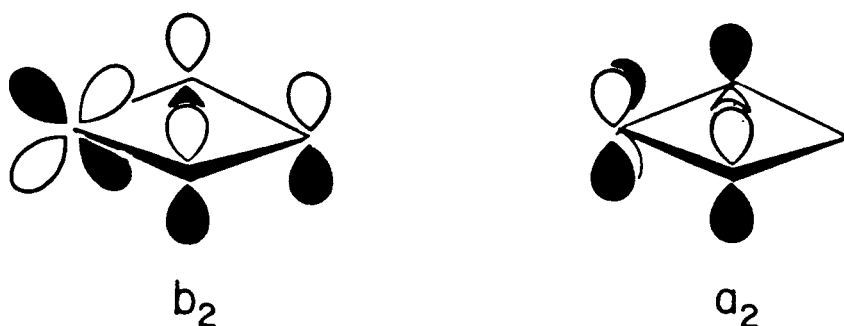
As is seen in the b_2 orbital, there is considerable W-β carbon bonding. Linear combinations of these orbitals do not produce localized π bonds as described in our GVB calculations.

The results from ab initio calculations are quite different. The $d\pi$ bonds that were used to build molecular orbitals in the PMOT approach are instead used to make localized π bonds which are then allowed to resonate (7a and 7b). This approach allows for a full 1.5 bond order between the carbons and also includes electron correlation in the bond pairs. This metalloaromatic system is thus stable because of the two $d\pi$ symmetry orbitals that allow the metal to form two π bonds simultaneously (by resonance) with bond orders each less than 1. In contrast, cyclobutadiene, uses a *single* carbon p orbital to form the π interaction with *both* adjacent carbon p orbitals.[14]

There is also an additional resonance structure which could arise from the PMOT approach by second-order mixing of the antibonding allyl orbital and the b_2 orbital. This would yield the valence bond structure shown below.
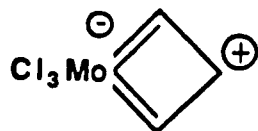
There is no significant mixing of this state in our ab initio calculations, as indicated by the positive charge of 0.86 found on the Mo and the small charge (-0.03) on the βC (see Section C and Figure 4).

To form the two Mo-αC bonds and two resonating π bonds, the Mo uses four of its five available d orbitals. The empty orbital is of d_{x^2} character and leads to a coordination of a ligand along the x axis. An acetylene coordinated along this axis could then insert into an Mo-αC bond to form a metallacyclohexatriene complex. In forming this insertion product, resonance is initially lost from the metallacyclobutadiene but is reintroduced in a hypothetical planar metallacyclohexatriene complex.

While the C-Mo-C angle prefers to be 125° to form the optimum directional dσ bonds, the axial Cl-Mo-Cl angle is expected to be large (166° in this case) due to high sp character (180° is optimal for two such bonds). Due to the high electronegativity of Cl, the Mo-Cl bonds are highly polarized toward Cl. These polar Mo-Cl bonds use Mo s orbitals since the ionization potential of the 5s electrons is less than for the 4d electrons. As a result of the charge transfer to the chlorines, the metal is positive, leading to covalent bonds to the carbons that are 4d-like and highly directed. This is the case in both the metallacyclobutadiene and the metallatetrahedrane.

243
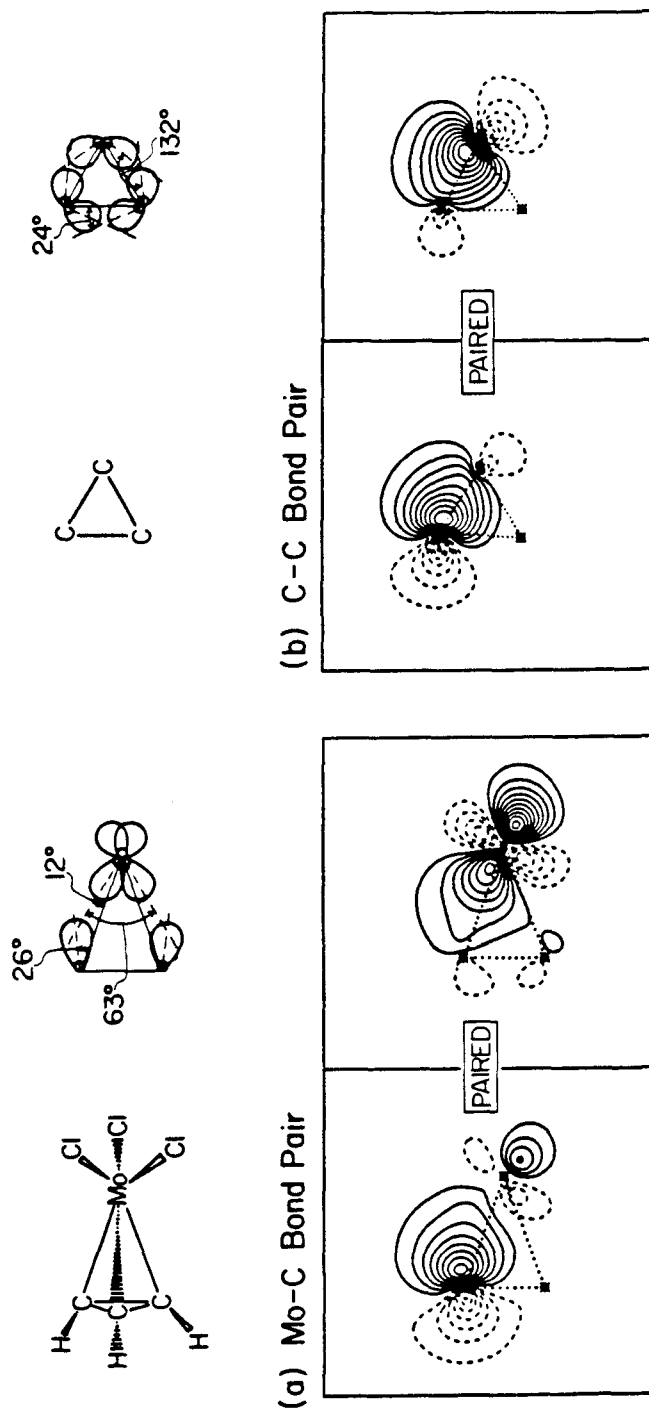
Figure 3: Contour plots for the metallatetrahedrane.

(a) Mo–C Bond Pair

(b) C–C Bond Pair

2. Bonding in the Metallatetrahedrane

For the metallatetrahedrane, all GVB wavefunctions led to three covalent Mo-C bonds. All attempts to force another description, such as a π allyl complex, only resulted in reversion to the three covalent bond description. A typical Mo-C σ bond is in Figure 3a.

Each Mo-C bond involves a Mo d σ orbital pointing at an sp^3-like orbital of the C_3H_3 fragment to form a σ bond. The metallatetrahedrane Mo-C σ bonds are less directional (more spatially diffuse) than in the metallacyclobutadiene because the metal now is forced to make three σ bonds rather than two. The bond is slightly bent ($\sim 12°$) from the bond axis, leading to an angle of 63° between ends of the Mo-d orbitals involved in each Mo-C bond. This small angle is created by the short C-C distance compared with the Mo-C distance. Rappé and Goddard[22] showed that the equivalent orthogonal d orbitals, each rotationally symmetric about its bond axis, must be at an angle of 54.7°, in reasonable agreement with the calculated results. A contour map of the C-C bond is shown in Figure 3b. It involves typical sp^3 orbitals localized on each carbon with no interaction with the metal.

C. Charges

Reactivity in transition metal complexes is controlled by the charge distributions between the metal and its ligands and by the nature of the metal-ligand bonds. The proposed reactivity of the metallacyclobutadiene in coordinating an acetylene requires that the metal center have an empty orbital and be electrophilic. The metallacyclobutadiene is a 12-electron species, and therefore, has empty orbitals. It is also calculated to be electrophilic, with the metal having a high positive charge of 0.86. In this complex, each chlorine takes approximately 0.34 electrons (see Figure 4 for all Mullikan populations). The alpha carbons are slightly negative and the

beta carbon is neutral. This charge distribution of the organic ligand is basically covalent, with no large charge polarization between the Mo and the C's. This is also apparent by viewing the contour maps 2a and 2b. Each one-electron orbital is essentially centered on the individual atoms.

The chlorine-to-molybdenum bonds behave the same in both complexes. The chlorines serve to remove s electron density from the metal. In each case, the chlorines take about 1.1 electrons and leave the positive charge to be dispersed among the Mo and the organic fragment.

The metallatetrahedrane has a similar charge distribution as the metallacyclobutadiene. Each chlorine takes about 0.36 of an electron and leaves the Mo with a positive 0.74 charge and the ring with a positive 0.34 charge (0.34 for the tetrahedrane, 0.19 for the butadiene). Again, the carbons have a slight negative charge, reflecting a higher electronegativity than Mo or H. This is as expected for a covalent Mo-C interaction.

In order to explore how charge transfer is affected by geometry of the C_3H_3 ring, the wavefunction was recalculated with a flat C_3H_3 ring (the original geometry had the H's bent back by 44°). Since $C_3H_3^-$ is "anti-aromatic", this might lead to a propensity for $C_3H_3^+$ and, hence, charge transfer to the metal. Indeed, the carbons lose 0.18 electrons to obtain a net charge of +0.52, while the metal gains 0.12 electrons to obtain a net charge of 0.86. Basically, the strong tendency for the Mo and the C's to form covalent Mo-C bonds prevents charge flow from the ring in either the flat or bent up hydrogen geometry. Furthermore, metallatetrahedrane with the flat C_3H_3 geometry is 6 kcal/mol [GVB (6/12)] above the system with a nonplaner C_3H_3 geometry. Although this bent back geometry is favored by steric interactions with the metal ligands, the dominant factor is believed to be the co-
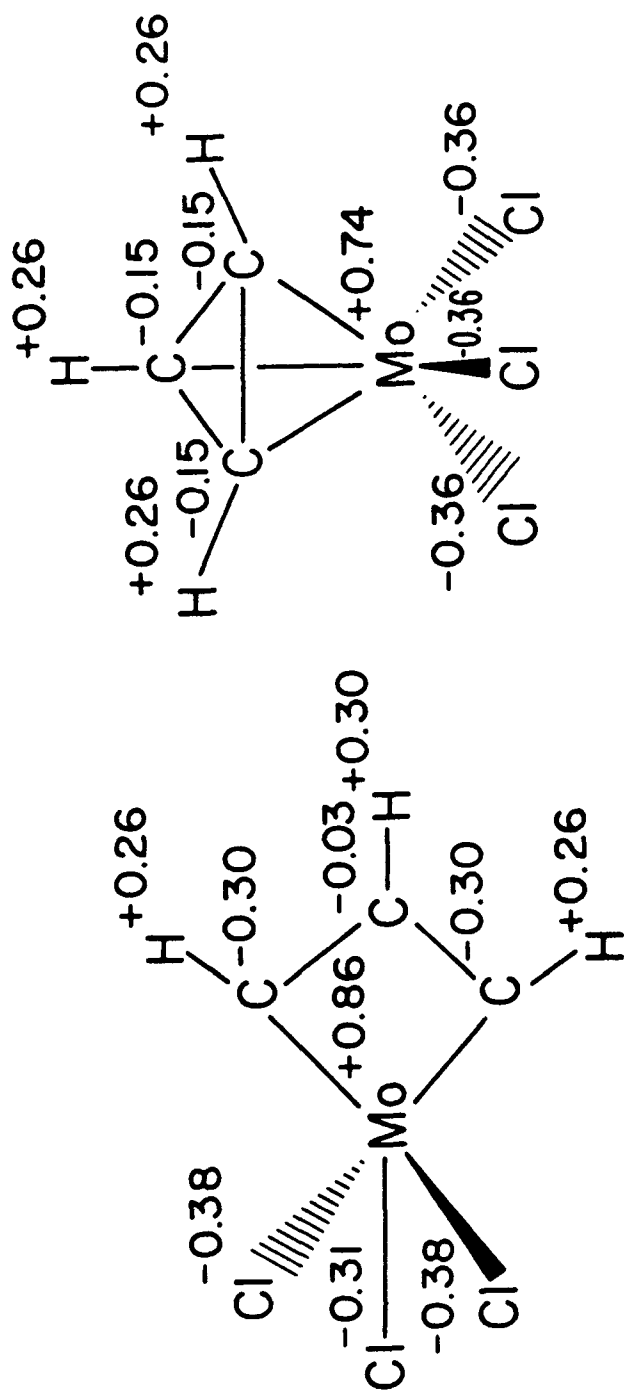
Figure 4: Mullikan populations for each atom in the metallatetrahedrane and metallacyclobutadiene.

valent metal-carbon bonding. Hence, the "bend-back angle" is a guide to the true metallatetrahedrane character in the bonding. Every metallatetrahedrane may have different bend-back angles depending on the charge distribution between the metal and the carbon ring, the oxidation state of the metal, and the steric requirements of the ligands on the metal and the alkyl groups on the carbon ring. In summary, the charge transfer is dominated by the nature of the M-C bonds. Because of the greater polarity in its Mo-C σ bond, the Mo in the metallacycle is more electrophilic than in the metallatetrahedrane.

D. Geometries and Energies

A dominant factor in the interconversion of the metallacyclobutadiene and metallatetrahedrane is the difference in ground state energies. In Figures 5 and 6, the energy separations between the metallacycle and the metallatetrahedrane are shown for various levels of theoretical treatments.

The metallacycle has four σ bonds, two of which are Mo-C and two are C-C. It also has one Mo-C π bond and one C-C π bond. The metallatetrahedrane also has six covalent bonds, three of which are Mo-C and three are C-C. Taking GVB overlaps as a rough guide to relative bond strengths, the total bond strength would be approximately the same since the sums of the overlaps are approximately the same (Table I). This neglects strain effects and resonance, which favors the metallacycle, and also neglects the energetics associated with the chlorine ligand geometries.

The placement of the chlorine ligands in the metallatetrahedrane was calculated in several geometries. Calculations were done at both 109° and 90° for the angle between the Cl's (the Cl-Mo-Cl angle). The 109° geometry is lower in energy by 44.0 kcal (for $MoCl_3$ high spin quartet, the 109° geometry is favored by 24.8

Table I: Orbital overlaps for the GVB pair orbitals.

Metallacyclobutadiene		Metallatetrahedrane	
Bond	Overlap	Bond	Overlap
Mo-Cα	0.74	Mo-C	0.67
Mo-Cα	0.74	Mo-C	0.67
Mo-Cπ	0.53	Mo-C	0.67
C-Cπ	0.71	C-C	0.83
C-Cσ	0.87	C-C	0.83
C-Cσ	0.87	C-C	0.83
	--		--
Total	4.46	Total	4.50
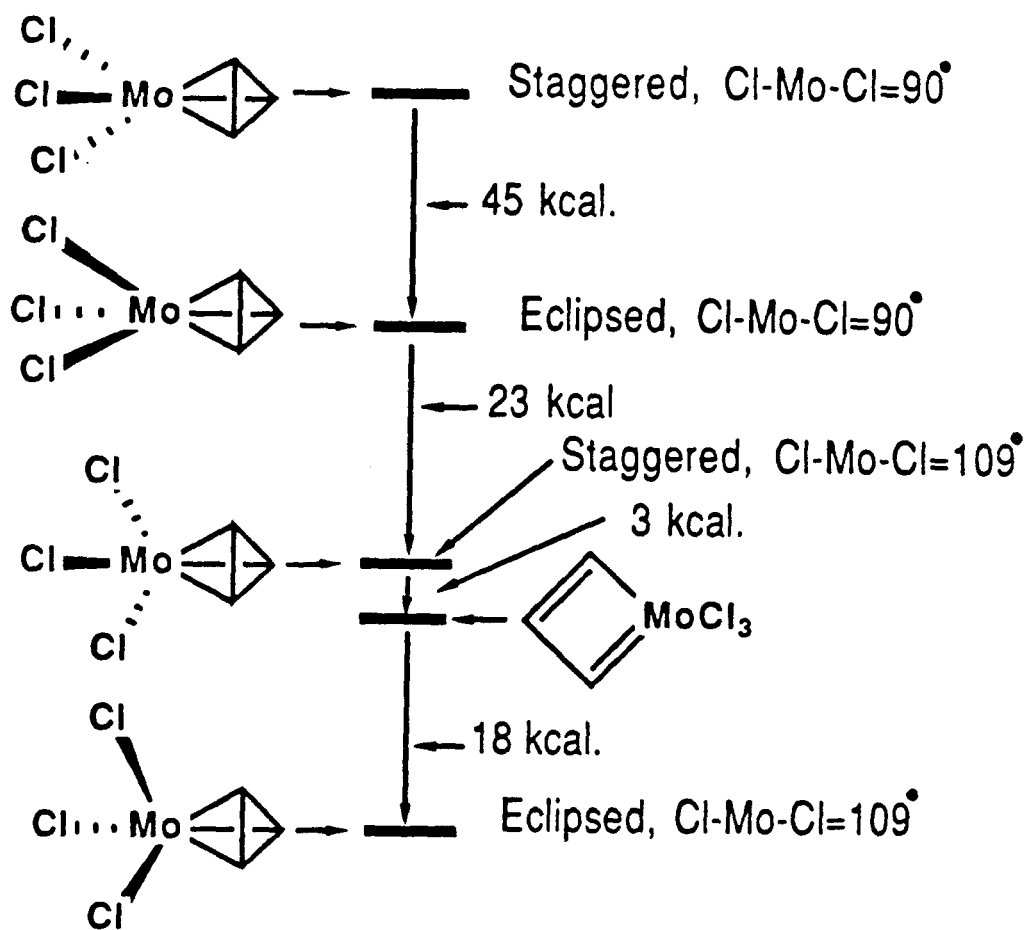
Figure 5: Ground state energy difference of several metallatetrahedranes and the metallacyclobutadiene at the GVB(6/12) level.
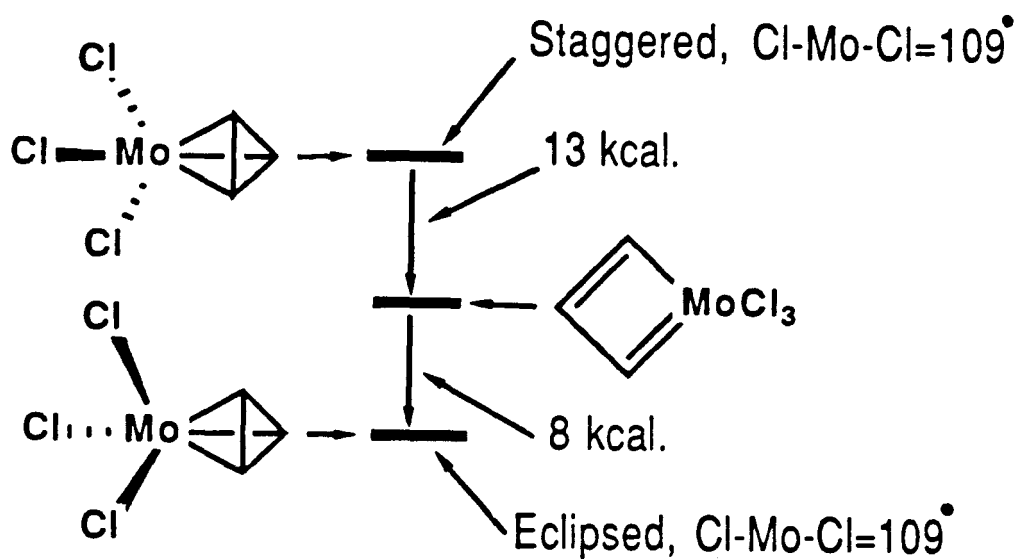
Figure 6: Ground state energy differences of the metallatetrahedrane and the metallacyclobutadiene at the CI level.

kcal). These energy differences are due to the decreased steric interaction between the chlorines in the 109° geometry.

The second geometry change was to stagger or eclipse the Cl's with the carbons of the C_3H_3 ring. The various geometries and their relative energies are presented in Figures 5 and 6. From calculations of the staggered and eclipsed geometries of the metallatetrahedrane with respect to the Cl's, the eclipsed conformation was found to be significantly lower than the staggered (by 18 to 45 kcal). In order to investigate the origin of this effect, the quartet state of free $MoCl_3$ was calculated, arriving at the localized orbitals for the $MoCl_3$ fragment presented in Figure 7. These orbitals are the ones used to bond the C_3H_3 fragments and are linear combinations of the orbitals in Figure 8. These localized high spin orbitals are *eclipsed* with respect to the chlorines. Thus, the origin of the eclipsed preference for the tetrahedrane is in the $MoCl_3$ fragment. Since the free $MoCl_3$ quartet state prefers to have an eclipsed set of d orbitals, the metallatetrahedrane bonds to the C_3H_3 fragment and leads to the eclipsed geometry. The staggered geometry requires rehybridization of $MoCl_3$ orbitals in order to bond to the C_3H_3 fragment.

Calculations on $MoCl_3$ at several Cl-Mo-Cl angles reveal the preference for the high spin orbitals to lie in the nodal planes of the Mo-Cl bonds. Figure 9a shows that the high spin orbitals are dz^2, dxz, and dyz combinations when the Cl-Mo-Cl angle is 120°. As the Cl-Mo-Cl angle diminishes the dyz mixes in dxy and tilts over two chlorines so that its horizontal angular node remains along the Mo-Cl bonds. The dxz orbital mixes in dx^2-y^2 and becomes $d\sigma$ appearing in character. The bottom positive lobe remains wedged between two chlorines. Finally, at a Cl-Mo-Cl angle of 90° (Figure 9b), the hybrid d orbitals are quite tilted from their original $d\pi$ character and are starting to appear as $d\delta$ type orbitals.
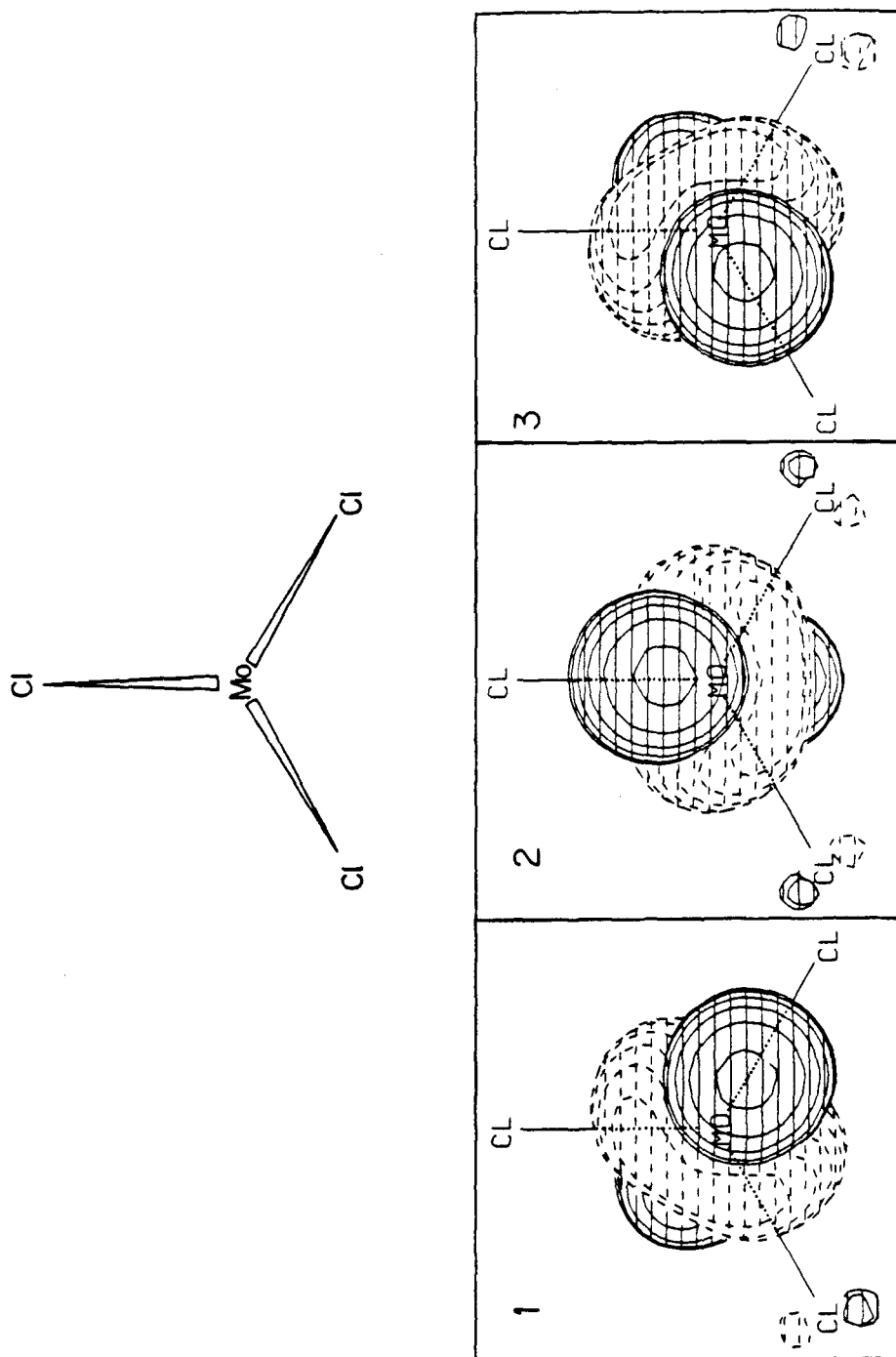
Figure 7: Singly-occupied orbitals localized over the Cl's of the quartet state of $MoCl_3$.

Mo dxz^{67},(dx^2−dy^2)^{26},Cl$^{.06}$ Mo s$^{.06}$,(2dz^2−dx^2−dy^2)$^{.90}$,Cl$^{.03}$ Mo dyz^{67},(dxy)^{26},Cl$^{.06}$
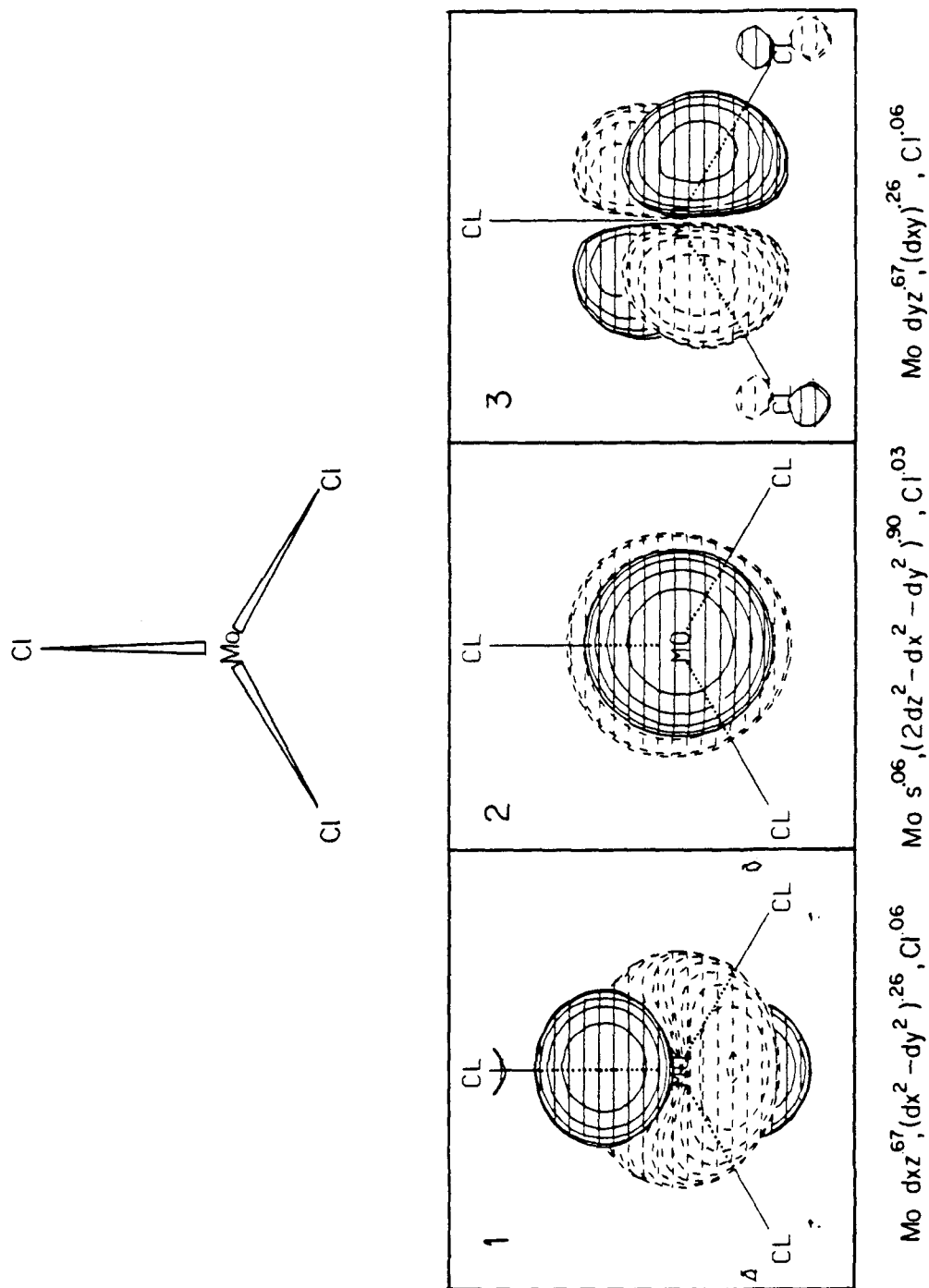
Figure 8: Singly-occupied orbitals of the quartet state of MoCl$_3$.

254
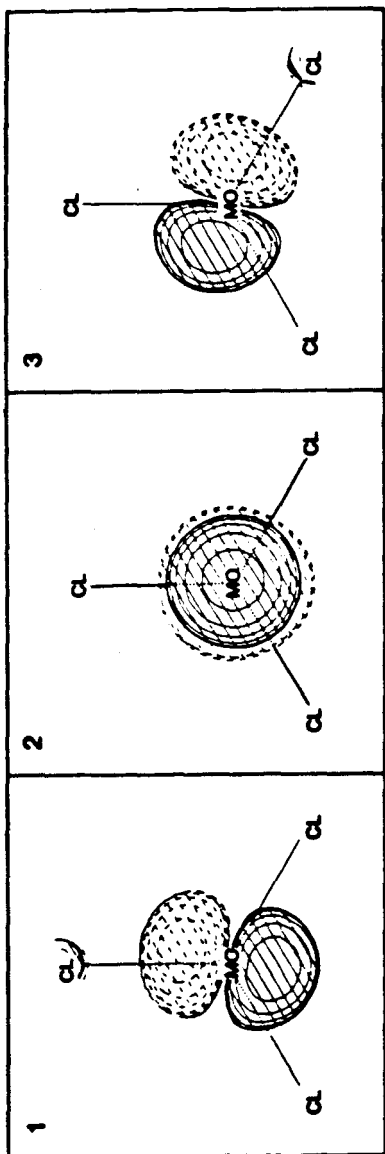
Figure 9a:High spin orbitals for MoCl₃ with a Cl-Mo-Cl angle of 120 degrees.
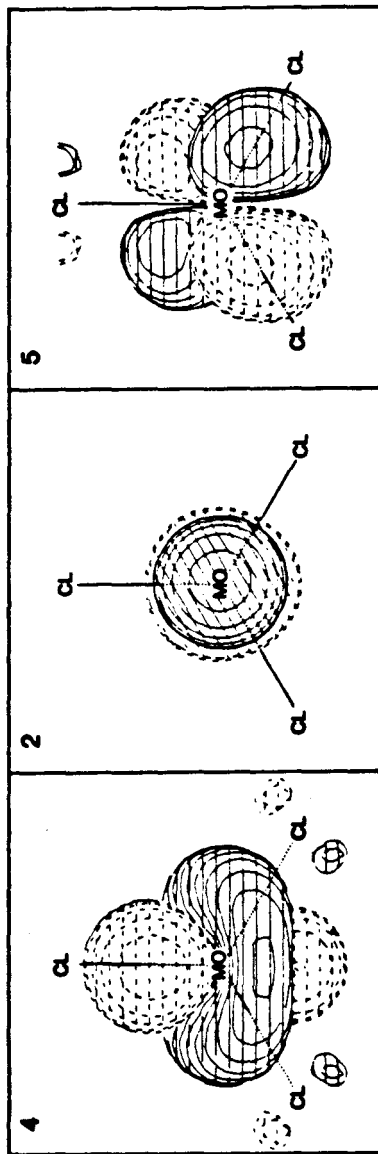
Figure 9b:High spin orbitals for MoCl₃ with a Cl-Mo-Cl angle of 90 degrees.

The high spin orbitals for the $MoCl_3$ fragment are presented in Figure 8. Mixing these frontier orbitals with the frontier orbitals of the cyclopropenium quartet state lead to the orbital interaction diagram of Figure 10 (no energy scale intended). The 1e and $1a_1$ orbitals on the metal are of the correct symmetry to mix with the equivalent symmetry orbitals of the cyclopropenium fragment only in an eclipsed geometry. Thus, covalent three-coordinate early transition metal systems (where the $1a_1$ and 1e set of orbitals is only singly-filled) prefer to make covalent bonds to three other substituents in an eclipsed geometry. As these orbitals fill, the preference for a staggered (octahedral) geometry becomes stronger. Steric interactions could also lead to a preference for staggered and are probably the dominant interactions in most experimental systems. Thus, in Group VIII metal systems, where these orbitals are filled (e.g., $Cl_3Fe^{\ominus}Me_3$,[23]), the geometry would be staggered due to the symmetry of the high lying 2e and $2a_1$ orbitals.[23]

Literature structures related to these conclusions are limited to the trigonal prism complexes of early transition metals with dithiolato bidentate ligands.[24] It has been suggested that these complexes are eclipsed due to S-S bonding interactions.[25] Since this suggestion, dithiolato complexes have been isolated with S-S distances greater than the sum of the covalent radii.[26] It is proposed that the eclipsed preference is due to the electronic effects presented above.

The preference for eclipsed geometries derives from the high-spin $MoCl_3$ fragment. This fragment has been calculated previously, and our calculations confirm the past results.[27,28] The $1e_1$ orbitals are tilted from the axis due to mixing of d_{xy} with d_{xz} and $d_{x^2-y^2}$ with d_{yz}. The question of bonding then reduces to why the $1e_1$ orbitals mix in such a fashion so as to prefer eclipsing. Calculations on $MoCl_3$ at several Cl-Mo-Cl angles reveal the preference for the high-spin orbitals to lie in
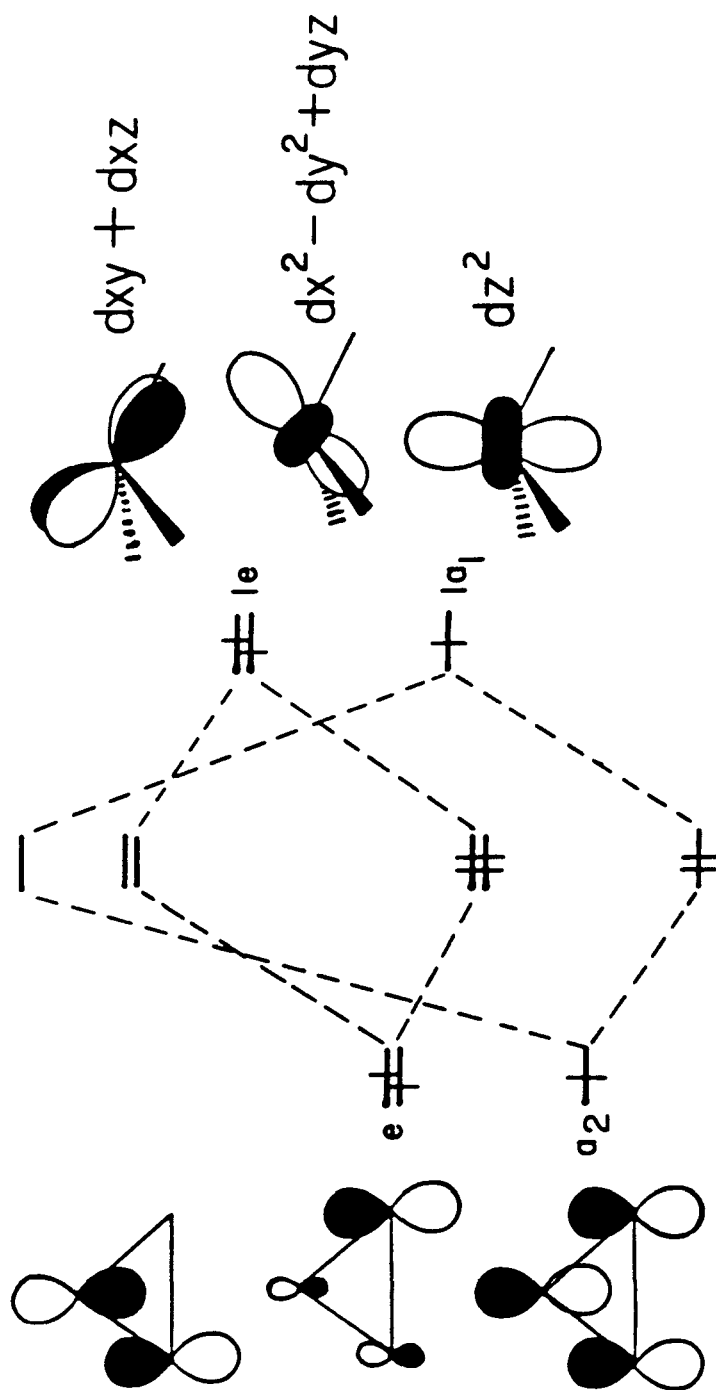
Figure 10: Orbital interaction diagram showing the preference for the eclipsed geometry arises from the ground state high-spin orbitals of $MoCl_3$.

the nodal planes of the Mo-Cl bonds. This allows for the least repulsion due to orthogonality between various occupied orbitals. It can be seen in Figure 8 that the $d_{x^2+y^2}$ and d_{yx} combination lies with the positive lobe directly between two Mo-Cl bonds. Conversely, the d_{xy} and d_{xz} combination has an angular node placed directly along an Mo-Cl bond. In this manner, the high-spin orbitals prefer to make bonds directly over the Mo-Cl bonds. This effect can be further visualized by looking at a schematic cross section of the Mo-C and Mo-Cl bonds (Figure 11). The orbitals of the Mo-C and Mo-Cl bonds directly overlap one another in the staggered geometry. In the eclipsed geometry, however, the Mo-C and Mo-Cl bonds lie roughly in the nodal planes of one another.

To further substantiate the stabilization of eclipsed bonds, several geometries of Cl_3MoH (triplet state, GVB(1/2)) were calculated, varying the hydrogen atom from an eclipsed to a staggered conformation with respect to the chlorines. It was found that an angle of 32° from the z axis (Figure 12), the eclipsed geometry was more stable by 1.7 kcal. If the stabilization of an eclipsed geometry lies in the bonding orbitals, then a trihydride geometry Cl_3MoH_3 should be 5.1 kcal (3x1.7 kcal) lower in the eclipsed geometry. A GVB (3/6) calculation with the three hydrogens of Cl_3MoH_3 at the same angle from the z axis as in the Cl_3MoH_3 geometry showed the eclipsed geometry to be 6.5 kcal lower than the staggered geometry. This is in agreement with our explanation rooted in orthogonality of the Mo-Cl and Mo-H or Mo-C bonds.

E. Electron Correlation

The above calculations used the simple GVB-PP wavefunction where the orbitals are optimized for a single bonding structure (for spin coupling). Thus, these calculations are biased against this fully delocalized metallacycle, which requires

258
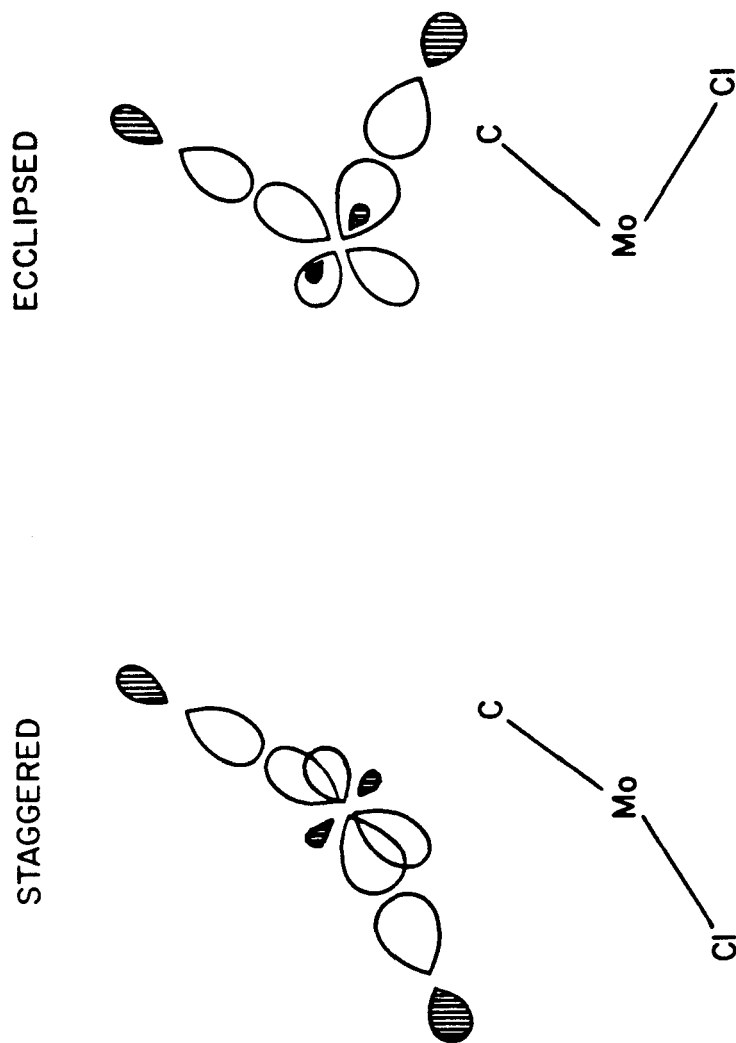
Figure 11: Schematic cross sections through the Mo-C and Mo-Cl bonds in the staggered and eclipsed geometries. The orbitals occupy roughly the same space in the staggered geometry but in the eclipsed geometry, the orbitals lie roughly in each others nodal planes.
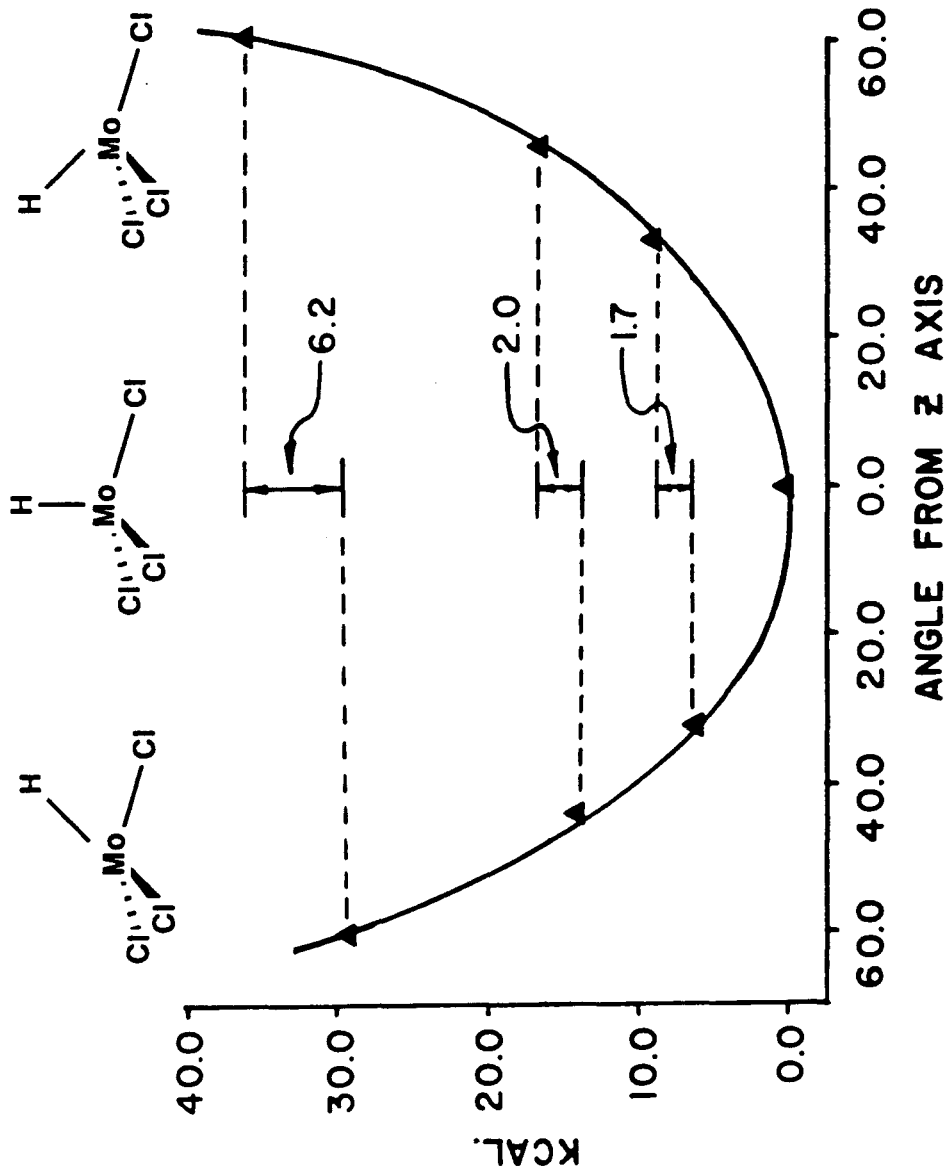
Figure 12: Plot of the energy of the triplet state of $MoHCl_3$ versus the angle the hydrogen makes with the z axis. Both staggered and eclipsed geometries are shown.

two configurations.

In order to elucidate further the energetic differences between the metallate-trahedrane and the metallacyclobutadiene, several calculations designed to allow resonance in the metallacyclobutadiene were performed.

An Mo atom with three unpaired d orbitals prefers the high spin state (Hund's rule) in which all three d electrons have the same spin, say α. However, bonding these electrons to ligands requires that the two electrons in the bond have opposite spins and that each electron has both α and β.
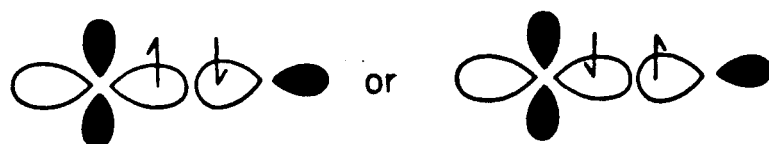
As a result, the d electrons on the metal can no longer all have the same spin. Thus, the high spin coupling of the metal tends to inhibit full bonding to the ligands and vice versa. A proper description of these spin coupling effects requires bonding structures in which the two electrons of a given pair are allowed to be coupled either low spin (bonding) or high spin (antibonding). Such configurations are included in the GVB-RCI wavefunction, and it was found that the metallacycle energy drops 6.28 kcal/mol more in the RCI than does the tetrahedrane. The contribution from such excitations within each GVB π bond pair resulted in a 19.8 kcal/mol lowering (half the total RCI lowering). Comparison to the analogous excitations from the C-C σ bonds of the metallatetrahedrane shows only a 7.63 kcal/mol lowering.

In order to allow resonance to build into the metallacycle, a full GVB-CI in the π space was allowed, with simultaneous σ relaxations (single excitations out of the σ bonds). This gave a further lowering of 9.86 kcal/mol. The tetrahedrane was then subjected to a comparable calculation. It consisted of a full GVB-CI

in the Mo-C space while leaving the RCI in the C-C space. This gave a further lowering of 6.56 kcal/mol. The final separation between the two geometries is 8 kcal/mol, favoring the metallatetrahedrane structure 2a. Due to the incorporation of resonance into the π system, these final CI's introduced a greater lowering for the metallacyclobutadiene than for the metallatetrahedrane.

The long Mo-C bond distances (in comparison to C-C bond distances) places the π bonds much further from one another than in cyclobutadiene.[14] This means that the repulsion from orthogonality that is so destabilizing in cyclobutadiene is much less evident in the metallacyclobutadiene, and therefore, the metallacycle takes advantage of some resonance stabilization.[14] Analysis of the resonance configurations shows a resonance stabilization of 8.68 kcal/mol.

F. Implications for Chemistry

This study allows us to speculate about the mechanism of metathesis performed by metallacyclobutadienes. It is viewed as decomposition of the metallacycle to an acetylene-alkylidyne, adduct which then loses the initial acetylene before or after coordinating a second acetylene. This reaction, thus, involves the slipping of an acetylene from a metallacycle to pi-coordination at the metal. The initial metallacyclobutadiene is a 12-electron species, whereas the acetylene-alkylidyne complex is a 14-electron species. The movement of the acetylene, thus, increases the electron richness of the metal. A strong π electron donor ligand should slow this reaction. This is a direct consequence of filling the orbitals the acetylene is moving into, and thus, making them less accessable. This logic is supported by the calculation of Rappé and Upton[29] for titanium metallacyclobutane olefin metathesis. In the titanium case, electron donating substituents on the titanium slow the metathesis reaction.[30] This is in direct contrast to the tungsten acetylene metathesis reaction

where electron withdrawing groups are indicated by Schrock *et al.* to slow the metathesis reaction.[5] Thus, there is a contradiction, and it would seem that the major effect operating in the tungsten metathesis systems is the steric environment imposed by the axial-equatorial ligands.

IV. SUMMARY

The Mo-C bonding in both the metallacyclobutadiene and the metallatetrahedrane is covalent with no large polarization toward either Mo or C. The Cl's remove 5s electron density from the Mo, leaving the d electrons to form hybrids that bond to the carbon fragments. The positive charge induced by the large electronegative chlorines is dispersed among the metal and the organic fragments. The metallacyclobutadiene is more electrophilic than the metallatetrahedrane. This supports the notion that the metallacycle can coordinate an acetylene. The electrophilicity of the Mo in the metallacycle argues in favor of accepting electron density from the axial-equatorial ligands. However, in contrast to the proposal by the original investigators,[5] this acceptance would (on an electronic basis) slow the metallacycle decomposition to an acetylene-alkylidyne. The energy difference between the metallacycle and metallatetrahedrane shows that the two geometries are very close in energy (within 20 kcal/mol by all calculational procedures). This is due to covalent bonds in the metallatetrahedrane that make up for the increased strain energy. In contrast to cyclobutadiene, the metallacyclobutadiene shows resonance stabilization. There is no bonding interaction between the Mo and the β carbon in the metallacycle ring. The bending of the ring substituents out of the plane of the carbons in the metallatetrahedrane is due to bonding effects (hybridization at the carbons forming covalent bonds to the Mo) not steric interactions with the axial-equatorial ligands. There is a considerable barrier to rotation of the C_3H_3 ring in the metallatetrahedranae due to strong electronic preference for the eclipsed geometry.

References and Notes

(1) (a) Wengrovious, J. H.; Sancho, J.; Schrock, R. R. *J. Am. Chem. Soc.* **1981**, *103*, 3932; (b) Sancho, J.; Schrock, R. R. J. Mol. Catal. **1982**, *15*, 75.

(2) (a) Dragutan, V.; Balaban, A. T.; Dimone, M. "Olefin Metathesis and Ring Operning Polymerizations of Cyclo-Olefins"; Wiley-Interscience: Chichester, 1985; (b) Ivin, K. J. "Olefin Metathesis"; Academic Press: London, 1983; (c) Mol, J. C. *Chemtech* **1983**, *13*, 250; (d) Grubbs, R. H. in "Comprehensive Organometallic Chemistry"; Wilkinson, G., Ed.; Pergamon Press, Ltd.: Oxford, 1982; Vol. 8, pp 499-551; (e) Banks, R. L. *Catalysis* **1981**, *4*, 100.

(3) Pedersen, S. F.; Schrock, R. R.; Churchill, M. R.; Wasserman, H. J. *J. Am. Chem. Soc.* **1982**, *104*, 6808.

(4) Churchill, M. R.; Ziller, J. W.; Freudenberger, J. H.; Schrock, R. R. *Organometallics* **1984**, *3*, 1554.

(5) Freudenberger, J. H.; Schrock, R. R.; Churchill, R. M.; Rheingold, A. L.; Ziller J. W. *Organometallics* **1984**, *3*, 1563.

(6) (a) Schrock, R. R.; Clark, D. N.; Sancho, J.; Wengrovious, J. H.; Rocklage, S. M.; Pedersen, S. F. *Organometallics* **1982**, *1*, 1645; (b) Schrock, R. R.; Listermann, M. L.; Sturgeoff, L. G. *J. Am. Chem. Soc.* **1982**, *104*, 4291.

(7) Schrock, R. R.; Pedersen, S. F.; Churchill, M. R.; Ziller J. S. *Organometallics* **1984**, *3*, 1574.

(8) Jemmis, E. D.; Hoffmann, R. *J. Am. Chem. Soc.* **1980**, *102*, 2570.

(9) Huzinaga, S. *J. Chem. Phys.* **1965**, *42*, 1293.

(10) Hay, P. J., personal communication to Goddard, W. A. III.

(11) Dunning, Jr., T. H. *J. Chem. Phys.* **1970**, *53*, 2823.

265

(12) Bobrowicz, F. W.; Goddard III, W. A. in "Modern Theoretical Chemistry, Methods of Electronic Structure Theory"; Schaefer,H. F., III, Ed.; Plenum Press: New York, 1977; Vol. 3, Chapter 4, pp 79-127.

(13) Voter, A. F.; Goddard, W. A., III *Chem. Phys.* **57**, *3*, 253.

(14) Voter, A. F.; Goddard, W. A., III *J. Am. Chem. Soc.* **1986**, *108*, 2830.

(15) (a) Fischer, E. O.; Kreis, G.; Kreiter, C. G.; Müller, J.; Huttner, G.; Lorentz, H. *Angew. Chem., Int. Ed. Engl.* **1973**, *12*, 564; (b) Clark, D. N.; Schrock, R. R. *J. Am. Chem. Soc.* **1978**, *100*, 6774; (c) Schrock, R. R.; Clark, D. N.; Sancho, J.; Wengrovious, J. H.; Rocklage, S. M.; Pedersen, S. F. *Organometallics* **1982**, *1*, 1645; (d) McCullough, L. G.; Schrock, R. R.; Dewan, J. C.; Murdyck, J. C. *J. Am. Chem. Soc.* **1985**, *107*, 5987.

(16) Drew, M. G. B.; Bresdon, B. J.; Day, A. J. *J. Chem. Soc., Dalton Trans.* **1981**, 1310, and references therein.

(17) (a) Mortreux, A.; Delgrange, J. C.; Blanchard, M.; Lubochinsky, B. *J. Mol. Catal.* **1977**, *2*, 73; (b) Devarajan, S.; Wlaton, O. R. M.; Leigh, G. J. *J. Organomet. Chem.* **1979**, *181*, 99; (c) Bencheick, A.; Petit, M.; Mortreux, A.; Petit, F. *J. Mol. Catal.* **1982**, *15*, 93; (d) Villemin, D.; Cachiot, P. *Tetrahedron Lett.* **1982**, 5139; (e) Petit, M.; Mortreux, A.; Petit, F. *J. Chem. Soc., Chem. Commun.* **1982**, 1385.

(18) Weast, R. C. "CRC Handbook of Chemistry and Physics"; CRC Press: Boca Raton, 1980.

(19) Rappé, A. K.; Goddard, W. A., III *J. Am. Chem. Soc.* **1982**, *104*, 297.

(20) Bursten, B. E. *J. Am. Chem. Soc.* **1983**, *105*, 121.

(21) Hall, M. B.; Fenske, R. F. *Inorg. Chem.* **1972**, *11*, 768.

(22) Rappé, A. K.; Goddard, W. A., III, unpublished results.

(23) Albright, T. A.; Hofmann, P.; Hoffmann, R. *J. Am. Chem. Soc.* **1977**, *99*, 7546.

(24) (a) Brown, G. F.; Stiefel, E. I. *Chem. Commun.* **1970**, 728; (b) Brown, G. F.; Stiefel, E. I. *Inorg. Chem.* **1973**, *12*, 2140; (c) Eisenberg, R.; Ibers, J. A. *J. Am. Chem. Soc.* **1965**, *87*, 3776; (d) Smith, A. E.; Schranger, G. N.; Mayweg, V. P.; Heinrich, W. *J. Am. Chem. Soc.* **1965**, *87*, 5798.

(25) Gray, H. B.; Eisenberg, R.; Stiefel, E. I. *Advances in Chemistry Series* **1966**, *62*, 641.

(26) (a) Bennett, M. J.; Cowie, M.; Martin, J. L.; Takats, J. *J. Am. Chem. Soc.* **1973**, *95*, 7504; (b) Cowie, M.; Bennett, M. J. *Inorg. Chem.* **1976**, *15*, 1584, 1589.

(27) (a) Elian, M.; Hoffmann, R. *Inorg. Chem.* **1975**, *14*, 1058; (b) Elian, M.; Chen, M. M. L.; Minges, D. M. P.; Hoffmann, R. *Inorg. Chem.* **1976**, *15*, 1148; (c) Burdett, J. K. *Inorg. Chem.* **1975**, *14*, 375.

(28) Orgel, L. E. "An Introduction to Transition Metal Chemistry"; Wiley: New York, 1960; p 174.

(29) Upton, T. H.; Rappé, A. K. *J. Am. Chem. Soc.* **1981**, *103*, 5582.

(30) See Chapter 1, Substituent effects.

APPENDIX I

Crystal Structure Data for $Cp_2^*Ti(Cl)O(CH_3)CCr(CO)_5$

Table 1: Summary of Crystal Data and Intensity Collection Information

Formula	$C_{27}H_{33}O_6ClCrTi$
Formula Weight	588.91/mol
Crystal System	Monoclinic
Space Group	$P2_1/C$
a	12.490(2)
b	13.472(3)
c	17.791(4)
β	109.83(2)
v	2816(2)
z	4
D_{calc}	1.39g/cc
λ	0.710733Å
μ	8.31 cm^{-1}
Scan Range	1.0° above $K_{\alpha L}$, 1.0° below $K_{\alpha z}$
Reflections	$\pm h$, $\pm k$, $\pm l$
Collected	11168 4101>0

Table 2: Selected Bond Distances for $Cp_2*Ti(Cl)O(CH_3)CCr(CO)_5$.

Distance(Å)

Cr	–C	2.089(6)
Cr	–C1	1.880(7)
Cr	–C2	1.897(7)
Cr	–C3	1.876(7)
Cr	–C4	1.892(7)
Cr	–C5	1.844(7)
Cr	–Me	3.136(7)
Ti	–O	2.007(4)
Ti	–Cl	2.347(2)
Ti	–C11	2.460(7)
Ti	–C12	2.477(7)
Ti	–C13	2.402(6)
Ti	–C14	2.390(6)
Ti	–C15	2.435(7)
Ti	–C21	2.458(7)
Ti	–C22	2.437(7)
Ti	–C23	2.406(7)
Ti	–C24	2.437(7)
Ti	–C25	2.438(7)
C	–O	1.269(7)
C	–Me	1.528(10)
Cl	–Me	3.502(7)
C1	–O1	1.146(9)
C2	–O2	1.138(8)
C3	–O3	1.151(9)
C4	–O4	1.136(9)
C5	–O5	1.166(9)
C11	–11M	1.492(10)
C12	–12M	1.487(10)
C13	–13M	1.498(9)
C14	–14M	1.503(9)
C15	–15M	1.500(9)
C21	–21M	1.489(10)
C22	–22M	1.489(10)
C23	–23M	1.499(9)
C24	–24M	1.498(10)
C25	–25M	1.510(10)

Table 3: Selected Bond Angles for Cp₂*Ti(Cl)O(CH₃)CCr(CO)₅.

Angle(°)

C	–Cr	–C1	91.5(3)
C	–Cr	–C2	95.3(3)
C	–Cr	–C3	91.7(3)
C	–Cr	–C4	86.0(3)
C	–Cr	–C5	177.1(3)
C1	–Cr	–C2	89.5(3)
C1	–Cr	–C3	176.1(3)
C1	–Cr	–C4	91.5(3)
C1	–Cr	–C5	88.8(3)
C2	–Cr	–C3	88.1(3)
C2	–Cr	–C4	178.4(3)
C2	–Cr	–C5	87.6(3)
C3	–Cr	–C4	90.8(3)
C3	–Cr	–C5	88.1(3)
C4	–Cr	–C5	91.1(3)
Cr	–C1	–O1	177.2(6)
Cr	–C2	–O2	176.9(6)
Cr	–C3	–O3	176.3(6)
Cr	–C4	–O4	178.8(6)
Cr	–C5	–O5	179.5(6)
Cr	–C	–O	129.2(5)
Cr	–C	–Me	119.4(5)
O	–C	–Me	111.3(5)
C	–O	–Ti	158.3(4)
O	–Ti	–Cl	97.2(1)

Tah

Table 4: Atom Coordinates (x 10^4) and U_{eq}'s for $Cp_2^*Ti(Cl)O(CH_3)CCr(CO)_5$.

Atom	x	y	z	U_{eq}
Cr	482.2(9)	115.8(8)	3471.1(6)	398(3)
Ti	3188.8(9)	231.9(8)	1920.8(7)	338(3)
Cl	4353.3(15)	−1161.7(13)	2387.2(11)	596(6)
O	2245(3)	86(3)	2630(2)	352(11)
C	1878(5)	−297(5)	3147(4)	388(18)
Me	2656(6)	−1134(6)	3602(4)	692(23)
C1	369(6)	1343(5)	2946(4)	468(20)
O1	254(5)	2093(3)	2624(3)	741(19)
C2	−627(6)	−415(5)	2545(4)	439(20)
O2	−1329(4)	−716(4)	2002(3)	697(17)
C3	488(5)	−1108(5)	3977(4)	474(21)
O3	437(4)	−1842(4)	4293(3)	783(19)
C4	1564(6)	634(5)	4413(4)	444(21)
O4	2226(5)	933(4)	4977(3)	812(20)
C5	−699(6)	503(5)	3806(4)	488(21)
O5	−1444(4)	742(4)	4021(3)	724(17)
C11	2796(5)	−93(5)	491(4)	398(18)
C12	2581(5)	−994(5)	819(4)	419(20)
C13	1699(5)	−840(5)	1122(4)	334(19)
C14	1325(5)	159(5)	942(3)	302(16)
C15	1995(5)	623(5)	557(4)	356(21)
C11M	3558(6)	−5(6)	5(4)	779(24)
C12M	3083(6)	−1970(5)	731(4)	710(26)
C13M	1185(5)	−1637(5)	1478(4)	484(21)
C14M	297(5)	616(5)	1063(4)	446(20)
C15M	1682(5)	1570(5)	89(4)	527(22)
C21	4802(6)	971(5)	2985(4)	425(21)
C22	3848(6)	1562(5)	2899(4)	375(18)
C23	3482(5)	1991(5)	2130(4)	343(18)
C24	4252(5)	1682(5)	1749(4)	360(19)
C25	5040(5)	1040(5)	2266(4)	438(22)
C21M	5520(6)	464(5)	3729(4)	646(25)
C22M	3413(6)	1826(5)	3555(4)	621(23)
C23M	2607(5)	2796(5)	1867(4)	507(21)
C24M	4439(5)	2166(5)	1046(4)	564(22)
C25M	6076(5)	607(5)	2133(4)	656(25)

Table 5: Gaussian Amplitudes for $Cp_2^*Ti(Cl)O(CH_3)CCr(CO)_5$.

Atom	U_{11}	U_{22}	U_{33}	U_{12}	U_{13}	U_{23}
Cr	448(7)	393(7)	369(7)	−55(6)	161(6)	−12(6)
Ti	285(7)	349(7)	359(8)	5(6)	83(6)	−12(7)
Cl	515(12)	494(12)	687(14)	158(10)	82(11)	37(11)
O	319(25)	403(28)	315(27)	−59(23)	81(21)	−30(24)
C	404(41)	352(42)	343(43)	−1(36)	41(34)	6(36)
Me	611(55)	821(60)	727(59)	302(47)	335(47)	414(50)
C1	503(49)	448(51)	491(53)	3(42)	220(42)	−57(42)
O1	1166(50)	390(35)	781(45)	125(33)	478(38)	141(31)
C2	461(49)	458(50)	447(53)	−36(39)	219(41)	−10(39)
O2	580(38)	892(42)	586(40)	−277(31)	155(31)	−116(33)
C3	377(45)	519(52)	483(53)	−116(42)	90(39)	5(43)
O3	970(46)	576(39)	728(44)	−267(34)	192(35)	125(33)
C4	597(55)	345(46)	427(53)	−113(39)	221(44)	−10(38)
O4	998(48)	797(43)	498(40)	−321(35)	66(34)	−211(33)
C5	568(54)	567(55)	406(50)	−71(42)	264(43)	−62(38)
O5	698(42)	884(44)	726(42)	21(33)	419(34)	3(32)
C11	305(38)	588(52)	339(41)	−56(39)	157(33)	−211(40)
C12	333(44)	467(49)	436(49)	−26(38)	103(37)	−114(40)
C13	317(42)	327(44)	301(43)	−77(34)	29(34)	−79(34)
C14	259(36)	358(41)	253(37)	10(34)	40(30)	−61(34)
C15	362(43)	482(47)	194(41)	−87(36)	56(34)	−82(34)
C11M	629(53)	1148(71)	738(58)	−260(53)	463(47)	−364(56)
C12M	563(55)	598(55)	889(67)	61(44)	143(48)	−362(49)
C13M	424(46)	432(46)	519(51)	−45(37)	58(39)	−13(39)
C14M	299(40)	582(49)	393(46)	62(36)	32(36)	−97(37)
C15M	547(52)	613(52)	372(48)	−77(41)	93(40)	91(40)
C21	283(42)	456(49)	456(51)	−155(36)	21(38)	−4(40)
C22	391(46)	394(45)	371(47)	−176(35)	169(39)	−70(37)
C23	307(43)	356(42)	387(48)	−61(32)	144(36)	−51(35)
C24	364(44)	385(45)	325(46)	−92(35)	109(36)	−56(36)
C25	238(41)	500(49)	546(56)	−75(36)	93(40)	−91(42)
C21M	544(51)	724(59)	483(53)	−92(44)	−68(42)	120(42)
C22M	714(58)	647(56)	512(55)	−237(44)	222(46)	−232(43)
C23M	514(48)	398(46)	543(52)	75(37)	93(40)	−9(38)
C24M	539(51)	623(54)	551(55)	−175(41)	212(43)	65(43)
C25M	349(46)	810(61)	828(63)	68(42)	225(45)	5(48)

Table 6: Hydrogen Atom Coordinates for Cp$_2$*Ti(Cl)O(CH$_3$)CCr(CO)$_5$.

Atom	x	y	z	B
H1	3280	−1289	3393	6.5
H2	3145	−913	4158	6.5
H3	2297	−1699	3670	6.5
11M1	4393	−24	381	7.2
11M2	3531	−585	−316	7.2
11M3	3454	553	−297	7.2
12M1	3922	−2034	1098	7.2
12M2	3089	−2102	205	7.2
12M3	2731	−2524	886	7.2
13M1	1808	−1944	1960	7.2
13M2	864	−2150	1122	7.2
13M3	662	−1376	1697	7.2
14M1	431	1332	1190	7.2
14M2	137	281	1484	7.2
14M3	−342	578	586	7.2
15M1	2381	1898	34	7.2
15M2	1357	2029	353	7.2
15M3	1199	1459	−442	7.2
21M1	6297	394	3765	6.2
21M2	5498	802	4205	6.2
21M3	5202	−216	3769	6.2
22M1	3832	2418	3856	6.2
22M2	3460	1313	3907	6.2
22M3	2637	2074	3336	6.2
23M1	2815	3356	2230	6.2
23M2	2556	3046	1324	6.2
23M3	1879	2565	1825	6.2
24M1	5049	2601	1177	6.2
24M2	4535	1646	657	6.2
24M3	3745	2503	720	6.2
25M1	6566	252	2629	6.2
25M2	6541	1114	2032	6.2
25M3	5868	130	1710	6.2
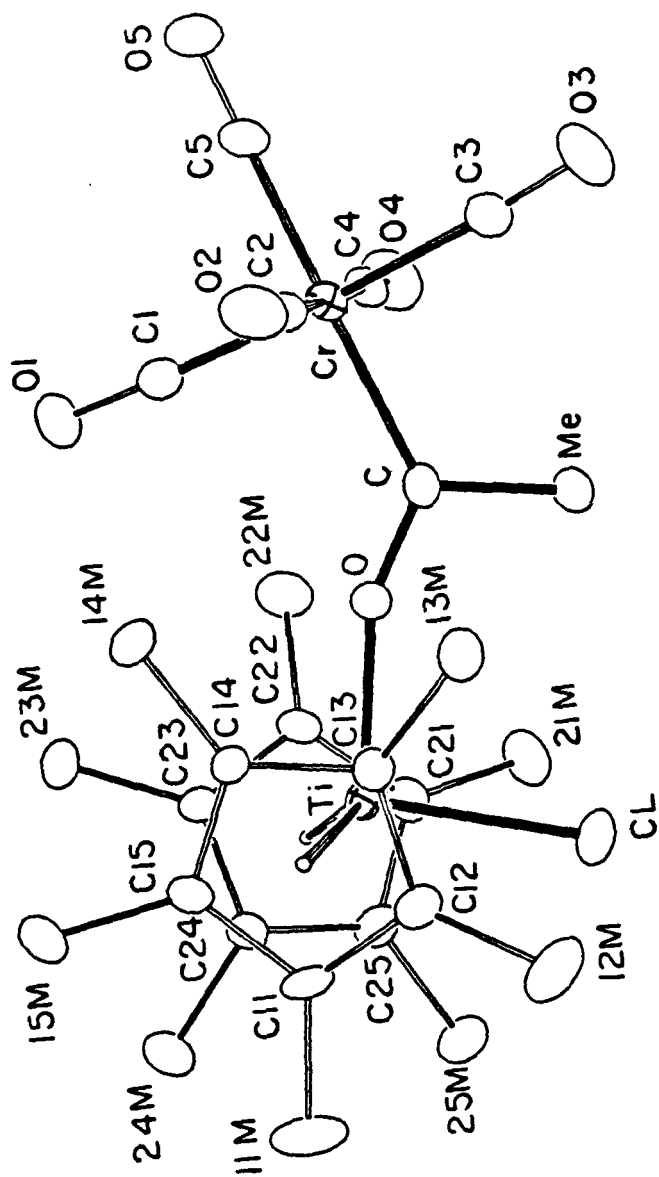
Figure 1: Numbering Scheme for $Cp_2*Ti(Cl)O(CH_3)CCr(CO)_5$.

APPENDIX II

Crystal Structure Data for Cp$_2$*Ti(O(CH$_3$)CCr(CO)$_5$)$_2$

Table 1: Summary of Crystal Data and Intensity Collection Information

Formula	$C_{34}H_{36}O_{12}Cr_2Ti$
Formula Weight	788.55/mol
Crystal System	Monoclinic
Space Group	$P2_1/n$
a	9.958(2)
b	32.226(8)
c	11.998(3)
β	108.21(2)
v	3657(3)$Å^3$
z	4
D_{calc}	1.43(1)g/cc
λ	0.710733$Å$
μ	8.92 cm^{-1}
Scan Range	1.0° above $K_{\alpha 1}$, 1.0° below $K_{\alpha 2}$
Collected	~14,000 5860 > 0

Table 2: Selected Bond Distances for Cp$_2$*Ti(O(CH$_3$)CCr(CO)$_5$)$_2$.

		Distance(Å)		Distance(Å)
Ti	–O1A	2.051(2)	C13A–C23A	1.509(5)
Ti	–O1B	1.973(2)	C14A–C15A	1.410(5)
Ti	–C11A	2.477(4)	C14A–C24A	1.510(5)
Ti	–C12A	2.462(4)	C15A–C25A	1.505(6)
Ti	–C13A	2.405(4)	C11B–C12B	1.410(5)
Ti	–C14A	2.389(4)	C11B–C15B	1.412(5)
Ti	–C15A	2.486(4)	C11B–C21B	1.496(5)
Ti	–C11B	2.420(3)	C12B–C13B	1.413(5)
Ti	–C12B	2.458(4)	C12B–C22B	1.500(5)
Ti	–C13B	2.411(4)	C13B–C14B	1.417(5)
Ti	–C14B	2.434(4)	C13B–C23B	1.507(5)
Ti	–C15B	2.425(4)	C14B–C15B	1.409(5)
Cr1	–C1A	2.107(4)	C14B–C24B	1.511(5)
Cr1	–C2A	1.847(4)	C15B–C25B	1.509(5)
Cr1	–C3A	1.874(5)	C1A –O1A	1.270(4)
Cr1	–C4A	1.873(5)	C1B –O1B	1.268(4)
Cr1	–C5A	1.851(4)	O1A –C1A	1.270(4)
Cr1	–C6A	1.897(5)	C1A –C7A	1.501(5)
Cr2	–C1B	2.096(4)	O2A –C2A	1.150(6)
Cr2	–C2B	1.862(4)	O3A –C3A	1.146(6)
Cr2	–C3B	1.887(4)	O4A –C4A	1.149(6)
Cr2	–C4B	1.886(4)	O5A –C5A	1.152(6)
Cr2	–C5B	1.872(5)	O6A –C6A	1.131(7)
Cr2	–C6B	1.884(4)	O1B –C1B	1.268(4)
C1A	–C7A	1.501(5)	O2B –C2B	1.151(5)
C1B	–C7B	1.524(5)	O3B –C3B	1.145(5)
C11A–C12A		1.413(5)	O4B –C4B	1.142(5)
C11A–C15A		1.401(5)	O5B –C5B	1.141(6)
C11A–C21A		1.508(6)	O6B –C6B	1.138(5)
C12A–C13A		1.404(5)		
C12A–C22A		1.503(6)		
C13A–C14A		1.417(5)		

Table 3: Selected Bond Angles for Cp$_2$*Ti(O(CH$_3$)CCr(CO)$_5$)$_2$.

			Angle(°)		Angle(°)
O1A	–Ti	–O1B	99.6(1)	C14A–C13A–C12A	108.1(3)
Ti	–O1A	–C1A	150.1(2)	C23A–C13A–C12A	125.2(3)
Ti	–O1B	–C1B	161.2(2)	C23A–C13A–C14A	126.2(3)
O1A	–C1A	–C7A	114.1(3)	C15A–C14A–C13A	107.6(3)
O1B	–C1B	–C7B	113.5(3)	C24A–C14A–C13A	125.7(3)
O1A	–C1A	–Cr1	127.8(2)	C24A–C14A–C15A	126.1(3)
O1B	–C1B	–Cr2	127.5(3)	C14A–C15A–C11A	108.1(3)
C7A	–C1A	–Cr1	118.0(2)	C25A–C15A–C11A	123.3(3)
C7B	–C1B	–Cr2	119.0(2)	C25A–C15A–C14A	126.2(3)
C1A	–Cr1	–C2A	178.0(2)	C15B–C11B–C12B	108.0(3)
C1A	–Cr1	–C3A	91.6(2)	C21B–C11B–C12B	125.2(3)
C1A	–Cr1	–C4A	87.2(2)	C21B–C11B–C15B	125.8(3)
C1A	–Cr1	–C5A	91.8(2)	C13B–C12B–C11B	108.0(3)
C1A	–Cr1	–C6A	92.3(2)	C22B–C12B–C11B	124.0(3)
C2A	–Cr1	–C3A	89.3(2)	C22B–C12B–C13B	127.4(3)
C2A	–Cr1	–C4A	92.1(2)	C14B–C13B–C12B	107.8(3)
C2A	–Cr1	–C5A	86.3(2)	C23B–C13B–C12B	125.1(3)
C2A	–Cr1	–C6A	89.5(2)	C23B–C13B–C14B	125.3(3)
C3A	–Cr1	–C4A	176.8(2)	C15B–C14B–C13B	107.9(3)
C3A	–Cr1	–C5A	91.3(2)	C24B–C14B–C13B	127.4(3)
C3A	–Cr1	–C6A	88.5(2)	C24B–C14B–C15B	122.2(3)
C4A	–Cr1	–C5A	91.7(2)	C14B–C15B–C11B	108.1(3)
C4A	–Cr1	–C6A	88.6(2)	C25B–C15B–C11B	126.3(3)
C5A	–Cr1	–C6A	175.8(2)	C25B–C15B–C14B	125.1(3)
C1B	–Cr2	–C2B	178.1(2)	C7A –C1A –O1A	114.1(3)
C1B	–Cr2	–C3B	88.9(2)	C7B –C1B –O1B	113.5(3)
C1B	–Cr2	–C4B	88.7(2)	C15A–C11A–C12A	108.2(3)
C1B	–Cr2	–C5B	92.0(2)	C21A–C11A–C12A	125.5(3)
C1B	–Cr2	–C6B	92.8(2)	C21A–C11A–C15A	124.4(3)
C2B	–Cr2	–C3B	91.4(2)	C13A–C12A–C11A	107.8(3)
C2B	–Cr2	–C4B	91.1(2)	C22A–C12A–C11A	126.7(3)
C2B	–Cr2	–C5B	89.8(2)	C22A–C12A–C13A	124.7(3)
C2B	–Cr2	–C6B	85.3(2)		
C3B	–Cr2	–C4B	176.0(2)		
C3B	–Cr2	–C5B	88.2(2)		
C3B	–Cr2	–C6B	94.4(2)		
C4B	–Cr2	–C5B	88.6(2)		
C4B	–Cr2	–C6B	89.0(2)		
C5B	–Cr2	–C6B	174.6(2)		

Table 4: Atom Coordinates (x 104) and U_{eq}'s for $Cp_2Ti(O(CH_3)CCr(CO)_5)_2$.

Atom	x	y	z	U_{eq}
Ti	4525.9(7)	3892.1(2)	2803.0(5)	337(1)
Cr(1)	1240.7(7)	4116.5(2)	−1369.8(5)	508(2)
Cr(2)	1531.7(7)	2760.8(2)	3565.4(5)	448(1)
O(1A)	3159(2)	3969(1)	1138(2)	362(6)
C(1A)	2096(4)	3847(1)	303(3)	390(9)
O(2A)	102(4)	4545(1)	6308(3)	1064(12)
C(2A)	507(5)	4371(1)	−2812(4)	709(13)
O(3A)	3469(4)	3730(1)	−2265(3)	996(11)
C(3A)	2632(5)	3869(1)	−1900(3)	638(12)
O(4A)	−1081(4)	4464(1)	−515(3)	1219(14)
C(4A)	−189(5)	4334(2)	−832(4)	752(15)
O(5A)	2977(4)	4892(1)	−721(3)	983(11)
C(5A)	2332(5)	4589(1)	−913(3)	589(11)
O(6A)	−664(5)	3383(1)	−2340(3)	1430(16)
C(6A)	68(6)	3650(2)	−1947(4)	864(17)
C(7A)	1361(5)	3476(1)	596(3)	668(12)
O(1B)	3582(2)	3428(1)	3333(2)	391(6)
C(1B)	3288(4)	3157(1)	3985(3)	430(9)
O(2B)	−1070(4)	2221(1)	2906(3)	892(10)
C(2B)	−66(5)	2424(1)	3173(3)	578(11)
O(3B)	2271(3)	2472(1)	1424(3)	796(9)
C(3B)	1975(4)	2591(1)	2216(3)	526(10)
O(4B)	1027(4)	3014(1)	5832(3)	958(11)
C(4B)	1220(4)	2921(1)	4976(4)	587(11)
O(5B)	3225(4)	2037(1)	4865(3)	1189(13)
C(5B)	2622(5)	2317(1)	4373(4)	677(12)
O(6B)	−535(3)	3428(1)	2348(2)	777(9)
C(6B)	287(5)	3184(1)	2783(3)	497(10)
C(7B)	4369(4)	3132(1)	5206(3)	584(11)
C(11A)	4720(4)	4263(1)	4656(3)	467(10)
C(12A)	3265(4)	4230(1)	4025(3)	454(9)
C(13A)	3016(4)	4454(1)	2977(3)	409(9)
C(14A)	4317(4)	4627(1)	2958(3)	444(9)
C(15A)	5351(4)	4521(1)	4024(3)	476(10)
C(21A)	5398(5)	4140(1)	5921(3)	741(13)
C(22A)	2130(5)	4054(1)	4468(3)	615(11)
C(23A)	1577(4)	4545(1)	2119(3)	587(11)
C(24A)	4510(5)	4922(1)	2042(4)	624(11)
C(25A)	6732(4)	4742(1)	4572(4)	692(13)
C(11B)	5521(4)	3422(1)	1698(3)	397(9)
C(12B)	6113(4)	3301(1)	2880(3)	454(9)
C(13B)	6920(4)	3637(1)	3500(3)	442(10)
C(14B)	6911(4)	3954(1)	2678(3)	433(10)
C(15B)	6033(4)	3822(1)	1570(3)	420(9)
C(21B)	4722(4)	3143(1)	718(3)	570(10)
C(22B)	6055(4)	2868(1)	3318(3)	598(11)
C(23B)	7912(4)	3617(1)	4739(3)	647(13)
C(24B)	7957(4)	4305(1)	2818(3)	592(12)
C(25B)	5848(4)	4047(1)	429(3)	563(10)

Table 5: Gaussian Amplitudes for $Cp_2^*Ti(O(CH_3)CCr(CO)_5)_2$.

Atom	U_{11}	U_{22}	U_{33}	U_{12}	U_{13}	U_{23}
Ti	260(4)	424(3)	317(3)	17(3)	77(3)	−39(3)
Cr(1)	444(4)	683(4)	357(3)	−31(4)	68(3)	105(3)
Cr(2)	432(4)	486(3)	442(3)	39(3)	161(3)	90(3)
O(1A)	306(15)	452(13)	319(11)	18(12)	85(11)	−37(10)
C(1A)	327(22)	495(21)	370(19)	16(18)	141(18)	17(16)
O(2A)	971(30)	1487(31)	582(18)	129(24)	22(20)	452(20)
C(2A)	551(31)	1023(34)	478(23)	10(27)	54(23)	183(24)
O(3A)	1176(34)	1191(28)	731(22)	297(25)	457(22)	21(19)
C(3A)	770(36)	765(29)	372(22)	132(28)	167(23)	55(21)
O(4A)	732(29)	1825(40)	1215(31)	504(28)	469(25)	394(27)
C(4A)	515(33)	1057(37)	655(29)	161(30)	142(27)	245(26)
O(5A)	1224(34)	767(22)	953(24)	−253(23)	335(23)	132(19)
C(5A)	677(34)	607(27)	491(23)	27(25)	195(23)	139(21)
O(6A)	1682(45)	1670(38)	732(24)	−1059(35)	80(26)	−122(24)
C(6A)	1015(46)	1080(39)	403(25)	−408(35)	84(28)	63(25)
C(7A)	598(31)	833(29)	443(22)	−248(26)	−25(22)	163(20)
O(1B)	356(15)	461(14)	374(12)	33(12)	139(12)	15(11)
C(1B)	410(25)	505(22)	386(19)	109(20)	140(19)	23(17)
O(2B)	751(26)	1033(25)	886(23)	−368(22)	247(21)	−30(19)
C(2B)	630(33)	592(26)	551(24)	−38(25)	239(25)	84(20)
O(3B)	879(27)	897(22)	729(20)	−185(19)	422(20)	−241(17)
C(3B)	482(28)	536(24)	565(24)	−86(21)	169(22)	9(20)
O(4B)	826(27)	1556(31)	549(19)	223(24)	298(19)	−19(20)
C(4B)	459(28)	754(28)	556(25)	101(23)	169(23)	108(22)
O(5B)	1269(37)	949(25)	1338(31)	578(25)	392(27)	485(23)
C(5B)	696(35)	670(29)	702(28)	186(26)	272(27)	163(22)
O(6B)	747(24)	853(21)	691(19)	346(19)	167(18)	169(16)
C(6B)	510(29)	561(24)	438(22)	−5(22)	174(21)	32(18)
C(7B)	463(27)	813(28)	438(21)	−3(23)	85(21)	117(20)
C(11A)	449(26)	535(23)	399(20)	26(21)	108(20)	−164(17)
C(12A)	426(26)	507(22)	478(21)	8(20)	211(20)	−160(18)
C(13A)	331(23)	442(21)	447(20)	39(18)	113(19)	−124(16)
C(14A)	441(26)	397(20)	510(22)	23(19)	173(21)	−115(17)
C(15A)	343(24)	520(23)	555(23)	−9(20)	127(21)	−223(19)
C(21A)	792(36)	955(32)	401(22)	49(29)	78(23)	−196(22)
C(22A)	596(30)	701(27)	660(26)	−24(24)	356(24)	−164(21)
C(23A)	417(26)	684(26)	631(24)	125(22)	122(22)	−129(20)
C(24A)	665(33)	495(23)	749(27)	10(23)	275(25)	−40(20)
C(25A)	476(29)	692(27)	870(30)	−88(24)	155(25)	−343(23)
C(11B)	334(23)	448(21)	453(20)	61(18)	187(18)	−62(17)
C(12B)	389(25)	507(22)	526(23)	116(20)	228(20)	16(18)
C(13B)	314(23)	583(23)	428(20)	131(20)	115(18)	−2(18)
C(14B)	271(22)	514(22)	541(22)	53(19)	166(19)	−77(18)
C(15B)	306(23)	529(22)	453(21)	69(19)	161(19)	−8(17)
C(21B)	602(30)	604(24)	567(23)	25(22)	274(23)	−144(19)
C(22B)	609(31)	585(25)	680(26)	163(22)	319(24)	82(20)
C(23B)	381(27)	879(30)	588(25)	188(24)	19(22)	−8(22)
C(24B)	359(26)	686(26)	762(27)	−36(22)	220(23)	−105(22)
C(25B)	475(27)	765(27)	523(23)	−3(22)	263(21)	25(20)

Table 6: Hydrogen Atom Coordinates for Cp$_2$*Ti(O(CH$_3$)CCr(CO)$_5$)$_2$.

Atom	x	y	z	B
H(7A1)	1977	3378	1441	5.0
H(7A2)	1356	3240	−69	5.0
H(7A3)	315	3574	522	5.0
H(21A1)	6297	4327	6270	5.0
H(21A2)	5721	3813	5938	5.0
H(21A3)	4629	4175	6349	5.0
H(22A1)	2618	3804	5083	5.0
H(22A2)	1760	4290	4914	5.0
H(22A3)	1307	3925	3743	5.0
H(23A1)	1755	4642	1322	5.0
H(23A2)	1136	4798	2499	5.0
H(23A3)	969	4267	2037	5.0
H(24A1)	5331	5136	2531	5.0
H(24A2)	4833	4741	1430	5.0
H(24A3)	3536	5075	1678	5.0
H(25A1)	7566	4509	4844	5.0
H(25A2)	6921	4950	3937	5.0
H(25A3)	6657	4905	5346	5.0
H(7B1)	5201	3329	5180	5.0
H(7B2)	4691	2801	5297	5.0
H(7B3)	3819	3215	5786	5.0
H(21B1)	5440	3033	270	5.0
H(21B2)	4295	2882	1085	5.0
H(21B3)	3883	3316	116	5.0
H(22B1)	6551	2887	4249	5.0
H(22B2)	6577	2676	2844	5.0
H(22B3)	4940	2799	3097	5.0
H(23B1)	8946	3600	4670	5.0
H(23B2)	7721	3885	5160	5.0
H(23B3)	7628	3327	5105	5.0
H(24B1)	8669	4216	2359	5.0
H(24B2)	8469	4353	3725	5.0
H(24B3)	7345	4579	2427	5.0
H(25B1)	6729	3970	164	5.0
H(25B2)	5850	4384	642	5.0
H(25B3)	4866	3953	−145	5.0

RING A - TOP
RING B - BOTTOM

Figure 1: Numbering Scheme for $Cp_2*Ti(O(CH_3)CCR(CO)_5)_2$.